PROCESSING- STRUCTURE- PROPERTY RELATIONSHIP IN NEEDLE-PUNCHED NONWOVEN NATURAL FIBER MAT COMPOSITES

By

MAHBOOBEH FAHIMIAN

A Thesis submitted to the Faculty of Graduate Studies of the University of Manitoba in partial fulfillment of the requirements of the degree of

DOCTOR OF PHILOSOPHY

Department of Mechanical and Manufacturing Engineering

University of Manitoba

Winnipeg, Manitoba, Canada

ABSTRACT

Natural fibers, such as hemp and flax, are emerging as cheaper reinforcing fibers for polymer composites. Renewability, comparable specific properties, and biodegradability make natural fibers more attractive than glass fibers. Vacuum Assisted Resin Transfer Molding (VARTM) is widely used to manufacture medium-to-large sized composites. The nonwoven mats used in VARTM must meet manufacturing (permeability) and structural (volume fraction (V_f), thickness, fiber orientation, properties) requirements. Unlike glass mats, natural fiber mats are not available commercially. Design and development of natural fiber mats require knowledge on the relationship among manufacturing, structure and properties of these mats and their composites. Developing this knowledge is the objective of this thesis. Effect of needle punch density on hemp fiber mat structure (areal density, V_f, fiber orientation distribution (FOD), thickness, permeability) was systematically studied. The FOD was characterized non-destructively using X-ray tomography. The Effect of consolidation pressure during composite manufacturing on its structure (V_f, thickness, FOD) was studied. The modulus and strength of needle-punched hemp mat – thermoset polyester composites, manufactured using VARTM and compression molding, were measured. A predictive model for these properties and a modeling approach for the evolution of FOD and thickness during mat manufacturing were developed and validated. The results of these studies were used to understand the relationship. The modulus and the strength of the composites were significantly influenced by the V_f and the FOD, the evolution of which during composite manufacturing depended on the consolidation pressure and the mat structure. The latter depended on mat manufacturing parameters, namely the punch density used

to bind the fibers together and the areal density of the web of fibers formed during air laying, and the FOD in the web. The permeability of the mat decreased with increasing the punch density and was found to be a function of both the V_f and the FOD. Despite this, the manufacturing of composite was not adversely affected, and the tensile modulus increased with punch density. The mat composite was modeled as an equivalent laminate, whose lay-up was determined using its FOD. The properties of equivalent laminate that was predicted using lamination theory compared well with the experimental results.

ACKNOWLEDGMENT

I would like to express my sincere gratitude to my thesis advisor **Dr. Raghavan Jayaraman**, for his invaluable guidance, academic support and financial assistance throughout my thesis work.

I would like to thank **Manitoba Rural Adaptation Council** (MARC), **Agriculture and Rural Development Initiative** (ARDI), **Stemergy renewable Fiber Technologies**, **Carlson Engineered Composites Inc**. and **New Flyer** for funding this research work.

I would like to thank **Brain O'Conner**, **Frank Wheeler** and **Mike Boskwick** for providing me the assistance during the research work.

I would like to thank **Kathy Davis** for her editorial help during writing my thesis.

I would like to thank **Don MacDonald** and **Fred Doern** and all my coworkers at Red River College for their support and encouragements during my research.

Last, but not the least, my very special thanks to **my family** for their constant support and encouragement during my graduate studies.

TABLE OF CONTENTS

LIST OF FIGURES

LIST OF TABLES

LIST OF ACRONYMS

FOD	Fiber Orientation Distribution
RTM	Resin Transfer Molding
VARTM	Vacuum Assisted Resin Transfer Molding

LIST OF SYMBOLS

$[A]$	Extensional stiffness matrix (Pa)
A_m	Cross section area of mat (m^2)
A_s	Preform compression factor
$[a]$	Compliance Matrix
B_c	Mats compression factor
C	Experimental factor related to ratio of axial and transverse deformation in a mat
D_f	Diameter of a fiber (µm)
E_{11}	Longitudinal tensile modulus of a lamina (GPa)
E_{22}	Transverse tensile modulus of a lamina (GPa)
E_f	Young's modulus of fibers (GPa)
E_x	Effective modulus of composite laminate in longitudinal direction
E_y	Effective modulus of composite laminate in transverse direction
$E_{x,T}$	Tensile Modulus of the mat (GPa)
$E_{z,c}$	Compressive modulus of the mat (GPa)
e_x	Axial strain on the mat
e_y	Transverse strain of the mat
e_z	Compressive strain of the mat
F_x	Tensile force action on mat (N)
f_a	Axial orientation factor
f_p	Planar orientation factor
GSM	Area density of needle punched mats (g/m^2)
h_c	Composite thickness (mm)

h_{mat}	Thickness of mats (mm)
h_{lamina}	Thickness of each lamina (ply) (mm)
h_p	Thickness of ply group (mm)
K_x	In-Plane permeability (m^2)
K_z	Through thickness permeability (m^2)
k_x	In-plane Kozney constant factor
k_z	Through thickness Kozney constant factor
L_0	Initial length of the mat
l	Length of a fiber (cm)
l_c	Critical length of the fiber
M_i	Moment per unit length (N)
m_f	Mass of a fiber (g)
m_l	Number of laminas in composite
N_i	Force per unit length (N/m)
N_0	Number of needles per unit length (Needle/cm)
N_z	Axial force exerted by needle board
n_f	Number of fibers per cm^2
$n(\theta_p)$	Number of fibers oriented in θ
P	Punch density (Punch/cm^2)
P_c	Compressive force (Pa)
Q	Volumetric flow (m^3/sec)
$[Q^k]_{x,y}$	Stiffness matrix of a lamina k (Pa) in global coordination
$[Q^k]_{1,2}$	Stiffness matrix of a lamina k (Pa) in local coordination
S	Strokes per unit time (Strokes/sec)
T	Transformation matrix
V	Volume of a fiber (cm^3)
V_f	Fiber Volume Fraction

V_0	Critical volume of fibers that fibers start sharing load bearing with matrix
V_x	Rate of fabric delivery (cm/sec)
V_z	Vertical speed of the needle board(cm/sec)
V_s	Saturated volume fraction, that preform cannot be compacted more with more compaction force.
w_f	Width of mat (cm)
w_0	Original width of mat (cm)
x	Coordination of end of a fiber in x direction
x_f	Final position of end of a fiber in x direction
x_0	Initial position of end of a fiber in x direction
y	Coordination of end of a fiber in y direction
y_0	Initial position of end of a fiber in z direction
y_f	Final position of end of a fiber in z direction
z	Coordination of end of a fiber in z direction
z_0	Initial position of the mat along z axis
z_1	Final position of the mat along the z axis
ΔP	Pressure gradient (MPa)
Δx	Amount of displacement of end of fiber in x direction
Δy	Amount of displacement of end of fiber in z direction
γ_s^0	Laminate shear strain for lamina
ε_{ij}	Strain of lamina
ε_x	Laminate strain in x direction for a lamina
ε_y	laminate strain in y direction for a lamina
θ	Angle of projection of fibers in x-y plane with x-axis
μ	Viscosity of the fluid (Pa.s)
μ_f	Average friction coefficient for fibers
ρ_f	Density of fibers (g/cm^3)

σ_x	Global stress on the lamina in *x* direction
σ_y	Global stress on the lamina in *y* direction
$(\sigma_i^T)_{ult}$	Ultimate tensile strength of the lamina in *i* direction
$(\sigma_i^C)_{ult}$	Ultimate compression strength of the lamina in *i* direction
σ_C	Strength of the composite laminate
σ_{fu}	Ultimate strength of the fibers
σ_{fuavg}	Average tensile strength of fiber in a mat
σ_1	Local stress on the lamina in fiber direction
σ_2	Local stress on the lamina transverse to fiber direction
$\bar{\sigma_f}$	Average strength of fibers over their length
σ_m'	Stress on the resin at composite failure
τ_C	Interfacial bond strength of resin and fiber (MPa)
τ_{xy}	Global shear stress on the lamina
$(\tau_{12})_{ult}$	Ultimate shear strength of the lamina
τ_{12}	Local shear stress on the lamina
v_f	Poisson's ratio of the fibers
v_m	Poisson's ratio of the matrix
v_{12}	Poisson's ratio of the lamina
φ	Angle of fibers with z-axis
ω	Porosity of the mat

CHAPTER 1

INTRODUCTION

Polymer matrix composites consist of high strength and high modulus fibers embedded in a polymeric matrix. They provide a combination of properties that cannot be achieved with either of the constituents alone. Their high specific properties result in lighter parts. A design engineer has a large number of options while choosing the fiber, the resin matrix, the fiber architecture, and the manufacturing method. This design freedom allows optimization of material and manufacturing to produce a composite product tailored to meet the requirements of performance and cost. Due to these advantages, polymeric composites have been steadily increasing their market share in non-structural and high performance structural applications in a number of industries such as aerospace, automobile, infrastructure, building materials, recreation and sports.

Close to 90% of composites used in the automotive industry are glass fiber composites and the rest are carbon fiber or aramid fiber composites [1]. Natural fibers such as hemp, flax, abaca and jute either have replaced (in certain applications) or are currently being evaluated to replace glass fibers in composites. In addition to offering a specific modulus comparable to glass fibers, as observed in Table 1.1, the natural fibers also offer additional advantages such as renewability, potential to be cheap, and no health or environmental concerns. New industrial markets for these fibers would add value to these fibers, which are currently disposed as waste, and improve farmers' income. Further research and development is required to make these new classes of

materials acceptable to industries. Hence, natural fiber composites, also known as bio-composites, are the focus of this thesis.

1.1 Background

Polymer composites can be classified based on the geometry of reinforcement as particulate composites, short fiber composites, and continuous fiber composites, as illustrated in Figure 1.1. Particulate composites contain randomly dispersed particles with aspect ratio (length/diameter) in the range of 1 to 20. Discontinuous or short fiber composites contain short fibers with aspect ratio in the range of 20 to 1000. Continuous fiber composites consist of fibers with aspect ratio greater than 1000 that span the entire length and width of a composite part. Normally, the percentage of the load shared by fibers and the properties of composite increase with an increase in the aspect ratio.

Continuous fiber composites are used in structural applications in the aerospace industry where the desired mechanical performance outweighs the cost. In the automotive industry, discontinuous fiber composites are used in semi-structural or non-structural applications, where cost is the primary consideration. Natural fibers, when extracted from the plant stalk, are normally short and discontinuous. Although they can be spun into continuous fibers, for use in composites [2], extensive processing degrades the mechanical properties and increases the cost of fibers. Hence, this study is focused on discontinuous hemp fiber composites.

The most common manufacturing processes for manufacturing short fiber composites are injection molding, compression molding and liquid molding. While the first process is used for manufacturing thermoplastic composites, the last two are used for manufacturing thermoset composites, which is the focus of this thesis.

Table 1.1. Comparison of Mechanical Properties of Natural Fibers with Synthetic Fibers [4]

Fiber	**Density (g/cm^3)**	**Elongation at break (%)**	**Tensile strength (GPa)**	**Specific Tensile strength ($\frac{MPa}{g/cm^3}$)**	**Young's Modulus (GPa)**	**Specific Young's Modulus ($\frac{GPa}{g/cm^3}$)**
Cotton	1.5-1.6	3-10	287-579	180-386	5.6-13	3.66-8.4
Jute	1.46	1.5-1.8	393-773	270-530	9.52-29.9	6.8-20.5
Flax	1.4	2.7-3.2	345-1035	245-739	59.9- 79.8	42.8-57
Hemp	1.48	1.6	550-900	370-610	69.85	47.2
Ramie	1.5	3.6-3.8	400-938	265-625	43.9	29.3
Sisal	1.33	2.0-2.5	511-700	340-526	37.9	28.5
E-glass	2.5	2.5	2000-3500	800-1400	70	28
S-glass	2.5	2.8	4570	1828	86	34.4
Aramid	1.4	3.3-3.7	3000-3150	2100-2250	63-65.8	45-47
Carbon	1.4	1.4-1.8	4000	2850	229.6-233.8	164-167

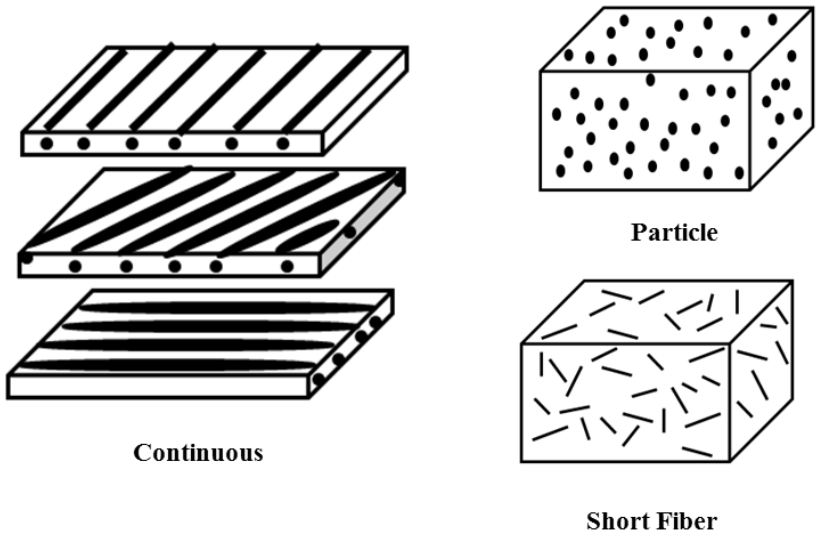

Figure 1.1. Composite Classification

Compression molding, illustrated in Figure 1.2, consists of two matched mold die halves. The thermoset resin, the discontinuous fibers, and other additives are mixed into a "charge" that is loaded into the mold cavity of the bottom mold half. The mold is closed, heated, and pressure is applied through the top half of the mold. Under heat and pressure the charge melts, flows to fill the mold cavity, and cures to yield a solid composite part. Compression molding is used to manufacture small to medium sized composite parts cost effectively.

Liquid molding and its variants such as Resin Transfer Molding (RTM), Light Resin Transfer Molding (LRTM), and Vacuum Assisted Resin Transfer Molding (VARTM) are used to manufacture short (i.e. discontinuous) fiber thermoset polymer composites. VARTM, whose schematic is shown in Figure 1.3, is suitable for manufacturing large composite parts. This process involves manufacturing a nonwoven fiber mat, placing it in a properly designed mold, and injecting the resin into the mold to impregnate the fiber mat under vacuum. The part is allowed to cure inside the mold at room temperature and is removed after resin cures completely. This study is focused on manufacturing the discontinuous natural fiber composites using VARTM, and additional details on this process are presented in Chapter 2.

The discontinuous reinforcing fibers used in VARTM are in the form of a nonwoven mat, as shown in Figure 1.4. The most common method of manufacturing these mats is air-laying. Well-separated short fibers are suspended in air and dropped by gravity on to a moving conveyor belt to form a web of fibers. The fibers in this web are subsequently bound together by a process known as needle punching. The use of needle punching in the textile industry dates back to 1800 [3]. In this process, illustrated in Figure 1.5, a board containing barbed needles reciprocates in a direction perpendicular to the surface of the fiber web.

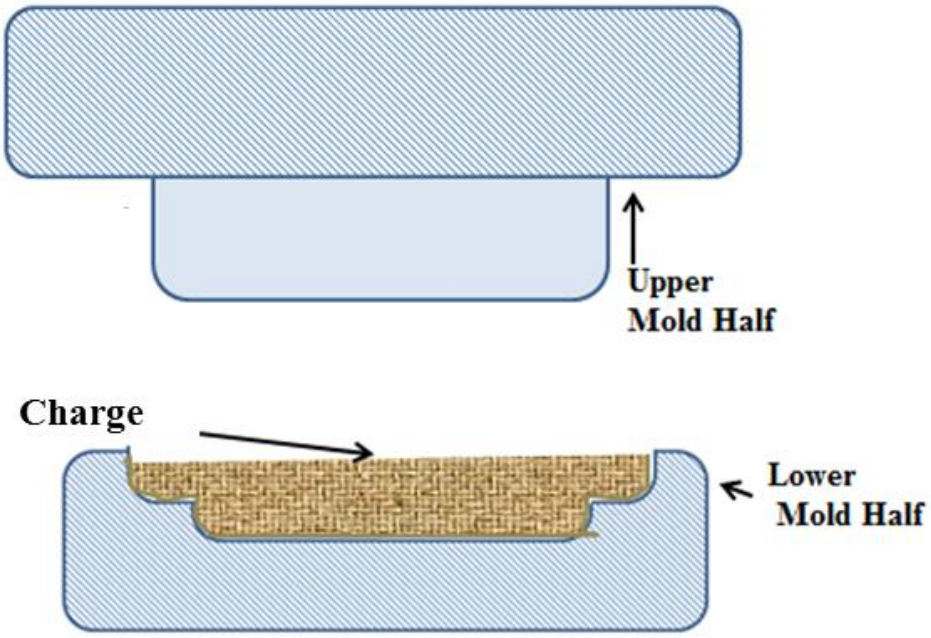

Figure 1.2. Compression Molding

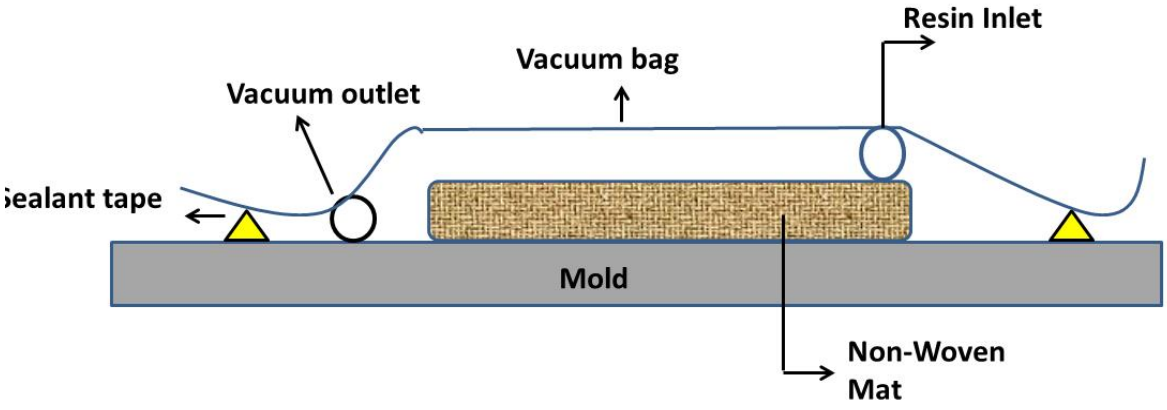

Figure 1.3. Vacuum Assisted Resin Transfer Molding

During this penetration or punching action, the grooves in each barbed needle would engage some fibers in the in-plane direction and reorient them along the thickness direction. These reoriented out-of-plane fibers bind the in-plane fibers together to result in a consolidated web, known as non-woven mat. The needle punching step is normally quantified by needle punch density (P), which is the number of punches per square centimeter (cm^2) of the mat. The amount of fibers deposited onto the moving conveyor belt and needle punching process would determine the areal density of the mat. The areal density of the mat is the weight of the mat per unit area measured in grams per square meter (GSM). The thickness of the mat is dictated by the areal density and the needle punch density. For a given needle punch density, the thickness of the mat is proportional to the areal density and for a given areal density, the thickness of the mat is inversely proportional to the needle punch density.

In contrast, the glass fibers are bound together using a binder to result in a nonwoven glass mat. Glass fiber mats are normally thinner than the hemp fiber mats of the same areal density due to smaller fiber diameter ~ 8 to 15 μm for glass fibers compared to 50 to 400 μm for hemp fibers. Due to this, the orientation of fibers in a glass fiber mat are essentially in the plane of the mat (i.e. 2D) while the orientation of the fibers in a hemp fiber mat could be in-plane as well as out-of-plane (i.e. 3D) directions.

A proper mat design is required to meet the functional and the manufacturing requirements of the composite part. Functional requirements include desired mechanical properties and thickness of the composite part.

Figure 1.4. Randomly Oriented Glass Mat

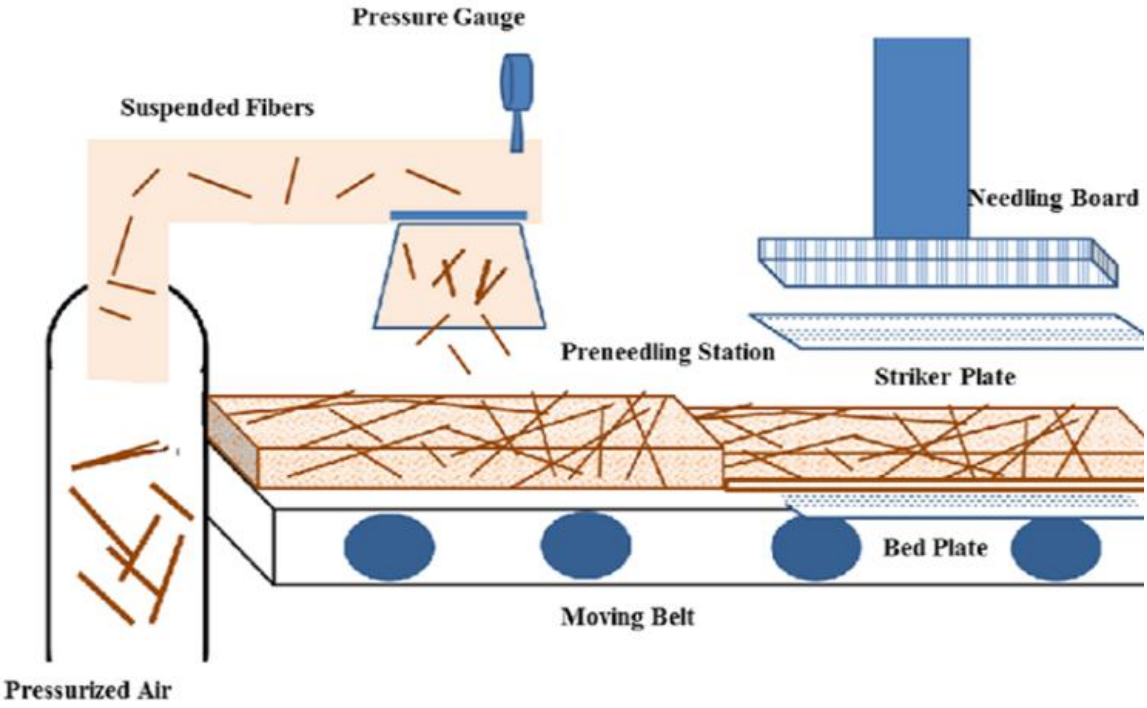

Figure 1.5. Schematic of Nonwoven Hemp Fiber Mat Manufacturing Process

Manufacturability requirements include easy conformability of the mat to the shape of the VARTM mold, successful resin impregnation of the mat to yield quality parts without voids and dry spots, and consolidation to yield desired fiber volume fraction in the manufactured composite part.

Mechanical properties are dictated by the volume fraction and the orientation of fibers in the composite, which in turn are influenced by *the volume fraction* and *the orientation of fibers in the mat* and changes to these due to consolidation during manufacturing. The thickness of the composite is dictated by *the thickness of the mat* and changes to it due to consolidation during manufacturing. The conformability of the mat depends on the *thickness and the stiffness of the mat*. Successful resin impregnation is dictated by the *permeability of the mat*. The consolidation (i.e. the compressibility of the mat during manufacturing) is influenced by *the stiffness of the mat*, which in turn depends on *the volume fraction and the orientation of fibers in the mat*.

All of these mat structural parameters, highlighted in italics in the above paragraph, are influenced by mat manufacturing parameters such as areal density in the fiber web before needle punching and needle punch density. Hence, optimizing the nonwoven mat structure by optimizing the manufacturing of the mats is required.

Optimized glass fiber mats are commercially available. However, optimized hemp mats are not available commercially. Hence, developing the knowledge on the relationship among mat manufacturing, mat structure, composite manufacturing and composite property is the focus of this thesis.

1.2 Scope and Organization of Thesis

The goal of this thesis is to generate the above-mentioned knowledge required to develop optimized nonwoven hemp fiber mats for designing and manufacturing thermoset polymer composite parts using VARTM.

This thesis is organized as follows:

- Chapter 2: A brief introduction to natural fiber microstructure and properties is followed by an introduction to nonwoven mats and their application in the composite industry. Then, a detailed literature review on published studies on bio-composite manufacturing and properties is presented and discussed to establish the knowledge gaps in support of the objectives of this thesis.
- Chapter 3: A modeling approach for predicting the evolution of fiber orientation distribution (FOD) during mat and composite manufacturing and an analytical model for predicting the tensile modulus and strength of needle punched mat composites are presented in this chapter.
- Chapter 4: Details on materials, experimental procedures, and simulations are presented in this Chapter.
- Chapter 5: Experimental and model predictions are presented, compared and discussed in this chapter.
- Chapter 6. Conclusions to support the thesis objectives are presented in this final chapter.

CHAPTER 2

LITERATURE REVIEW

2.1 Introduction

This chapter provides a comprehensive review of published literature on natural fibers, natural fiber mats, manufacturing of mats and natural fiber composites, and properties of natural fiber composites. The objective is to identify the knowledge gaps that challenge the use of natural fibers in composite applications, in support of the scope and objectives of this thesis.

First, a brief introduction to natural fiber microstructure and properties is presented, followed by an introduction to nonwoven mats and their application in the composite industry. Subsequently, a detailed review of previous studies on natural fiber composite manufacturing and properties is presented. Knowledge gaps, motivation, and objectives of this thesis follow.

2.2 Background Information

2.2.1 Natural Fibers

Natural fibers have been the subject of several research studies over the past decade because of several advantages that they have over synthetic reinforcement materials such as glass fibers. Natural fibers are low cost fibers with low density, resulting in high specific properties. Their abundance, coupled with high specific properties, makes them competitive to glass fibers [5, 6]. However, disadvantages such as lack of commercial availability of optimized nonwoven

mats that result in desired composite properties, tendency to aggregate during the processing, poor resistance to moisture and flame spread, and vast variability in the aspect ratio and the properties of the fibers are currently impeding their applications in load bearing structures [7].

Natural fibers can be sourced from plants, animals or minerals. Generally, plant or vegetable fibers are used to reinforce polymers in composite industry. Plant fibers can be grouped into three types: seed hair (such as cotton, kapok), bast fibers (such as flax, hemp, jute and ramie) and leaf or hard fibers (such as sisal and abaca fibers) [8]. Properties of various natural fibers that have been evaluated for use in composites are listed in Table 1.1. The specific Young's modulus of flax, hemp, ramie and sisal are higher than that of E-glass fibers. The properties of natural fibers greatly vary due to variation in their chemical composition, which depends on the source and the level of extraction from the source and purification. The various constituents of natural fibers are cellulose, hemicellulose, lignin, pectin and waxes. The amount of each component in a fiber depends on the fiber source, as shown in Table 2.1.

"Cellulose" was first isolated by Anselme Payen in 1830 [9]. He discovered that when plant tissue, cotton linters, and root tips from plants were purified with an acid ammonia treatment followed by extraction in water, a fibrous material was formed, which he named "Cellulose." Subsequent systematic studies have delineated the composition of these fibrous materials and the structure of a plant stalk containing these materials. A good review can be found in Ref.[10]. The cross-section of a cell that makes up plant stalk is shown in Figure 2.1 and it consists of a middle lamella, a primary wall, and three layers of secondary cell wall. The primary and secondary walls consists of "micro-fibrils" that are basic structural units of a cell wall. These microfibrils are 10 to 30 nm in diameter and 500 to 1000 nm in length [11]. These microfibrils, made-up of crystalline cellulose, are arranged within a cell wall as a core

surrounded by amorphous hemicellulose. The microfibrils are oriented at an angle to the longitudinal axis of the cell wall, which is known as a "microfibril angle" [12, 13]. The molecular weight of cellulose in the micro-fibril (which determines the properties of the cellulose), the amount of microfibrils (which determines the amount of cellulose), and the micro-fibril angle differ with plant type.

The hemi-cellulose, together with lignin, acts as matrix binding these micro-fibrils. The modulus of elasticity of a perfect crystal of cellulose has been estimated to be between 130 GPa and 250 GPa [8, 14]. Similarly, the tensile strength has been estimated to be in the range of 0.8 GPa to 10 GPa [9, 14]. However, the properties of natural fibers, tabulated in Table 1.1, are much lower than these estimates since they are not 100% cellulose. A typical mechanical extraction process results in natural fibers with diameters in the range of 50 to 800 microns, which are composite fibers consisting of cellulose (in the form of micro-fibrils) bound by a matrix of hemi-cellulose and lignin. Since the properties of amorphous hemi-cellulose and lignin are lower than that of cellulose, the properties of natural fibers vary with plant type since the amount of these constituents varies with plant type. For instance, it can be observed from Table 2.1 that the cellulose content of flax fiber is lower than that of hemp fibers; therefore, the Young's modulus of hemp fibers is slightly higher than that of flax fibers as shown in Table 1.1.

The amount of cellulose and hence, the properties of a natural fiber increase with a decrease in fiber diameter. Since mechanical extraction of natural fibers from plant stalk (known as mechanical decortication) results in fibers with a wide-distribution in fiber diameter, the properties of these fibers in a given batch vary widely. *Such mechanically decorticated fibers were used in this thesis.* In contrast, a chemical purification process, mechanical decortication,

Table 2.1. Chemical Composition of Natural Fibers (%) [15]

Bast Fiber	Cellulose (%)	Lignin (%)	Hemicellulose (%)	Ash (%)
Flax	43-47	21-23	24-26	5
Kenaf	44-57	15-19	22-23	2-5
Jute	45-63	21-26	18-21	0.5-2
Hemp	57-77	9-13	14-17	0.8
Ramie	87-91	-	5-8	-

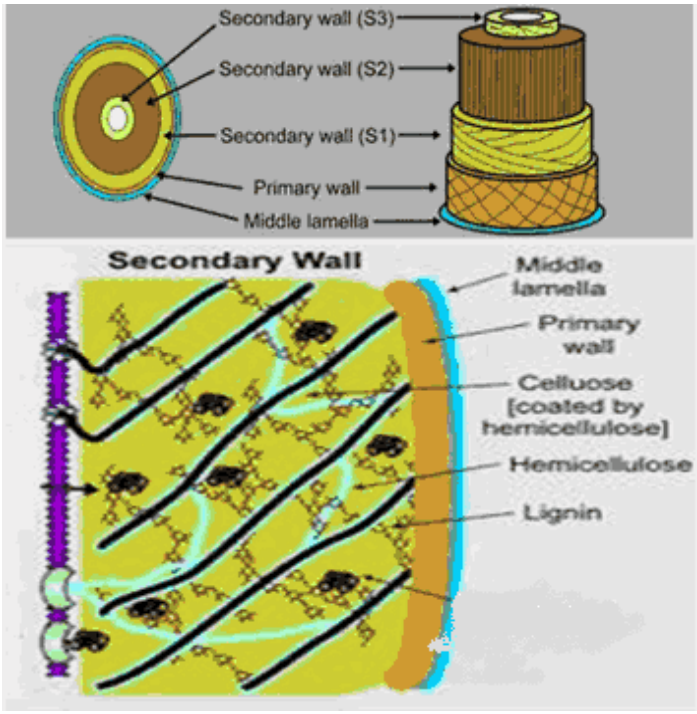

Figure 2.1. Cross section of a plant stem (top image) and cross section of secondry wall (bottom image)[16]

results in a relatively finer fiber with a narrow distribution in fiber diameter and enhanced properties. However, this increases the cost of fibers and hence, is not usually pursued by fiber suppliers.

2.2.2 Nonwoven Mat

Non-woven mats are also known as nonwoven or nonwoven fabric. In the composite industry, "mat" is normally used to refer to nonwoven mats. Apart from composites, mats are also used in disposable products, such as diapers, sanitary wipes and napkins, as well as durable products such as apparel, home building, packaging, and industrial applications [17]. Nonwoven products are replacing the woven and knit materials due to their lower cost and lighter weight. The global annual demand for nonwoven mat composites for applications in automotive interior parts is estimated to be about 120,000 tons, and the share of North American annual demand is nearly one-third of this global market [18]. Nonwoven mats are also used by the geotextile industry because of their higher permeability, better friction, and better conformability when compared to woven products [19]. Bio-based nonwoven geotextiles made from hemp, flax, jute, kenaf and bagasse have been used for temporary (several months to several years) applications where biodegradability is required [20]. Two major steps in mat manufacturing are web formation and binding.

Three methods of forming a web are (1) air laying, (2) wet laying, and (3) spun laying [19]. *Air laying, which is the focus of this study* is illustrated in Figure 1.1. In this method, fibers are separated by a mechanical comb, suspended in air, and dropped on to a moving conveyor belt to form the web of fibers. In wet laying, fibers suspended in water are collected on a screen, drained of any entrapped water, and dried to form the web. In spun laying, hot and continuous

synthetic filaments that were extruded through the spinnerets are blown onto a moving belt where they are bonded together to form the web.

The American Society for Testing of Materials defines non-woven fabric as "a structure of fibers held together with a binding material." However, some of the nonwovens do not have a binding material and the fibers are held together by entanglement of the fibers, caused by various binding techniques. This study has used a mat without a binding material.

The various mat binding methods [21] include thermal, mechanical and chemical. In thermal binding, the thermoplastic component of a mat softens upon application of heat and binds the fibers together. The mechanical binding includes hydro-entanglement and needle punching. Hydro-entanglement uses fine jets of highly pressurized water to entangle and bind the fibers. In needle punching, entanglement of fibers is achieved by a set of barbed needles punching through the web. *This study has used needle punching to bind the fibers in the mat.*

2.2.2.1 Needle Punching

Needle punching was developed in the late 1800s for producing carpet underlays and spring padding of mattresses and furniture from coarse animal hair and vegetable fibers [22]. Natural fibers such as wool, cotton, jute, sisal and synthetic fibers such as polypropylene, polyethylene, rayon and nylon have been used in manufacturing needle punched mats.

In the needle punching process, the web of fibers, formed by air-laying, is fed into a needling press (also known as a needler) using a conveyor belt. A needle board fitted with needles (as shown in Figure 1.5) strike the web of fibers from the top, and the needles descend through the web by a pre-determined needle depth. During this downward stroke, the grooves in the needles pick up in-plane fibers (parallel to the surface of the web) and reorient them in the out-of-plane (i.e. along the thickness of the web) direction. These reoriented fibers mechanically

interlock the rest of the fibers resulting in the mat. Further discussion on this process can be found in Chapter 3.

The punch density (P) measured in punches per cm^2 is calculated as follows [22],

$$P = \frac{N_O \times S}{V_x} \tag{2.1}$$

where N_O is the number of needles per unit length of the needle board (needles/cm), S is the number of strokes per unit time (Punches/sec) of the needle board, and V_x is the speed of the conveyor (cm/sec). *In this study, the punch density was varied between 0 and 150 (the maximum possible value for the needler) to understand its effect on the structure of the mat.*

Needle depth is another parameter that may be varied during needle punching. This is the distance travelled by the needle beyond the bottom surface of the web. When the depth of needle penetration is varied, keeping the areal density of the mat (i.e. GSM) constant, it may alter the structural parameters (identified in Chapter 1) of the mat, which in turn can influence subsequent manufacturing and properties of the composite. *In this study, the depth was kept constant at 8 mm.*

2.2.3 Composite Manufacturing Using VARTM

As illustrated in Figure 1.3, one half of the mold is solid and the other half is a flexible vacuum bag. The low cost VARTM process involves following steps.

1. <u>Mold preparation and non-woven mat lay-up:</u> The solid half of the mold is usually made of wood and its surface is coated with gel to ensure a good surface finish. The mold is prepared with a coat that allows subsequent priming and painting. The non-woven mat is cut to shape and placed on the mold surface. Sometimes a porous flow medium is placed on top of the mat to assist with even flow and distribution of the resin.

2. <u>Sealing the mold and creating a vacuum:</u> A vacuum bag (nylon or silicone sheet) is placed over the mat to cover it and sealed along the edges to the bottom mold using tacky tapes or appropriate seals. This bag isolates the mat from the surrounding atmosphere. Vacuum is applied at one end of the mat and the thermoset resin is introduced at the opposite end. Resin injection strategies such as point injection, edge injection, or peripheral injection are used depending on the part geometry to ensure appropriate mold filling.

3. <u>Resin impregnation</u>: The resin is mixed with an initiator, degassed, and sucked into the mat under the action of vacuum.

4. <u>Curing</u>: The mat impregnated with the resin is normally allowed to cure at room temperature on the mold and the cure time is normally a few hours depending on the resin. The composite would not completely cure at the time of manufacturing and may continue to cure to completion while in use. Alternatively, the composite part can be post-cured in an oven, after de-molding, to complete the cure.

A natural fiber mat composite part manufactured using VARTM should be of high quality with the desired fiber volume fraction and thickness to meet the functional requirements of the part. While the quality of composite is affected by the permeability of the mat, the volume fraction and thickness of the manufactured composite part are influenced by the mat compaction behavior. The relationships between mat structure and permeability, and between mat structure and compaction, are discussed below.

2.2.3.1 Permeability

Permeability is a measure of the amount of void spaces between the fibers and how they are connected within the mat. During mold filling, the resin flows through void spaces among the

fibers of the mat and fills them to impregnate the entire mat. The resin flow through a fibrous mat is related to its permeability by Darcy's Law as per Equation (2.2),

$$Q = -\frac{kA}{\mu L}\Delta P \tag{2.2}$$

where Q is the volumetric flow rate (m^3/sec), μ is the viscosity of the fluid (Pa.s), ΔP is the pressure gradient in flow direction (MPa), k is the permeability of the mat (m^2), A is the cross-sectional area perpendicular to flow (m^2) and L is the length of mat parallel to the flow (m). If the fibers in the mat are randomly oriented in 3D, then the permeability along the length, the width, and the thickness of the mat would be same. Since the fiber orientation in mats is seldom random, the permeability of the mat has to be measured along the in-plane and out-of-plane directions to completely characterize its permeability.

In this study, the in-plane and out of plane (through the thickness or transverse) permeability of the hemp fiber mats were measured and compared to understand the effect of mat manufacturing parameters.

The knowledge on the permeability would allow prediction of resin flow path in a mat of given shape. This can be used to adjust the location of resin inlets and vacuum outlets to enable complete impregnation of a mat without any dry spots. In addition, the permeability would allow determination of the impregnation (i.e. fill) time and use it to adjust the gel time of the resin. Since the resin ceases to flow upon gelation, the fill time has to be more than the impregnation time to manufacture quality composites without any dry spots.

2.2.3.2 Mat Compaction

While manufacturing a composite part using VARTM, the nonwoven mat is subjected to compressive stress under the action of the applied vacuum. The mat consolidates under this stress, resulting in a decrease in mat thickness and an increase in fiber volume fraction as shown

in Figure 2.2. It can be observed that the level of compaction depends on the pressure applied during manufacturing and the level of consolidation determines the final composite thickness, fiber volume fraction, and properties of the composite. There have been a number of studies focused on modeling the compaction behavior of fiber beds and this will be discussed later in Section 2.3.3.

2.2.3.3. Fiber Orientation Distribution

One important structural parameter in natural fiber mats is the orientation of the fibers which significantly influences the properties of natural fiber mat composites. In this section the important terminologies related to fiber orientation distribution $f(\theta)$ (FOD) are introduced.

A single fiber in an arbitrary orientation in 3D is shown in Figure 2.3. The thickness of the mat is aligned with the z-axis. The angle between the fiber axis and *z* axis is φ. The angle between the *x*-axis and the projection of the fiber in the *x*-*y* plane is θ.

The fibers within a mat exhibit a distribution in φ and θ as shown in Figures 2.4 and 2.5 respectively. The number of fibers with a certain orientation is normalized to the total number of fibers to obtain the normalized frequency plotted in these figures. The distribution in φ and θ is known as Fiber Orientation Distribution (FOD) in this thesis.

Since the experimental FOD is difficult to interpret, it may be represented by a single function in order to make it easier to compare any two FODs. Extending Herman's approach [23] two factors have been defined to represent the state of fiber orientation in short-fiber composites and used in the past by a number of composite researchers [24].

A planar orientation factor (f_p) defined as

$$f_p = 2 < cos^2(\theta) > -1 \tag{2.3}$$

where

$$< cos^2(\theta) >= \int_0^{\frac{\pi}{2}} f(\theta) cos^2(\theta) \theta d\theta \quad (2.4)$$

This assumes that all fibers are oriented in 2-D. An axial orientation factor, which assumes orientation of fibers in 3D is defined as

$$f_a = \frac{[3 < cos^2(\varphi) > -1]}{2} \quad (2.5)$$

where

$$< cos^2(\varphi) >= \int_0^{\frac{\pi}{2}} f(\varphi) cos^2(\varphi) sin\varphi d\varphi \quad (2.6)$$

Both these factors have been used in this thesis.

2.3 Review of Published literature

2.3.1 Properties of Natural Fibers

Properties of natural fibers are required in any model to predict the properties of composites. As noted in Section 2.2.1, properties of natural fibers vary widely due to variation in their chemical composition.

Mwaikambo et al. [25], have completed a major study on the effect of alkalization on natural fibers such as hemp, sisal, jute and kapok. They have extensively studied the effect of alkalization on fiber diameter, fiber strength, modulus, and surface topography. The SEM images of the fiber surface showed a relatively smooth surface for all the un-treated fibers. However, after alkalization, all fibers showed uneven surface. The fiber diameter reduced with increasing concentration of NaOH. There was no correlation between cellulose content and diameter of the fibers since the cellulose structure changed due to alkalization.

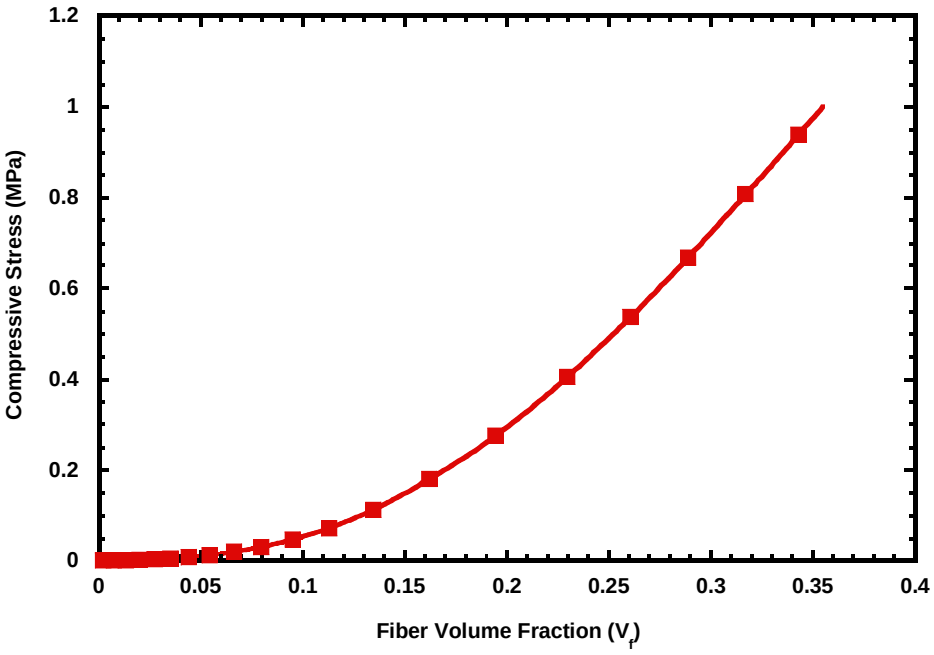

Figure 2.2. Compression of a saturated needle punched hemp mat

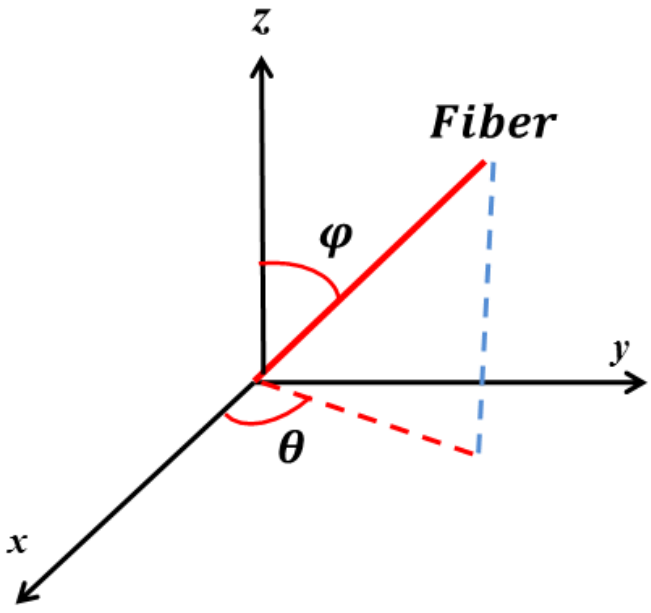

Figure 2.3. In-plane (θ) and out of plane (φ) orientation of a fiber in a mat

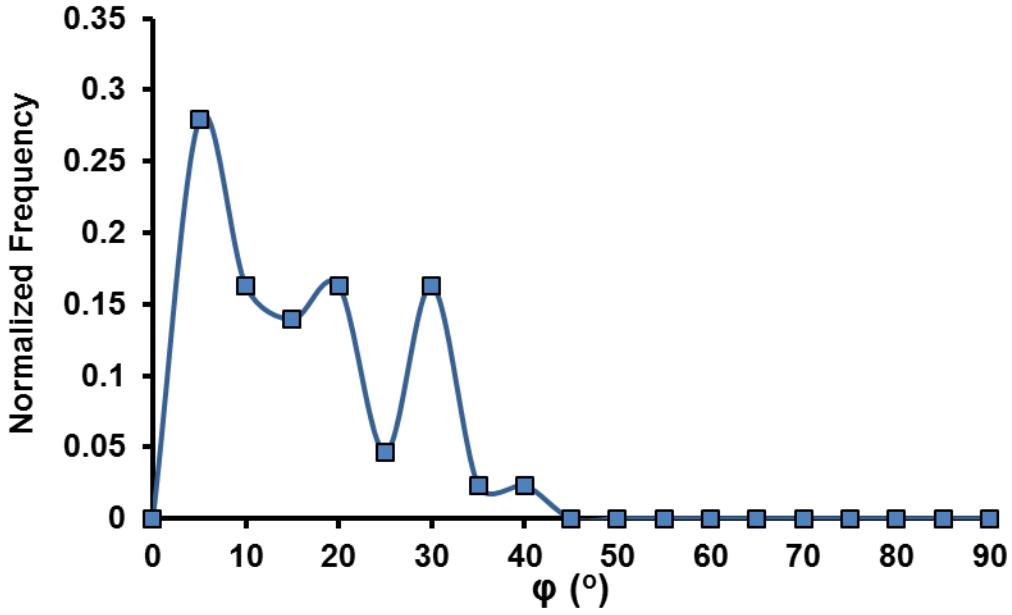

Figure 2.4. Fiber orientation (φ) distribution (FOD) in a hemp mat

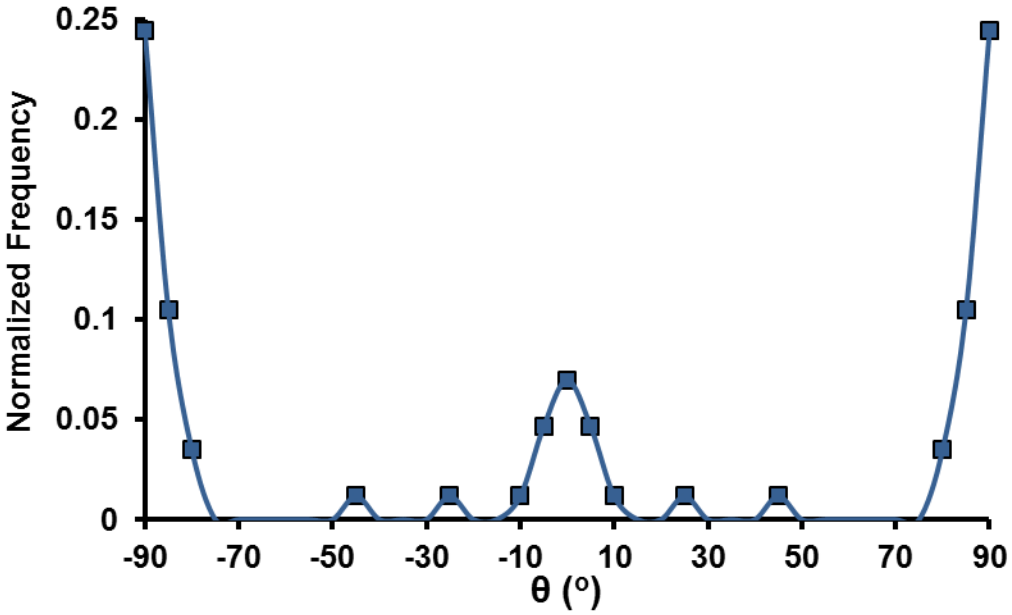

Figure 2.5. Fiber orientation (θ) distribution (FOD) distribution in a hemp mat

It transformed from long thread of “cellulose I” to smaller chains of “cellulose II”. An average diameter of 42μm, a maximum modulus of 45 GPa, and a maximum strength of 1100 MPa were obtained after treating the fibers with 16% NaOH for 48 hours.

In another study with sisal fiber [26] the authors observed the same trend. With decreasing fiber diameter, the strength and modulus increased. The maximum strength and modulus of 800 MPa and 27 GPa respectively, were obtained after treating. The diameter of fibers was reported to be around 120 μm.

A recent review by Placet et al. [27] has catalogued all previous studies on the dependence of hemp modulus and diameter, and has tried to relate this dependence to the structure and chemical composition of hemp fibers. However, the listed studies were focused on European grown hemp fibers. Such studies on Canadian grown hemp fibers are rare and many studies have focused on the effect of agricultural parameters such as seeding rate on the structure of hemp fibers [28]. In this thesis, the distribution in the diameter, the modulus and the strength of Canadian grown hemp fibers is generated and used in modeling.

2.3.2 Mat Permeability

There are numerous studies on the permeability of continuous and discontinuous synthetic fiber beds and they will not be reviewed here for sake of brevity. Moreover, they are not needle-punched and hence, not directly relevant. Hence, this review is focused on publications that studied permeability of needle-punched glass and natural fiber mats, which are very limited.

Rebenfeld [29] compared two spun-bonded fiber glass mats with one needle punched mat. The study was more on the comparison in variation of in-plane permeability between the mats. They did not provide areal density or volume fraction of mats in order to understand the effect of

mat structure on the permeability. However, they showed that needle punched mats had higher permeability.

Rouison [30] measured the in-plane permeability of hemp mats with an areal density of 600 g/m^2 and 8 mm thickness. His experimental study showed that the rate of in-plane impregnation of hemp mats by Stypol 8086 unsaturated polyester was an order of magnitude lower than that for glass mats with an areal density of 200 g/m^2 and thickness of 3 mm.

Xiaoye et al. [31] compared the permeability of a jute mat with 60 μm diameter randomly oriented jute fibers and a glass fiber mat with 17 μm diameter randomly oriented glass fibers, using molten polypropylene. They assumed one dimensional flow through the thickness of the mat and measured the polymer flow with time. Their study indicated that the impregnation rate for jute mats was 3.5 times higher than that for glass mats. The permeability of jute fibers was reported to be 10×10^{-10} m^2, while the permeability of glass fibers was 3×10^{-10} m^2.

Li [32] studied the in-plane permeability of sisal woven mats. The focus of this study was to understand the effect of fiber surface treatments and fiber volume fraction on the permeability of the woven mats, using vinyl ester resin. The volume fraction of fibers being the same, the permeability of the woven sisal fiber mat was 25% more than that of the woven glass fiber mats. He reasoned this to be due to the larger sisal fiber diameter that created larger passages for the resin to flow. The reported permeability values are 0.001 times the value reported by Xiaoye et al. [30].

Currently, a correlation between permeability and mat manufacturing parameters has not yet been determined.

2.3.3. Mat Compaction

One of the first studies on compaction of fibrous materials was on compressive behavior of wool by Van Wyk in 1946 [33], who suggested a power law correlation between the compressive force and volume fraction of fibers in a 3D random network, using

$$P_c = B_c V_f^{\,3} \tag{2.7}$$

where P_c (Pa) is the compressive force, B_c is a constant related to the fibrous material structure, and V_f is the fiber volume fraction. Since then, there have been a number of studies on compressive behavior of fibrous beds with varying structure and evaluating the B_c value for different materials.

Gutowski et al. [34] have studied this extensively using continuous fiber beds. They suggested that the fibers did not share any load below a certain volume fraction of fibers (V_o) and this share increased rapidly with increase in fiber volume fraction beyond V_o. Hence, the load required to compact the fiber bed, above V_o, increased rapidly and the fiber volume fraction (V_f) increased to a saturation level (V_s) level when it could not increase anymore. V_s is between 0.785 for a square array of fibers and 0.907 for a hexagonal array of fibers ($0.785 < V_s < 0.907$). They developed a mathematical expression for the compression load (P_c) that fibers can take based on their volume fraction and alignment. For perfectly aligned fibers

$$P_c = A_s \frac{\left(\sqrt{\frac{V_f}{V_o}} - 1\right)}{\left(\sqrt{\frac{V_s}{V_f}} - 1\right)^4} \tag{2.8}$$

where A_s (Pa) is a constant that depends on the geometry of the fiber network in the mat obtained by fitting the experimental data with the model. Several studies have extended this concept and evaluated it for different arrangements of fiber networks.

Toll et al. [35] have extended the above formulation for random fiber mats. They assumed that a power law was applicable to describe the relationship between the applied stress and the fiber volume fraction, as

$$P_c = E_f f^4 V_f^{\,5} \tag{2.9}$$

where E_f is the Young's modulus of fiber and f is a function dependent on the orientation of fibers. For a completely random fiber network f was 0.64 and it decreased with an increase in the alignment of fibers. They evaluated their model for short fiber glass mat manufactured by slurry deposition. The initial volume fraction of fibers in the mat was 8%. Their experimental results showed good correlations with predictions from Equation (2.10).

Colin et al. [36] extended the Toll model for needle punched glass mats bonded with thermoplastic powders. The results of their study showed that although the needle punch mats showed a power law compaction behavior, the power of V_f in Equation (2.9) decreased from 5 to 3. This means that the compressibility of the mats decreased with an increase in the needle punch density.

Roack et al. [37] evaluated the compressibility of glass mats with different fiber orientation. Unidirectional spun roving glass mat had the lowest compressibility and reached saturation at 52% volume fraction of fibers and the straight roving glass fibers had the saturation at 75% volume fraction.

Apart from the study by Van Wyk cited above, studies on compaction behavior of natural fiber composites are very limited. In one study by Lee et al. [38], composites of kenaf fibers and polypropylene as well as jute fibers and polypropylene were manufactured using compression molding under 6 MPa pressure and 200 ^{o}C. They reported a maximum fiber volume fraction of 23%.

In another study by Xiaoye et al. [31] the porosity of jute fiber mat was shown to be 10% more than the needle punched glass mat, under the same compressive stress. The study did not provide any information regarding mat areal density or manufacturing methods.

Recently, Francucci et al. [39] compared the compaction behavior of natural fiber mats with glass fiber mats during liquid composite molding. They used bidirectional jute fiber mats and random sisal mats. Maximum volume fraction attainable for random sisal mat was 35% at 1.6 *MPa*, while it was 52% for bidirectional mat and 55% for glass mat.

The above review indicates that a thorough study correlating the mat structure and mat manufacturing parameters with mat compaction is not available for needle punched mats. For successful VARTM manufacturing of natural fiber mat composites, knowledge of the compression behavior of the natural fiber mat is necessary. The level of compaction for a given compressive load depends on the mat structural parameters such as mat areal density, mat thickness, fiber modulus, and the needle punch density. Understanding this relationship is important for the design of an optimal natural fiber mat and such knowledge is not currently available.

2.3.4 FOD and Its Relation to Properties of Composites

Traditionally, the studies on the effect of FOD on composite properties are in the area of injection molded composites [40-43]. In this category of studies, the effect of different manufacturing parameters such as the flow velocity, the pressure or the viscosity of the resin on the FOD has been investigated both theoretically and experimentally. The FOD measurements have been done using contact microradiography of thin sections or reflected light optical microscopy of polished surfaces [44, 45].

Earlier studies on the FOD of nonwoven mats had focused on the orientation of small fibers in paper or nonwoven textiles. Johnson [46] used tracer fiber (pigmented fibers) in non-woven mat and introduced a method to calculate the orientation of curled fibers in nonwoven mats. However, his study was on the hot bonded polypropylene mat.

Fourier transform has been used by Enomae et al. [47] to analyze the digital image of the surface of fibers. This type of image analysis has been evaluated in terms of the error that it creates since a continuous function is used to define the distribution of a limited number of fibers in a digital image [48]. The standard error in orientation distribution of fibers is about 7% in references 40 and 48. An increase in the number of fibers to 100 decreased the error in digital analysis to 1% when compared to manual orientation analysis. There are numerous papers on various techniques for experimental and theoretical analysis of FOD; however, experimentally measured FOD of mats has not been correlated to mat manufacturing and the properties of mat composites.

2.3.5 Manufacturing and Properties of Discontinuous Fiber Mat Composites

Discontinuous fiber nonwoven mat composite parts are manufactured by VARTM or compression molding using the film stacking method. The size of the parts manufactured using these methods are relatively larger than the parts manufactured by injection molding. While both manufacturing methods are used to manufacture thermoset composites, compression molding is used to manufacture thermoplastic composites. Published studies on glass mat composites are extensive. Glass mats with well-defined properties are currently available commercially. In contrast, natural fiber mats are not available commercially and published studies on them are very limited. Published studies on non-woven mat composites consisting of glass and natural fiber mat are reviewed here. As mentioned earlier, the binding methods used in manufacturing

the non-woven mats can be bonding of fibers using binders or thermoplastic polymers or mechanical interlocking of fibers using needle punching. Only those studies focused on needle punching are reviewed here to identify the knowledge gaps.

2.3.5.1 Synthetic fiber mat composites

While the commercially available synthetic fiber mats are bonded, few published studies have focused on needle punched glass mats. Zhao et al. [49] studied the effect of needle punch density (which varied in the range of 0 to 80 Punch/cm^2) on the properties of glass mat polypropylene composites manufactured by film stacking method with 26 ±2% weight fraction of fibers for all the punch densities. In their study, 60 Punch/cm^2 resulted in the highest tensile modulus (4.68 GPa), although the modulus varied only about 400 MPa when the punch density was increased from 0 to 60 Punch/cm^2. The void content decreased with increase in the punch density, 4.7% for random glass mat with no punching to 0.71 % for 80 Punch/cm^2.

Sung Ho Lee et al. [50] studied the tensile and flexural properties of needle punched glass mat impregnated with polyester resin. They compared the properties of needle punched composite to those of plain weave composite with 60% weight fraction of continuous fibers. The needle punched composite had 55% weight fraction of fibers. In their study, the tensile strength increased by 20% by increasing the punch density from 15 to 90 Punch/cm^2. The tensile modulus improved 20% in the cross-machine direction and 12% in the machine direction due to needle punching. The difference between the tensile modulus of mat and woven composites decreased with increasing the punch density. In addition, the flexural modulus of woven composites with continuous fibers was lower than that of the short fiber needle punched composite. In terms of thickness, the thickness of the needle punched composites with 90 *Punch /cm^2* was equal to the thickness of the woven composite.

Tae Jin Kang and Sung Ho Lee [51] studied the fiber length and orientation in needle punched glass-polyester composite. Optical images of the surface of the mat composite were analyzed by image processing to evaluate the distribution in fiber orientation. They calculated the planar orientation factor, which showed that the fiber orientation on the surface became increasingly isotropic with increasing the punch density and it changed from 0.015 to 0.05. They also measured the fiber length variation with punch density and found out that the mean length of fiber decreased by 30% with increase in punch density from 0 to 90 Punch/cm^2. They did not study the effect of fiber length degradation or fiber orientation on the composite properties.

Kang et al. [52] evaluated the mechanical properties of needle punch mat composites, consisting of oxidized polyacrylonitrile (PAN) fibers and polyacrylic resin manufactured by film stacking method. They measured the tensile strength, the interlaminar shear strength, the flexural strength, and the thermal conductivity of composites manufactured using mats with punch densities of 200 to 700 Punch/cm^2. The interlaminar shear strength increased from 3 MPa at 200 Punch/cm^2 to 8 MPa at 500 Punch/cm^2 and then decreased at higher punch densities. A similar trend was observed for the tensile strength of the composites, which increased from 15 MPa at 200 Punch/cm^2 to 30 MPa at 500 Punch/cm^2. However, the thermal conductivity increased with increasing the needle punch density. The authors related the optimal punch density, corresponding to maximum tensile and shear strength of composites, to the amount of fibers oriented in the third direction.

The effect of needle punching on the wool fiber damage was studied by Menghe Miao et al. [53]. They quantified the fiber damage as fiber breakage and fiber weakening. They used water soluble fibers mixed with 8% wool fibers. After needle punching, the water soluble fibers were dissolved revealing the wool fibers, which were subsequently measured for their length variation

and tensile strength. At 50 Punch/cm^2 the fibers exhibited 28.8% fiber breakage and 7.8% strength degradation.

In a comprehensive study, Wang [54] compared the mechanical properties of 4 different glass mat-epoxy composites. He studied the consolidation behavior of different glass mats during resin transfer molding and hand layup process. He introduced a bulk factor (*S*) calculated using Equation:

$$S = \frac{h_{mat}}{h_c} \tag{2.11}$$

where h_{mat} is the mat thickness under 5 *kPa* pressure and h_c is the thickness of composite panel. He studied the volume fraction, the composite bulk factor, and the mechanical properties of 4 different glass fiber mats, namely stitch-bonded chopped strand mat, powder bonded chopped strand mat, continuous filament strand mat and woven glass mat. The continuous fiber mats did not have any binding method applied to them. The bulk factor for the woven mat was the lowest. The bulk factor of stitch-bonded and powder-bonded mats were higher than that of woven mats but lower than that of continuous filament mats. The fiber volume fraction, the tensile modulus and the tensile strength increased in the following order: woven mat composites, stitch-bonded composites, powder-bonded mat composites and continuous strand mat composites. The areal densities of the four mats were not same and the volume fraction of fibers was different. Therefore, drawing any conclusion on the effect of mat binding method on composite properties is difficult. Mat thicknesses for all four composite panels were the same. This shows mat binding method in glass fibers has little effect on composite panel thickness. Such effect was also observed, in the properties, by Zhao et al. [49] as shown in Table 2.2. It can be observed that the tensile modulus and strength of non-woven glass mat composite manufactured with needle punched mats are same as those of composites manufactured with bonded mats.

2.3.5.2 Natural fiber mat composites

Published studies on natural fiber mat composites are more limited than glass composites. The numbers of studies on needle punched mat composites are even less. Therefore, this review is extended to all natural fiber mats and binding methods.

Wuzella [55] manufactured nonwoven mats from mixtures of kenaf and flax fibers. He impregnated the fiber mats with acrylic thermoset resin and manufactured binded mats by compression molding. The flexural modulus for 85% weight fraction of fibers was reported to be 8 GPa in the machine direction and 4.9 GPa in the cross-machine direction. Although the results of this study showed properties comparable to some glass fiber composites, it did not present any details on the mat manufacturing method, mat areal density, thickness, and diameter, length and volume fraction of fibers in the composite. He did not correlate these parameters to the properties of the composite.

Chen [56] manufactured hemp-polypropylene composites and compared their tensile strength and modulus with those of composites manufactured with kenaf, ramie and bagasse fibers. The weight fraction of fibers was 30%. Since the areal density of needle punched mats were different, the properties were normalized by the areal density of mats and reported in terms of index values. Hemp composites showed the highest index. However, the needle punch density and depth used in manufacturing the mats were not reported in this study.

Van den Oever et al. [57, 58] studied the mechanical properties of wet-laid flax mat composites. The flax mat composite with 20% volume fraction of fibers had a tensile modulus of 5 GPa. Their study showed that the transverse strength and modulus of composites were considerably lower than the longitudinal properties. But, they did not study the effect of mat manufacturing parameters.

Van De Velde et al. [59] studied the effect of needle punching, fiber treatment and press temperature on mechanical properties of needle punched flax/polypropylene composite. The weight fraction of flax fibers in composites was 60%. The areal density of needle punched mat decreased from 918 g/m^2 to 887 g/m^2 after needle punching the mat for the second time. The properties of composite degraded for twice needle punched panels especially at higher press temperatures. The alkalization treatment of fibers also degraded the tensile modulus and the strength of the composite. The needle punch density and depth were not reported in their study.

Exequiel et al. [60] evaluated the addition of long jute fibers to wood particles while manufacturing wood particle boards. Their study concluded that an addition of 5% of 40 *mm* long jute fibers increased the modulus of the wood board. They related the improvement in modulus to increase in entanglement among the fibers due to needle punching. However, they did not report any quantitative data to support their claim.

Gillah et al. [61] studied the effect of adding sisal fiber to wood fiber board in order to improve its mechanical properties and dimensional stability in humid environments. They used sisal fibers, 30 mm and 40 mm in length and in contents of 5 and 10% in needle punched wood board manufactured with urea formaldehyde resin. Sisal content of 5% was effective in improving the modulus of the wood board by 20%. The length of the sisal fiber had minimal effect on improving the wood board properties. Although the authors claimed that the interlocking effect improved the properties of wood boards they did not do any investigation other than mechanical testing to support their suggestion. They did not consider the effect of needle punch density and depth.

Mwaikambo et al. [62] manufactured cashew nut shell oil based thermoset composite using hemp fibers and compression molding. Although they did not report the volume fraction of fibers

or the mat manufacturing method, they reported relatively high tensile modulus of 7 GPa for the random mat composites. The modulus of fiber they utilized for manufacturing the composites was in range of 40 to 60 GPa, which is among the highest modulus reported in literature for hemp fibers.

Williams et al. [63] manufactured natural fiber composite with soybean based thermoset resin by the VARTM process. They manufactured random flax and pulp cellulose mat composites. The mats, used in this study, were bonded by 5% (weight fraction) of a starch adhesive, before composite manufacturing. The modulus of flax composites with 15% weight fraction of fibers was around 2 *GPa*. They did not provide details on punch density and depth.

O'Donell et al. [64] manufactured flax composites using VARTM with canola oil based resin. Two types of adhesive bonded flax mats were used. They were bonded by polyethylene (PET). The weight fraction of fibers to adhesive was 60/40 for one adhesive and 85/15 for another. Composites manufactured using flax mats with 60/40 mats had a higher volume fraction of fibers (25%) than 85/15 mats (22%). But both composites showed the same tensile modulus of 2.07 GPa. The focus of their study was to evaluate the manufacturability and properties of composites; therefore there was no information about mat thickness or fiber orientation.

Mieck et al. [65] studied the properties of needle punched flax mat (two different punch densities) impregnated with polypropylene. The tensile modulus of composites with 30% weight fraction of fibers was 8 GPa and 6 GPa, in transverse and longitudinal directions respectively. The mat composite with 220 g/m^2 had 10% higher tensile modulus than mat composites with 150 g/m^2. This was due to an increase in volume fraction of fibers in composites. This study did not include any information on the needle punch density and depth.

Motje et al. [66] compared various treatments of hemp fibers and their effect on hemp - polypropylene (PP) composites manufactured by injection molding. This study is interesting since they used both the fiber refining (alkalization) and the surface treatments on the fibers and compared their effect on composite properties. However, none of the treatments improved the mechanical strength of the composite. Their study did not include any information on hemp fiber properties.

Hajnalka Hargitai et al. [67, 68] studied the effect of hemp fiber content and anisotropy in needle punched hemp mats. Hemp fibers were blended with polypropylene fibers in 30, 40, 50 and 70% weight fractions. They were carded and needle punched. The needle punched mat composites were manufactured using compression molding. The tensile modulus increased with increasing the fiber content, reaching a maximum value of 6.5 *GPa* at 50% fiber weight fraction. Composites with double-carded mats had lower modulus. The modulus of 30% hemp fiber composite was 5 GPa for double carded mat composites. The needle punch density and depth were not reported.

The properties of natural fiber composites published in the literature are compared with the properties of glass fiber mat composites in Table 2.2 to highlight the effect of needle punching in natural and synthetic fiber mat composites. For each fiber category, results for the needle punched composite are compared with those for bonded-mat composites, with the exception of hemp fibers, which were in the form of loose short fibers. Since polypropylene is the matrix used in all composites, the observed difference in properties is due to needle punching. It can be inferred from table 2.2, that needle punching significantly enhanced the properties of natural fiber mat composites when compared to glass mat composites.

Since the diameter of glass fiber is smaller (4 to 20 μm) than that of natural fiber (50 to 400 μm), the thickness of glass fiber mats is significantly smaller than that of natural fiber mats, for a given areal density (GSM). Hence, the fibers in glass mats are oriented in the in-plane direction and needle-punching does not orient the fibers in the thickness direction due to lack of interaction between the small fibers and thicker needles. However, due to its large diameter fibers and thicker mats, the interaction between the fibers and the needle are likely to be higher during needle punching. Hence, the likelihood and the magnitude of reorientation of the fibers along the thickness direction and ensuing fiber entanglement are higher in natural fiber mats, resulting in a positive influence of needle punching on composite properties.

The properties of natural fiber nonwoven mat composites reported in the literature are summarized in Table 2.3. Results for injection molded composites, consisting of discontinuous fibers but not mat, are included for comparison. The tensile modulus of injection molded Polypropylene (PP)-hemp composites are lower than that of non-woven hemp fiber mat-PP composites, highlighting the advantage of needle punching in enhancing the properties. The thermoset matrices used in composites identified in Table 2.3, have similar moduli. Despite this, the moduli of the composites varied in the range of 1 to 10 GPa, which can't be explained by variation in fiber volume fraction. Additional information, such as fiber properties, needle punch density, needle punch depth, and FOD, that could have helped in understanding this variation were not provided in these publications.

Table 2.2. Comparison between needle punched natural fiber mat composites and needle punched glass composite with polypropylene resin

Fiber	(w/w)%	Tensile modulus (GPa)	Tensile strength (MPa)	Reference
Glass	26.6	3.7	68	[49]
Glass (Needle punched)	26.3	3.24	55.7	[49]
Flax	23	2.07	--	[64]
Flax (Needle punched)	30	7	70	[65]
Hemp	30	2.6	32.9	[66]
Hemp (Needle punched)	30	4.5	50	[68]

Table 2.3. Tensile modulus of hemp fiber composite reported in literature

Thermoplastic composites	**Fiber content (%)**	**Reinforcement**	**Manufacturing Method**	**Tensile Modulus (GPa)**	**Ref.**
Cashew nut shell	N/A[1]	Mat[1]	Compression molded	7.2(±1.94)	[62]
MAESO (Soy based resin)	20(w/w)	Mat[1]	Resin transfer molding	4.4	[63]
Polypropylene	30(w/w)	Hemp (aspect ratio of 100)	Injection molded	2.3	[66]
Polypropylene (PP)	50(w/w)	Needle punched Hemp mat	Compression molded	6.5	[68]
Polypropylene	30(w/w)	hemp subjected to various refining treatments	Injection molded	2.5 - 4.2	[69]
Thermoset resin					
Unsaturated polyester	35%(v/v)[2]	Hemp mat	Resin transfer molding/0.2 MPa	1.74	[70]
Unsaturated polyester	20%(v/v)	Hemp mat/ Kenaf	Resin transfer molded	1.42	[71]
Epoxy	51(w/w)	Needle punched Hemp mat	Compression molded	6.4(±0.5)	[72]
Poly vinyl alcohol	10(w/w)[3]	Mat[1]	Wet lay out	9.8(±1.5)	[73]

[1] The type of hemp mat was not specified
[2] Volume fraction
[3] Weight fraction

2.3.6. Modeling of Properties of Natural Fiber Mat Composites

There are numerous studies on the theoretical modeling of tensile properties of short fiber (mostly glass) composites. The effect of various parameters such as resin and fiber tensile properties, volume fraction of fiber, interfacial strength between fibers and resin, and the orientation of fibers has been studied and quantified.

References 74 and 75 provide a comprehensive review of various approaches that are available for the prediction of tensile modulus of short fiber composites. This section focuses on the studies of tensile properties of natural fiber composites.

To predict the tensile modulus and tensile strength of discontinuous fiber composites, the orientation of fibers is an important factor that needs to be quantified. The studies on calculating and measuring FOD of mats are reviewed in Section 2.3.4. There are numerous studies correlating the orientation of fibers and composites properties in injection molded composites. But, such studies on mat composites are few. Most of the studies fitted the experimental values of tensile modulus to micromechanical models and introduced an empirically fitted factor as an orientation factor without correlating the factor to the actual orientation of the fibers [74-77].

Some researchers have suggested mathematical cosine and sine functions to model the FOD, without validating the mathematical function using experimental fiber orientation distribution [78-81]. Kim et al. [82] introduced a mathematical fiber orientation distribution. In their study, the effect of different aspect ratio of fiber orientation distribution was studied. However, their study was not validated with experimental fiber orientation distribution.

Esmaeili et al. [83] introduced a mathematical model and used it, along with experimental FOD, to show that the latter has a normal distribution. However, they did not correlate the experimental FOD with the experimentally measured properties of the composites.

There are a few published studies on applying micromechanical models to predict the modulus of natural fibers composites [84-88]. They did not measure the orientation of fibers or the properties of fibers; they fitted the experimental data with the micromechanical models. Therefore, the models did not provide any insight into the composites microstructure. Ansell, in chapter 8 of ref. [85], discusses on various parameters required for optimizing the properties of natural fiber composites. He briefly touches on the necessity of predicting the tensile modulus of natural fiber composites as important design parameters. However, in the case of hemp composite manufactured by resin transfer molding that he introduces as a case study, he uses a simple rule of mixture with orientation factor of $\eta_o = 0.25$ and tensile modulus of hemp fiber taken from literature (E_f = 45 GPa) to predict the modulus, which deviates by 100% from the experimental results.

In a comprehensive review by Facca et al. [84], several micromechanical models in literature were used to predict the modulus of natural fiber composites. They showed that there was a large difference between the predicted and the experimental results. They used the published values for fiber modulus and overlooked the variation of modulus of natural fibers with diameter due to change in chemical composition [26, 62, 89].

The study by Patel et al. [90] appears to be the sole study on modeling the tensile modulus of needle punched natural fiber composites. They manufactured needle punched hemp mat with areal density of 500 g/m^2; however, they didn't reveal other manufacturing parameters for the hemp mat. They used compression molding at 10 MPa pressure to manufacture the composite. They used Cox-Krenchel model for tensile modulus predictions. The model predictions showed a large deviation from experimental results for hemp fiber composites. They related the deviation

to the void in composites. They modified the model using a parameter for the void content, the value for which was obtained by empirical fitting.

There are a lot of experimental studies on tensile strength of natural fiber composites [6, 91-93]. However, the studies are very limited on needle punched natural composites. Chen et al. [56] manufactured hemp-polypropylene mat with compression molding using needle punched mat and reported the tensile strength 12 MPa at 30% weight fraction of hemp with areal density of 1959 g/m^2.

Patel et al. [90] manufactured the needle punched hemp composite with 500 g/m^2 areal density mat. The fiber's volume fraction was 35%. The maximum achievable strength was for 2% NaOH treated composite with 50 MPa.

Similar to tensile modulus, most of the studies on tensile strength are focused on the effect of fiber chemical and mechanical treatments on the tensile strength. The effect of mat characteristics and natural fiber properties on tensile strength of the composites is not studied.

A recent study by Ku et al. [86] reviews all the studies on tensile strength of natural fiber composites, the study lacks theoretical modeling in order to quantify or qualify the effect of mat macrostructure on the tensile strength of the composites.

2.4 Summary and Motivation for the Thesis

Manufacturing of medium-to-large size natural fiber mat composite parts using liquid injection molding processes such as VARTM requires natural fiber mats. These mats should be appropriately designed to meet both the manufacturing and the functional requirements as defined in Section 1.1. Understanding the relationship among mat manufacturing, mat structure, composite manufacturing, and composite properties is the key to successful development of

optimized natural fiber mats and natural fiber mat composites. It can be recalled from Section 1.1 that the mat structural parameters include mat permeability, mat areal density (GSM), mat thickness and mat architecture. Similarly, the mat manufacturing parameters include areal density, needle-punch density, and needle-punch depth. Composite manufacturing parameters includes mat permeability and compaction under pressure used in manufacturing.

Unlike glass fibers, the aspect ratio and properties of natural fiber feed stock widely varies, which can significantly affect the mat structure, bonding with the polymer matrix, and the properties of the composite. Hence, knowledge on the distribution in fiber aspect ratio, effect of aspect ratio on fiber properties (modulus and strength), and fiber-matrix interfacial bond strength is a necessary prerequisite to develop any reliable model to predict the properties of natural fiber mat composites.

Based on the literature review presented in this chapter, it can be concluded that such a comprehensive knowledge is yet to be generated. Previous studies have focused on one or more of the aforementioned areas. However, the following knowledge gaps exist.

- Most of published studies have focused on natural fiber refining, fiber surface treatment, fiber-matrix bonding. A systematic study of the variability in fiber properties and its impact on properties of natural fiber composites is lacking. Moreover, while most of the studies have focused on natural fibers grown in Europe, similar studies on natural fibers grown in Canada/North America are limited. This is important since the agronomical conditions can affect the fiber composition, the aspect ratio and the properties.
- While manufacturing of glass fiber mats is well established, manufacturing of natural fiber mats is yet to be standardized; there are no commercial manufacturers of natural fiber mats. While there are published studies on the relationship between composite

properties and glass mat structure, similar studies are lacking in the case of natural fiber mats. Limited published studies on natural fiber mat composites suggests that the impact of mat structure on composite properties is more in the case of natural fibers than glass fibers. The relationship between natural fiber mat structure and mat manufacturing is not known at this time and there is no analytical model to predict the evolution of mat structure (i.e., areal density, thickness, FOD, and V_f) during mat manufacturing

- An analytical study correlating the mat consolidation (characterized by thickness, FOD, and V_f) during composite manufacturing and properties of natural fiber mat composite is currently lacking.

2.5 Thesis Objectives

In view of these knowledge gaps, the overall goal of this thesis is to address some of the critical knowledge gaps that would aid in the design and development of optimized non-woven natural fiber mats for manufacturing of natural fiber thermoset composite parts using VARTM. The specific objectives focused in this thesis to achieve this goal are

1) Study, experimentally, the effect of needle punching on the mat structure characterized by the areal density, the thickness, the fiber volume fraction, the fiber orientation, the permeability, and the compressibility.
2) Study, experimentally, the effect of pressure applied during composite manufacturing on the structure (i.e. the fiber volume fraction and the fiber orientation) and properties of the natural fiber mat composite.
3) Develop a modeling approach for predicting the change in FOD during mat and composite manufacturing. Develop a model to predict the tensile modulus and the

strength of hemp fiber composites using matrix properties, experimentally determined distribution in fiber properties in the mat, and the FOD.

4) Use the results of the above objectives to understand the manufacturing–structure-property relationship in needle-punched hemp fiber mat composites.

CHAPTER 3

MODEL FOR FOD AND MAT COMPOSITE PROPERTIES

3.1 Introduction

Properties of a mat composite, such as tensile modulus and strength, depend on its microstructure, characterized by the fiber volume fraction (V_f) and the FOD in that composite. The mat structure, which defines the microstructure of the composite, changes during manufacturing. Hence, the magnitude of V_f and FOD in the composite depends on the history of manufacturing, as illustrated in Figure 3.1. The fiber volume fraction (V_f) in a mat is inversely proportional to its thickness,

$$V_f = \frac{GSM}{\rho_f h_{mat}} \tag{3.1}$$

where GSM is the areal density of mat (g/m^2) , ρ_f is the density of fibers, and h_{mat} is the thickness of the mat. It can be observed in Figure 3.1 that the thickness of the mat (hence, V_f) changes continually during mat manufacturing and composite manufacturing. Unlike glass fiber mats, hemp fiber mats are thicker, for a given GSM, due to large diameter hemp fibers. This allows the hemp fibers to orient along the thickness direction (out-of-plane *z*-direction in Figure 3.1) as well as along in-plane directions (*x* and *y* in Figure 3.1). Due to change in the thickness, the FOD would also change during mat and composite manufacturing.

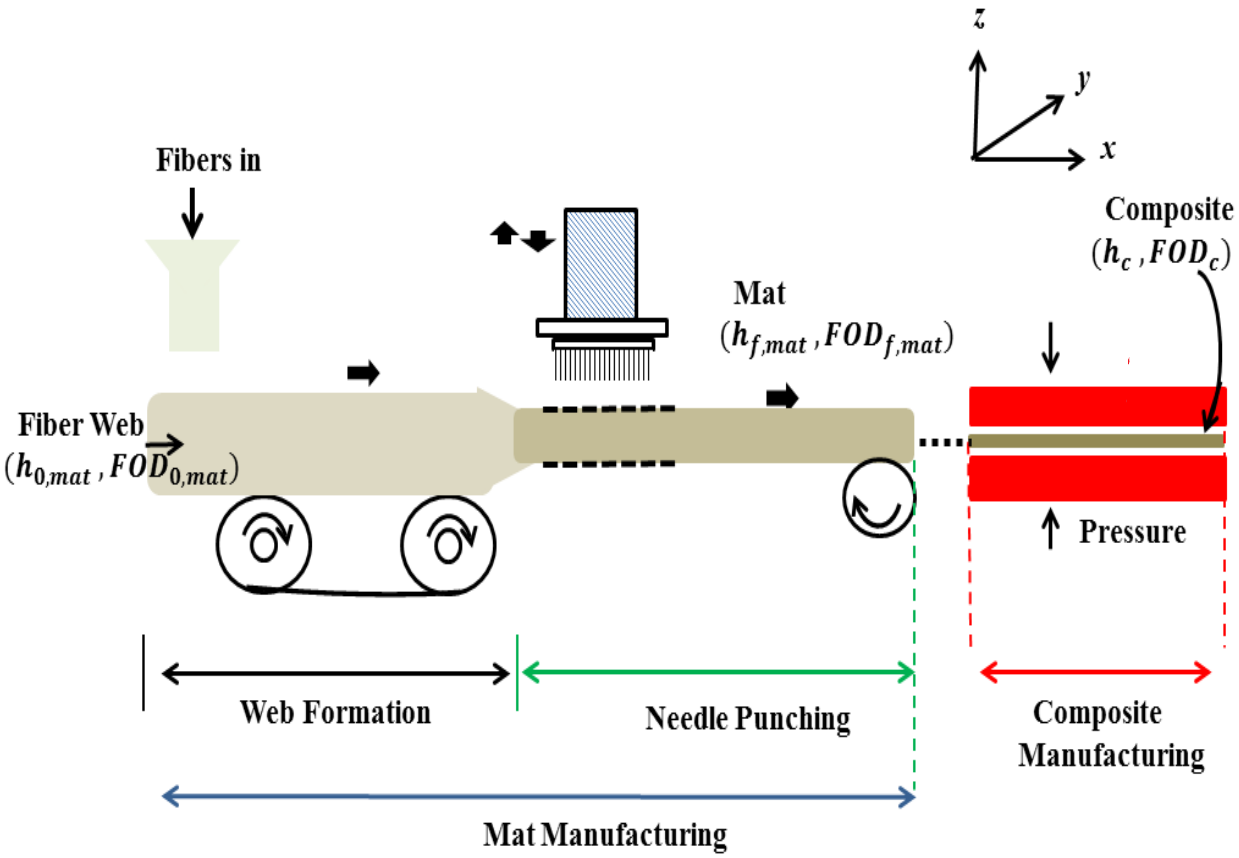

Figure 3.1. Process of needle punching and composite manufacturing

A model for predicting the modulus and the strength of a mat composite requires input values for V_f and FOD in that composite. These values cannot be the starting values in the web of fibers shown in Figure 3.1 since these values change during manufacturing. Hence, a model for the evolution of the mat thickness, the V_f, and the FOD during mat and composite manufacturing is required to accurately predict the properties of a mat composite and to understand the variation in composite properties with variations in manufacturing parameters. Development of an analytical model for this evolution and its validation is beyond the scope of this thesis. However, a modeling approach has been developed and applied to model the experimentally measured FOD to understand qualitatively the evolution of the mat structure during manufacturing and its impact on mat composite properties. This modeling approach is presented in Section 3.2. The model for the prediction of the tensile modulus and the tensile strength of mat composites is presented in Section 3.3

3.2 Model for Evolution of V_f and FOD

3.2.1 Mat Manufacturing

During mat manufacturing, the web of fibers is formed on a moving conveyor belt and is fed in to the needler by the conveyor at a desired conveyor speed (V_x,o), as shown in Figure 3.1. Within the needler, a needle board containing the needles reciprocates in the vertical direction and strikes the mat at a desired speed of V_z . A take-up roll moves the mat out of the needler at a speed of $V_{x,f}$. During the downward stroke, the needle board descends to a desired distance, known as the needle-punch depth. This is the distance, below the bottom surface of the mat, to which the needle tip travels. The needle punch density, P, (i.e., number of punches per cm^2) is determined by V_x, V_z, and the density of needles in the needle board (number of needles per cm^2).

The needle punch density and depth determine the level of compaction of the mat, i.e. reduction in mat thickness.

During the needle punching, the mat is subjected to

- The compressive force exerted by the needle board on the mat, during its time of contact with the mat ($t = 2 \times \frac{[h_{mat} + needle\ depth]}{V_z}$). The factor of 2 is used since the board is in contact during both the downward and return strokes.
- The compressive force exerted by the needles. The grooves in the needle pick up the fibers, during the downward stroke, and reorient them along the thickness direction. These fibers apply compressive force on other fibers that are in contact along their length in the in-plane direction. The magnitude of this force depends on the probability of interaction of needles with fibers, which reduces with decrease in areal density and increases with needle punch density.
- The tensile force exerted by the take-up rolls, when the mat is pulled out of the needler, at the desired $V_{x,f}$ overcoming the compressive forces mentioned above.

In response to these forces, the fibers within the mat slide and the free space among the fibers is eliminated, resulting in change in dimensions. This results in reorientation of the fibers, as illustrated in Figure 3.2 for a single fiber. The position of a fiber changes from *A* to *A'* at one end, and from *B* to *B'* at the other end. The orientation of the fibers within the mat is analyzed in this thesis in terms of φ (the angle between the fiber axis and *z*-axis) and θ (the angle between *x*-axis and either fiber axis or its projection onto the *x*-*y* plane as shown in Figure 3.2). These angles change due to reorientation of the fiber as illustrated in the Figure 3.2 (from φ_0 to φ_1 and θ_0 to θ_1). The mat compacts by$|z_1 - z_0|$.

If the change in the position of a fiber $(\Delta x, \Delta y, \Delta z)$ is known, then the final orientation of that fiber can be calculated using

$$\theta_f = tan^{-1}\left(\frac{y_{0+}\Delta y}{X_{0+}\Delta x}\right) \tag{3.2}$$

$$\varphi_f = cos^{-1}\left(\frac{(z_0-\Delta z)}{\sqrt{(x_{0+}\Delta x)^2+(y_{0+}\Delta y)^2+(z_0-\Delta z)^2}}\right) \tag{3.3}$$

Hence, the changes in the positions of the fibers have to be determined to predict the change in the FOD of the fibers in the mat.

Assuming pseudo-affine [94] deformation, changes in the position of fibers can be determined using the change in the dimensions of the mat during needle-punching,

$$\Delta x = p_1 \Delta X \tag{3.4}$$

$$\Delta y = p_2 \Delta Y \tag{3.5}$$

$$\Delta z = p_3 \Delta Z \tag{3.6}$$

where p_1, p_2, and p_3 are constants . The changes in dimensions of the mat are determined using

$$\Delta X = l_o \varepsilon_x$$

$$\Delta Y = w_o \varepsilon_y$$

$$\Delta Z = h_o \varepsilon_z$$

Where e_x, e_y, and e_z are strains in the mat and L_o, w_o, and h_o are the length, the width, and the thickness of the mat before needle-punching.

Affine deformation assumes that the strain is uniform throughout a material, at any size scale; i.e., a micrometer of the material would experience the same strain as the millimeter of the material. The deformation can involve both rotation and extension. Pseudo-affine deformation assumes that the deformation involves only rotation and has been applied to predict the

deformation of polymer chains [94-96] and orientation of short fibers in injection molded composites [97-98]. Applying this assumption to the deformation of the mats, it is assumed that the fibers within the mat do not extend but rotate to accommodate the deformation of the mat. This rotation is accomplished through sliding of the fibers at the areas of contact between them. A model to predict the change in the dimensions of the mat is presented below.

Needle punching is analogues to roll forming of metals, which is used to reduce the thickness of metal plates, as illustrated in Figure 3.3. The rolls are replaced with the needle board and the roll pressure is replaced with the compressive force exerted by the needle board and the needles. The entry and exit velocities of the mat are $V_{x,o}$ and $V_{x,f}$. Instead of plastic deformation, in the case of metals, the reduction in the thickness of the mat is achieved by frictional slip among fibers and elimination of free space among fibers. The first task is to determine the change in dimensions of the mat and subsequently relate this to the change in fiber positions to determine the change in FOD.

The final mat thickness is given by

$$h_{f,mat} = \frac{F_x}{\sigma_x w_f} \tag{3.7}$$

where F_x is the tensile force acting on the mat, σ_x is the stress acting on the mat, and w_f is the final width of the mat.

Analogous to the definition of slip in roll forming, the axial strain in the mat (e_x) can be defined as

$$e_x = \frac{V_{x,f} - V_{x,0}}{V_{x,0}} \tag{3.8}$$

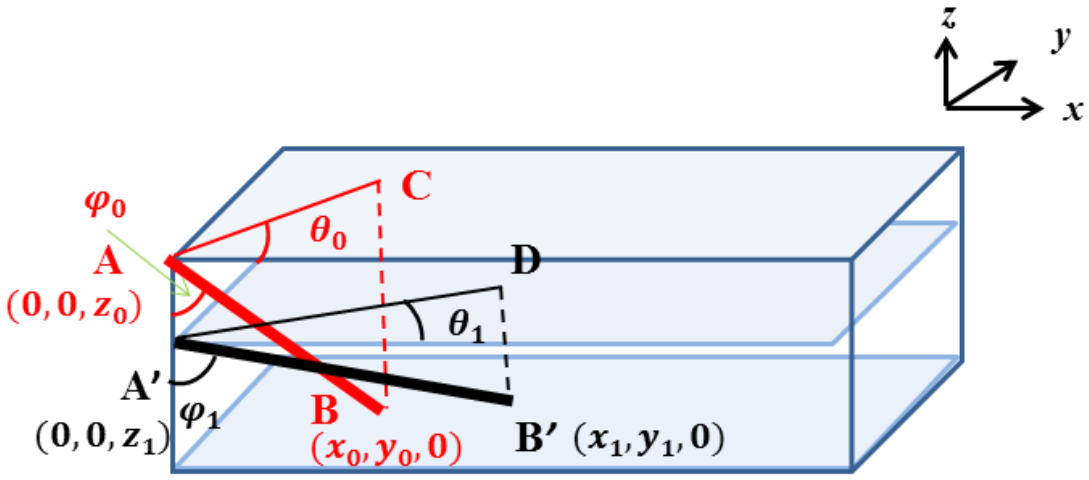

Figure 3.2. Change in fiber position due to needle punching

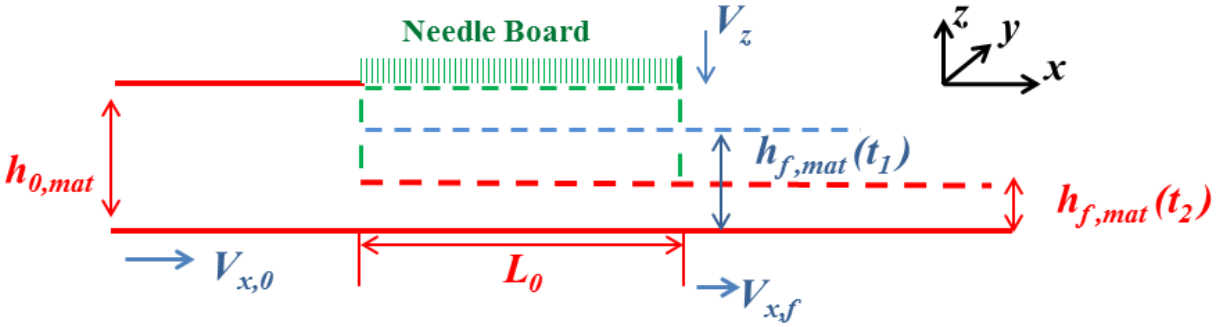

Figure 3.3. Change in mat thickness during needle punching

While slip in roll forming occurs between the roll and the material, the slip in the current situation occurs between fibers in the mat. The stress on the fiber can be related to this strain using

$$\sigma_x = E_{x,T} e_x \tag{3.9}$$

where $E_{x,T}$ is the tensile modulus of the mat. This tensile modulus is a function of strain as shown in Figure 3.4 for a representative mat.

The final width can be determined using Equation

$$w_f = w_0[1 + e_y] \tag{3.10}$$

where e_y is the transverse strain in the mat in the width direction and w_0 is the original width of the mat. Assuming the following relation between the axial and transverse strains:

$$e_y = C_f e_x \tag{3.11}$$

Equation (3.9) can be modified as

$$w_f = w_0[1 + C_f e_x] \tag{3.12}$$

C_f is a factor that needs to be determined experimentally.

The axial force on the mat (F_x) is related to the transverse compressive force (N_z) exerted by the needle board and the needles on the mat as per

$$F_x = \mu_f N_z \tag{3.13}$$

where μ_f is the average friction coefficient for fiber–fiber sliding in the mat. N_z is determined using:

$$N_z = \sigma_z A = E_{z,c}\, \varepsilon_z w_0 L_0 \tag{3.14}$$

where $E_{z,c}$ is the compressive modulus of the mat and L_0 is the length of the needle beam in contact with the mat as shown in Figure 3.3.

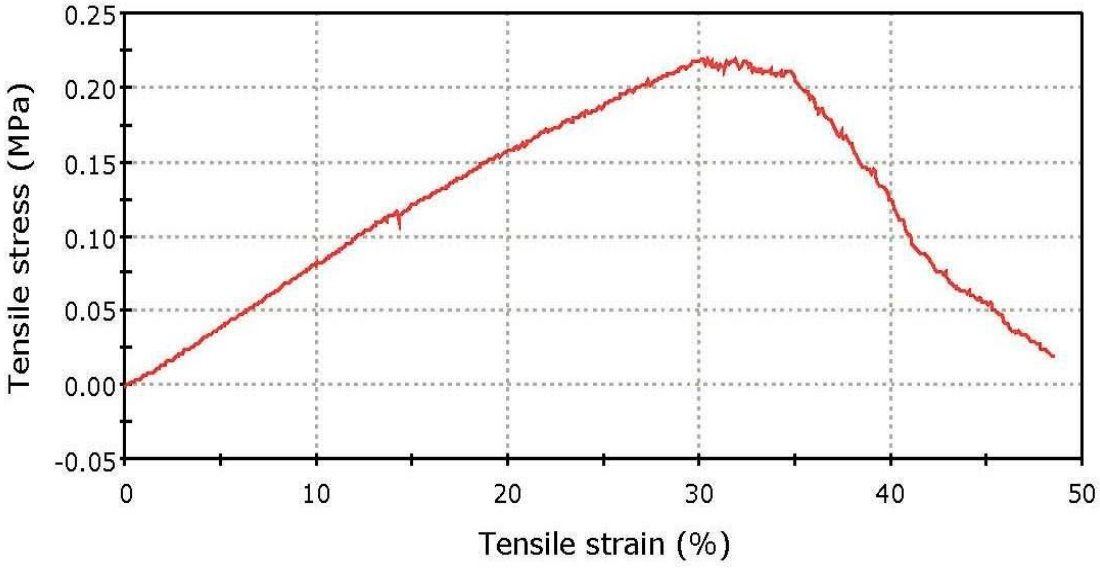

Figure 3.4. Stress–Strain curve of hemp mat under tensile load

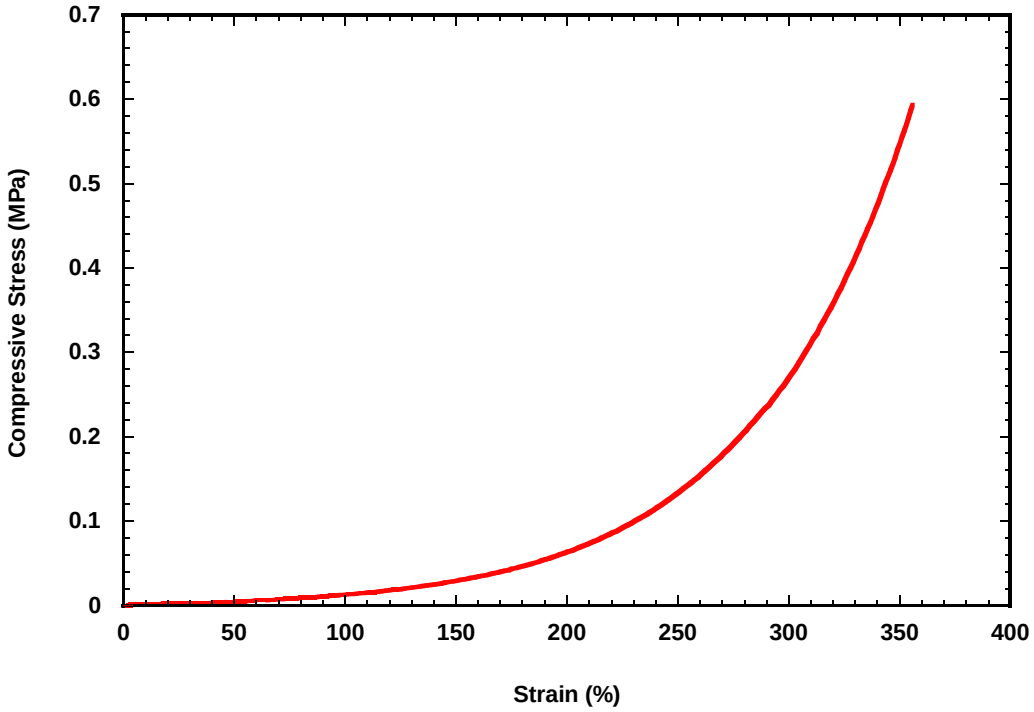

Figure 3.5. Stress–Strain curve of hemp mat under compressive load

The compressive modulus varies nonlinearly with strain as shown in Figure 3.5 for a representative mat. The transverse strain ε_z is related to stroke speed:

$$e_z = \frac{V_z\, t}{h_{0,mat}} \tag{3.15}$$

Substituting Equations (3.9) and (3.10) into Equation (3.8), the axial force can be calculated

$$F_x = \frac{\mu_f\ E_{z,c}\, V_z\, w_0\, L_0\, t}{h_0} \tag{3.16}$$

where *t* is time. Using Equations (3.4), (3.7), and (3.11), Equation (3.2) can be written as

$$h_f = \frac{\mu_f\, E_{z,c}\, V_z\, L_0\, t}{E_{x,t}\, e_x\, h_{0,mat}\, [1+Ce_x]} \tag{3.17}$$

where e_x is given by Equation (3.3).

While the final thickness and the width of the mat due to needle punching can be determined using Equations (3.12) and (3.7) respectively, the final length of the mat can be determined using

$$L = L_0[1 + e_x] \tag{3.18}$$

Using the final thickness and Equation (3.1), V_f can be determined.

Equations (3.12), (3.17), and (3.18) yield mat dimensions at a time, *t*, during one stroke of the needle beam. Figure 3.2 shows that the compressive force exerted by the needle board and the needles changes with time during a stroke resulting in a variation of compaction with time. Hence, the above equations have to be recast in a differential form and integrated with respect to time to get the final dimensions of the mat that exits the needler. Moreover, an area of mat can be punched multiple times by multiple strokes of the needle beam, as the punch density increases. Table 3.1 tabulates the number of strokes of needle board per unit time as a function of punch density. Accounting for these increases the complexity of the model and this is beyond the scope

of this thesis. Besides, many factors in the above equations, such as C_f, μ_f, V_z, $V_{x,f}$ are not known. Moreover, the pilot-plant facility used for mat manufacturing did not allow controlled experiments to determine these parameters.

Hence, the experimental FOD (Section 4.6.2) for each mat is fitted with Equations (3.2) and (3.3) to obtain the optimal values of Δx and Δy that yielded the best fit. The experimentally measured thickness of the mat after needle punching and the initial positions of fibers in the 0-P mat (obtained using experimentally measured FOD) are used in this modeling. The curve fitting and the results obtained by this procedure are used to (i) support the modeling approach discussed in this section and (ii) understand the effect of needle punching on mat structure.

3.2.2 Composite Manufacturing

Unlike needle punching, composite manufacturing is a batch process and hence, there are no entry and exit velocities. The mat impregnated with a resin matrix is subjected to consolidation pressure and the resin cures and solidifies under this pressure at room temperature. Reduction in the thickness of the impregnated mat and thus the increase in the fiber volume fraction is proportional to the applied pressure. Many studies in the area of manufacturing of composites have studied this and modeled it empirically or numerically [34, 99]. However, these studies have not focused on change in other dimensions, Δx and Δy, which are required to determine the change in FOD. Hence, the procedure presented in the previous section has been extended to study the effect of compaction pressure on V_f and FOD in mat.

Table 3.1. Numbers of strokes per second as a function of needle punch density

Mat	$\frac{Stroke}{sec}$
2.6-P	1
7-P	3
20-P	7
30-P	10
70-P	25
150-P	53

Experimentally measured FOD in mats, subjected to a consolidation pressure is fitted using Equations (3.2) and (3.3), the experimentally measured thickness of the mat after application of the required pressure, and fiber positions in the needle-punched mat before the application of pressure (obtained using experimentally determined FOD in that mat).

The empirically determined values for Δx and Δy for various consolidation pressures and needle-punch densities are used to understand the effect of consolidation pressure on the structure of mats manufactured with various needle punch densities.

3.3 Model for Tensile Modulus and Strength of Needle-punched Mat Composites

A needle punched mat composite consists of discontinuous fibers with a distribution in their orientations. The properties of this composite are predicted by defining an equivalent multi-directional laminate composite, made-up of unidirectional continuous fiber laminae as illustrated in Figure 3.6. The laminate analogy first introduced and used by Halpin et al. [100] to model the modulus of discontinuous glass fiber composite. However, the model developed in this thesis, by extending the model by Halpin et al. [100], is different from the latter, with distinct contributions, as follows:

(a) While the study by Halpin et al. [100] considered the equivalent laminate to be quasi-isotropic $[0/\pm45/90]_S$, no such restriction is placed in this thesis on the laminate lay-up. No limitation has been placed on the fiber orientation. The FOD in needle punched mat composites has been determined experimentally for the first time and used in the determination of the lay-up sequence of the equivalent laminate.

(b) To the best knowledge of the author, this thesis is the first study to apply this model to needle-punched mat composites and natural fiber composites. This model together with the model for FOD discussed in the previous section has enabled the delineation of the relationship among manufacturing, structure, and composite properties.

(c) Distribution in fiber modulus and strength due to distribution in fiber diameter has been quantified experimentally and used in the model. This is essential to accurately predict the modulus and the strength of the composite since the composition and the properties of natural fibers vary with diameter. The latter exhibits a distribution due to the nature of the fiber extraction process from the plant stalk.

The model assumptions are as follows:

- The equivalent laminate is balanced and symmetric.
- The lamina of the equivalent laminate is transversely isotropic.
- Despite the presence of fibers in the out-of-plane direction, the needle-punched composite is modeled as 2D composite.

The lay-up sequence of the equivalent laminate is $\left[(\pm\theta_1)_1, (\pm\theta_2)_2, \ldots, (\pm\theta_p)_q\right]_S$ where θ_p is the angle between the longitudinal axis of the fibers (i.e. principal material coordinates) in an equivalent lamina/ply and global *x*-axis of the laminate as shown in Figure 3.6. q is the number of pairs of plies per ply group $(\pm\theta_p)$; it should be noted that there are two plies $(+\theta, -\theta)$ in each ply group of $(\pm\theta)$. The values for these angles and the number of layers in each ply group and in the laminate are determined using experimental FOD.

Representative plots of experimentally measured FOD in $(\varphi \; and \; \theta)$ are shown in Figures 3.7 and 3.8, respectively, for a 0-P mat. The frequency of fibers in each angle is determined using

$$f(\theta_p)=\frac{n(\theta_p)}{\sum n(\theta_p)} \tag{3.19}$$

where $n(\theta_p)$ is the number of fibers oriented in θ angle. The detailed procedure used in determining the FOD is presented in Section 4.6.2. It should be noted that the frequency of fibers in Figure 3.8 include in-plane projection of fibers in the out-of-plane direction. Figure 3.8 shows that the frequency of fibers at an angle $+\theta$ is not equal to $-\theta$. Since the equivalent laminate is assumed to be balanced, the frequency of fibers at $+\theta$ is made equal to that at $-\theta$ as per

$$f(\pm\theta_p)=\frac{[n(+\theta_p)+n(-\theta p)]/2}{\sum n(\theta_p)} \tag{3.20}$$

and the resulting FOD in θ is shown in Figure 3.8. This FOD is used to determine the lay-up sequence of an equivalent laminate. For example, the lay-up of the equivalent laminate based on FOD plotted in Figure 3.8 is

$$[(\pm 90^o)_2\,,(\pm 85^o)_2,(\pm 80^o)_1,(\pm 55^o)_1,(\pm 30^o)_1,(\pm 10^o)_1\,,(\pm 5^o)_1,(0^o)_2]_S.$$

The thickness of each ply is estimated. The minimum thickness of ply (h_{lamina}) would be less than the average diameter of the hemp fibers in mat. The diameter distribution is measured for each mat and the range is tabulated in Table 3.2. On the other hand the thickness of a ply (h_{lamina}) should satisfy the equation $h_{lamina} \times N_l = h_c$. For all composites manufactured with mats with various punch densities and consolidation pressures, N_l is the total number of plies in the laminate and h_c is the thickness of the composite. Based on the analysis of all data, $h_{lamina} = 0.25$ mm has been found to satisfy both conditions.

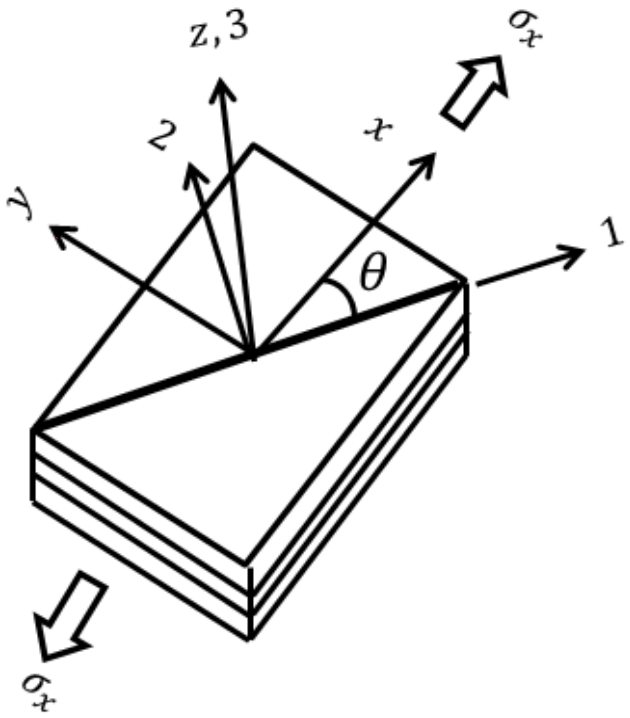

Figure 3.6. A laminated composite shown with principal and global coordination

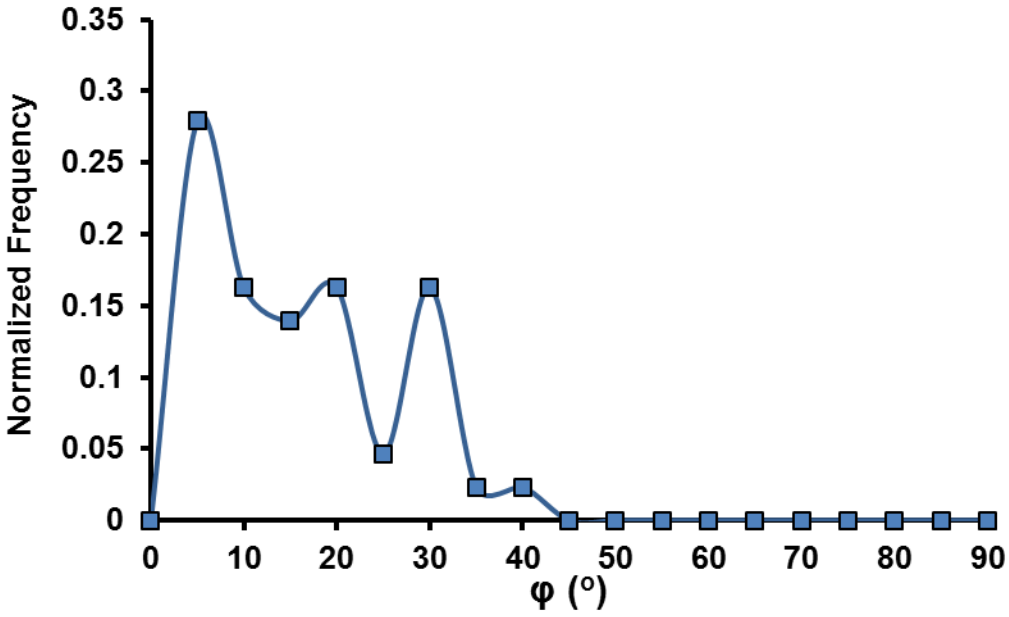

Figure 3.7. Normalized frequency distribution in φ for 0-P mat

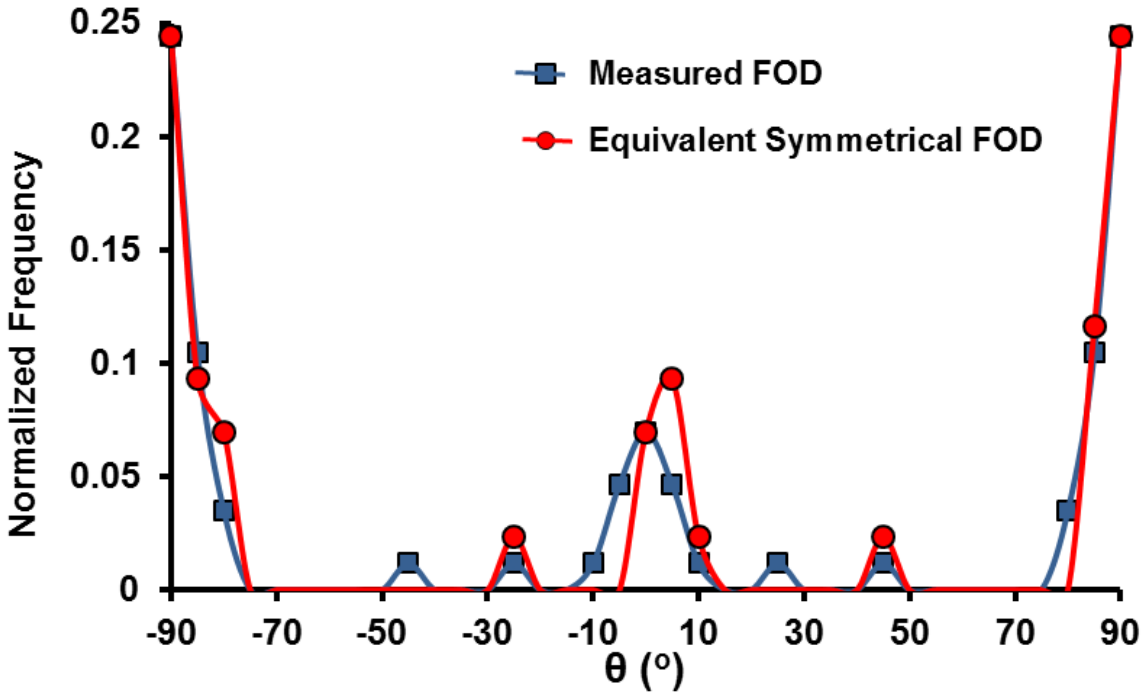

Figure 3.8. Normalized frequency distribution in θ for 0-P mat

and equivalent symmetrical frequency

The thickness of a ply group (h_p) with orientation ($\pm\theta_p$) is determined using the frequency of fibers in that orientation:

$$h_p = f(\pm\theta_p) \times h_c \tag{3.21}$$

where h_c is the thickness of the composite. The number of ply pairs in each ply group is

$$q_p = \frac{h_p}{h_{lamina}} \tag{3.22}$$

and the total number of plies in each ply group is $2q$. The total number of plies in the laminate (N_l) is

$$N_l = \sum_{p=1}^{p_{max}} 2q \tag{3.23}$$

where p_{max} is the total number of ply groups.

The modulus and strength of the equivalent laminate, defined as per the procedure discussed above, are determined using 2D lamination theory [101]. The lamination theory relates the stiffness and compliance constants of a laminate to the stiffness's and compliance constants of the plies that make-up the laminate. For in-plane loading of symmetric and balanced laminate along the global *x*- axis, the load per unit width (N_i) is related to applied strain (ε_i),

$$\begin{bmatrix} N_x \\ N_y \\ N_s \end{bmatrix} = \begin{bmatrix} A_{xx} & A_{xy} & 0 \\ A_{yx} & A_{yy} & 0 \\ 0 & 0 & A_{ss} \end{bmatrix} \begin{bmatrix} \varepsilon_x \\ \varepsilon_y \\ \gamma_s \end{bmatrix} \tag{3.24}$$

where A_{ij} is the extensional stiffness and $i, j = x, y, s$. The stiffness constants are defined [101], as

$$A_{ij} = \sum_{k=1}^{N_l} Q_{ij}^k (z_k - z_{k-1}) \tag{3.25}$$

where Q_{ij}^k (are the stiffness constants of the ply (k) along global-axes. z_k and z_{k-1} represent the distance between mid-plane (i.e. reference plane) of the laminate and the top and bottom surfaces of a ply, respectively, as shown in Figure 3.9. The stiffness constants of a ply along global axes

$[Q^k]_{x,y}$ are related to stiffness constants of the ply along the principal material coordinate axes $[Q^k]_{1,2}$ and transformation matrix (T). It is given in matrix form as

$$[Q^k]_{x,y} = [T]^{-1}[Q^k]_{1,2}[T] \tag{3.26}$$

The components of $[Q^k]_{1,2}$ are given by

$$Q_{11} = \frac{E_1}{1-v_{12}v_{21}} \quad , \quad Q_{22} = \frac{E_2}{1-v_{12}v_{21}} \tag{3.27}$$

$$Q_{12} = \frac{v_{12}E_2}{1-v_{12}v_{21}} = \frac{v_{21}E_1}{1-v_{12}v_{21}} \quad , \quad Q_{66} = G_{12}$$

where E_1, E_2, G_{12} and v_{21} are engineering constants of a unidirectional lamina measured along principal material axes, and

$$\text{T}=\begin{bmatrix} cos^2\theta & sin^2\theta & 2sin\theta cos\theta \\ sin^2\theta & cos^2\theta & -2sin\theta cos\theta \\ -sin\theta cos\theta & sin\theta cos\theta & (cos^2\theta - sin^2\theta) \end{bmatrix} \tag{3.28}$$

3.3.1 Tensile Modulus

To predict the tensile modulus of the equivalent laminate, a uniaxial tensile load ($N_x \neq 0, N_y = 0,\ N_s = 0$) is applied to the laminate. The relation in equation (3.24), can be inverted to obtain the relation between induced strain and applied load,

$$\begin{bmatrix} \varepsilon_x \\ \varepsilon_y \\ \gamma_s \end{bmatrix} = \begin{bmatrix} a_{xx} & a_{xy} & 0 \\ a_{xy} & a_{yy} & 0 \\ 0 & 0 & a_{ss} \end{bmatrix} \begin{bmatrix} N_x \\ 0 \\ 0 \end{bmatrix} \tag{3.29}$$

where $[a]_{x,y} = [A]_{x,y}^{-1}$ is the compliance matrix. The in-plane longitudinal modulus (E_x) of the laminate is

$$E_x = \frac{\sigma_x}{\varepsilon_x} = \frac{\frac{N_x}{h_c}}{a_{xx}N_x} = \frac{1}{h_c a_{xx}} \tag{3.30}$$

For a uniaxial tensile load applied in y direction ($N_x = 0,\ N_y \neq 0, N_{xy} = 0$) the relation between induced strain and applied load is

$$\begin{bmatrix} \varepsilon_x \\ \varepsilon_y \\ \gamma_s^0 \end{bmatrix} = \begin{bmatrix} a_{xx} & a_{xy} & 0 \\ a_{xy} & a_{yy} & 0 \\ 0 & 0 & a_{ss} \end{bmatrix} \begin{bmatrix} 0 \\ N_y \\ 0 \end{bmatrix} \tag{3.31}$$

The in-plane transverse modulus (E_y) is

$$E_y = \frac{\sigma_y}{\varepsilon_y} = \frac{\frac{N_y}{h_c}}{a_{yy} N_y} = \frac{1}{h_c a_{yy}} \tag{3.32}$$

Engineering elastic constants are required to determine Q, *A*, *a*, and the modulus of the laminate. They can be measured by testing unidirectional lamina or can be predicted using micromechanical models and the engineering constants for the fiber and the matrix. Since unidirectional hemp fiber lamina could not be prepared and tested due to the discontinuous nature of the fibers, the latter approach has been used in this thesis. Details on these are provided in Chapter 4.

Using Equation (3.21), Equation (3.25) can be modified replacing $(z_k - z_{k-1})$ with $\frac{h_p}{2} = f(\pm\theta_p) \times \frac{h_c}{2}$ for the chosen equivalent laminate and

$$A_{ij} = \sum_{k=1}^{N_l} f(\pm\theta_k) \times \left(Q_{ij}^k\right)_k \times \frac{h_c}{2} \tag{3.33}$$

Using this, unidirectional lamina properties (predicted using fiber and matrix properties), and Equations (3.26) and (3.27), the moduli of the needle-punched hemp fiber mat composites given by Equations (3.30) and (3.32), are predicted and compared with experimental results.

Table 3.2. Diameter of fibers in hemp mat with different needle punch density

Mat	**Maximum Diameter (µm)**	**Minimum Diameter (µm)**	**Average diameter** $D_{avg} = \frac{\sum n_i D_i}{\sum n_i}$
0-P	547.67	22.98	126.98
2.6-P	562.70	16.55	191.92
7-P	694.04	16.50	164.32
30-P	640.82	22.26	140.54
70-P	577.40	9.90	95.03
150-P	620	6.59	113.98

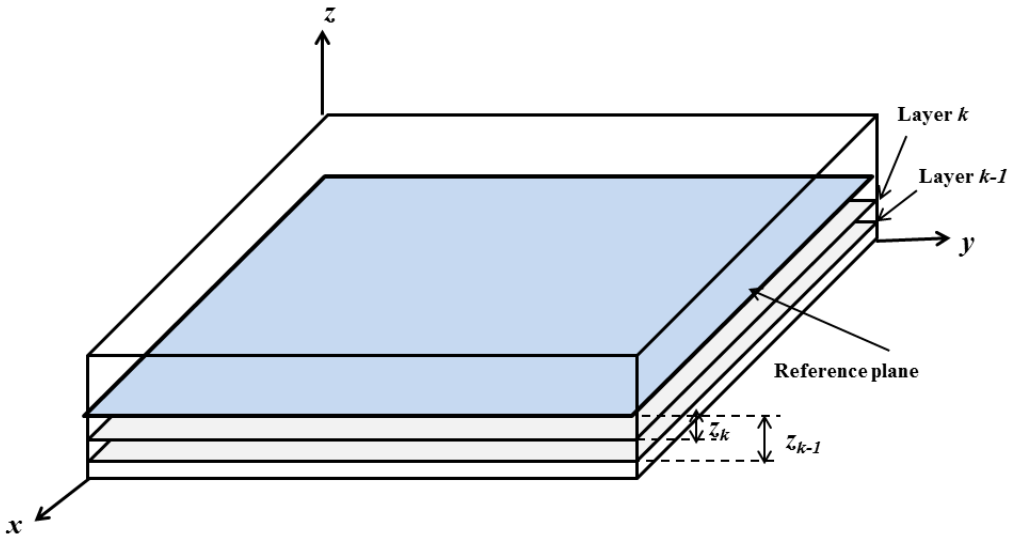

Figure 3.9. Composite laminate consisting of multiple laminaes

3.3.2 Tensile Strength

The tensile strength of mat composites is predicted using the equivalent laminate and a ply discounting method [105]. Even though multiple fracture modes can occur in a laminate, only transverse cracking is considered in this thesis while predicting the tensile strength.

The laminate analogy for predicting the tensile strength of discontinuous glass fiber composite was first introduced by Kardos [76]. The current approach differs in (i) use of lay-up sequence determined using experimental FOD, and (ii) application to needle punched mat composites, which has not been done before.

A laminate failure under the load may not be instantaneous. Some plies might fail under a certain load while the rest would still carry the load. Even failed plies might carry some load at locations away from cracked regions. Hence, composite laminates exhibit progressive (transverse) cracking of plies before ultimate laminate failure, starting with the most compliant ply (First Ply Failure) and ending with the strongest ply (Ultimate Laminate Failure). The modulus of the laminate would degrade with cracking as shown in Figure 3.10. In the ply discounting method used in this thesis, an incremental loading is used with the lamination theory to determine the Ultimate Laminate Failure (ULF) stress as discussed below.

An in-plane tensile load $N_i = \begin{bmatrix} N_{x,i-1} + \Delta N_x \\ 0 \\ 0 \end{bmatrix}$ is applied in increments along the global x-axis of the equivalent laminate. To start with $N_{x,i-1}$= 1. Mid-plane strains induced in the laminate are calculated by Equation (3.29). Since the laminate is symmetric and under in-plane loading, the strain in the plies would be equal to the strains in the laminate:

$$\begin{bmatrix} \varepsilon_x \\ \varepsilon_y \\ \gamma_s \end{bmatrix}^k = \begin{bmatrix} \varepsilon_x \\ \varepsilon_y \\ \gamma_s \end{bmatrix} \tag{3.34}$$

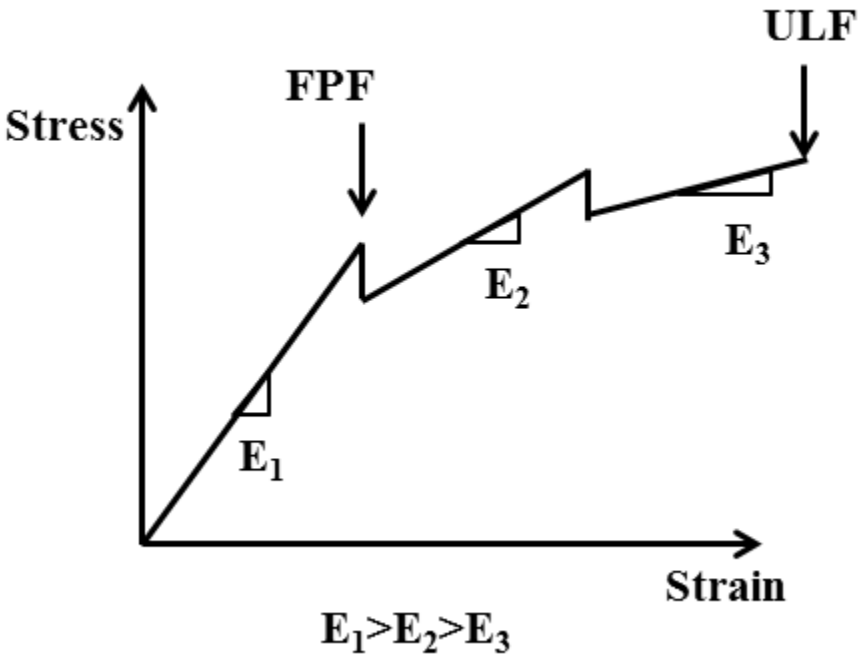

Figure 3.10. Progressive transverse cracking in multidirectional laminate during tensile testing

The stresses in a ply, along global axes, are

$$\begin{bmatrix}\sigma_x\\ \sigma_y\\ \tau_s\end{bmatrix}^k = [Q]^k_{x,y} \times \begin{bmatrix}\varepsilon_x\\ \varepsilon_y\\ \gamma_s\end{bmatrix}^k \tag{3.35}$$

Using transformation matrix (Equation 3.28), the stresses in each lamina ($\begin{bmatrix}\sigma_1\\ \sigma_2\\ \tau_{12}\end{bmatrix}^k$) along the principal material axes are calculated using

$$\begin{bmatrix}\sigma_1\\ \sigma_2\\ \tau_s\end{bmatrix}^k = [T]^k \begin{bmatrix}\sigma_x\\ \sigma_y\\ \tau_s\end{bmatrix}^k \tag{3.36}$$

Applying maximum stress failure criterion, the stresses along the principal material axes of each ply are compared with the ultimate longitudinal strengths($(\sigma_1^T)_{ult}$ or $(\sigma_1^C)_{ult}$), ultimate transverse strength($(\sigma_2^T)_{ult}$ or $(\sigma_2^C)_{ult}$), and ultimate shear strength of the lamina (τ_{12}^{ult}) to determine if a ply would fail [101]. Superscripts of "*T*" and "*C*" correspond to tensile and compressive loading, respectively. If any of these limiting values are exceeded in any ply, then that ply is deemed to have failed and unable to bear additional loading. The stiffness constant $[Q^k]_{1,2}$ for the failed ply is reduced to negligible values ([10^{-8}]).

The new stiffness matrix $[A]_{x,y}$ for the laminate is determined using Equation (3.30) and the negligible values for the stiffness constants of the failed ply. New compliance constants, $[a]_{x,y}$ of the laminate are determined by inverting the stiffness matrix. The load is incremented and added to the current load to determine the new load. Using this load, the above procedure is repeated until the ply with least θ fails. The load at which this ply fails is divided by the thickness of the laminate to determine the tensile strength of the composite.

CHAPTER 4

EXPERIMENTAL AND SIMULATION DETAILS

4.1 Introduction

Details on materials, manufacturing of mat and composites, test procedures, and simulations using the models developed in Chapter 3 are presented in this chapter.

4.2 Materials

Fibers were provided by Stemergy Renewable Fiber Technology Inc. in ON, Canada. Stypol 8086, unsaturated polyester, was used as the thermoset polymer matrix and was procured from Cook Polymers and Composites. Luperox 224 initiator, purchased from Sigma Aldrich (Oakville, Ontario, Canada), was used as the catalyst for curing the resin matrix.

4.3 Manufacturing

4.3.1 Nonwoven Mat Manufacturing

Nonwoven mat was manufactured using the non-woven pilot plant facility at North Carolina State University, Raleigh, USA. The fibers from Ontario were shipped to this facility. Subsequently, they were air-laid into a web of fibers on a moving conveyor belt, which subsequently fed the web into a needler shown in Figure 4.1. The web of fibers was needle-punched at this needler resulting in a mat. The needle punch depth was set to 8 *mm* and needle

punch density was varied in the range of 0 to 150 Punch/cm^2 (the maximum capacity of the needler). The needle-punched mats were collected in take-up rolls (48" wide) and shipped back to the University of Manitoba for further testing.

4.3.2 Manufacturing of Composite Panels

Hemp fiber mat composites were manufactured using VARTM. A schematic of the VARTM set-up is shown in Figure 4.2. All mats were dried at $70^{\circ}C$ for 24 hours prior to impregnation by the matrix. The mats were cut to 10 inch by 10 inch size and placed at the center of the bottom part of the VARTM mold with a gel coated surface for easy removal of the panel after impregnation. The resin was introduced at one end of the mat, and a chopped glass mat placed at the opposite edge of the mat connected the mat to the vacuum port, as shown in Figure 4.2. Tacky tape was placed along the longitudinal edge of the mat to prevent race tracking and dry spots. A silicone pad, which covered the mat, acted as the vacuum bag and was held in position using the top part of the mold. The latter also doubled as the conduit connecting the mat to the vacuum port. Subsequent to the application of vacuum to the mat, the resin, prepared in a beaker, was allowed to flow into the mat under negative pressure through the inlet port at the center of the silicone bag. After complete impregnation, some panels were cured in the mold at room temperature. Additional panels were removed from the VARTM mold, sandwiched between two silicone pads, and subjected to pressures of 260 kPa and 560 kPa, using a G50 H-24-CLX hydraulic press manufactured by WABASH MPI, IN, USA. The panels were cured at room temperature under these pressures. The consolidation pressure was varied to study its effect on FOD and properties of hemp mat composites.

Figure 4.1. Needler (Courtesy – Dr. R.Jayaraman)

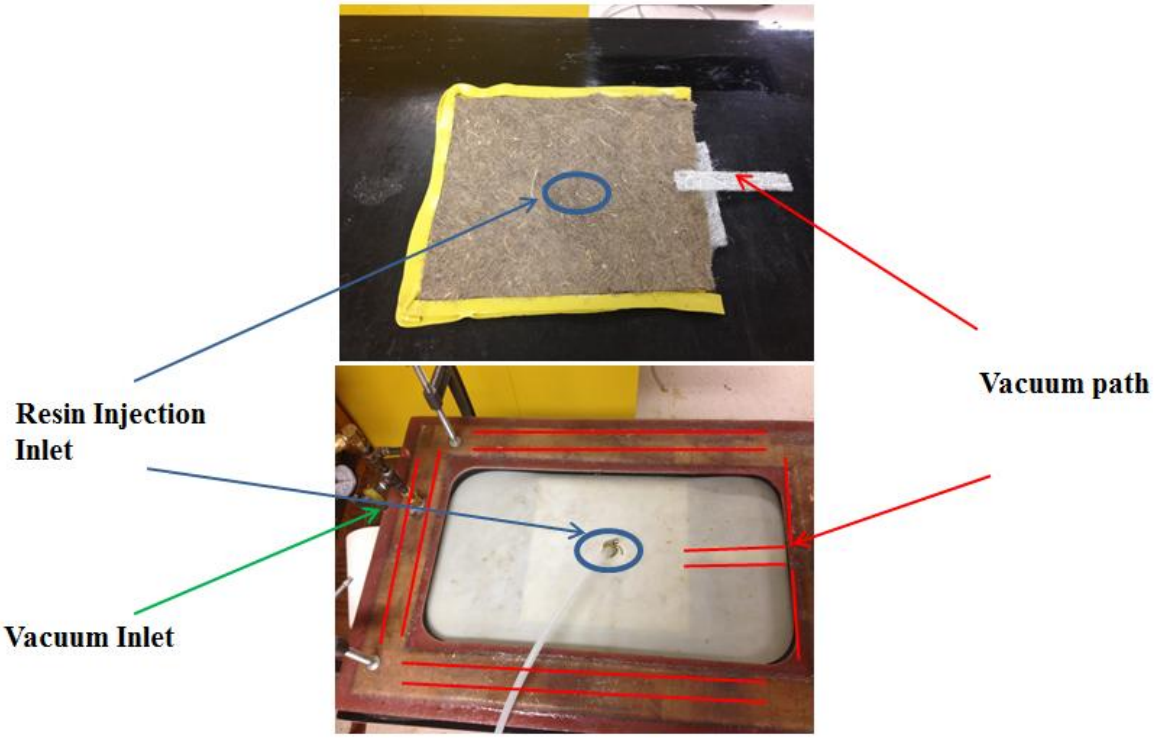

Figure 4.2. VARTM mold set up

The composition of the resin mixture injected into the mold consisted of Stypol 8086 mixed with 1.25 (w/w%) of Luperox 224 initiator. The composition was decided based on an optimization study by Brian O'Conner as a part of his undergraduate thesis in Mechanical and Manufacturing Engineering department at the University of Manitoba. A total of 18 composite panels, are tabulated in Table 4.1 were manufactured.

4.4 Test Coupon Preparation

4.4.1 Tabbing

Tabs were bonded to the gripped ends of the tensile test coupons to avoid crushing the ends during gripping. Tabs cut from woven carbon fiber epoxy composite laminates, (F263-8/T300), were used. Four plies of the fabric prepreg of this material were hand-laid and cured at 180^0C and 80 psi for 2 hours using the G50 H-24-CLX hydraulic press. The tabs, cut from these panels, were bonded to the edges of the natural fiber composite panels using room temperature curing M-bond 200 adhesive procured from Vishay Micro-Measurements Group Inc. The adhesive was allowed to cure at room temperature for 24 hours under the pressure of spring clamps.

4.4.2 Cutting

Composite test coupons, 127 mm long and 20 mm wide were cut from the panels with bonded tabs using a slow-speed 39-1471 Handimet-I diamond saw from Buehler Ltd. A feed rate of 10 *mm/min* was used. A slow feeding rate was used to avoid any overheating of the saw, and damage to the coupon edges. The panel was held to the cutting platform using double sided tape.

Table 4.1. List of manufactured needle punched hemp mat composites

Mat Type	**Consolidation Pressure (kPa)**		
	101	260	560
0-P	✓	✓	✓
2.6-P	✓	✓	✓
7-P	✓	✓	✓
30-P	✓	✓	✓
70-P	✓	✓	✓
150-P	✓	✓	✓

4.4.3 Polishing

Edges of all coupons were ground and polished. The edges were progressively ground using 80, 180, 240, 320, 400 and 600 grit silicon carbide papers. Subsequently they were polished using 6 μm alumina powder. The polished surfaces were thoroughly cleaned and wiped using ethyl alcohol to remove all loose particles.

4.4.4 Strain gaging

Strain gages of type EA-06-250AE-350, manufactured by Vishay Micro-Measurements Group Inc., were used to measure the strain during tensile testing. All strain gages were bonded to the test coupons using M-Bond 610 supplied by the strain gage manufacturer. The bonded strain gauges were cured at room temperature. Prior to bonding the strain gages to the test coupon, the desired area was cleaned using M-prep Conditioner A (alkaline) followed by M-prep Neutralizer B (acidic). A strain gaged sample is shown in Figure 4.3.

4.5 Testing

4.5.1 Fiber Volume Fraction Measurement

The volume fraction of fibers (V_f) was calculated using

$$V_f = \frac{\rho_c - \rho_m}{\rho_f - \rho_m} \tag{4.1}$$

where ρ_f, ρ_m, ρ_c are the density of the fiber, resin, and composite respectively. These densities were measured as follows. Mass (m) of test samples was accurately weighed to 0.1 mg accuracy using a balance. Subsequently, the volume of these samples was measured using AccuPyc's 1330 helium pycnometer, as per ASTM D4892-89. Using the mass and volume, the density of the sample was determined. The measured density of hemp fiber and Stypol resin is tabulated in Table 4.2. The density of composites and the fiber volume fraction are presented in the next chapter.

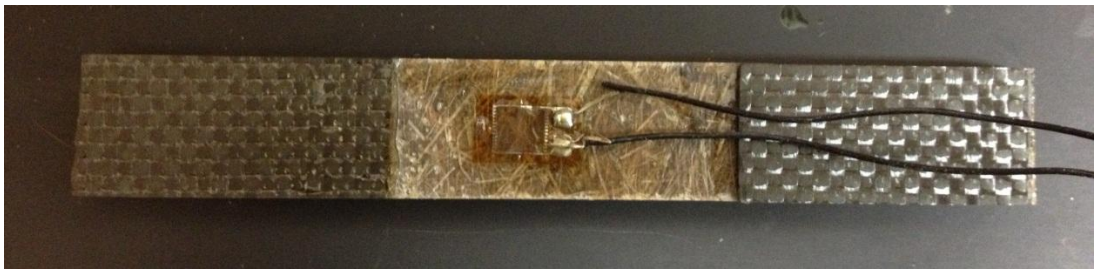

Figure 4.3. The test coupon with strain gauge

Table 4.2. Density of resin and fibers measured as per ASTM D4892-89

Material	**Density (g/cm^3)**
Stypol 8086	1.30 (±0.05)
Hemp	1.51 (±0.03)

4.5.2 Fiber Characterization

4.5.2.1 Fiber length, diameter and aspect ratio

The distribution in the aspect ratio of the natural fibers was determined using a sample batch of 0.5 gram of fibers randomly chosen from the batch of fibers obtained from the supplier. The length of the fibers was measured using a ruler and the diameter of the fibers was measured using Nikon's Eclipse LV100 microscope. A representative image of a fiber is shown in Figure 4.4. Assuming the cross sectional area of the fibers to be circular, the diameter was measured using these images at a minimum of 10 positions along the fiber's length and the average diameter was measured.

4.5.2.2 Fiber Modulus and Strength

The tensile modulus and strength of the hemp fibers were determined using TA Instruments' Q800 DMA and tension clamp, shown in Figure 4.5, as per ASTM D3822. Tests were run in ramp force mode at a rate of 1 N/min to 16 N. The gage length was 12 mm. Fibers were glued to a rectangular paper template with a hole in the center, as shown in Figure 4.6. This template was clamped at its ends and was cut in the center before starting the test. This ensured that only the fiber was loaded. The moduli of fibers were calculated from the slope of the stress-strain curve within a strain range < 0.5%. Figure 4.7 shows a representative stress strain curve. The stress-strain curve exhibits a sudden increase in strain at ~250 MPa. Such an increase is not observed in results for all tested fibers. This is believed to be due to damage developing within the fiber. Each fiber is made-up of a number of smaller fibers/fibrils. Failure of some of these fibrils, and delamination between them has been observed before the final failure of the tested fiber. Hence, these damage modes are believed to be the reason for this jump in strain. Since the testing was done at constant load rate, appearance of such damages would result in a jump in strain, observed in Figure 4.7. It should be noted that the cross-sectional area of the fiber

at the start of testing was used in determining the entire stress-strain curve; therefore, the effect of change in the cross-sectional area of the fiber that bears the applied load, due to the damages, on the stress-strain curve is not captured in Figure 4.7. The fiber tensile tests were done by Frank Wheeler as part of his undergraduate thesis in the Mechanical and Manufacturing Engineering Department at the University of Manitoba.

Ton-that et al. [118] determined the difference in standard deviation of the strength, calculated using cylindrical fiber cross-section assumption and the actual cross-sectional area near the location of fiber fracture, to be 19%. However, they did not take into account the change in the cross-sectional area of the fiber along its length while determining the modulus of the fiber. Since the change in the properties due to change in the diameter and the length of the fiber is more than the error introduced due to the assumption of cylindrical fiber cross-section, it is believed the assumption used in this thesis is valid. Moreover, the cross-section of the fibers used in this study had some empty spaces between the fibrils that made-up the fiber. Wei Hu et al. [118] have estimated this empty space to be about 1.5% only and hence, is believed to have resulted in negligible error while determining the strength and the modulus of the fiber.

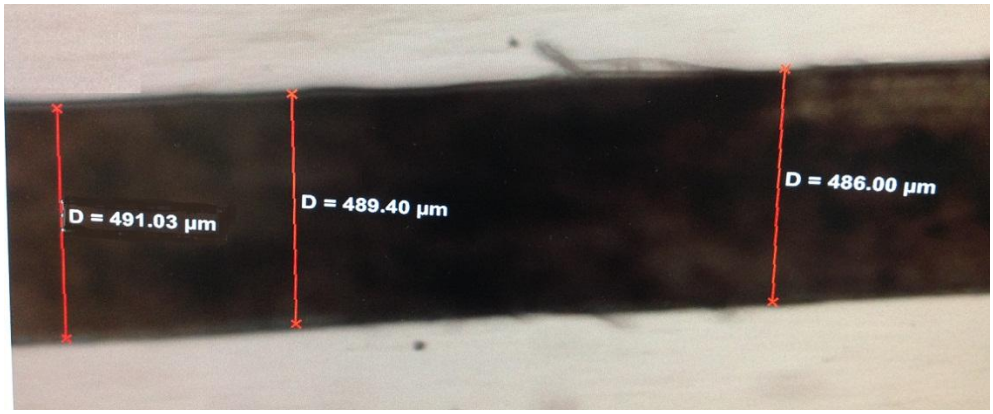

Figure 4.4. Representative image of a hemp fiber and diameter measurements

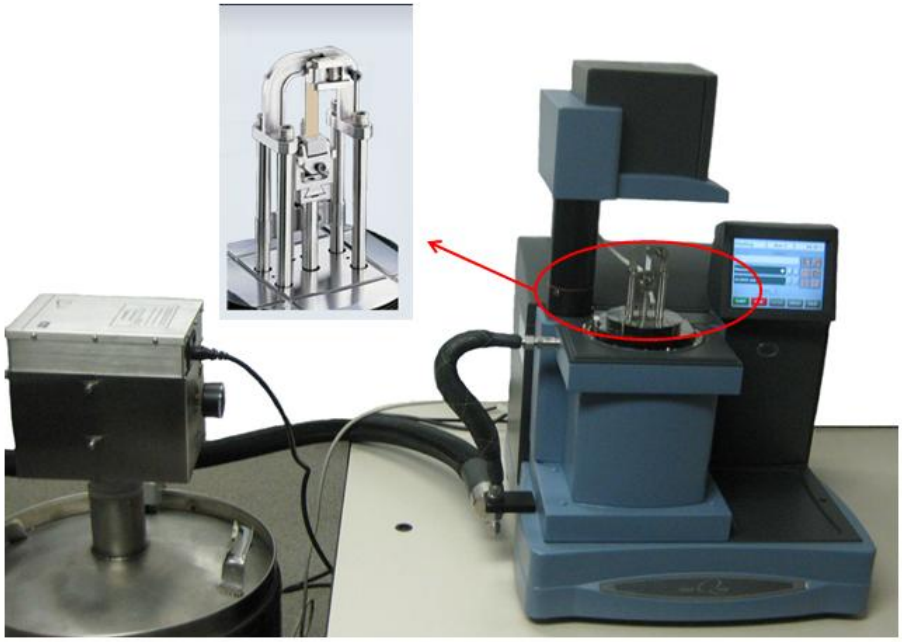

Figure 4.5. DMA Q800, TA instruments Dynamic Mechanical Analyzer with tension film clamp

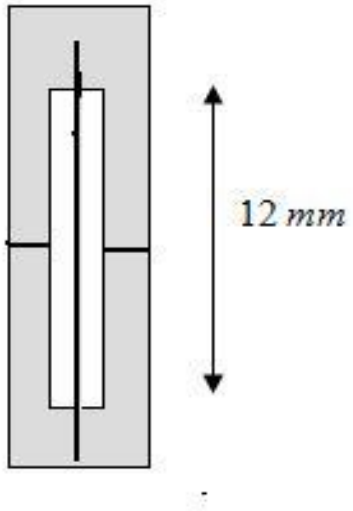

Figure 4.6. Tensile template for fiber and the fiber sample

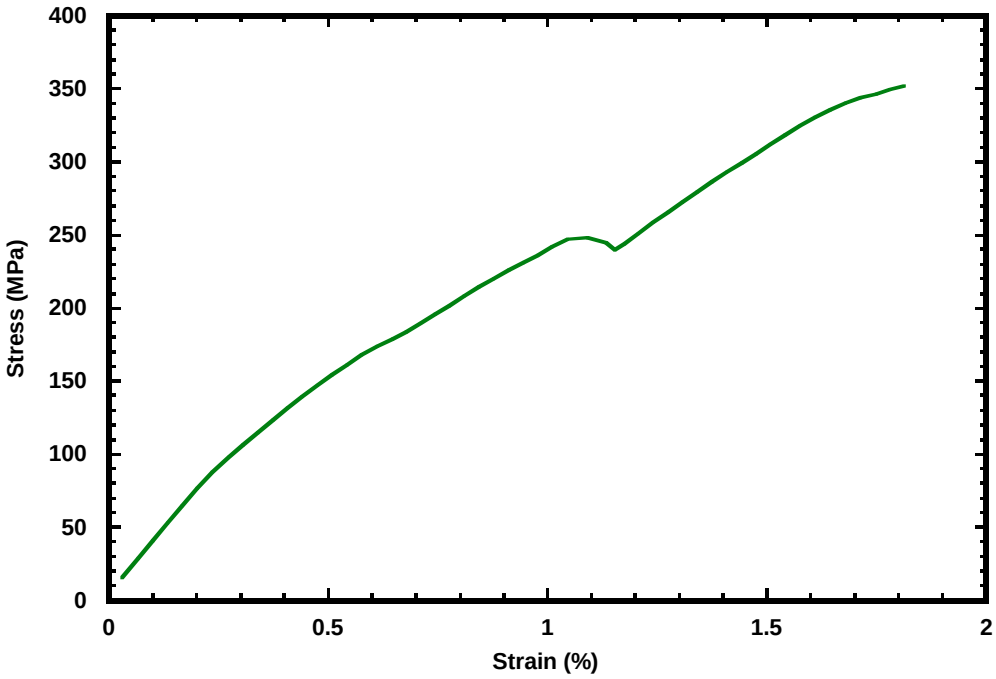

Figure 4.7. A representative tensile stress -strain curve for hemp fiber

4.5.3 Mat Permeability Characterization

4.5.3.1 Transverse Permeability

The transverse permeability of hemp mats was measured using a constant flow permeability cell as per ASTM D2434. The constant flow permeability cell, shown in Figure 4.8, consists of cylindrical cell with a mat holder at its center. The mat holder is hollow at the center and has two O-rings along its rim. These rings prevented any leakage of the test fluid through gaps between the holder and the cylinder walls and thereby guaranteed a flow strictly through the nonwoven mat that was held at the center of the holder using a highly porous metallic screen. The pressure drop across the thickness of the mat, during fluid flow through the mat, was measured using two manometers placed above and below the mat holder and used in determining the transverse permeability.

In a typical experiment, the mat was placed on the mat holder and the cylindrical column above the mat was filled with water. After the flow stabilized, the rate of change of height of water in the column was determined and used along with the diameter of the column to determine the flow rate. The pressure above and below the mat was recorded. Experiments with no fiber bed verified that the pressure drop created by the metallic screen and diameter constriction at the holder location was negligible. Using one dimensional Darcy's Law, the transverse permeability, K_z (m^2), can be calculated using Equation (4.2) [102]:

$$K_z = -\frac{Q\mu L}{A_m \Delta P} \tag{4.2}$$

where Q is the flow rate (m^3/s), A_m is the cross sectional area of the mat (cm^2), ΔP is the pressure drop (Pa), μ is the viscosity of the fluid (P, water here) and L is the distance over which pressure drop occurs which is equal to the thickness of the mat (mm) respectively. The

measurements were done using a saturated mat under steady state flow conditions. Three samples were tested for each mat.

4.5.3.2 In-plane Permeability

A unidirectional flow method was used to measure the in-plane permeability of the hemp mats. In this method, the fluid (Stypol 8086) was introduced at one end of a rectangular mat (101 mm wide and 610 mm long) under a vacuum as shown in Figure 4.9. The position of flow front (x_f), with respect to the resin injection location, was monitored with time. Applying Darcy's law for unidirectional flow, the x_f was related to longitudinal permeability in Equations (4.3) to (4.5):

$$x_f^2 = \frac{2K_x}{\mu}\int_0^t \Delta P dt \tag{4.3}$$

$$x_f^2 = \frac{2\Delta P t\, K_x}{\mu \Psi} = Bt \tag{4.4}$$

$$B = \frac{2\Delta P\, K_x}{\mu \Psi} \tag{4.5}$$

where x_f (m) is the distance the resin travels through the mat in time t *(sec)*, Ψ is the mat porosity, K_x is the in-plane permeability, and ΔP is the difference in pressure between the inlet and outlet locations. A plot of $x_f{}^2$ versus t yielded B, which was used to determine the in-plane permeability.

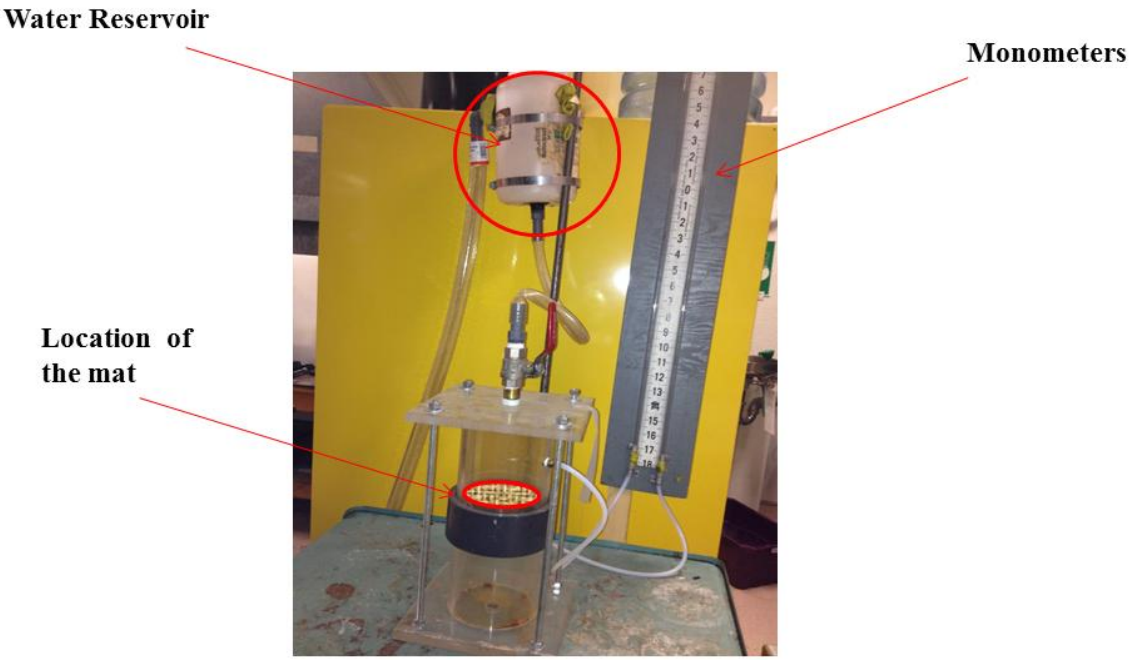

Figure 4.8. Transverse Permeability test setup

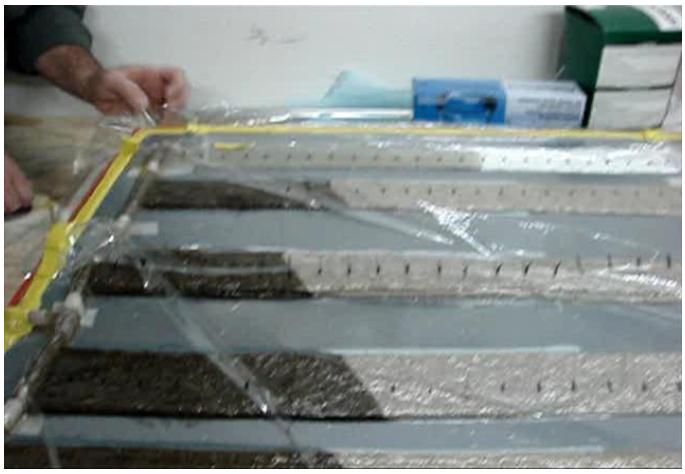

Figure 4.9. Unidirectional flow method used to measure in-plane permeability (Courtesy – Dr. R. Jayaraman)

4.5.4 Mat Compaction

The effect of the punch depth on the compressibility of the mat during composite manufacturing was studied by compression tests using INSTRON's 5500R screw driven test frame and a compression fixture. Samples, 100 ± 5 mm in diameter, were cut from the mat and subjected to compression at a cross-head displacement rate of 0.001 mm/s. The compressive load and displacements were recorded. To study the effect of lubrication of fibers by the resin matrix on mat compaction, a few 30-P mat samples were wetted by Stypol 8086, sandwiched between two non-stick films and tested. The number of samples tested per mat was three.

4.5.5 FOD Characterization

The needle punched mats were non-destructively imaged by 3D tomography using X-Radia's Micro X-ray CT shown in Figure 4.10. The re-constructed 3-D images were subsequently analyzed using commercial software, AVIZO-Fire 7 by VSG Company, to obtain the FOD. The mat sample size was 7×4 cm. An objective lens with a magnification of 4.3 X was used to maximize the scan area on the mat, which resulted in a reconstructed 3D image of 2212 × 2064 × 1640 μm. The smallest feature that could be resolved at this setting was 0.5 μm. The scanning was done by rotating the sample at 0.5^{o} intervals from -90^{o} to 90^{o}. The exposure time for each scan was 1 second. The reconstruction of the image was done by software that was linked to the acquisition software. One view of the 3D image of the hemp mat is shown in Figure 4.11. Slices of these images were imported to AVIZO Fire 7 and reconstructed for analysis, as shown in Figure 4.12. The diameter, the out-of-plane orientation (φ), and the in-plane orientation (θ) were determined for each fiber in the image using AVIZO-Fire 7.

Figure 4.10. X-Radia's Micro X-ray CT

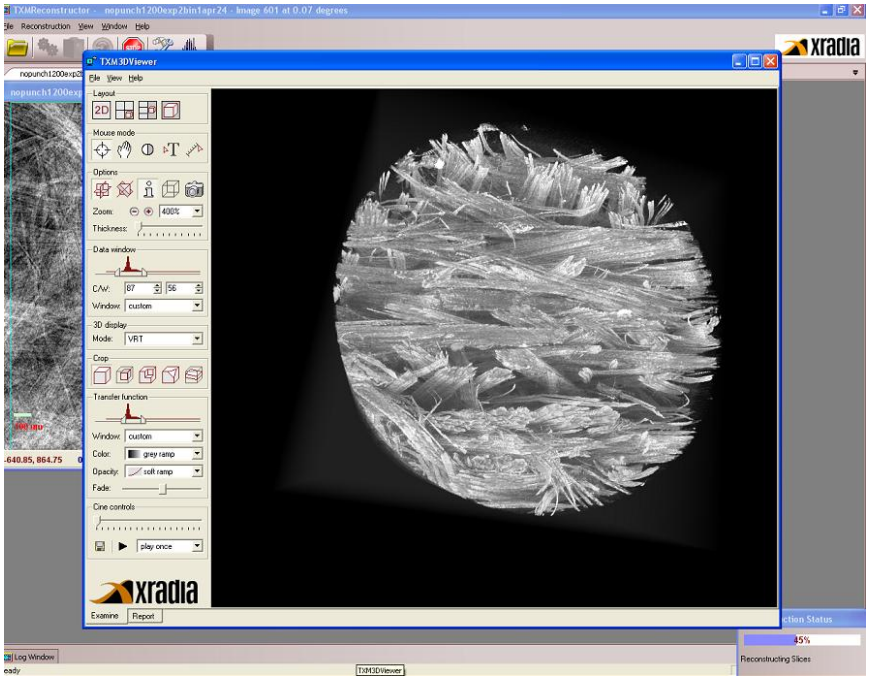

Figure 4.11. One view of the 3-D image of hemp mat acquired by X-Radia's Micro X-ray CT

To confirm that the FOD obtained using the scan volume, 2212 × 2064 × 1640 µm, was representative of the mat, the same 30-P was imaged at a higher scan volume (22000 × 20000 × 12000 µm) using Bruker's Micro CT (Skyscan) 1176 X- ray, operated by the Small Animal and Material's Imaging Group at the Human Anatomy and Cell Science department of the University of Manitoba. Additionally, 10 scans of contiguous areas of the mat were also completed using X-radia`s X-ray Mico-CT and compared to confirm that the scan size, 2212 × 2064 × 1640 µm, yielded a representative FOD for the entire mat.

4.5.6 Fiber-Matrix Interfacial Bond Strength Characterization

A single fiber fragmentation test was used to determine the bond strength between the natural fibers and the resin matrix. The single fiber fracture test was chosen because of its simplicity. Fibers with near-circular cross-section were carefully selected from the mat and dried overnight at 70ºC. A silicone mold with cavities, for manufacturing multiple dog-bone shaped samples, was manufactured and used. A single fiber was placed in the center of a mold cavity and held taut by gluing its ends to the edges of the mold. Stypol 8086 resin, mixed with the initiator, was poured into the mold cavity and allowed to cure at room temperature. A dog-bone single fiber sample is shown in Figure 4.13.

The dog-bone samples were loaded manually using the test frame shown in Figure 4.14. The load frame was held under a Nikon Eclipse LV100 microscope and the sample was viewed under a polarized light. During loading, the fiber begins to break when the stress on the fiber reaches its ultimate strength. The fracture location is observed as a dark region under polarized light, as shown in Figure 4.15. With an increase in load, the fiber continues to break until a state is reached when the length of the fibers are too small (i.e. $l \leq l_c$) to reach the fracture stress of the fiber as shown in Figure 4.15.

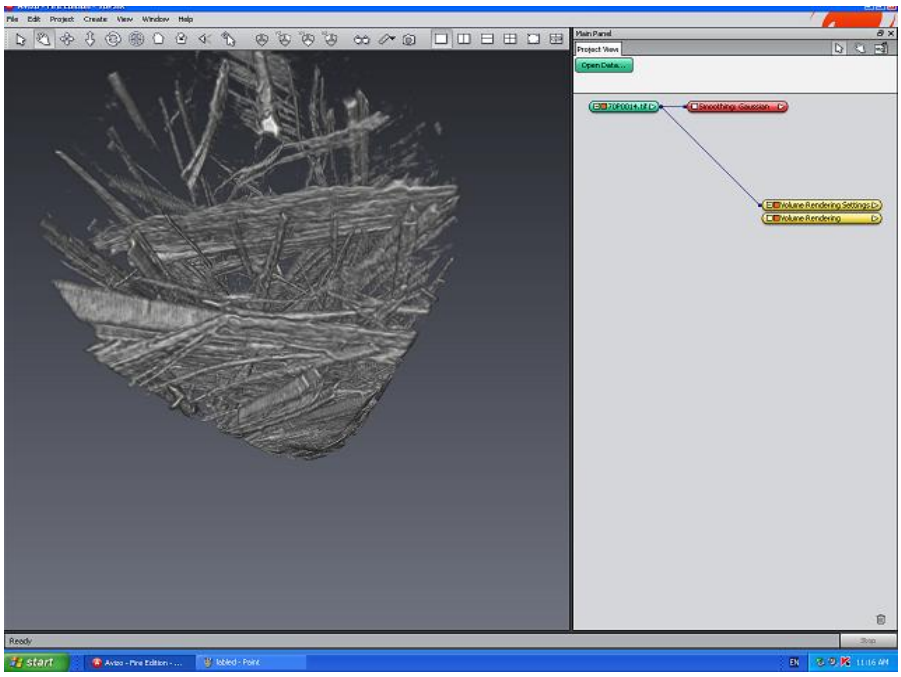

Figure 4.12. One view of the 3-D image of hemp mat reconstructed in AVIZO

Figure 4.13. Single fiber fragmentation test specimen

The length of the fibers at this state is known as critical length (l_c) and are equal to the length between the breaks in Figure 4.15, which was measured using Nikon's NIS-Elements Basic Research-3.0 image analysis software. Assuming that the average length of the fiber at saturation of breaks is equal to the critical length and that the shear stress at the interface is uniform, the interfacial bond strength was determined using Equation (4.6) [103]:

$$\tau_u = \frac{(\sigma_f d_f)}{2 l_c} \tag{4.6}$$

where σ_f , and *df* are the fracture strength, diameter of the fiber, respectively. Diameter of the fiber (d_f) was measured using the image of the fiber as shown in Figure 4.4. Ten samples were tested and the average value is reported.

4.5.7 Tensile Test

The tensile properties of the hemp fiber composite were determined as per ASTM D3039 using INSTRON's 5500R screw driven test machine. A dummy test coupon (material, punch density, and strain gage same as test coupon) was used with the test coupon in a half-bridge configuration to eliminate the effect of temperature fluctuations during testing on the strains measured using the strain gauges. The dummy coupon with a bonded strain gauge was under no load and was very near the test coupon. The load data was acquired by Instron's Blue Hill software and the corresponding strain data was acquired using National Instruments' SCXI 1100 data acquisition system and LabView software.

A loading rate of 0.006 mm/sec was used. All tests were done at room temperature. Three samples were tested for each punch density and consolidation pressure and average properties are reported. The tensile modulus of the composite was calculated based on the slope of the stress-strain curve in the strain range < 0.2%.

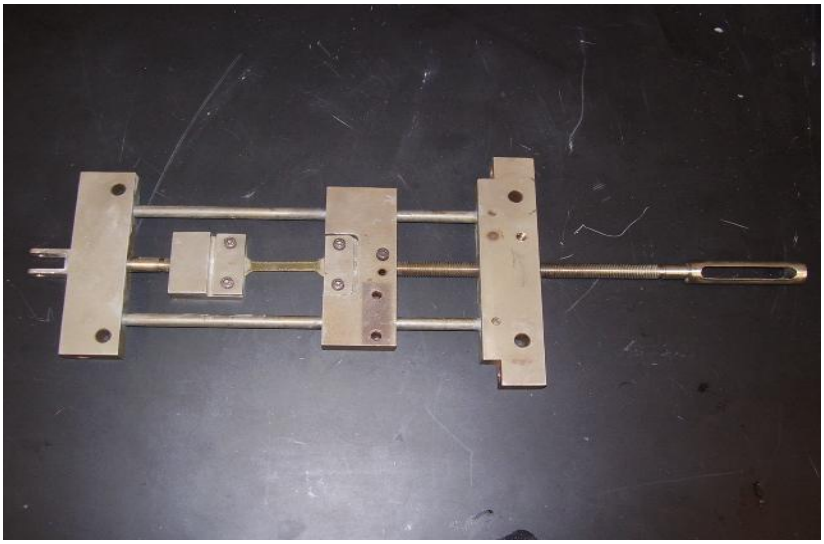

Figure 4.14. Tensile load frame

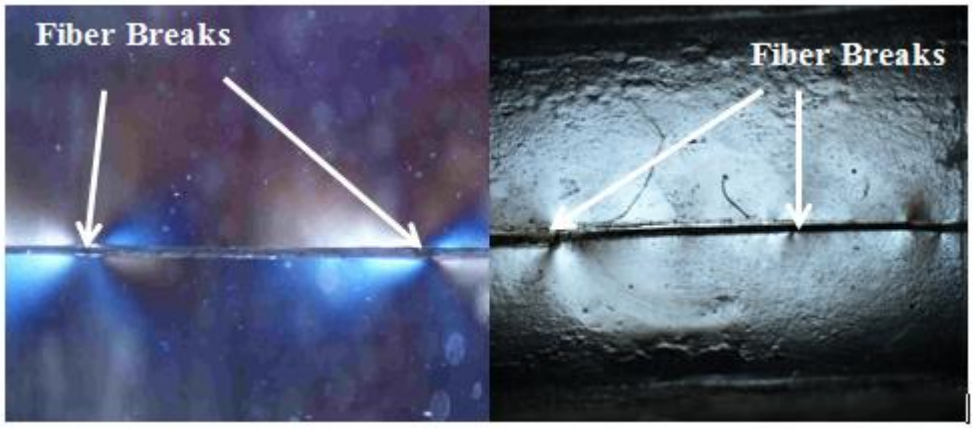

Figure 4.15. Fiber breaks observed under normal light (left picture)

and under polarized light (right picture)

4.6 Simulation Details

The tensile modulus and tensile strength of needle punched composites were predicted using the model discussed in Chapter 3. The model was programmed using MATLAB. The input values to the program and algorithm are discussed below.

4.6.1 Resin, Fiber, and Lamina Properties

Tensile modulus (E_m) and tensile strength (σ_m) of the resin were determined experimentally and are tabulated in Table 4.3. Poisson's ratio (ν_m) and shear modulus of the resin (G_m) were extracted from the manufacturer's data sheet [104] and is shown in Table 4.2. The values in Table 4.2 were input as resin properties to the program.

The experimentally measured Young's modulus and strength of hemp fibers (E_f) varied with the diameter of fibers due to the change in the chemical composition of fibers with diameter, as shown in Figure 4.16 and 4.17 respectively. As the fiber's diameter varied from 50 μm to 800 μm, its tensile modulus varied from 45 GPa to 2 GPa, and tensile strength varied from 500 MPa to 35 MPa. This variation was accounted for, while predicting the properties of the composite. The data in these figures were empirically fitted using nonlinear regression function in MATLAB:

$$E_f(d_f) = 56.43 \exp(-0.0064 d_f) \tag{4.7}$$

$$\sigma_f(d_f) = 456 \exp(-0.0098 d_f) \tag{4.8}$$

The equations with fitted values for the constants are shown Figure 4.17 and Figure 4.18. The distribution in the diameter of fibers in the mat was measured by the method discussed in Section 4.5.5.

Table 4.3. Resin elastic constants

E_m (GPa)	G_m (GPa)	ν_m	σ_m (MPa)
1.869 (±0.09)	1.2	0.32	34.6 (±1.5)

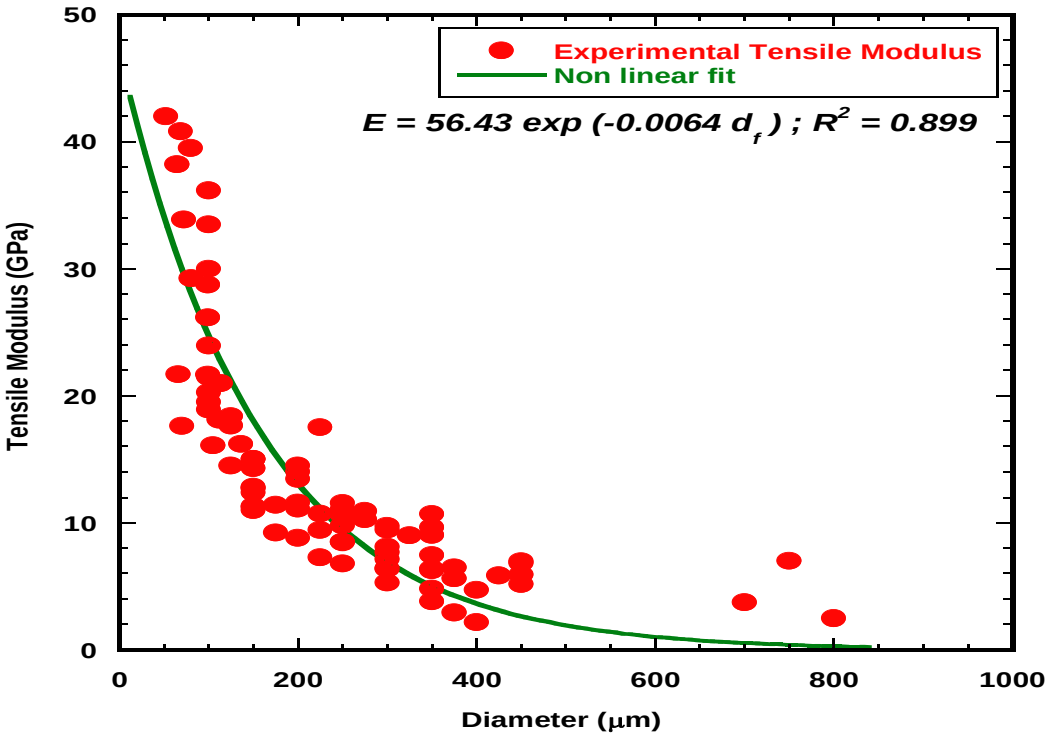

Figure 4.16. Variation of modulus of hemp fibers with diameter

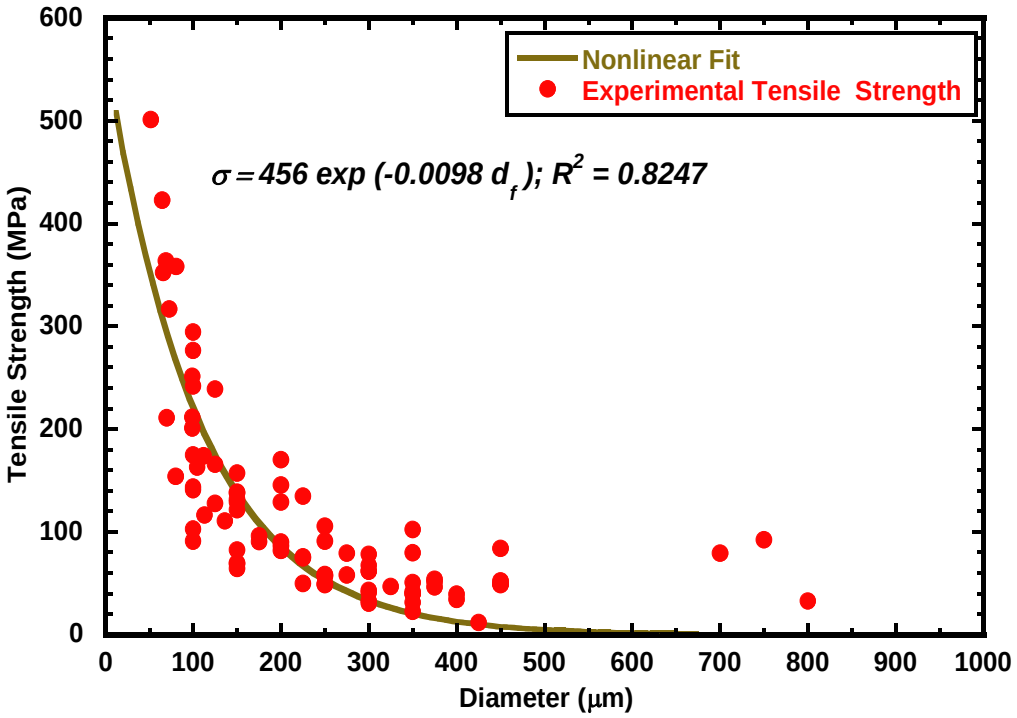

Figure 4.17. Variation of tensile strength of hemp fibers with diameter

A representative distribution in fiber diameter for 0-P hemp mat is shown in Figure 4.18. It can be inferred that the diameter varied in the range of 10 μm to 410 μm. Using the results in Figures 4.17 to 4.18, the distributions in the modulus and the strength were determined. Representative results for 0-P mat are given in Figure 4.19 and Figure 4.20. The average modulus ($E_{f,avg}$) and strength of fibers ($\sigma_{f,avg}$) in a mat were calculated using Equations (4.9) and (4.10) respectively:

$$E_{f,avg} = \frac{\sum n_f E_f}{\sum n_f} \tag{4.9}$$

$$\sigma_{f,avg} = \frac{\sum n_f \sigma_f}{\sum n_f} \tag{4.10}$$

where n_f is the frequency of fibers with a certain tensile modulus or tensile strength. The fibers were assumed to be isotropic and hence, the transverse modulus was taken to be same as the longitudinal modulus discussed above. The distribution of tensile modulus and tensile strength of hemp fibers for the rest of the mats are presented in Appendix A.2.

The shear modulus of the fibers (G_f) and the Poisson's ratio of the fiber (ν_f), were taken from the literature to be 6 GPa and 0.24 [105].

Using the resin and fiber properties, the lamina properties were determined using well known micromechanical models available in the literature.

The rule of mixtures was used to determine the longitudinal modulus (E_{11}) and the Poisson's ratio (ν_{12}) of the unidirectional lamina,

$$E_{11} = E_{f,ave} V_f + E_m V_m \tag{4.11}$$

$$\nu_{12} = \nu_f V_f + \nu_m (1 - V_f) \tag{4.12}$$

where V_f and V_m are fiber volume fraction and the resin volume fraction, respectively.

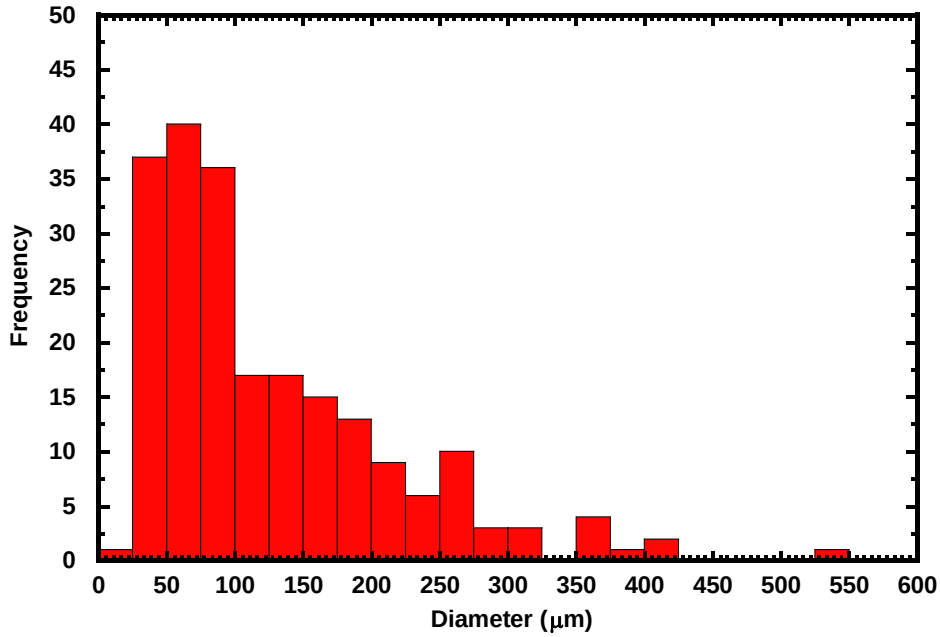

Figure 4.18. Distribution in diameter of fibers in 0-P hemp mat

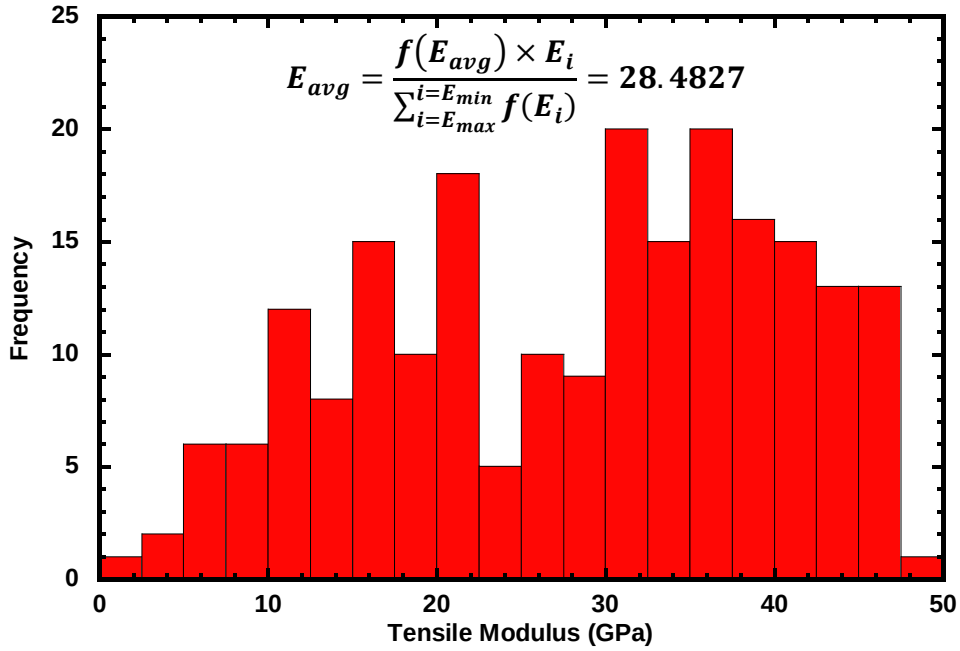

Figure 4.19. Distribution in tensile modulus of fibers in 0-P hemp mat

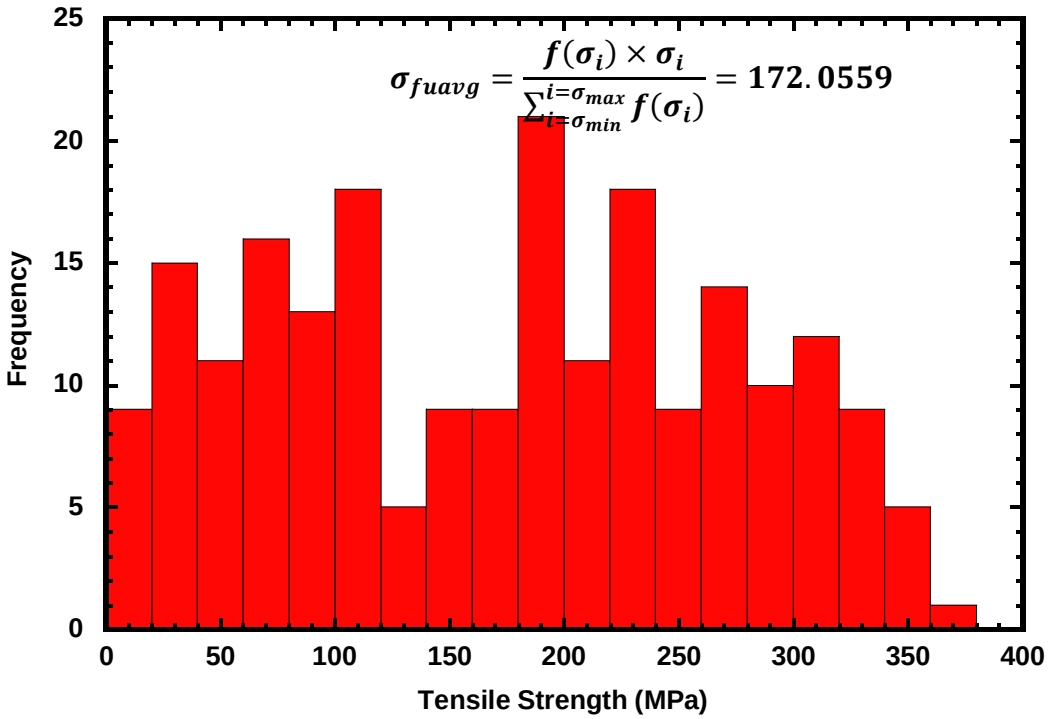

Figure 4.20.Distribution in the tensile strength of the hemp fibers in 0-P mat

The transverse modulus of the unidirectional lamina (E_{22}) was calculated using the micromechnical model developed by Morais [116], which was based on Aboudi's model:

$$E_{22} = \frac{\sqrt{V_f}}{\frac{\sqrt{V_f}}{E_f} + \left(1 - \sqrt{V_f}\right)\left(\frac{1-\upsilon_m^2}{E_m}\right)} + \left(1 - \sqrt{V_f}\right)\frac{E_m}{1-\upsilon_m^2} \tag{4.13}$$

The shear modulus of the unidirectional lamina (G_{12}) was calculated using the self consistent model developed by Whitney et al. [106,107].

$$G_{12} = G_m \frac{G_f + G_m + V_f\left(G_f - G_m\right)}{G_f + G_m - V_f\left(G_f - G_m\right)} \tag{4.14}$$

The experimentally measured volume fractions used in these equations are presented in Chapter 5.

The tensile strength of the lamina was calculated based on the micromechanical models available in literature. In this approach, the mat composite is modeled as a single layer with a distribution in fiber orientation. A modified rule of mixture [108], is used to estimate the tensile strength of needle punched lamina. Since the strain to failure of hemp fibers is much less than the failure strain of the Stypol matrix used in manufacturing the mat composite (see Figure 4.21), the longitudinal strength of unidirectional composite (σ_{LC}) can be predicted using

$$\sigma_{LC} = \sigma_{fu} V_f + \sigma'_m\left(1 - V_f\right) \tag{4.15}$$

where σ_{fu} is the fracture strength of fibers and σ'_m is the stress on the matrix at composite strain at failure. In the above equation, the strength is assumed to be a unique value. However, a statistical distribution in strength is observed in reality. Even though synthetic fibers have uniform chemical composition, they exhibit a distribution in strength because of a statistical distribution of defects introduced in fibers during manufacturing.

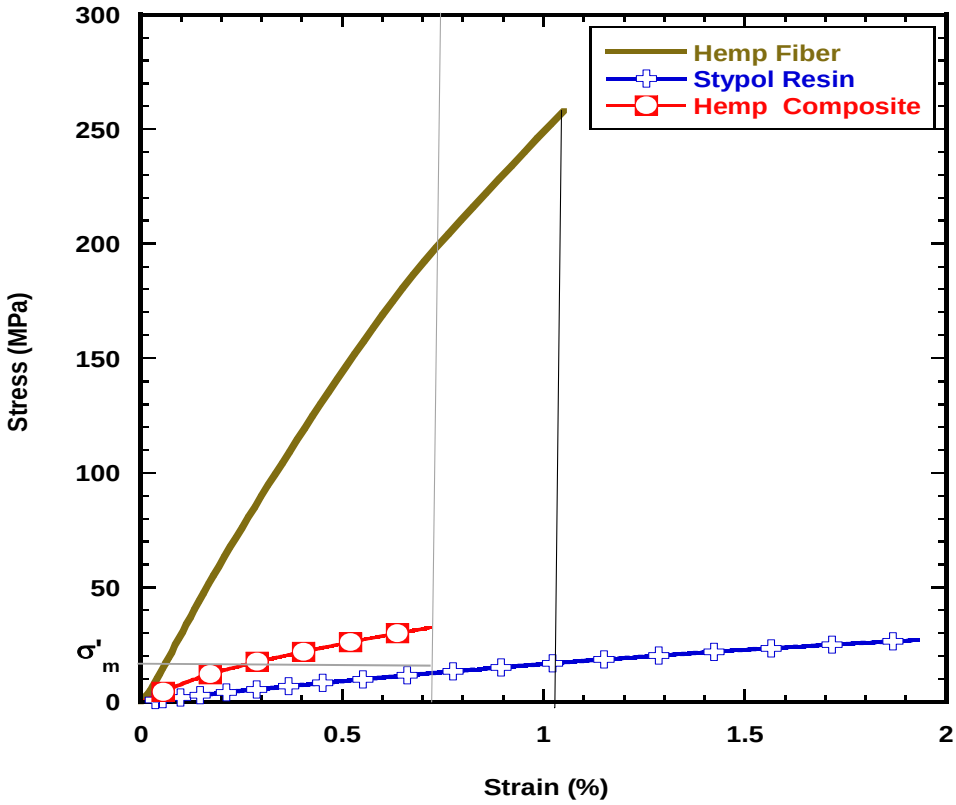

Figure 4.21. Stress–Strain curve for hemp fiber, resin and polymer matrix composites

In the case of natural fibers, additional variability is introduced by the distribution in the diameter of the fibers (due to the nature of the fiber extraction process from the plant stalk), which is related to variation in chemical composition of fibers. Hence, the distribution in fiber diameter and fiber strength (σ_{fu}) has been measured experimentally in this thesis, and the average fiber strength is calculated for each mat based on the frequency of fibers with a certain diameter (N_i):

$$\sigma_{fuavg} = \frac{\sum N_i \times \sigma_{fu}}{\sum N_i} \tag{4.16}$$

where σ_{fuavg} is used instead of σ_{fu} in Equation (4.15). Additional modification of Equation (4.15) is required to take in to account the effect of variation in fiber length and fiber orientation in needle punched hemp mat composites.

The effect of fiber length was first studied by Kelly and Tyson [109]. Their model was based on Cox's shear lag theory [110]. Applying this theory, the average fiber stress is given by

$$\bar{\sigma_f} = \frac{\tau_c l}{d} \qquad l \leq l_c \tag{4.17}$$

$$\bar{\sigma_f} = \sigma_{fuavg}\left(1 - \frac{l_c}{2l}\right) \qquad l > l_c \tag{4.18}$$

where l_c is the critical length, which was measured in this thesis using single fiber fragmentation test. The distribution in the length of hemp fibers was measured experimentally and fitted with a Weibull distribution function [83]:

$$f(l) = abl^{b-1}exp(-al^b) \quad for\ l > 0 \tag{4.19}$$

where *a* and *b* are Weibull parameters, obtained by fitting the experimental data with Equation (4.19). Substituting $f(l)$ for l in Equation (4.17) and (4.18) and integrating over the observed range for fiber lengths, the average fiber stress is calculated as

$$\bar{\sigma_f} = \left[\frac{\tau_c\, ab}{d}\int_{l_{min}}^{l_c} l^{b-1}exp(-al^b)d(l) + \frac{\sigma_{fuavg}}{ab}\int_{l_c}^{l_{max}}\left(1 - \frac{l_c}{2}\right)\left(l^{1-b}e^{al^b}\right)\, dl\right] \tag{4.20}$$

Using this, equation (4.15) becomes

$$\sigma_{LC} = \bar{\sigma_f} V_f + \sigma'_m (1 - V_f) \tag{4.21}$$

The distribution in the length of hemp fiber is shown in Figure 4.23. The length of fibers varied from 4 *mm* to 210 *mm.* The Weibull parameters (*a* and *b*) obtained by fitting the data in Figure 4.22 using Equation (4.19), and the measured critical maximum and minimum lengths of the fibers are tabulated in Table 4.4.

The transverse strength of the lamina (σ_2) was calculated using

$$\sigma_2 = \sigma_m (1 - V_f) \tag{4.22}$$

This equation was derived [10] based on the assumption that the transverse strength of a lamina is controlled by the strength and volume fraction of the matrix.

The shear strength of the lamina τ_{12} is controlled by the adhesion between the fiber and matrix [108] and was assumed to be equal to the interfacial strength of hemp and stypol resin (11.12 MPa).

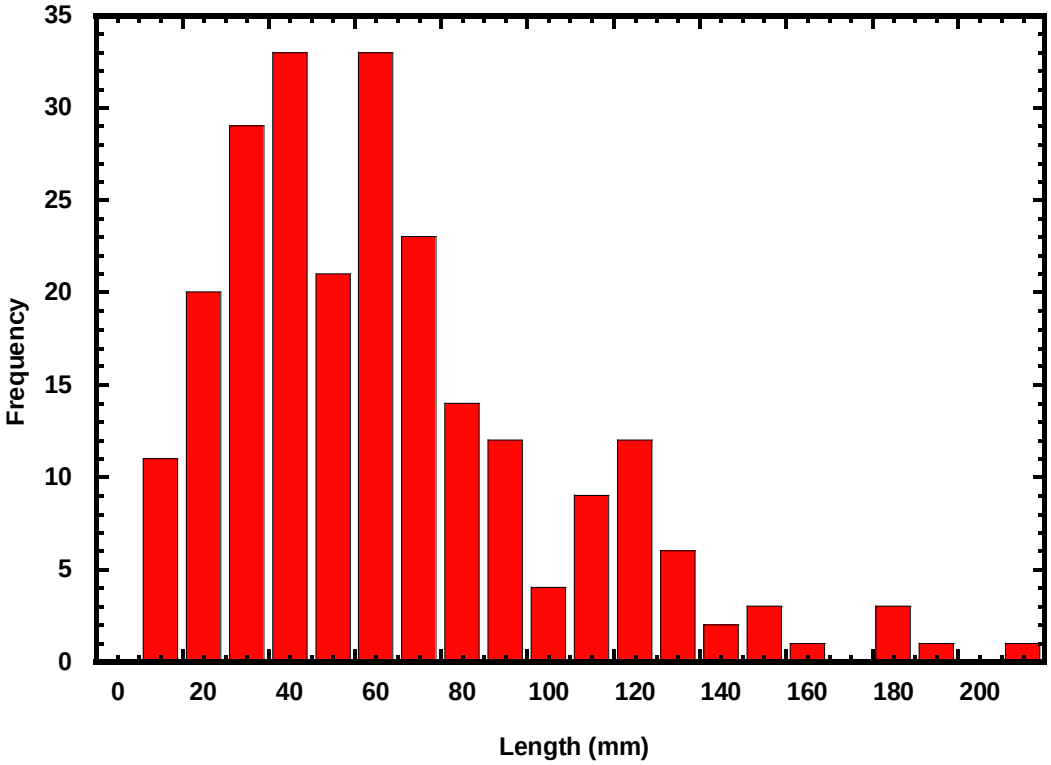

Figure 4.22. Distribution in length of hemp fibers

Table 4.4. Hemp fiber length variation and critical length measurements

l_c (mm)	l_{min} (mm)	l_{max} (mm)	a	b
2.67	4	210	74.91	2.47

4.6.2 FOD

To calculate the orientation distribution of fibers, fibers were grouped at orientation intervals of 5^o (referred to as bin size) to determine their frequency. For example, fibers with orientations in the range of 0^o to 5^o were grouped together and considered to have an average orientation of 2.5^o. Similarly, fibers found in the range of 5^o to 10^o were grouped together and considered to be with an average orientation of 7.5^o. This procedure was repeated for the entire orientation range.

The frequency of fibers in each bin was determined by

$$f(\theta_i) = \frac{n(\theta_i)}{\sum n(\theta_i)} \tag{4.23}$$

where $n(\theta_i)$ is the number of fibers oriented in that bin.

Representative results for distribution in θ in 30-P mat, determined using two bin sizes of 2^o and 5^o are compared in Figure 4.23. Even though a slight difference in FOD is noted, the planar orientation factor f_p, calculated using this data and Equation (2.4), varied by less than 0.05 when the bin size was changed from 2^o to 5^o. However, the data based on 5^o bin, is easier to visualize while comparing the FOD from different mats. Hence, it was chosen to determine FOD and all FOD data presented in this thesis based on this bin size.

It can be observed in Figure 4.23 that the FOD is not symmetrical. Since equivalent laminate used in the model for modulus and strength, discussed in Chapter 3, is assumed to be symmetric and balanced, the experimental FOD was corrected to satisfy this condition, before being input to the model. The procedure of correcting the FOD is as follows:

1. If fibers are present only in $+\theta$, then the frequency at this angle is divided by two and used as the frequency for $-\theta$ and $+\theta$. For instance, a frequency of 0.2 at 10^o is equal to 0.1 at 10^o and 0.1 at -10^o.

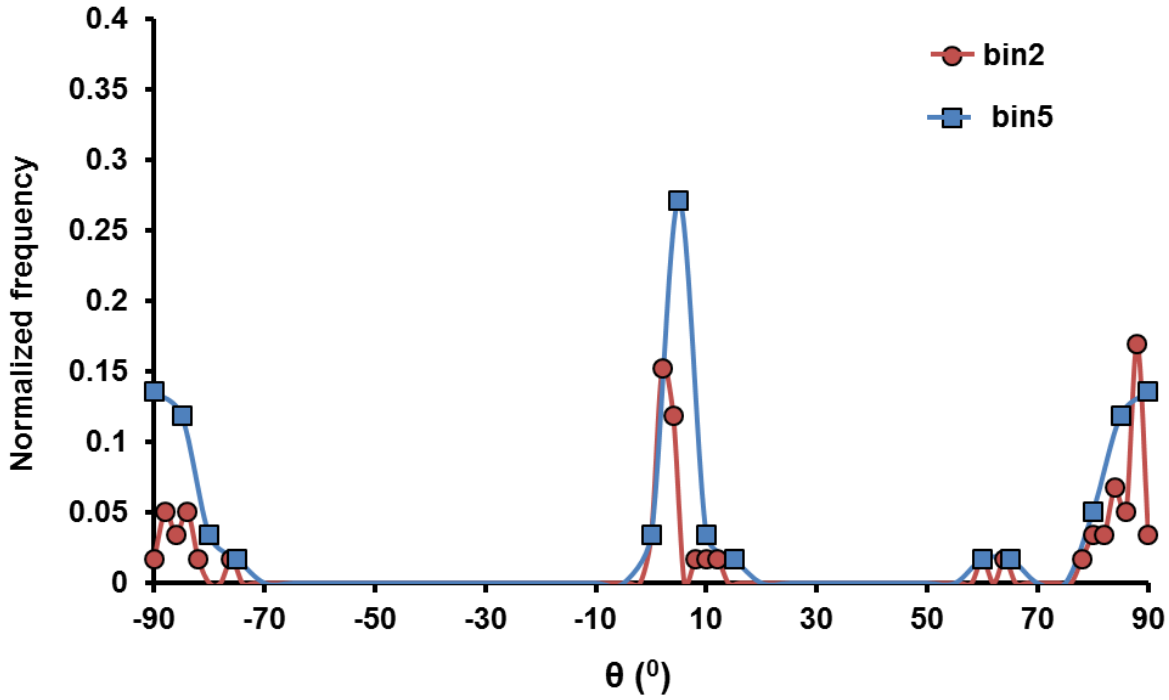

Figure 4.23. Effect of bin size on FOD for 30-P hemp mat

2. If the frequency of fibers at $-\theta$ and $+\theta$ were not the same, then they were added and divided by 2 to yield the average frequency at these two orientations (see Figure 3.8). The lamina lay-up was determined using this corrected FOD as per the procedure discussed in Chapter 3 (Section 3.3).

4.6.4 MATLAB Program for Predicting the Tensile Modulus of a Needle-punched Mat Composite

The various steps of the program for predicting the tensile modulus of a mat composite are presented as a flow chart in Figure 4.24. The program was based on lamination theory.

Step 1: For a given punch density and manufacturing pressure, input corresponding values for the corrected FOD for θ, the *fiber (E_f , G_f, υ_f) and resin (E_m, G_m , υ_m) properties,* the experimentally measured composite thickness (h_c), and the fiber volume fraction(V_f) .

Step 2: Determine laminate stacking sequence using the FOD and the procedure discussed in Section 3.3

Step 3: Calculate the elastic constants of a unidirectional hemp fiber composite lamina as per Equations (4.11)-(4.14).

Step 4: Determine stiffness matrices, $[Q^k]_{1,2}$ and $[Q^k]_{x,y}$ for each laminate layer, using Equations (3.27) to (3.26).

Step 5: Determine laminate stiffness $[A]_{x,y}$ and compliance matrices $[a]_{x,y}$ using Equation (3.25).

Step 6: Determine the longitudinal and transverse tensile moduli of the mat composite using Equations (3.30) and (3.32).

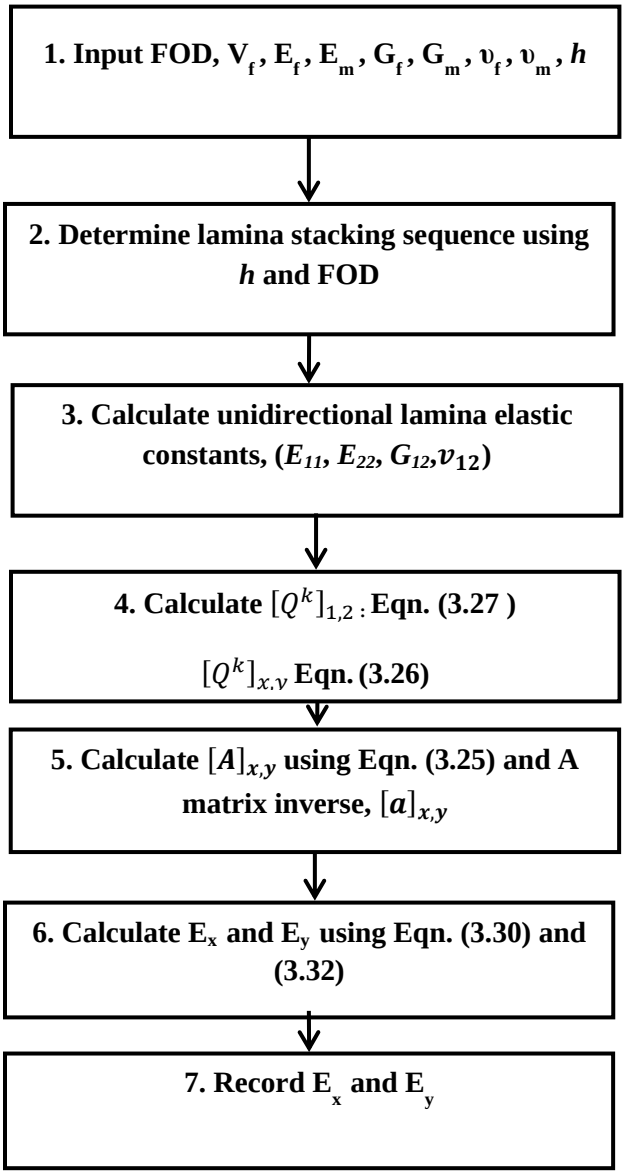

Figure 4.24. Flowchart of predicting the tensile modulus of a needle punched mat composite

4.6.5 MATLAB Program for Predicting the Tensile Strength

The various steps of the program for predicting the tensile strength of a mat composite are presented as a flow chart in Figure 4.25. This program is the second part of the program presented in 4.6.4.

Step 1: Read lamina and laminate stiffness's as well as laminate compliance from the program discussed in Section 4.6.4.

Step 2. Read strength values for fiber and resin and determine lamina strengths as per Equations (4.21) and (4.22).

Step 3. Initialize initial load to be 0 .

Step 4: Apply a load increment and add to the previous value to obtain current load per unit width.

Step 5: Using this load per unit width and laminate compliance, calculate the laminate strain as per Equation (3.29).

Step 6: Calculate ply stresses along global axes using the laminate strains (which are equal to ply strains) and ply stiffness values along global axes, using Equation (3.34).

Step 7: Transform the ply stresses along global axes to obtain ply stresses along principal material axes, as per Equation (3.36).

Step 8-10: Using these ply stresses and the maximum stress criterion to determine if any of the ply groups would fail.

Step 11. If a ply group is deemed to have failed, the properties of this lamina are reduced to a negligible value and the laminate stiffness and compliance matrix are calculated again.

Step 12-13. If the ply with least θ failed, output that load per unit width as the ultimate failure load for the composite and divide this value by the thickness of the laminate to obtain the

tensile strength of the composite. If not, increment the load by (0.1 N) and repeat steps 4 to 11. Load increment (0.1) is less than stress variation between two plies with 5^{o} differences in orientation angle.

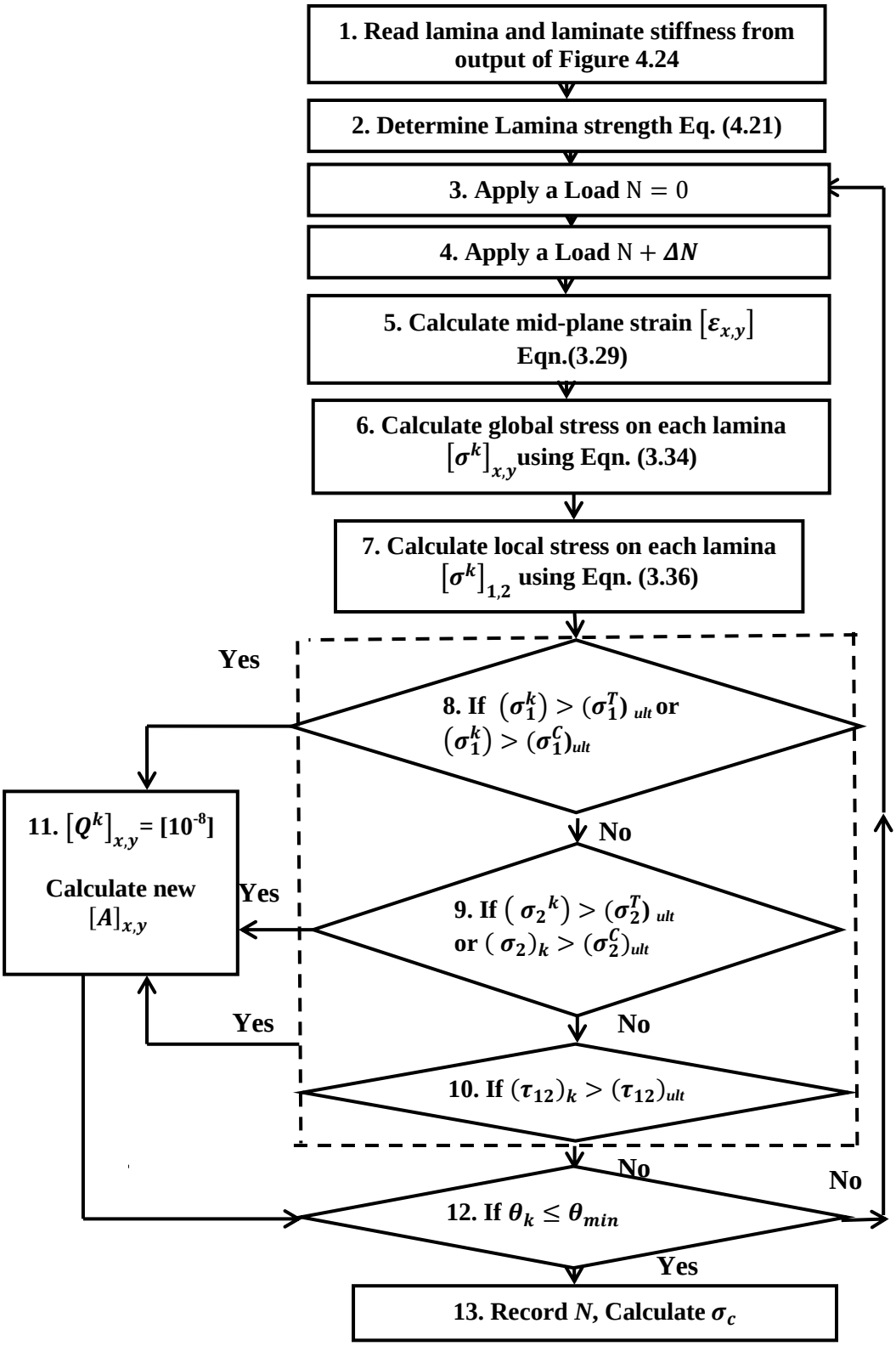

Figure 4.25. Flowchart of predicting the tensile strength of a needle punched mat

CHAPTER 5

RESULTS AND DISCUSSION

5.1 Introduction

In this chapter the results of experimental and theoretical study on needle punched mats and composites are presented and discussed. First, the results from the experimental study on the effect of needle punching on mat structure characterized by the areal density (GSM), thickness, fiber volume fraction, compressibility, permeability, and fiber orientation are discussed. Then, the predicted results for the evolution of FOD during needle punching and composite manufacturing are presented and compared with experimental results.

Subsequently, the experimental results for the modulus and the strength of mat composites are presented and discussed to highlight the processing-structure-property relationship. Finally, the predictions of the model, presented in Chapter 3, for modulus and strength are presented and compared with the experimental results to validate the model.

5.2 Effect of Needle Punching on Mat structure

5.2.1 Physical Properties of Needle Punched Mats

The areal density, the thickness, and the fiber volume fraction of mats, manufactured with various punch densities, are tabulated in Table 5.1.

The mats with punch density from 2.6 to 30 Punch/cm^2 were manufactured as one batch and the mats with punch densities of 0, 70 and 150 Punch/cm^2 were manufactured as a second batch. The areal density of the mats from the two batches varied by 240 to 340 g/m^2. This variation in areal density is due to variation in the manufacturing parameters, which was beyond the control of the author of this thesis. The manufacturing parameters include difference in air pressure (which was controlled to vary the areal density of the web of fibers) and difference in the speed of conveyor belt (0.8 m/s versus 1 m/s). Similarly, the variation in the areal density between 7-P mat and rest of the mats from the first batch is believed to be due to the occasional clogging of the comb that separates the fibers and feeds them into the air stream and the manual feeding of the fibers to the comb. Lack of good control over the location where the air stream dumps the fibers onto the moving conveyor belt is also believed to have contributed to the observed variation of the areal density.

Due to this variability, the trend in thickness and volume fraction is not readily apparent in Table 5.1. The areal density of 2.6-P, 20-P and 30-P mats were nearly the same and hence, results for these mats can be compared; with an increase in the punch density, the thickness of the mat decreased, and the fiber volume fraction in the mat increased. Similar conclusions can be drawn based on the results for 70-P and 150-P with similar areal density. Despite having an areal density lower than many mats, the 0-P mat was thicker than all other mats and had the least fiber volume fraction. This also supports the above conclusion that needle punching reduces the thickness of the mats.

5.2.2 Compressibility of Needle Punched Mats

As discussed in Chapter 3, the fiber volume fraction and the FOD, which control the properties of the mat composites, depend on the compaction of the mat during composite

manufacturing. Hence, the compaction behavior of various mats was studied to understand the effect of needle punching. The compressibility of various mats, in dry state, is plotted in Figure 5.1. Equation (3.1) was used to convert the mat thickness to fiber volume fraction in the mat. The observed difference in the slope of the curves clearly demonstrates the significant effect of needle punching on the compaction behavior of the mats.

At low compaction levels, when rotation of fibers is easy, the volume fraction would increase at nearly constant stress due to the elimination of voids among fibers. At higher compaction levels when fiber rotation becomes difficult, the stress would rapidly increase without much increase in the volume fraction due to elastic deformation of the fibers. The level of fiber rotation, resistance to fiber rotation, and elastic deformation of the fiber, depends on mat structure (V_f, FOD). Since needle punching influences the mat structure, the observed difference among mats is to be expected. However, a trend on the effect of needle punching on compressibility is not apparent. This will be discussed further in Section 5.3.1.

During composite manufacturing at 101 kPa by VARTM, the pressure of 101 kPa was first applied before impregnating the mat with resin. Hence, the mat compacted in a dry state. However, in case of composites manufactured at 260 kPa and 560 kPa, the mat was impregnated with resin by VARTM under 101 kPa before applying the pressure and hence, the mat compacted under lubricated condition. In order to study the difference in compaction between dry and lubricated states, the compressibility of 30-P mat was also studied under lubricated states. The compressibility of lubricated mats differed substantially from that of dry mats beyond ~200 kPa, as shown in Figure 5.2.

Table 5.1. Physical properties of manufactured needle-punched hemp mat

ID	**Mat areal density(g/m^2) (Variation %)**	**Thickness (mm)**	**V_f in Mat (%)**	**V_f in Composites at 101 kPa (%)**
0-P	941.34 (±17.9) [1]	12.45 (±3.1) [1]	6.6 (± 1.6) [1]	11.6 (± 2.1) [1]
2.6-P	1021.59 (±7)	8.07 (±1.53)	8.7 (±1.6)	12.8 (±1.1)
7-P	872.45 (±9.3)	5.86 (±0.65)	8.7 (±1.2)	13.8 (±0.7)
20-P	1014.84 (±7)	5.75 (±0.93)	11 (±3.5)	16.4 (±1.4)
30-P	1113.85 (±6.6)	5.39 (±1.24)	15 (±1.1)	20.8 (±1.2)
70-P	1241.28 (±11.2)	6.83 (±1.40)	12 (±1.5)	18 (±3.0)
150-P	1283.28 (±7.5)	6.12 (±1.37)	13.9 (±1.7)	22.9 (±2.4)

[1]Standard deviation

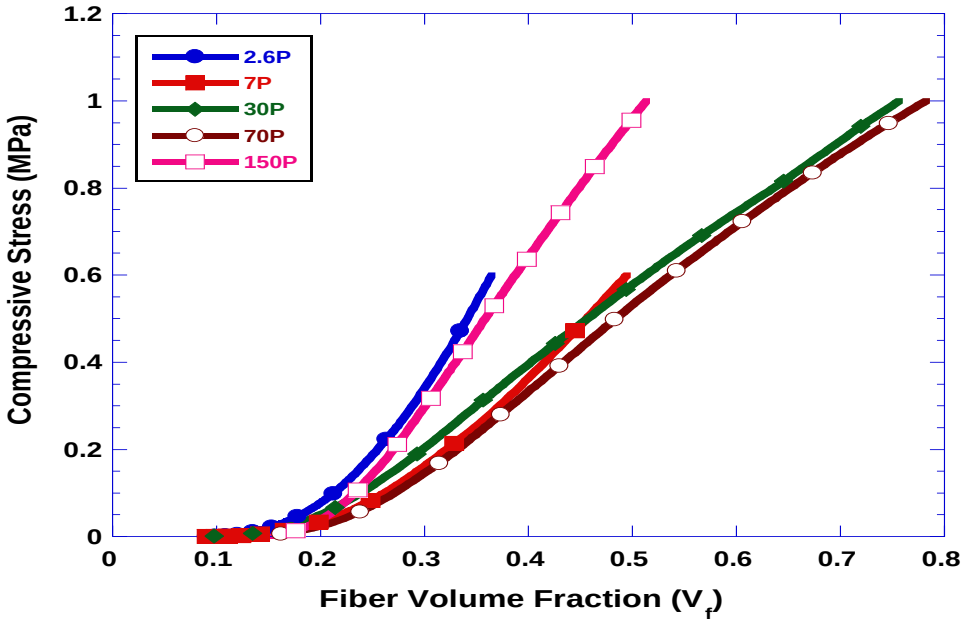

Figure 5.1. Effect of needle punching on the compressibility of dry mats

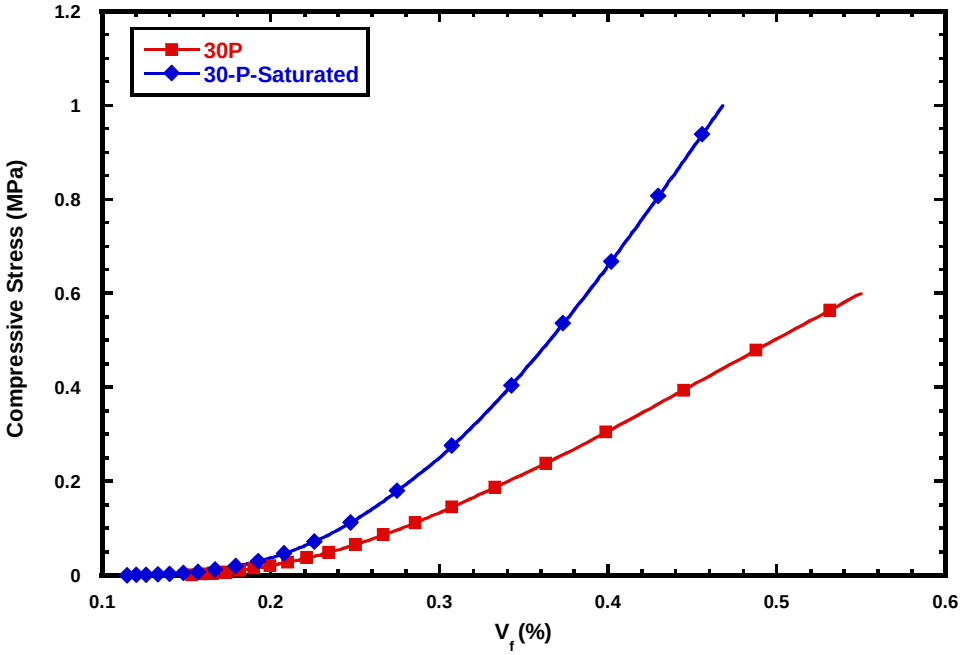

Figure 5.2. Effect of resin on compression behavior of 30-P mat

The lubricated mats required higher stress to reach the same level of compaction when compared to dry mats, which is due to the additional resistance offered by the resin (filling the void space between fibers in the dry mat) to compaction. The nonlinear change in slope suggest that lubrication could also be changing the rate of rotation of fibers with applied stress and the level of elastic deformation of fibers when compared to that in dry mats.

5.2.3 FOD of Needle Punched Mats

As discussed in Chapters 3 and 4, the FOD in φ and θ was non-destructively characterized. Typical distributions in φ and θ are plotted in Figures 5.3 and 5.4, respectively for both small scan volume (measured using X-Radia's Micro-Xray CT) and large scan volume (measured using SkyScan). The result from the smaller scan volume is slightly different than that from the larger scan volume; the larger scan volume detected more fibers with φ in the range of 50^o to 90^o when compared to the smaller volume scan. The 2D (using the FOD in θ) and 3D (using the FOD in φ) orientation factors were determined using Equations (2.3) and (2.5) and are plotted in Figures 5.5 and 5.6, respectively for both scan volumes. The 2D factor is referred as f_p and the 3D factor is referred as f_a in this thesis. The values for both volumes compared very well (difference was 0.27 for f_p and 0.12 for f_a). However, the difference in FOD observed in Figures 5.3 resulted in a modulus variation of 6.5% as predicted using the model developed in this study. Hence, the FOD obtained using smaller scan volumes was considered to be representative of the entire mat and the smaller scan volume was used in the characterization of all mats.

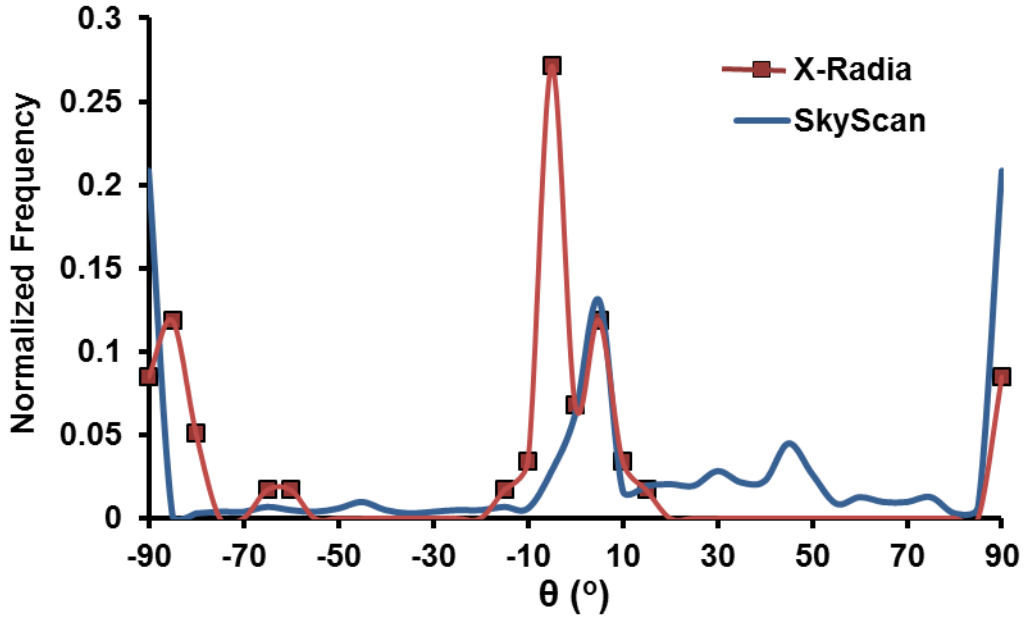

Figure 5.3. FOD in θ for 30-P mat for two different image sizes acquired by X-Radia and SkyScan

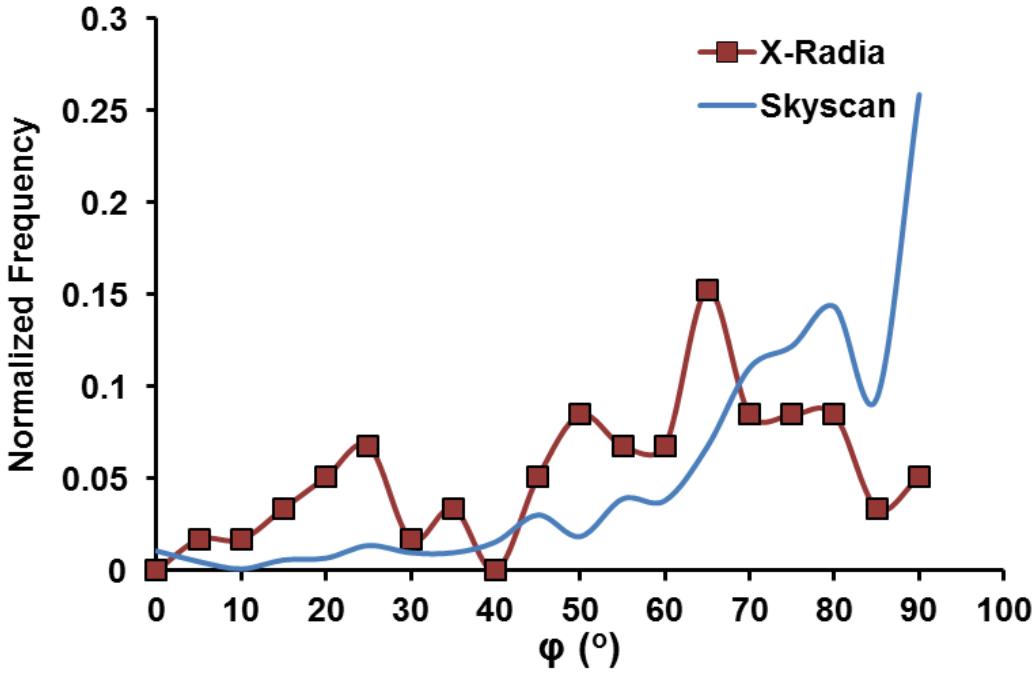

Figure 5.4. FOD in φ for 30-P mat for two different image sizes acquired by X-Radia and SkyScan

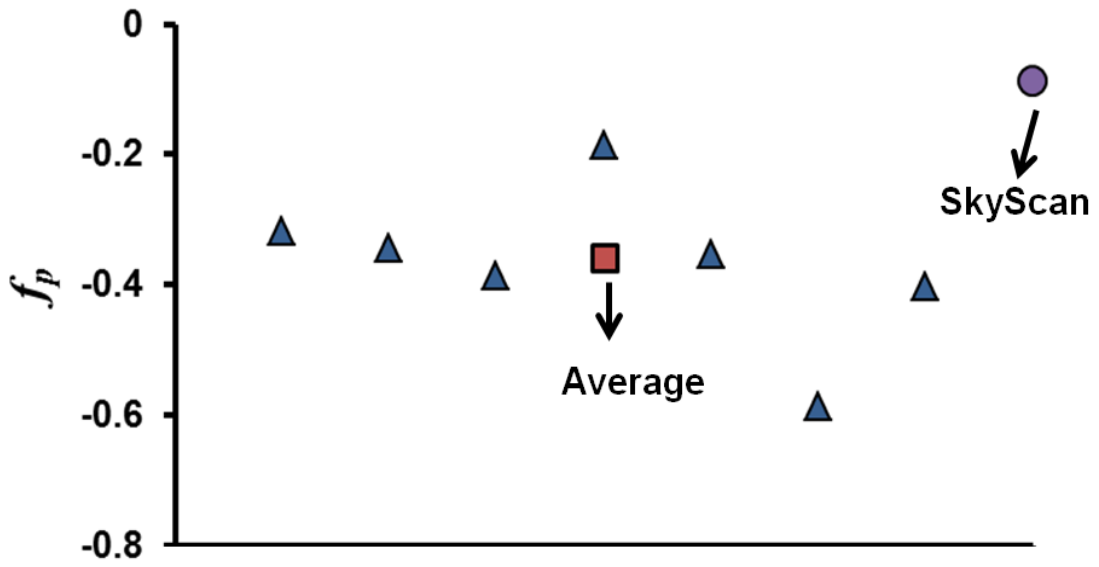

Figure 5.5. Comparison of f_p determined using multiple small scans in continuous area using X-Radia and large scan value by SkyScan

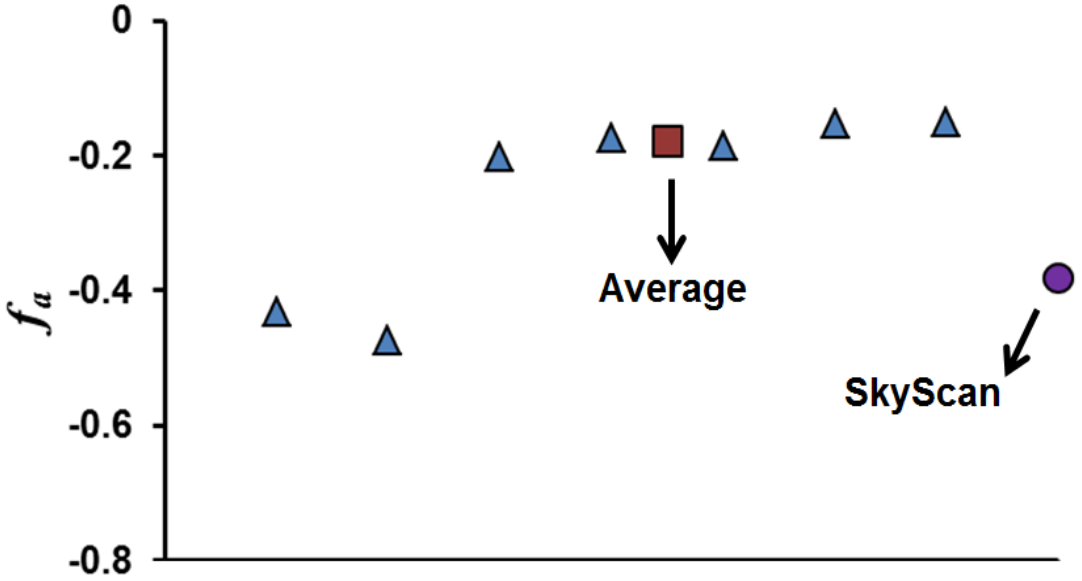

Figure 5.6. Comparison of f_a determined using multiple small scans in continuous area using X-Radia and large scan value by SkyScan

The FOD in φ for various mats are compared in Figures 5.7 and 5.8. Lines, connecting the data points, are drawn to aid in the interpretation but the observed FOD is not continuous in φ and θ.

The 0-P mat was from the second batch and was very fragile to handle. While due care was taken to minimize any change in its FOD due to handling, minor change in the FOD could not be ruled out. Since the results for 0-P mat is used in interpreting the effect of needle punching on FOD, the above two factors should be remembered while interpreting the results.

All fibers in 0-P mat were oriented in 3D and no fibers were found either at $\theta = 0$ or $\varphi = 0$. Most of the fibers in the 0-P mat were oriented with φ in the range of 0^o to 50^o. This is to be expected since the thickness of the web, formed at the location where the fibers were dropped by gravity onto the conveyor belt, was about 2" to 3", allowing the fibers to orient along the out-of-plane direction. The fibers were gradually reoriented towards the in-plane direction during a subsequent needling operation due to compaction and stretching.

The FOD in φ for 0-P is compared with the FOD for 2.6-P, 7-P, and 30-P in Figure 5.7. While the FOD for 0-P from batch 1 is not known, it is assumed to be same as that for 0-P from the second batch. Comparing 0-P with 2.6-P and 30-P, it can be inferred that φ increases with an increase in punch density. This is to be expected since compaction and stretching results in reorientation of the fibers towards the in-plane directions. The 7-P mat follows this trend weakly and this is thought to be due to the lower areal density, which reduces the probability of engagement of needles with fibers and hence, fiber reorientation.

A similar trend is observed in the FOD in φ for 70-P and 150-P (from the second batch) compared with the FOD for 0-P in Figure 5.8.

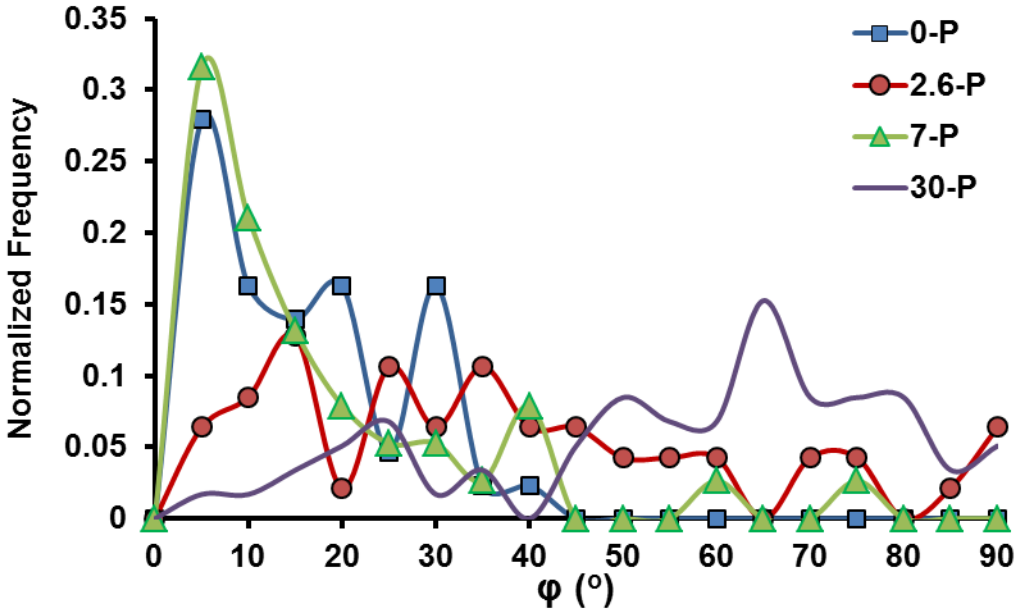

Figure 5.7. FOD in φ for the first batch of needle punched mats

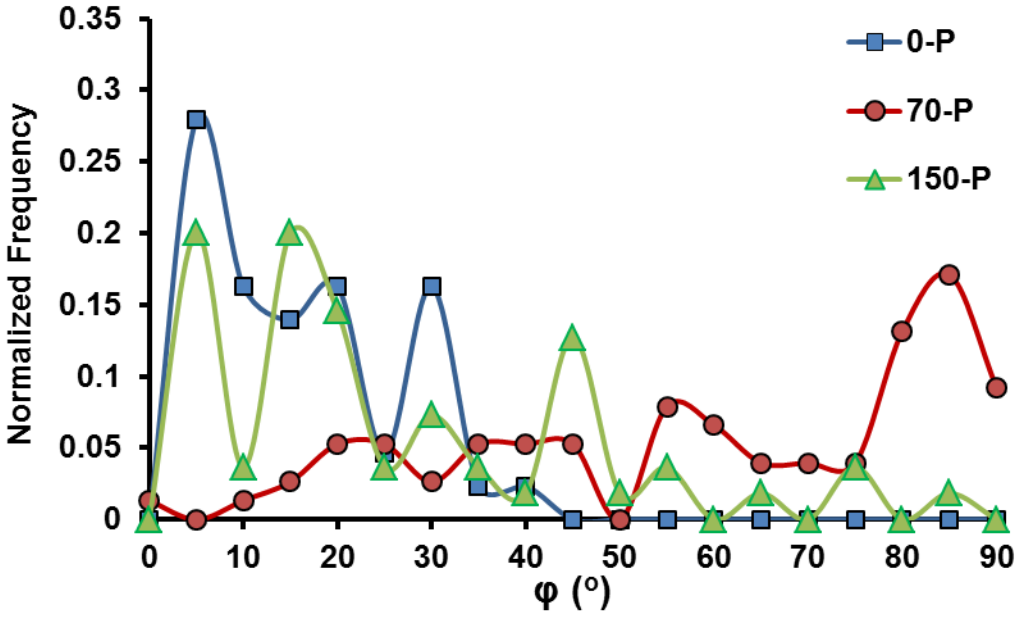

Figure 5.8. FOD in φ for the second batch of needle punched mats

The magnitude of reorientation for 150-P is relatively less than that for 70-P. The difference in the areal density is believed to be the reason for this. The f_a, determined using the FOD, is plotted in Figure 5.9. With increasing the punch density to 70-P, the φ increases and hence, the f_a decreases. The reorientation of fibers at 150-P is relatively less, which results in a higher f_a at 150-P than at 70-P. The observed trend is similar to that observed in the mat thickness's shown in Table 5 .1 and hence, is believed to be due to the combined effect of needle punch density and the difference in the areal density of various mats.

The FOD in θ for various mats are compared in Figures 5.10 and 5.11 for the first (2.6-P to 30-P) and second batches (70-P to 150-P) of mats, respectively. The distribution in θ was obtained by projecting the fibers onto the x-y plane. With an increase in the punch density, the frequency of fibers near $\theta = 0^o$ decreased and those near $\theta = 90^o$ increased, i.e. more fibers got reoriented towards the transverse direction (y-axis) than the longitudinal direction (x-axis).

The f_p determined using the FOD is plotted in Figure 5.12 as a function of punch density. All mats have negative values for f_p, which means more fibers are oriented in the transverse direction than in the longitudinal direction, reflecting the observed trend in the FOD. This is also corroborated by the higher transverse modulus of the composite than its longitudinal modulus, which is discussed later in Section 5.5.1. It can be observed from Figures 5.10 and 5.11 that the FODs in θ for 0-P and 7-P and for 2.6-P and 30-P are similar. Hence, the values for f_p are of the same magnitude, as observed in Figure 5.14.

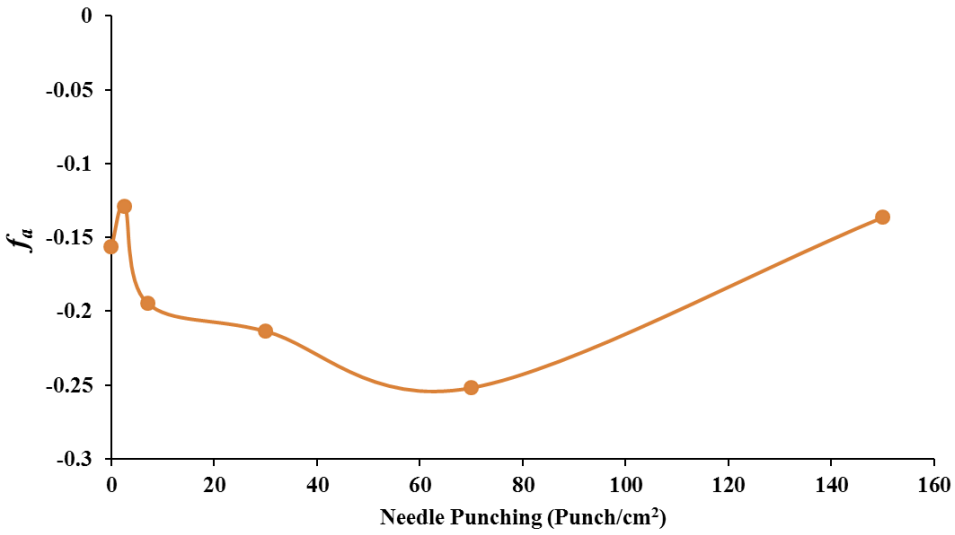

Figure 5.9. f_a for the hemp mat as a function of punch density

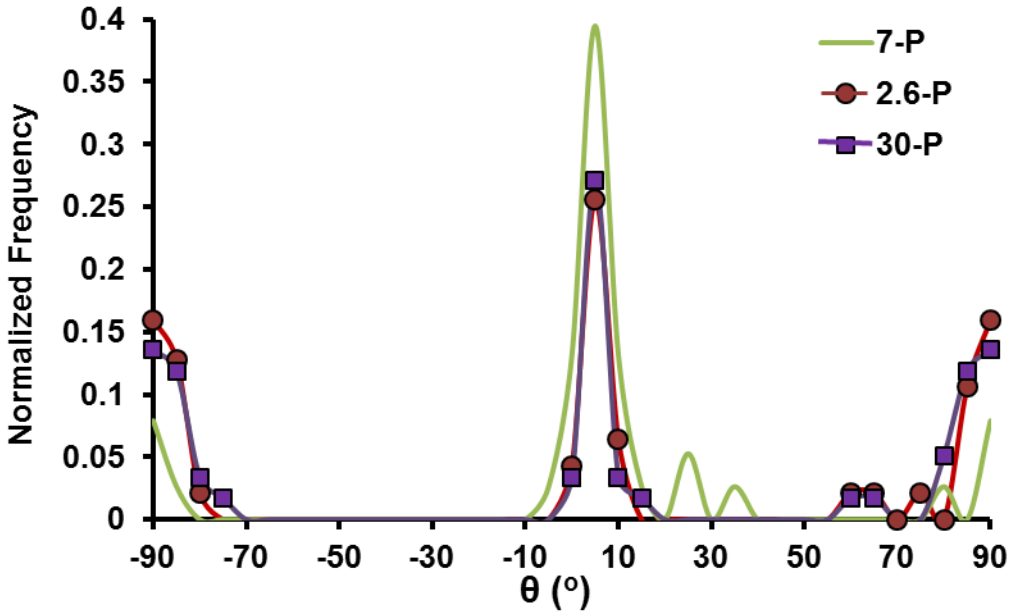

Figure 5.10. FOD in θ for the first batch of needle punched mats

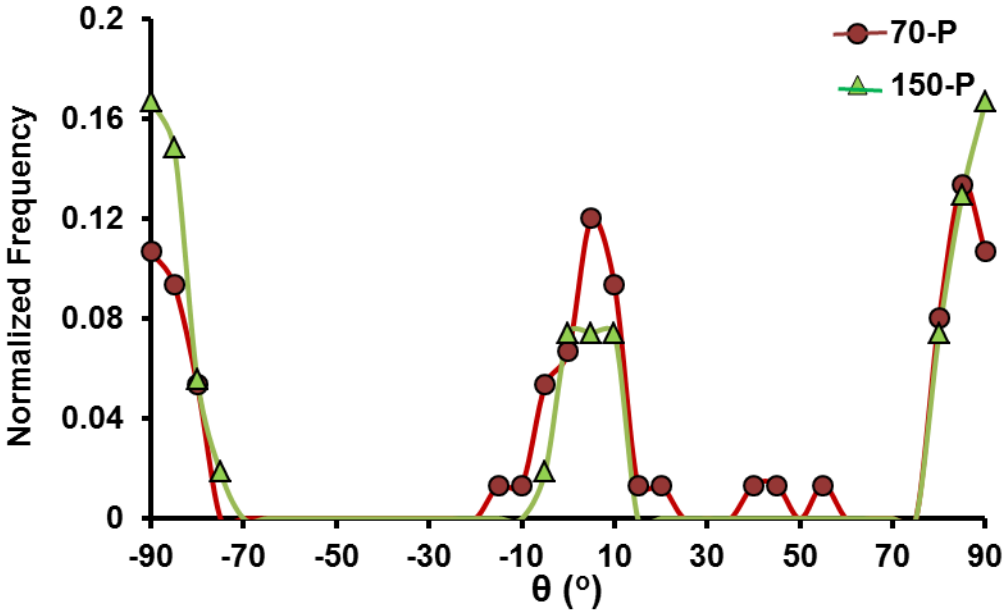

Figure 5.11. FOD in θ for the second batch of needle punched mats

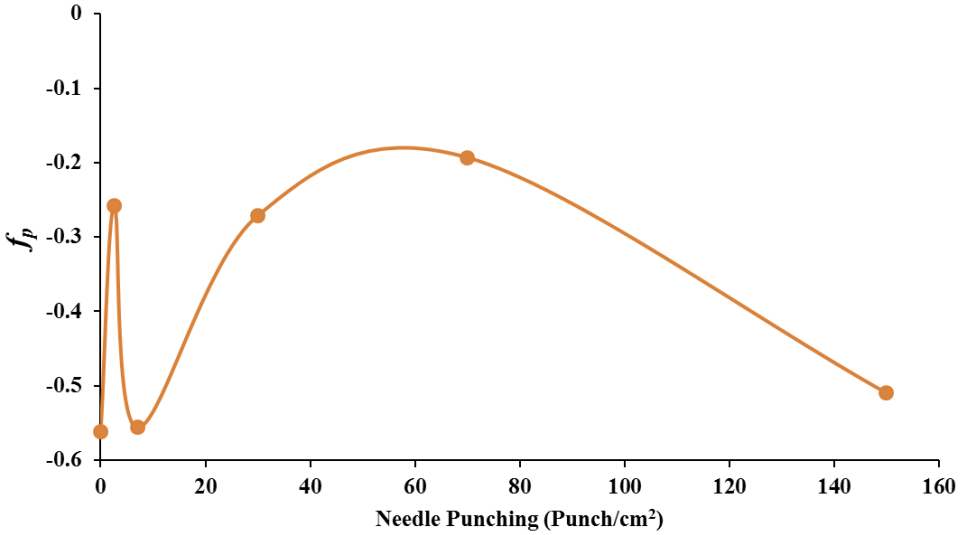

Figure 5.12. f_p for the hemp mat as a function of punch density

5.2.4 Permeability of Needle Punched Mats

The experimentally measured flow front location with respect to resin inlet position is plotted in Figure 5.13 as a function of time. It follows a linear trend as per Equation (4.5). The in-plane longitudinal permeability was determined from Figure 5.13 and Equation (4.4), is tabulated in Table 5.2 for various mats. It can be inferred from Table 5.2 that the in-plane longitudinal permeability of the mats decreased with an increase in punch density due to the reduction in void spaces (i.e. porosity). It was modeled using the well-known Kozney-Carman model [99]:

$$K_x = \frac{r_f^2(1-V_f)^3}{4k_x V_f^2} \tag{5.1}$$

$$K_x = \frac{C}{k_x} \tag{5.2}$$

$$C = \frac{r_f^2\,(1-V_f)^3}{4V_f^2} \tag{5.3}$$

where r_f is the radius of the fiber, V_f is the volume fraction of the fibers, and k_x is the Kozney constant.

In accordance with this equation, the experimentally measured K_x is linearly proportional to *C* as shown in Figure 5.14. The slope of this plot is $1/k_x$ and the value for k_x, determined from the slope of this plot, is 27.6. The C was determined using the data for three different mats with different volume fraction. Despite this, a linear relation with a constant value for k_x for all three mats is observed. This observation is consistent with published studies that have found the Kozney constant, for continuous fiber prepregs, to be independent of fiber volume fraction. Although the fiber diameter in the mat exhibited a distribution, the minimum value reported in

Table 3.2 was used in determining the "C" plotted in Figure 5.14. The reason for this is discussed later in this section.

The through-the-thickness permeability (K_z) of hemp mats is plotted in Figure 5.15 as a function of punch density. With increasing the needle punch density from 2.6 to 150, K_z decreased by a factor of 8. It can be inferred from Table 5.3, that the relation between K_z and % porosity is not clear, unlike K_x that increased with increase in porosity. K_z is plotted as a function of C in Figure 5.16. It should be noted that the C was determined using the minimum diameter in Table 3.2. Unlike K_x, the relation is not linear, suggesting that the Kozney constant for the through-the-thickness (k_z) is a function of punch density. This varied in the range of 0.007 to 0.018 due to variation in FOD with punch density, which is discussed in the next section.

The transverse permeability is roughly 100 times the in-plane permeability. This ensured a planar resin front during testing for in-plane permeability; i.e., the transverse permeability did not influence the in-plane permeability measurements.

The permeability values reported in the literature for glass and natural fiber mats are tabulated in Table 5.4. It can be inferred that the needle punched hemp mats of this study have higher transverse permeability than, and comparable in-plane permeability to, glass fiber mats. Possible reasons for higher transverse permeability in hemp mats are lower V_f and bigger pore sizes due to larger diameter fibers.

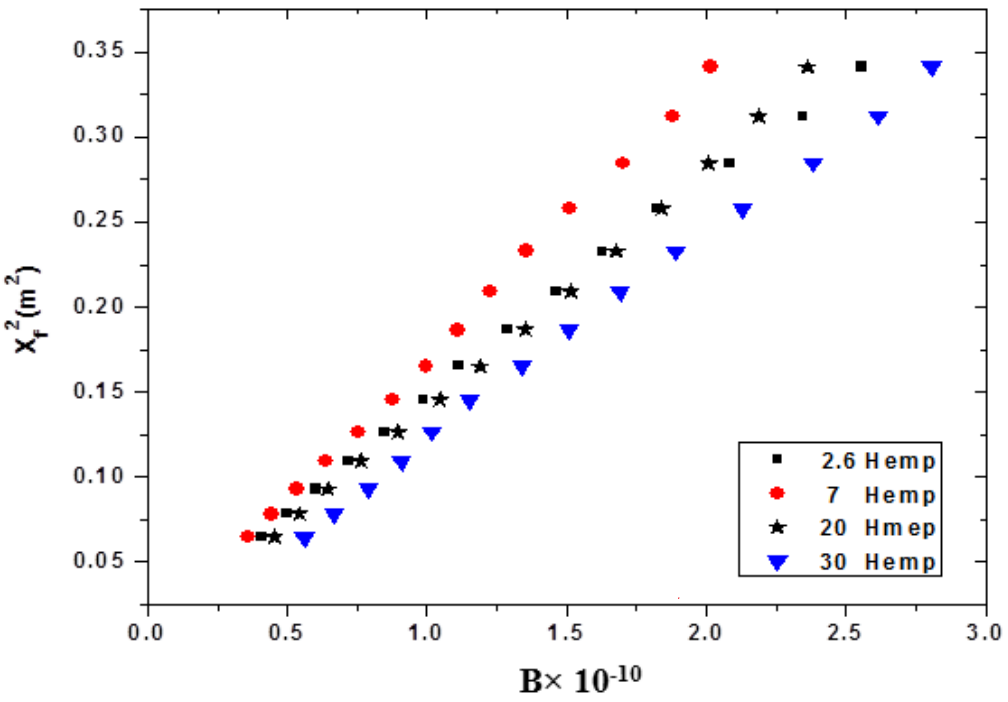

Figure 5.13. Square of the distance travelled by the flow front as a function of time for hemp mats with varying punch density

Table 5.2. In-plane permeability of needle hemp punch mats

Mat	**Porosity (1-V_f) %**	**K_X ×10 $^{-10}$ (m^2)**
2.6-P	80.63	1.30
7-P	82.79	1.65
30-P	75.27	1.20

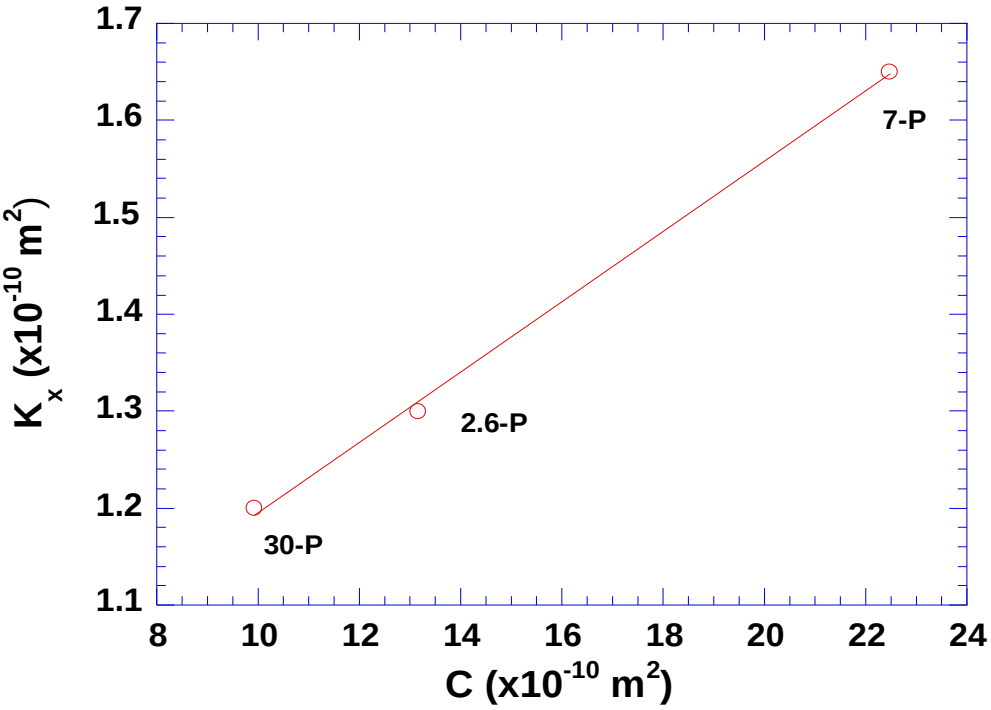

Figure 5.14. In-plane permeability plotted as a function of C using equation (5.3) for three mats

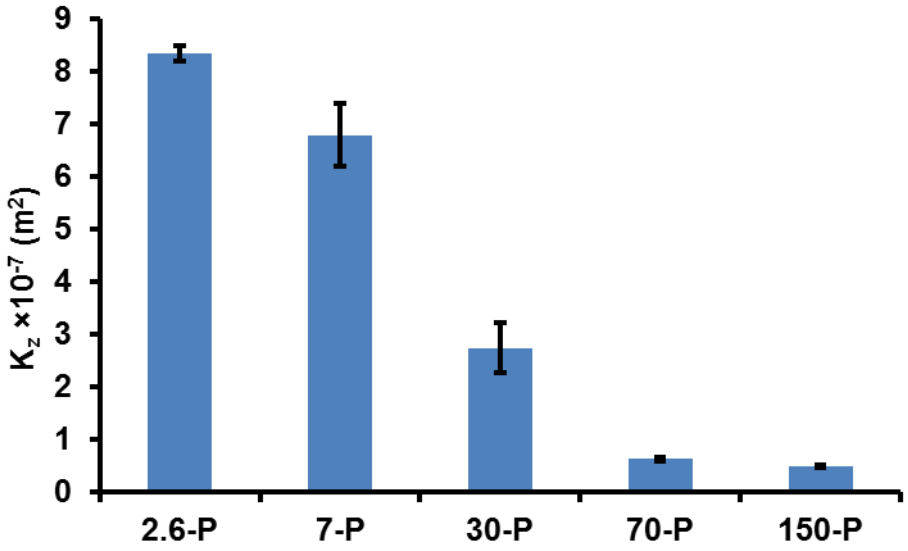

Figure 5.15. Through-the-thickness permeability as a function of needle punch density

Table 5.3. Through-the-thickness permeability of needle-punched hemp mats

Mat	**Porosity (1-V_f) %**	**$K_z \times 10^{-7}$ (m^2)**
2.6-P	91.3 (±1.6)	8.35 (±0.141)
7-P	91.3 (±1.2)	6.8 (±0.592)
30-P	85 (±1.1)	2.75 (±0.468)
70-P	88 (±1.5)	0.636 (±0.039)
150-P	86.1 (±1.7)	0.49 (±0.0259)

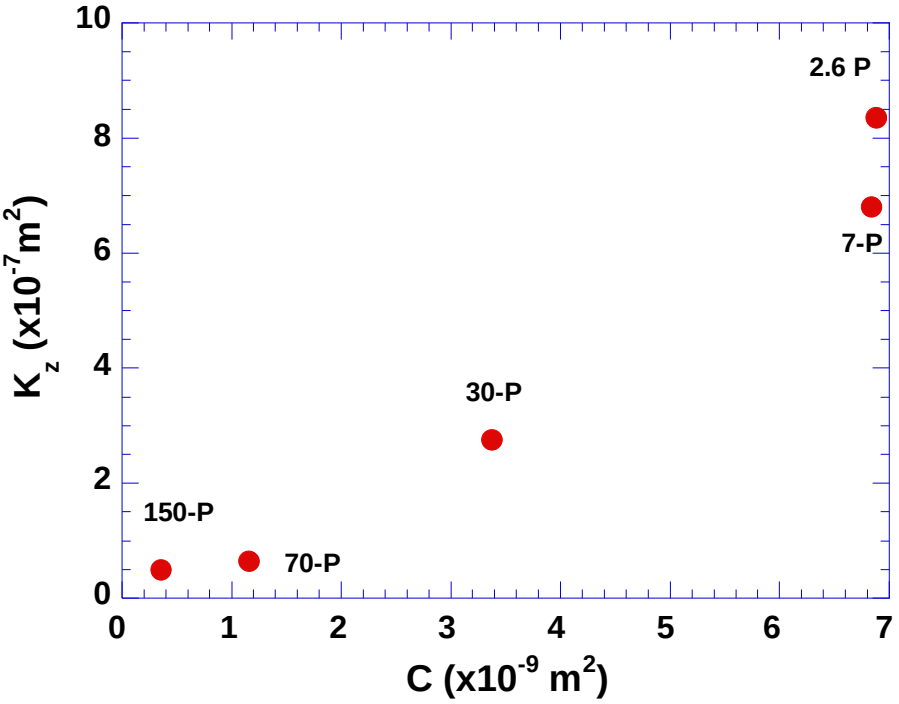

Figure 5.16. Through-the-thickness permeability plotted as a function of C, determined using equation (5.3) for five mats

Table 5.4. Permeability data from literature for various fiber mats

Mat	**In-plane permeability(m^2)**	**Out of plane permeability (m^2)**	**V_f *(%)***	**Reference**
Knitted glass mat	3.05×10^{-10}	3.064×10^{-10}	0.30	[111]
Long strand random mat	-	2×10^{-11}	0.2	[112]
Glass fiber fabric(±45)	-	3.09×10^{-12}	0.357	[113]
Compacted medium density wood fiber mats	1×10^{-11}	-	0.30	[114]
Flax mat	1.02×10^{-10}	-	0.31	[64]
Bidirectional Jute	0.82×10^{-6}	-	0.27	[115]
Random Sisal	1.25×10^{-6}	-	0.25	[115]

It can be inferred from Table 5.4 that the in-plane permeability of needle punched hemp mats of this study is comparable to that of flax and medium density wood fiber mats (in the order of 10^{-10} m^2). It is lower than that of bidirectional jute by 1000 times because the fibers in the latter are parallel to one another. It is also lower than that for sisal fiber mat by a factor of 1000 because of the larger sisal fibers

While the decrease in permeability due to needle punching increased the impregnation time during composite manufacturing by VARTM, it did not affect the quality of the composite part. Hence, it can be concluded that needle punching can be increased to increase the V_f and the properties of hemp mat composites without concern about permeability.

The Kozney constant (k_z) for the through-the-thickness permeability is plotted as a function of f_a in Figure 5.17. Note that this constant was determined using the values of C that was calculated using minimum fiber diameter in Table 3.2. The k_z decreased with increase in f_a. Increase in f_a means the fibers was increasingly oriented along the out-of-plane direction. Hence, the through-the-thickness permeability (K_z) increased and the Kozney constant (k_z) decreased with increase in f_a.

The f_a decreased with an increase in punch density from 2.6 to 70, and hence, k_z increased resulting in a decrease in K_z, as observed in Figures 5.14 and 5.17. Although K_z increased with porosity (similar to the trend in K_x), this is not apparent in Table 5.3 due to the additional influence of the FOD, that changed with punch density. These results demonstrate a clear relationship among the punch density, the FOD and the through-the-thickness permeability (K_z).

In contrast, the Kozney constant for in-plane longitudinal permeability (k_x) did not change with punch density despite the change in FOD with punch density. The negative values for f_p indicate that there are more fibers in the transverse direction than the longitudinal direction.

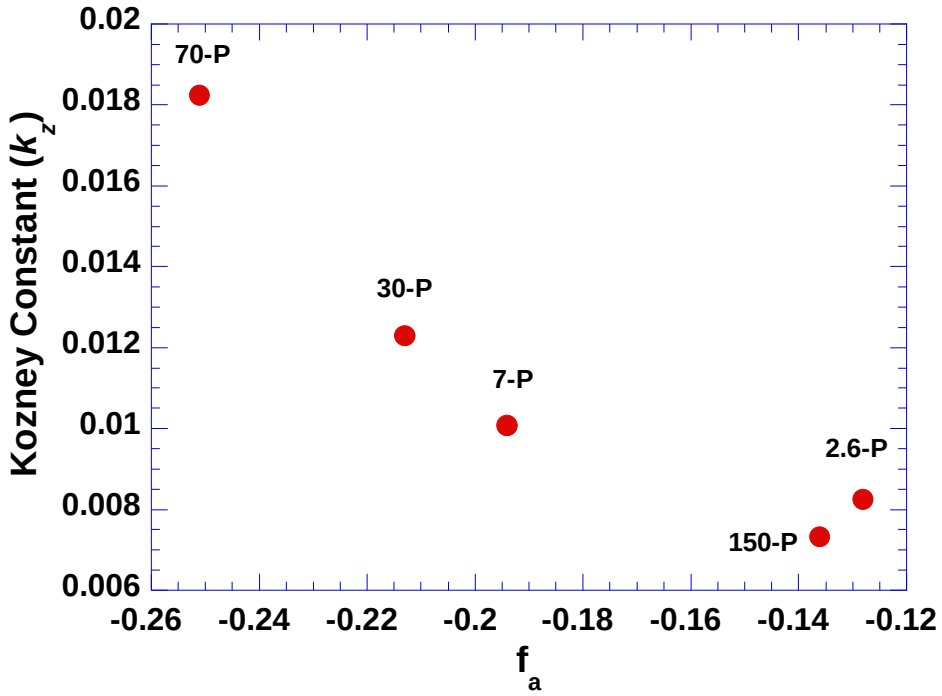

Figure 5.17. Relation between k_z (determined using smallest fiber diameter) and f_a

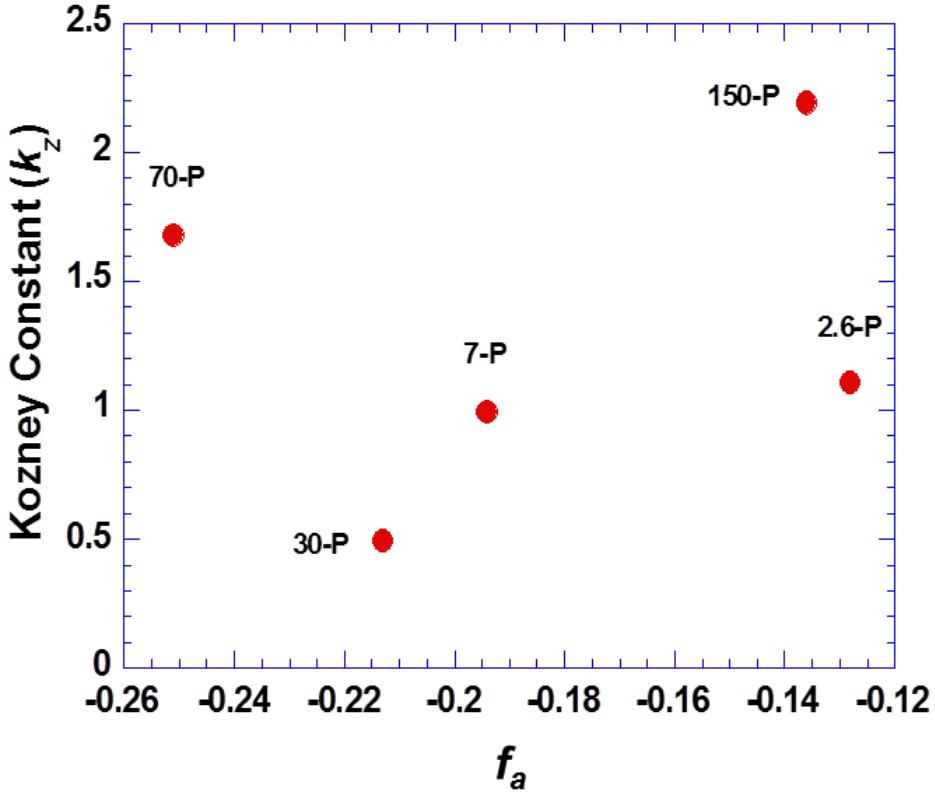

Figure 5.18. Relation between k_z (determined using average diameter) and f_a

The observed changes in f_p with punch density do not exceed "0". Since a value above zero would indicate a significant number of fibers aligned along the longitudinal direction, the changes in f_p indicate that the change in the frequency of fibers aligned along the longitudinal direction was not significant enough to cause a change in K_x and k_x. Hence, the dependence of K_x and k_x on f_p or f_a could not be discerned experimentally.

A value of f_a greater than -0.5 indicates that fibers are oriented in the out-of-plane direction and a value of 0 represents random orientation in 3D. The needle punched mats had f_a in the range of -0.128 and -0.251, suggesting more fibers are in the out-of-plane direction. Hence, the changes in the orientation of these fibers with needle punching are significant enough to cause the observed changes in K_z and k_z. A lack of correlation between f_p and k_z supports the above conclusion.

The value for k_x (27.6) was higher than those for k_z (0.007-0.019). The value for the Kozney constant reported in the literature [99] for unidirectional continuous graphite fiber prepregs varies from 0.68 for orientation parallel to the fiber axis, to 11 for orientation perpendicular to the fiber axis. However, there are no reports correlating fiber orientation with permeability in discontinuous mats. The negative values for f_p suggest that more fibers are oriented perpendicular to the longitudinal direction. Hence, the high value for k_x is believed to be due to more fibers being oriented in the direction perpendicular to the longitudinal axis along which permeability was measured. Similarly, values close to zero for f_a suggest that more fibers are oriented in 3D rather than in-plane alone. Hence, the low value for k_z is believed to be due to more fibers in the out-of-plane direction.

In order to study the impact of fiber diameter used to determine C in equation (5.3), the k_z determined using average fiber diameter is plotted in Figure 5.18 as a function of f_a.

Because of a correlation between k_z and f_a in Figure 5.18, the smaller diameter that showed a good correlation (see Figure 5.17) was used to determine C, which was correlated with K_x and K_z to determine k_x and k_z. Also, smaller diameter resulted in k_x and k_z values that are consistent with the values reported in the literature for Kozney constant. The reason for the lack of correlation at larger average fiber diameters is not understood. One possible reason is the idealization of the elliptical cross-section of the fibers to be circular.

5.3 Effect of Compaction Pressure during Composite Manufacturing on Structure of Composite

5.3.1 Thickness and Fiber Volume Fraction

The final thicknesses of composites, manufactured using various mats, are compared in Figure 5.18 for various molding pressures. The thickness of the mats used in manufacturing the composites is denoted as "As received" in Figure 5.19. It can be inferred that the degree of compaction (i.e. reduction in thickness) for a mat composite decreased with an increase in compaction pressures, which is in line with the observation in Figure 5.2 for lubricated compaction. Moreover, the trend in "As received thickness" due to variation in the areal weight of the mats was also observed in the composite thicknesses, which decreased with an increase in punch density until 30-P and increased beyond that. This highlights the influence of areal weight and thickness of mats on the thickness of mat composites.

The experimentally measured fiber volume fraction in the composites is plotted in Figure 5.20 as a function of compaction pressure for various mat composites. The V_f at zero pressure corresponds to fiber volume fraction in dry mats. Although the V_f increased with consolidation pressure as expected, the rate of increase and the V_f at a pressure varied with punch density used to manufacture the mats. The fiber volume fraction of the composite at a pressure increased with increase in punch density.

Despite having a higher thickness and lower V_f of the mat than 30-P composites (see Table 5.1), the 150-P composites had a higher V_f due to higher areal density of the mat. However, 70-P composite had a lower or equal V_f when compared to 30-P composite, despite having a higher areal density due to lower V_f of the mat.

Additional increase in the punch density (from 30 to 70) was not enough to compact the additional fibers due to higher areal density (see Table 5.1), resulting in the thickness and the V_f of 70-P mat to be lower than those of 30-P. These results confirm the variability in the compaction behavior, observed in Figure 5.2 for dry mats, due to needle punching.

5.3.2 FOD

Consolidation pressure, applied during manufacturing of composites, results in compaction as well as a change in FOD. The FOD in composites could not be obtained due to difficulties in imaging them. The small difference in density between the fiber and the matrix was not enough to resolve the fibers (specifically small fibers) during X-ray computed tomography. Hence, this FOD was obtained by an alternative method. The dry mat was subjected to various pressures (in the range encountered during manufacturing) and the FOD in the dry mat was determined as a function of pressure and used to interpret the effect of consolidation pressure.

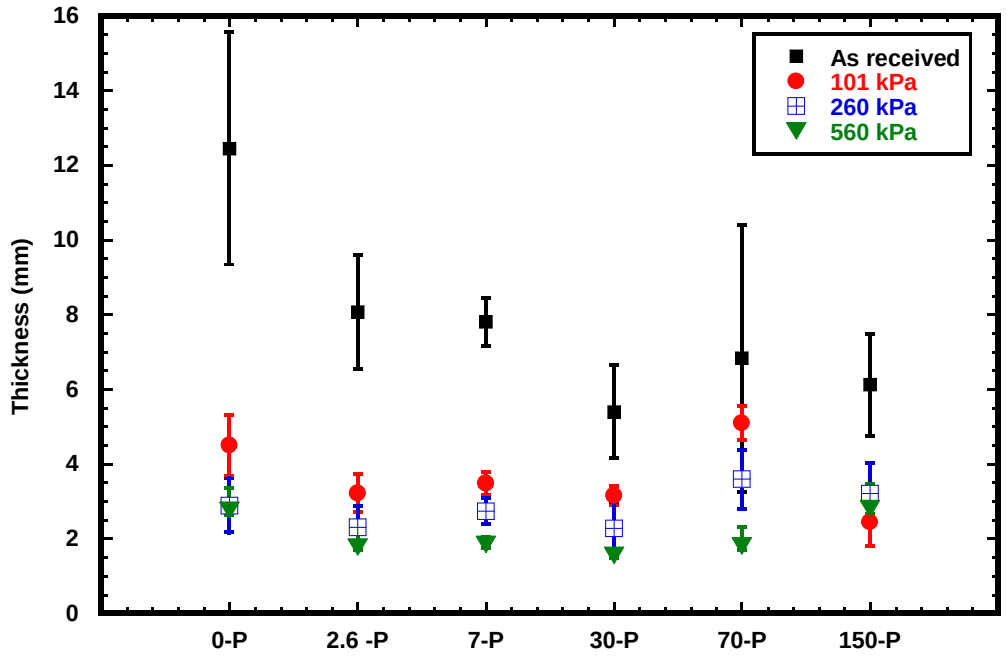

Figure 5.19. Thickness of composites as a function of consolidation pressure for various mats

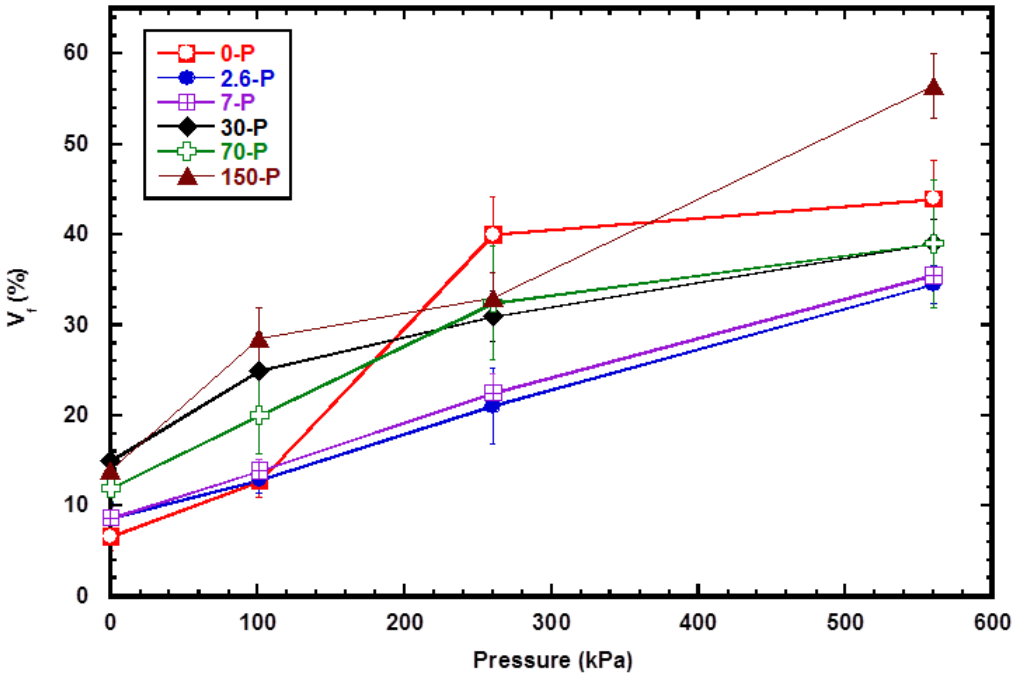

Figure 5.20. Effect of consolidation pressure on fiber volume fraction in composites

While this would be applicable for VARTM manufacturing where the pressure is applied before resin impregnation, at 260 kPa and 560 kPa, the mats impregnated with resin, were compacted. The liquid resin could lubricate the fibers altering the level of compaction (see Figure 5.2) and fiber reorientation during compaction. Hence, the influence of resin lubrication on the effect of pressure on FOD, presented below, has to be investigated in future work.

The influence of compaction pressure on FOD in 2.6-P is shown in Figures 5.21(a) and (b) for φ and θ respectively. With increasing the pressure to 101 kPa, the fibers rotated towards $\varphi = 0$ and $\theta = 90$. With a further increase in pressure to 260 kPa, the frequency of fibers near $\varphi = 0$ reduced and θ for fibers decreased towards 0^o. With further increase in pressure to 560 kPa the frequency of fibers reduced at certain angles and increased at others. Such a complex trend was observed in other mats also and plots for these mats are provided in Appendix C1 (Figure C.1 to C.4)

Due to the complexity in the interpretation of these curves, f_a and f_p are used to understand the effect of consolidation pressure on FOD. The f_p and f_a , determined using the FOD in Figures 5.21 and C.1 to C.4 are plotted as a function of pressure in Figures 5.22 and 5.23 respectively. The values at zero pressure correspond to the orientation factors for the dry mat before application of the pressure. It is obvious from these figures that the f_a and f_p changed with consolidation pressure and the magnitude of change in the FOD differed with punch density. When pressure was increased to VARTM (101 kPa) pressure, the f_p became more negative for all mats except 7-P. This means more fibers were rotated towards the transverse direction (i.e. $\theta = 90^o$). With further increase in pressure to 260 kPa, the f_p increased towards zero due to rotation to new angles as well as reduction in the frequency of fibers at certain angles.

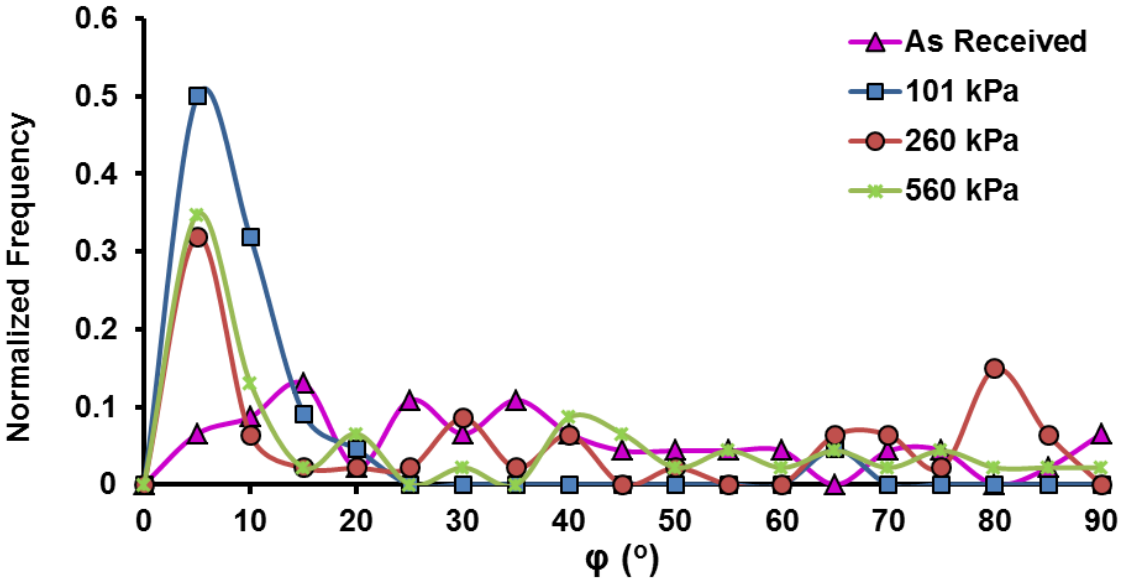

(a)

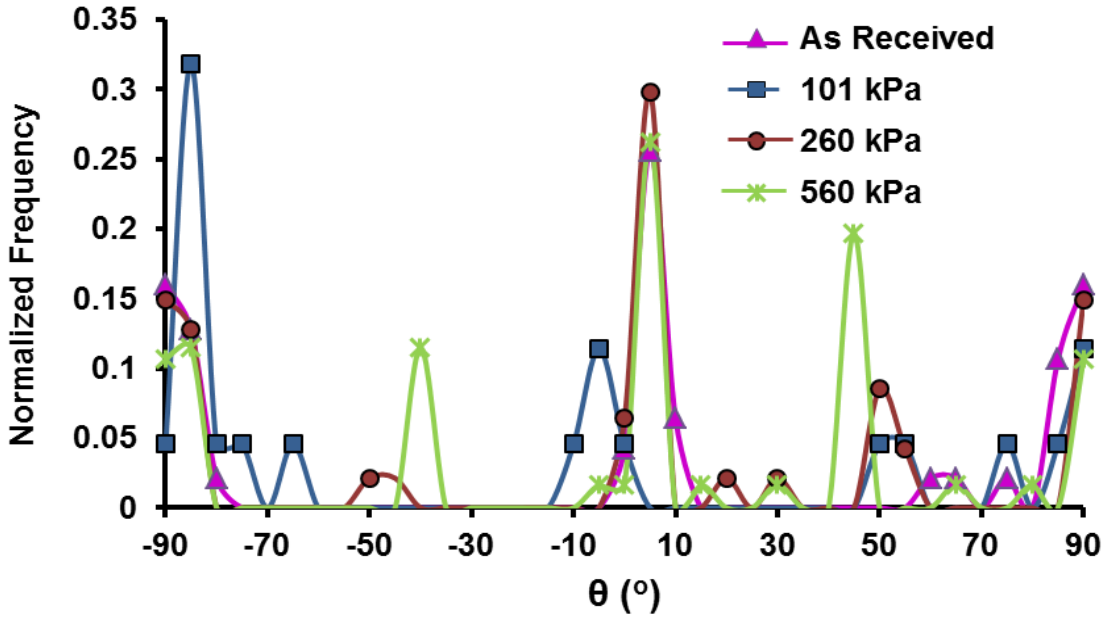

(b)

Figure 5.21. Effect of compaction pressure on FOD in 2.6-P
(a) out of plane orientation angle, φ (b) in-plane orientation angle, θ

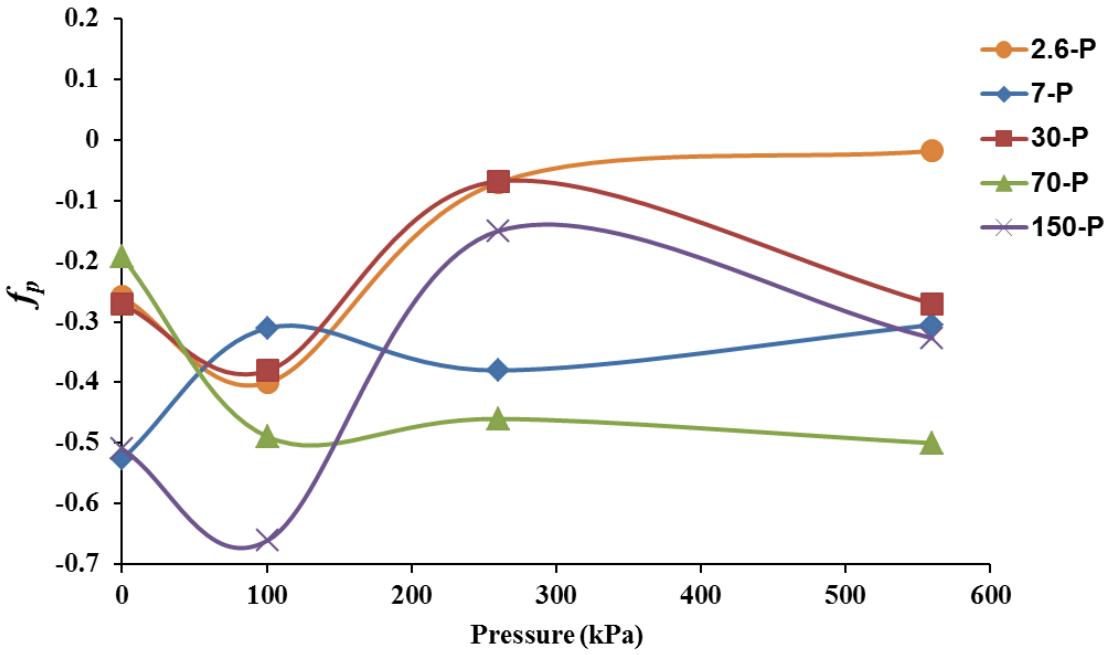

Figure 5.22. Effect of consolidation pressure on f_p

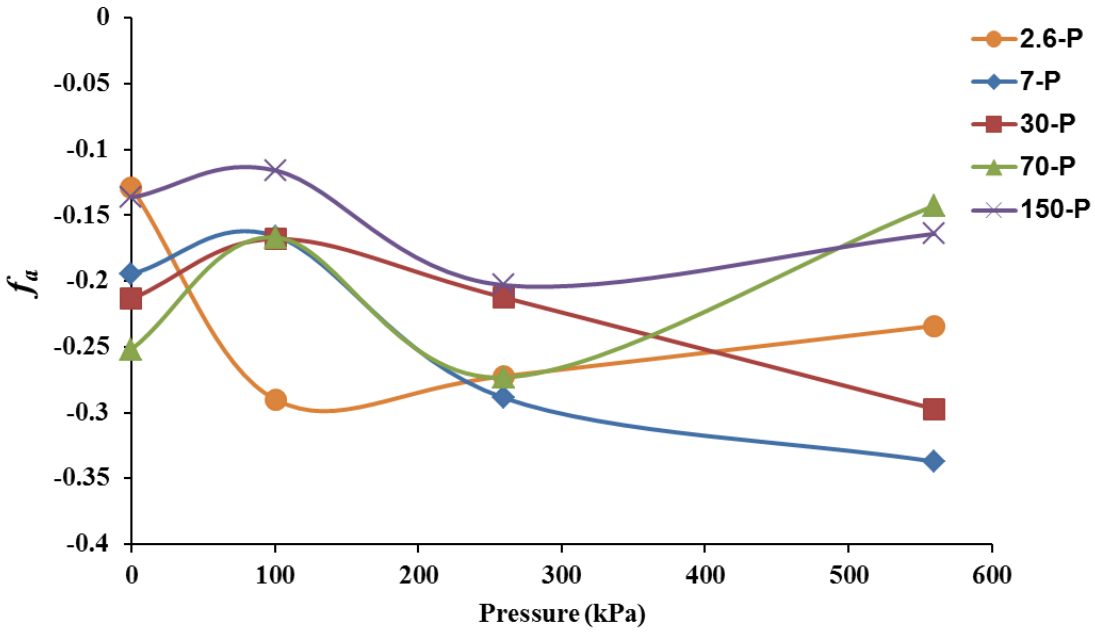

Figure 5.23. Effect of consolidation pressure on f_a

With further increase in pressure to 560 kPa, the f_p decreased for 30-P, 70-P and 150-P, and marginally increased for 2.6-P due to rotation and change in the frequency. The behavior at 560 kPa is similar (i.e. decrease in f_p) to that at 101 kPa. However, there is a sudden increase in f_p when pressure is increased from 101 to 260 kPa.

In order to understand this, a derivative of the curves in Figure 5.1 is plotted in Figure 5.24. This derivative corresponds to the rate of stiffening of the mat during compression. A monotonically increasing slope would represent stiffening; a decreasing slope would correspond to softening. All mats exhibited a peak in the curve beyond which the slope decreased. The compressive stress corresponding to this peak differed with punch density; however, the stress values were greater than 101 kPa. Such softening is believed to be the reason for the sudden increase in f_p at 260 kPa.

The cause for this softening is not clearly understood at this time. Buckling of these fibers, oriented in the out-of-plane direction during needle punching, could be one possible reason. Further investigation is required to confirm this.

A similar reversal of trend at 260 kPa is observed in f_a, plotted in Figure 5.23. Exceptions to these general trends in f_p and f_a are 7-P in Figure 5.22 and 2.6-P punch in Figure 5.23. Reasons for this deviation are not understood at this time. Nevertheless, the data in these figures highlight the complex interaction between the consolidation pressure applied during manufacturing and the mat structure after needle punching in deciding the FOD in composites.

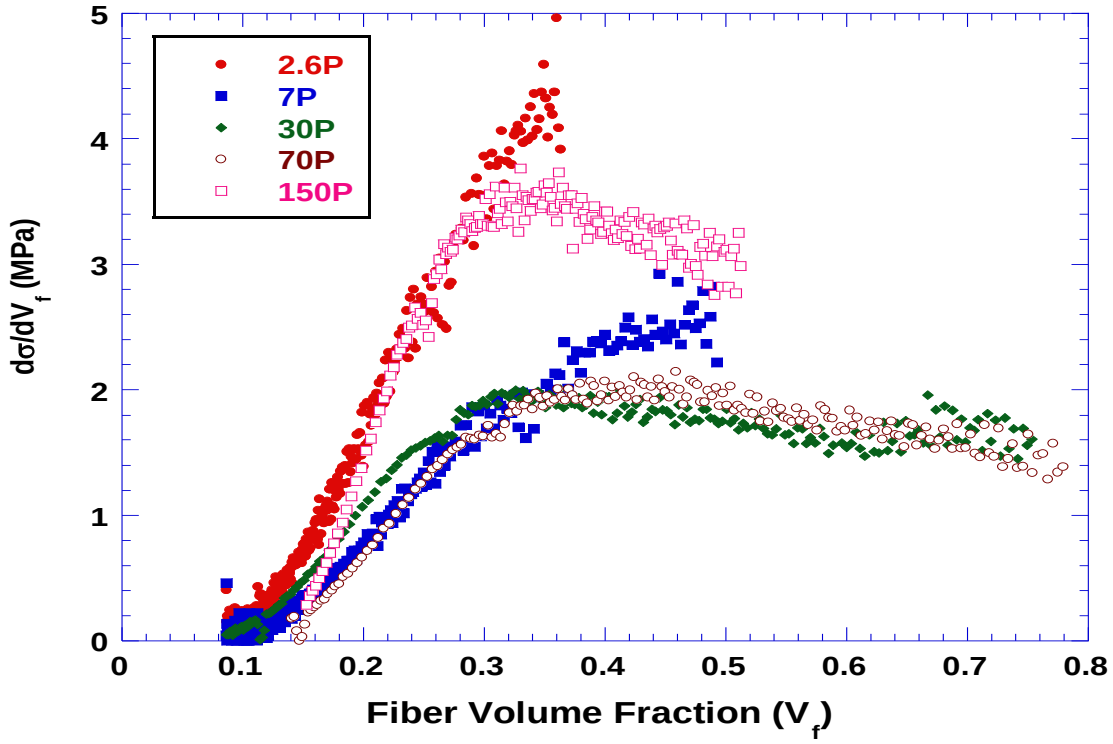

Figure 5.24. Derivative of volume fraction-pressure curves in Figure 5.1

5.4 Comparison of Predicted and Simulated FOD

As stated in Chapter 4, the modeling approach presented in Chapter 3 could not be used to predict the FOD due to the lack of information on inputs such as take-up roll velocity, friction coefficient, etc. These inputs are required to predict the change in the dimensions of the mat (Δx Δy, Δz) needed to predict the new orientations of the fibers using Equations (3.14) and (3.15).

A key assumption in this modeling approach is the pseudo-affine deformation assumption. According to this assumption, the deformation at the microscopic (i.e. fiber) level is the same as that at the macroscopic (i.e. mat) level. This allows the use of change in mat dimensions in Equations (3.14) and (3.15) to predict the rotation of fibers.

This key assumption was evaluated in this thesis by predicting the FOD using the FOD in 0-P mat and assumed values for Δx, Δy and Δz. These values were varied to obtain the best correlation between the experimental and the predicted FOD. The level of correlation was used to evaluate the pseudo-affine deformation assumption.

5.4.1 Influence of needle punch density on FOD in mats

The predicted FODs in φ and θ are compared with experimental FODs in Figures 5.25 and 5.26 respectively, for 2.6-P mat. The plots for other mats can be found in Appendix C.2 (Figure C.5 to C.8) While experimentally measured thickness of mats was used to determine Δz, the optimal values for Δx and Δy that resulted in the best correlation are tabulated in Table 5.5.

While the trend in FOD is predicted well, the accuracy of prediction of the frequency of fibers at an angle differed. It can be inferred from Figure 5.25 that the fiber reorientations in the range of $70 - 90^{o}$ for φ could not be predicted. This is thought to be due to lack of accurate description of FOD in the mat prior to needle punching for each punch density. The areal density of the 0-P mat was different from that of other mats. This difference, as well as heterogeneity in

fiber distribution within a mat could have resulted in a FOD for 0-P different from the FOD input to the model.

The orientation factors, f_p and f_a, determined using the predicted FODs are compared with orientation factors determined using experimental FODs in Figures 5.27 and 5.28, respectively for various punch densities. It can be observed that the proposed model could predict the experimental trend in FODs correctly. This supports the pseudo-affine assumption. The error in prediction of f_p is less than that of f_a.

One possible reason for the error is the accuracy of initial FODs input to the model, as discussed above. A second reason is the lack of accounting for the effect of multiple strokes. The number of strokes increases with punch density; 55, 150, 630, 1500 and 3214 strokes/min for 2.6-P, 7-P, 30-P, 70-P and 150-P respectively. A change in dimension per stroke would decrease with increase in the number of strokes since the mat would become increasingly stiffer due to compaction. Whereas, a constant average value for Δx, Δy, and Δz was used for each stroke. The error in f_p in Figure 5.27 increases with punch density, supporting this reasoning.

Table 5.5. The estimated amount of fiber displacement in a mat due to needle punching

Mat	Δx (mm)	Δy (mm)	Δz(mm)
2.6-P	-0.01	2.5	3.93
7-P	-0.01	0.5	4.20
30-P	-0.08	3	6.61
70-P	-0.01	2	5.17
150-P	-0.05	3	5.88

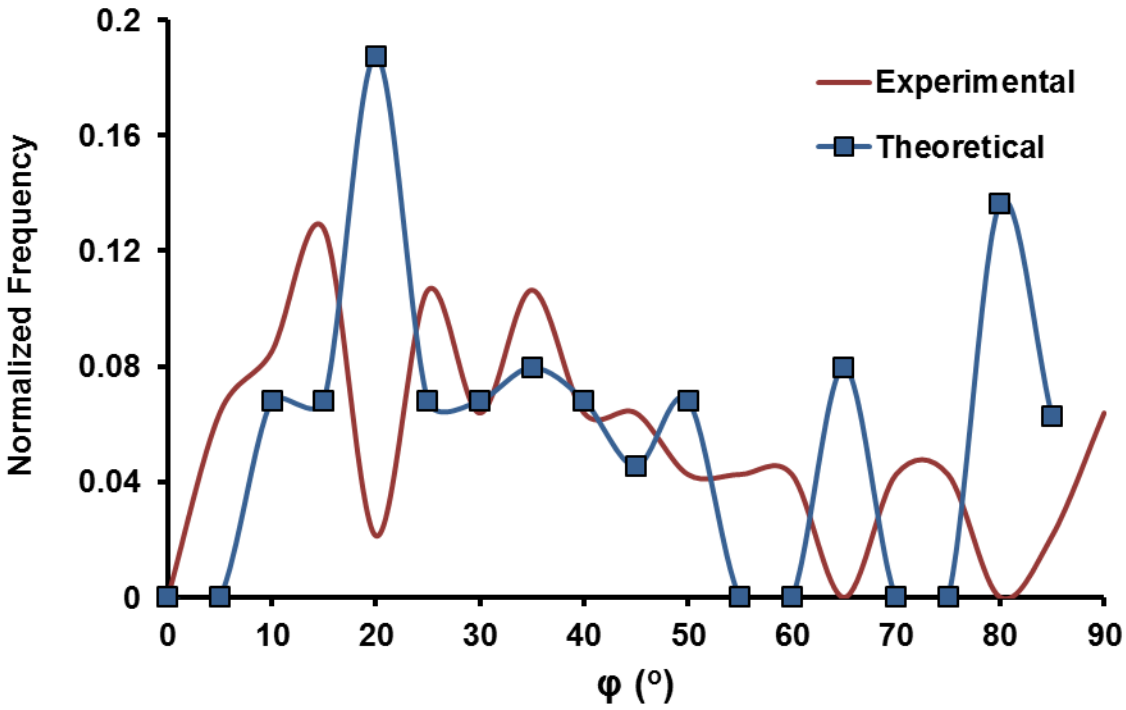

Figure 5.25. Predicted and experimental FOD for φ in 2.6-P mat

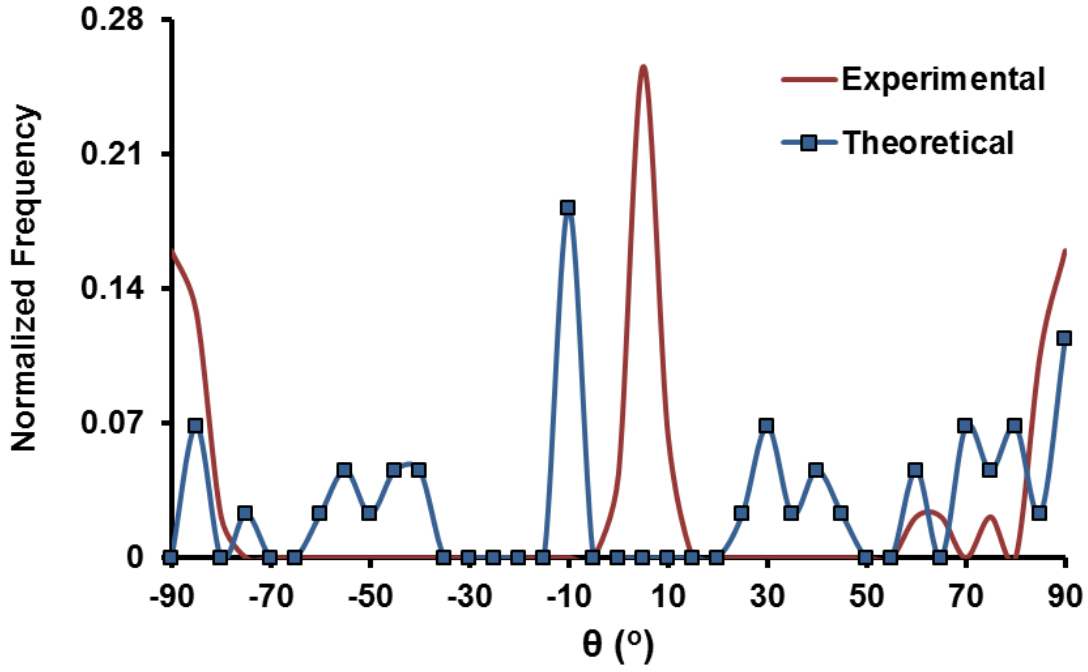

Figure 5.26. Predicted and experimental FOD for $\boldsymbol{\theta}$ in 2.6-P mat

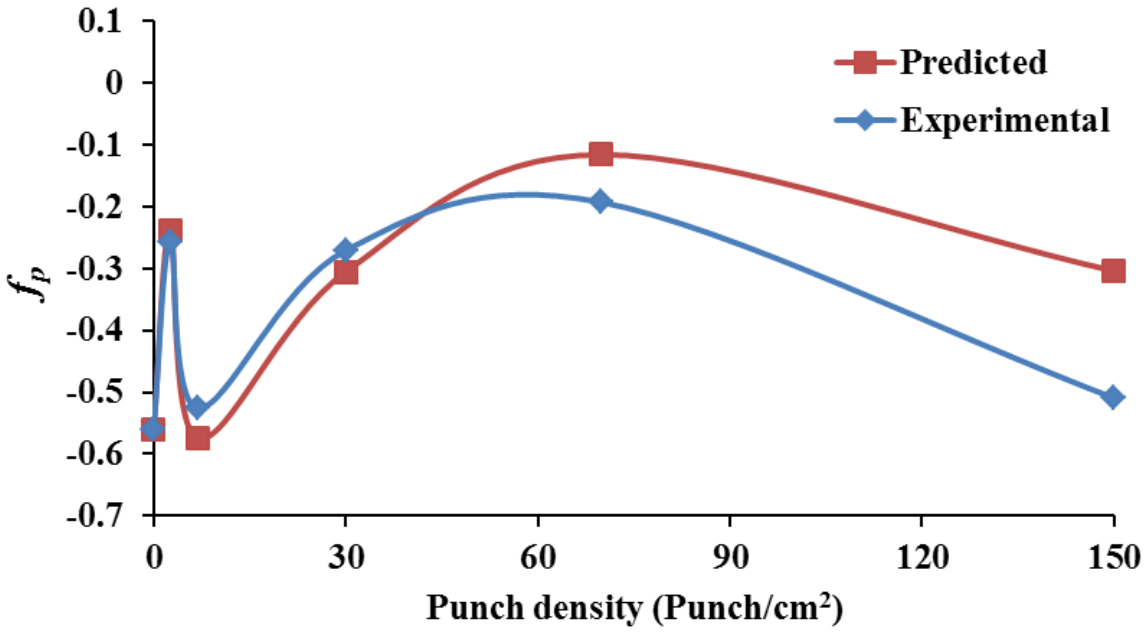

Figure 5.27. Predicted and experimental f_p for different needle punch density mats

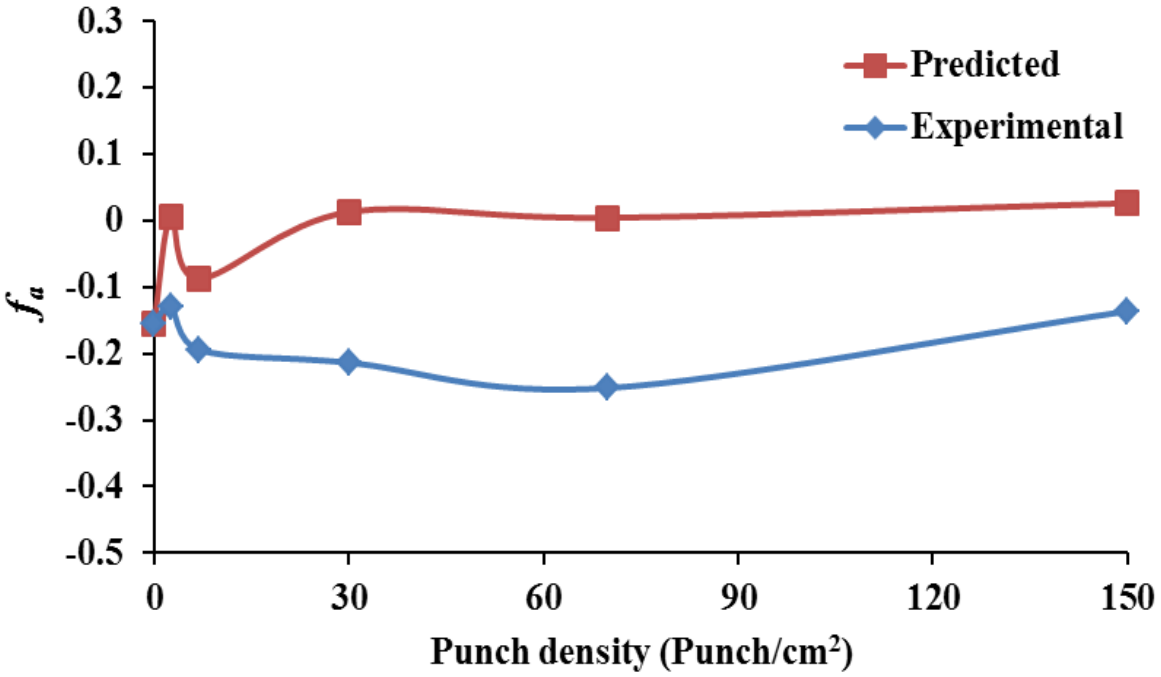

Figure 5.28. Predicted and experimental f_a for different needle punch density mats

5.4.2 Influence of consolidation pressure on FOD in composites

The change in FOD due to consolidation pressure was predicted using the FOD in a mat after needle punching. The predicted FOD in φ is compared with the experimental FOD at 101 kPa, 260 kPa, and 560 kPa in Figures 5.29 (a), (b), and (c), respectively, for 2.6-P mat. The predicted FOD in θ is compared with the experimental FOD at 101 kPa, 260 kPa, and 560 kPa in Figures-5.29 (d), (e), and (f), respectively, for 2.6-P mat. The plots for other mats can be found in Appendix C.3 (Figure C.9 to C.16) While experimentally measured thickness of mats was used to determine Δz, the optimal values for and Δx and Δy that resulted in the best correlation are tabulated in Table 5.6.

While the trend in the experimental FOD was predicted well, the accuracy of prediction of frequency at an angle differed.

The orientation factor, f_p, determined using the predicted FODs are compared with orientation factor, f_p, determined using experimental FODs in Figures 5.30(a) to (e) for 2.6-P, 7-P, 30-P, 70-P, and 150-P, respectively. The orientation factor, f_a, determined using the predicted FODs are compared with orientation factor, f_a, determined using experimental FODs in Figures 5.31 (a) to (e) for 2.6-P, 7-P, 30-P, 70-P, and 150-P, respectively. It can be observed that the model could predict the experimental trend in FODs correctly. This supports the pseudo-affine assumption. The error in prediction of f_p is less than that of f_a.

One major source of error in prediction is lack of accounting for elastic deformation of the fibers. The recovery in thickness after unloading is plotted in Figure 5.32 for all punch densities and pressures. (i.e. the difference between the thickness after unloading and thickness under load) is plotted in Figure 5.32 for all punch densities and pressures. There are Substantial recovery points to elastic deformation, which needs to be accounted for in any prediction.

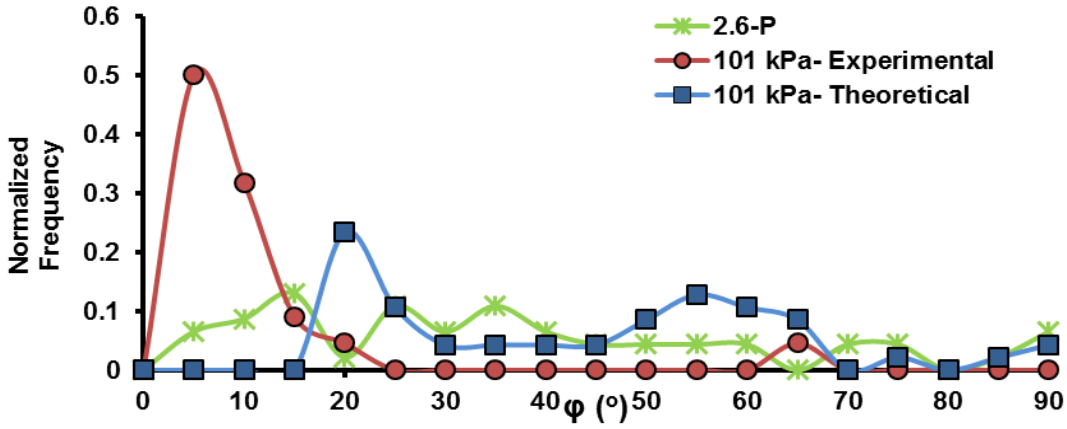

(a)

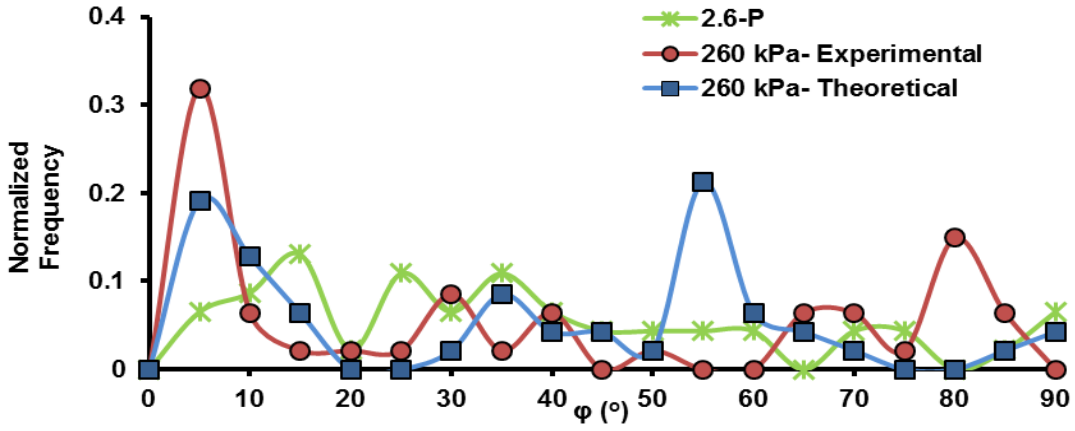

(b)

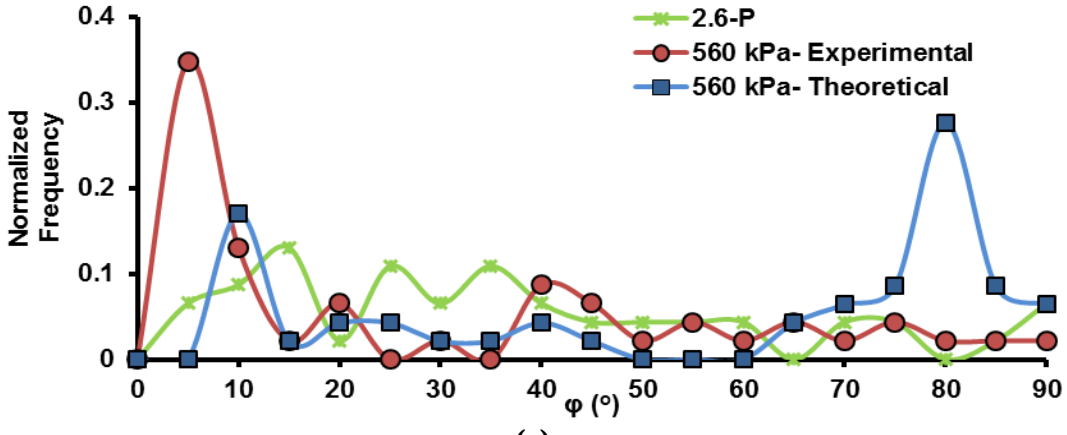

(c)

Figure 5.29. The predicted and experimental FOD in φ for 2.6-P mat in (a) 101 kPa and (b) 260 kPa (c) 560 kPa compaction pressure

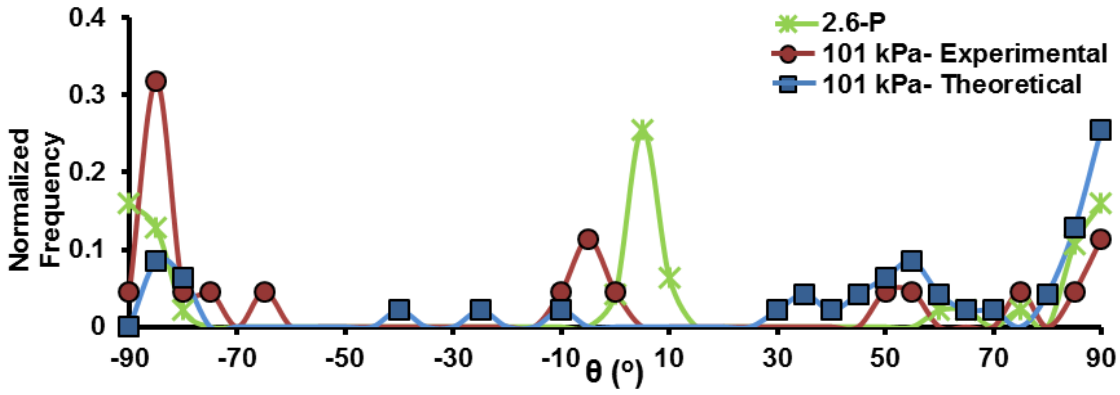

(d)

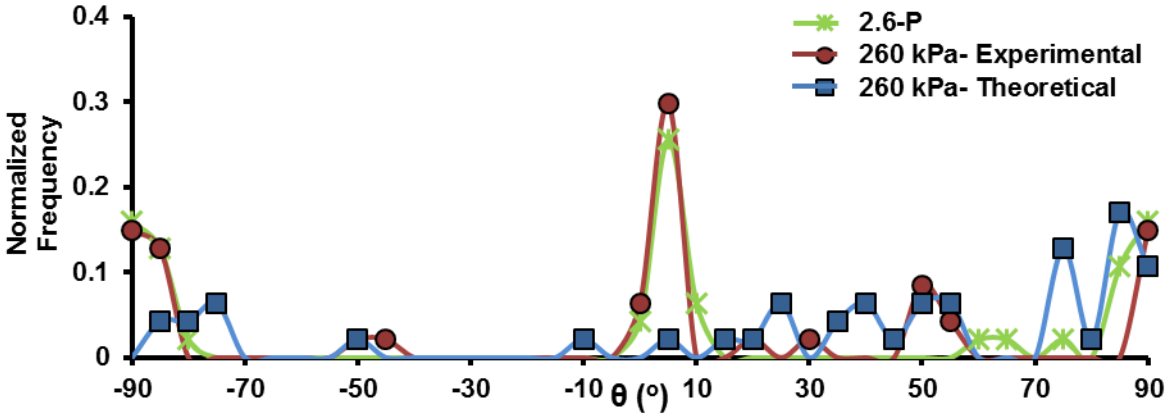

(e)

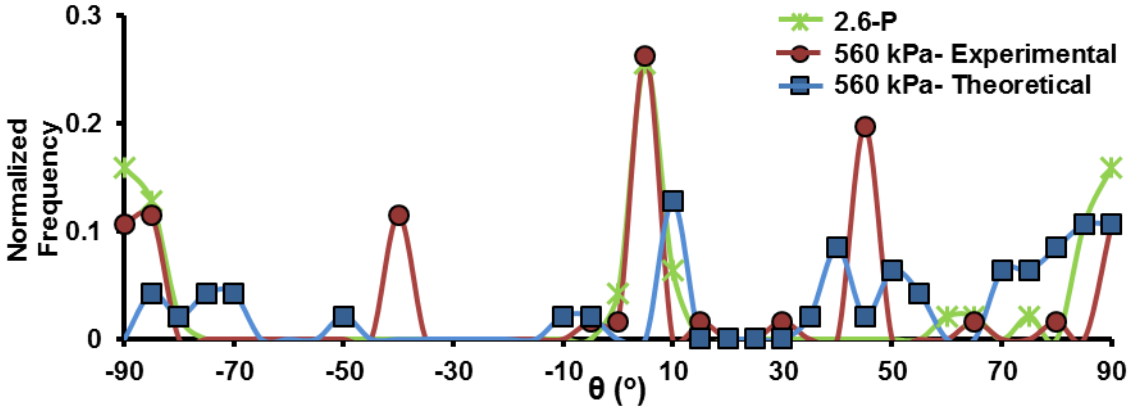

(f)

Figure 5.29. The predicted and experimental FOD in θ for 2.6-P mat in (d) 101 kPa, (e) 260 kPa, and (f) 560 kPa compaction pressure

Table 5.6. The estimated amount of fiber displacement in a mat due to manufacturing pressure

	101			260			560		
Mat	Δx *(mm)*	Δy *(mm)*	Δz *(mm)*	Δx *(mm)*	Δy *(mm)*	Δz *(mm)*	Δx *(mm)*	Δy *(mm)*	Δz *(mm)*
2.6-P	-0.01	2	1.56	-0.01	0.2	2.56	-0.01	0.16	3.27
7-P	-0.01	0.8	1.75	-0.01	1.5	2.59	-0.01	1.2	3.36
30-P	-0.01	8	0.46	-0.01	3	0.6	-0.01	4	1.02
70-P	-0.01	12	0.05	-0.01	9.5	0.53	-0.01	11.5	1.22
150-P	-0.01	6	0.24	-0.01	1.5	0.46	-0.01	2	1.04

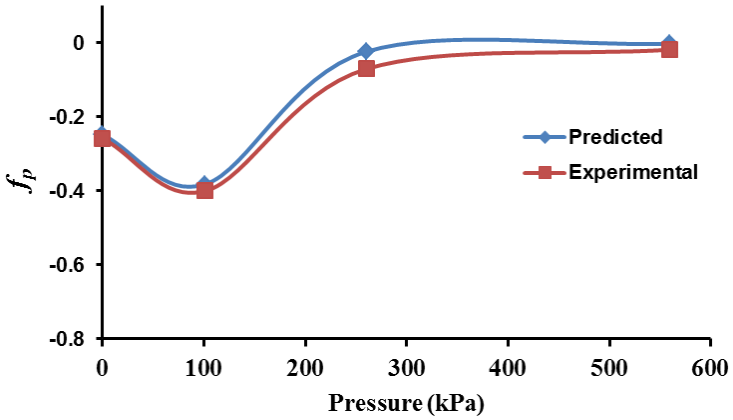

(a)

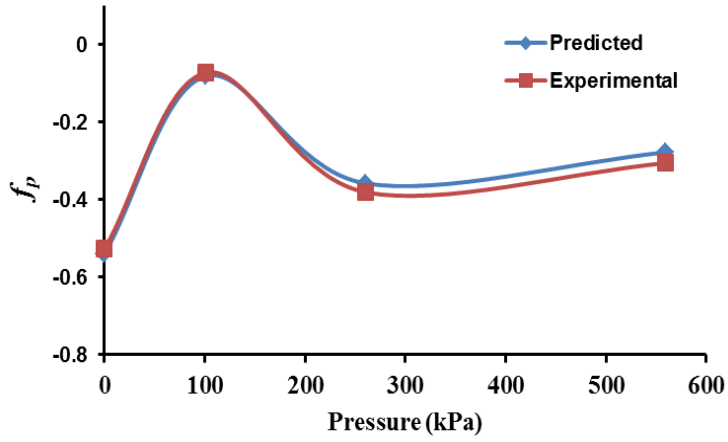

(b)

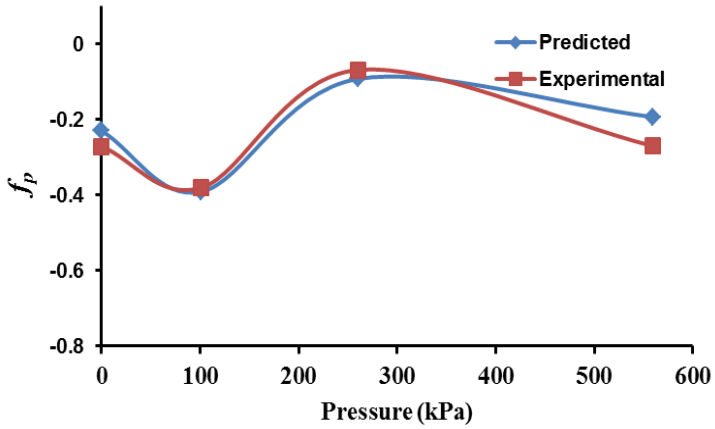

(c)

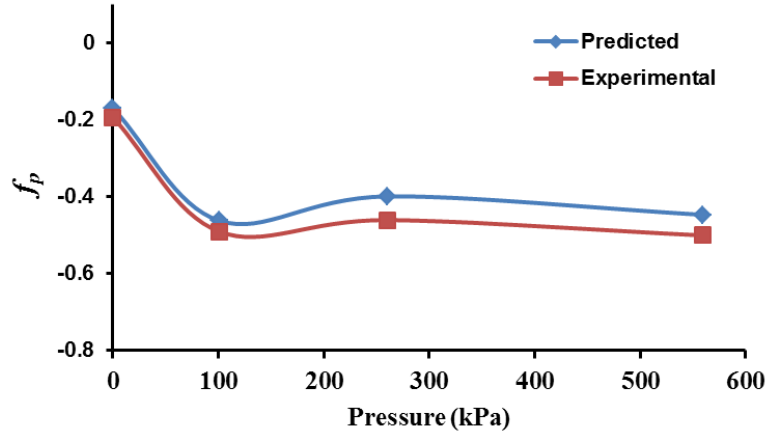

(d)

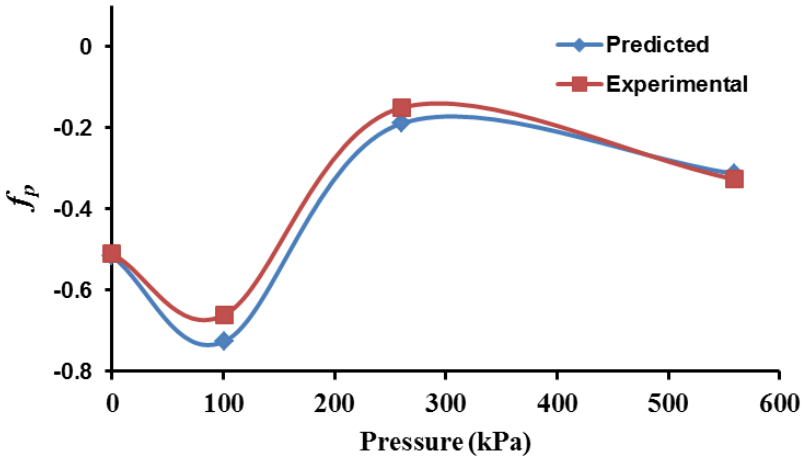

(e)

5.30. Comparison between predicted f_p and predicted values for (a) 2.6-P, (b) 7-P, (c) 30-P, (d) 70-P, and (e) 150-P

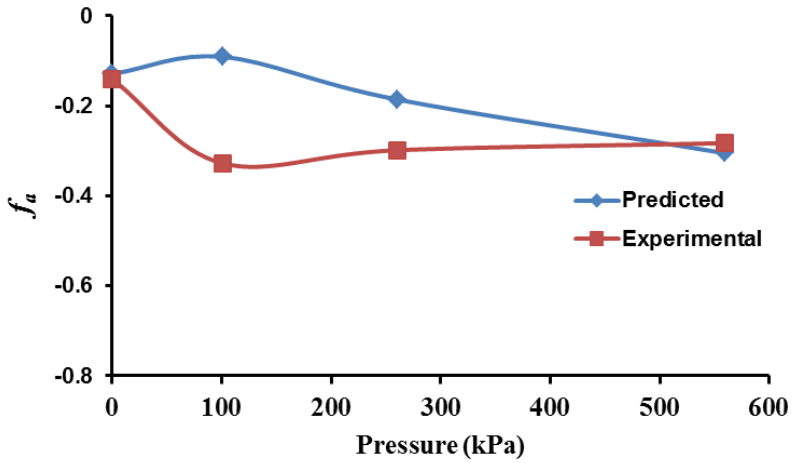
0
-0.2
-0.4
-0.6
-0.8
f_a
0
100
200
300
400
500
600
Pressure (kPa)
Predicted
Experimental

(a)

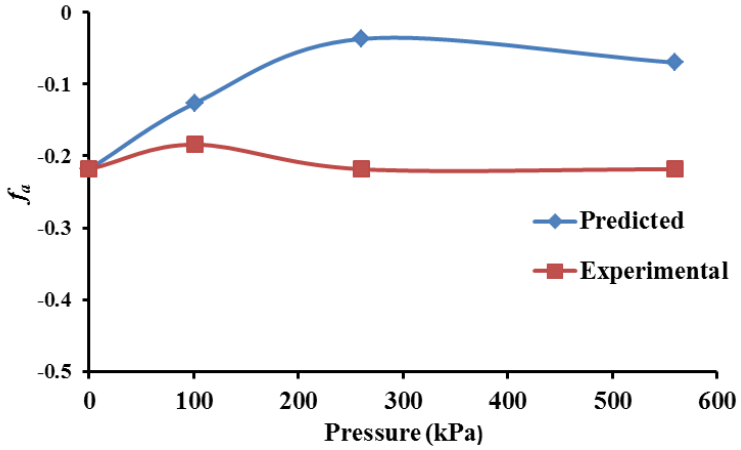
0
-0.1
-0.2
-0.3
-0.4
-0.5
f_a
0
100
200
300
400
500
600
Pressure (kPa)
Predicted
Experimental

(b)

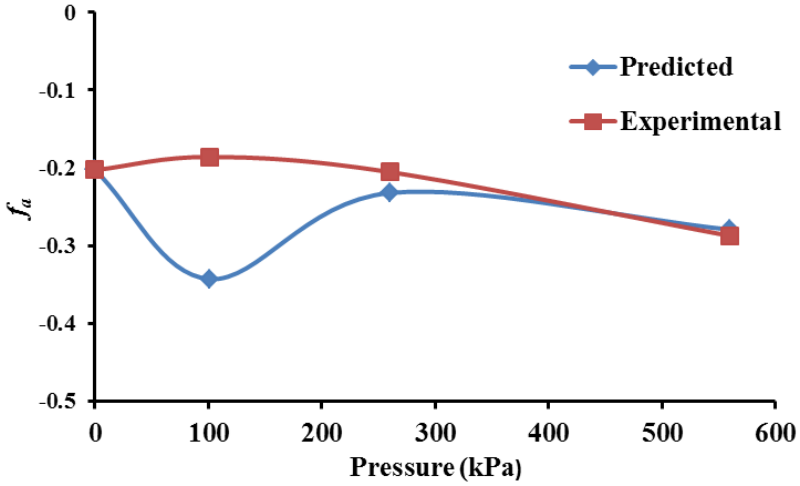
0
-0.1
-0.2
-0.3
-0.4
-0.5
f_a
0
100
200
300
400
500
600
Pressure (kPa)
Predicted
Experimental

(c)

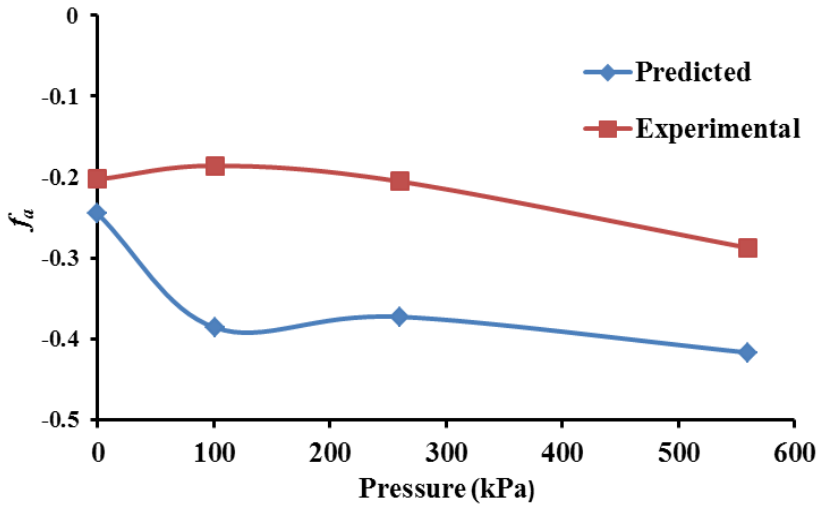

(d)

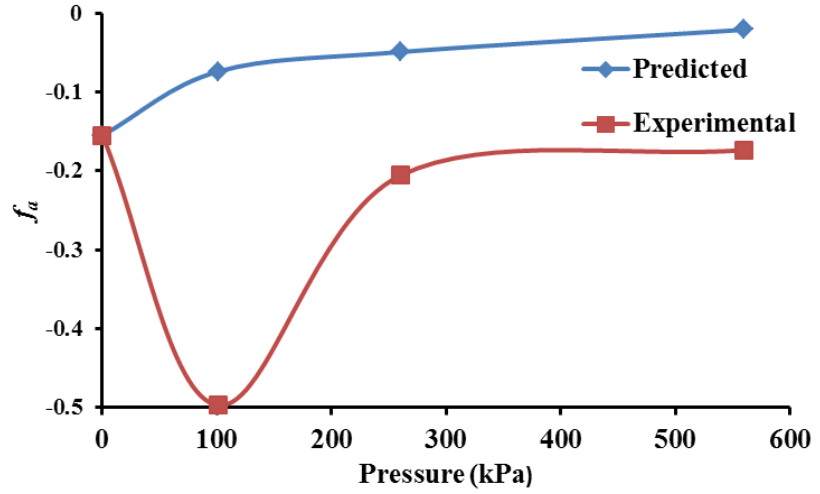

(e)

5.31. Comparison of predicted f_a with experimental values for (a) 2.6-P, (b) 7-P, (c) 30-P, (d) 70-P, and (e) 150-P

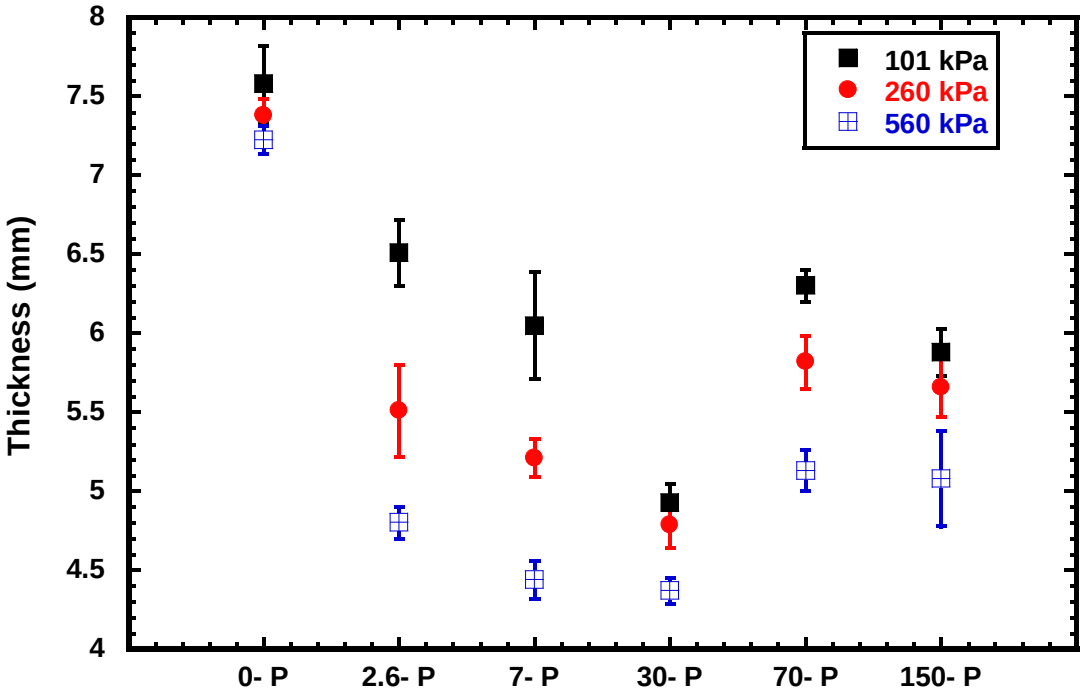

Figure 5.32. Recovered thickness after unloading from the compressive load

5.5 Composite Properties

5.5.1 Tensile Modulus – Experimental Results

A representative tensile test result is plotted in Figure 5.33. Results for neat resin (Stypol) and Stypol reinforced with glass fibers are also included for comparison. It is obvious that the hemp fibers reinforced the neat resin significantly; however, the level of reinforcement changed with mat density as indicated by the lack of superposition among stress-strain curves for various punch densities. It can also be inferred that the modulus of hemp fiber mat composites are comparable to that of glass-fiber composites.

All tensile test results are non-linear. The initial linear portion, identified in Figure 5.33, was used to determine the modulus of the composite. The experimentally determined modulus of composites manufactured using various mats are plotted as a function of fiber volume fraction in Figures 5.34 – 5.39. These values are also tabulated in Table 5.7. The modulus of the samples cut along the length of the mat (referred as longitudinal modulus) differed from the modulus of the samples cut along the width of the mats (referred as transverse modulus). Hence, results for these two moduli are plotted separately. The modulus for the neat resin is also plotted in all these figures. Three samples were tested at each pressure.

The composite panel manufactured at a given pressure exhibited spatial variation in fiber volume fraction (V_f) due to heterogeneous fiber distribution within a mat. Hence, the measured fiber volume fraction in each of the tested sample for a single compaction pressure varied. Therefore, the data point for each sample is plotted instead of plotting the average value for each pressure. The V_f of composites increased with consolidation pressure; however, the increase was not linear (except 2.6-P and 7-P) as observed in Figure 5.20 and discussed in Section 5.3.1.

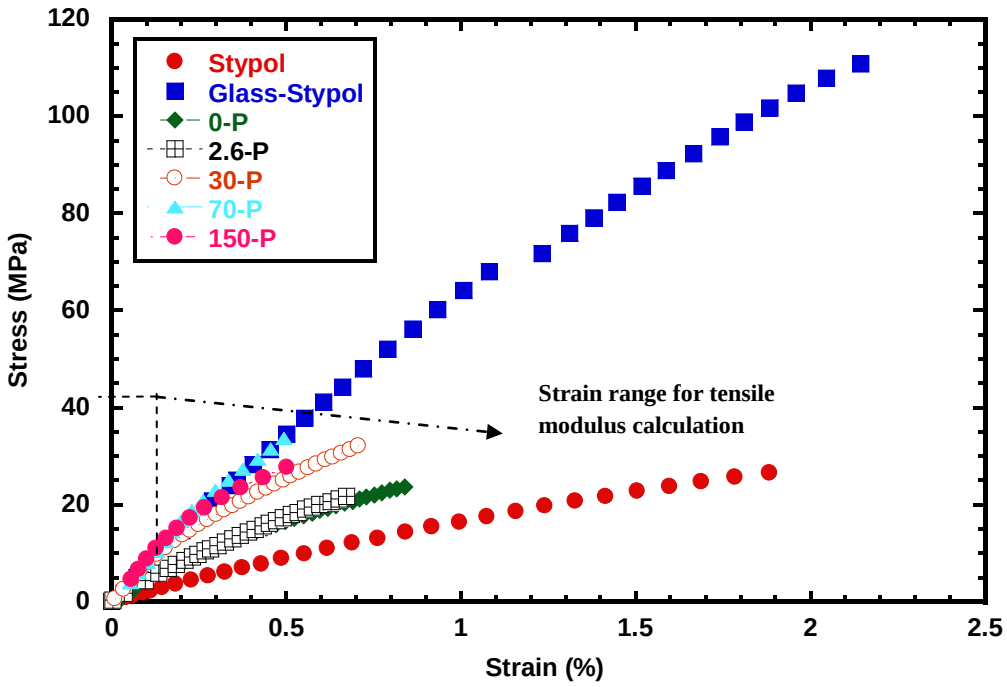

Figure 5.33. Stress-strain curve for needle punched composite manufactured at 101 kPa

Table 5.7. Experimental tensile modulus of needle punched composites at various manufacturing pressures

Composite	Manufacturing Pressure	V_f (%)	E_L (GPa)	E_T (GPa)		Composite	Manufacturing Pressure	V_f (%)	E_L (GPa)	E_T (GPa)
0-P	***101 kPa***	11-14	3.80	4.56		**30-P**	***101 kPa***	22-28	8.00	8.60
			4.29	5.25					8.20	9.30
			4.90	6.00					8.50	9.80
	260 kPa	42-43	7.80	8.90			***260 kPa***	29-33	7.19	6.90
			9.30	9.30					7.30	7.57
			9.50	10.30					8.10	7.90
	560 kPa	44-50	6.10	8.10			***560 kPa***	37-41	8.90	9.60
			6.80	10.30					9.25	10.30
			10.30	10.90					10.10	10.50
2.6-P	***101 kPa***	11.8-14	4.43	5.10		**70-P**	***101 kPa***	17-23	4.70	5.20
			5.50	5.30					4.80	6.40
			5.60	6.40					5.30	6.50
	260 kPa	18-24	4.60	4.60			***260 kPa***	28-37	7.30	5.27
			5.60	5.30					8.30	7.50
			5.70	5.70					13.00	8.00
	560 kPa	33-36	5.10	5.80			***560 kPa***	34-44	9.20	9.40
			5.50	5.80					10.00	13.50
			5.60	5.70					10.00	14.00
7-P	***101 kPa***	13-14.8	6.60	6.00		**150-P**	***101 kPa***	26-31	6.1	6.90
			6.90	7.60					6.9	7.50
			7.00	8.40					7	8.69
	260 kPa	21-24	3.60	4.60			***260 kPa***	31-35	7.8	8.30
			4.70	6.30					7.90	8.90
			4.70	6.30					7.95	8.95
	560 kPa	33-38	4.60	8.80			***560 kPa***	54-59	6.50	8.70
			4.90	8.80					9.00	10.10
			5.60	9.80					9.20	10.30

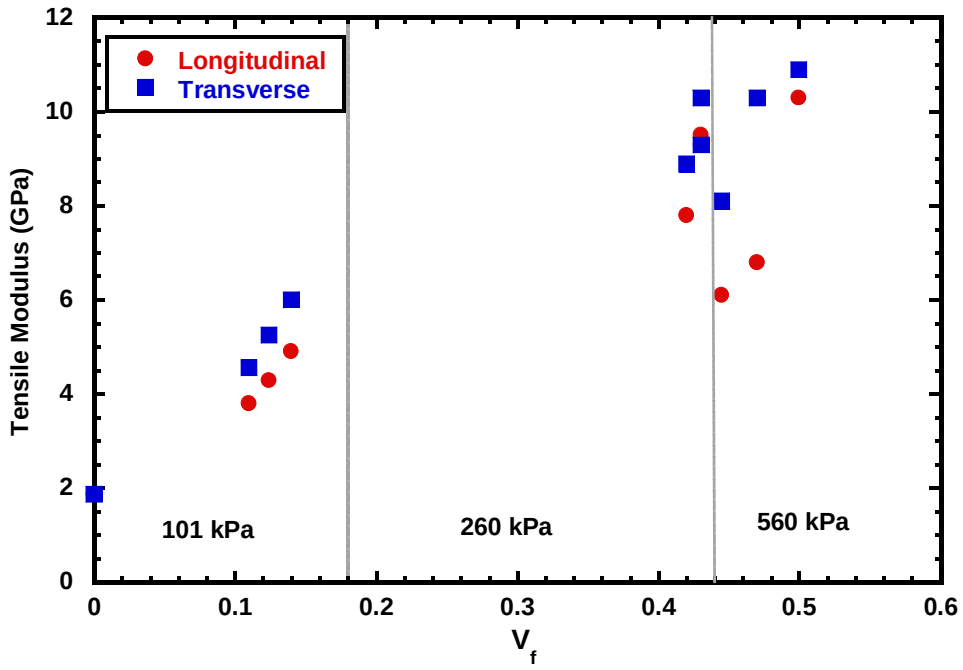

Figure 5.34. Experimental tensile modulus of 0-P composite in longitudinal and transverse direction

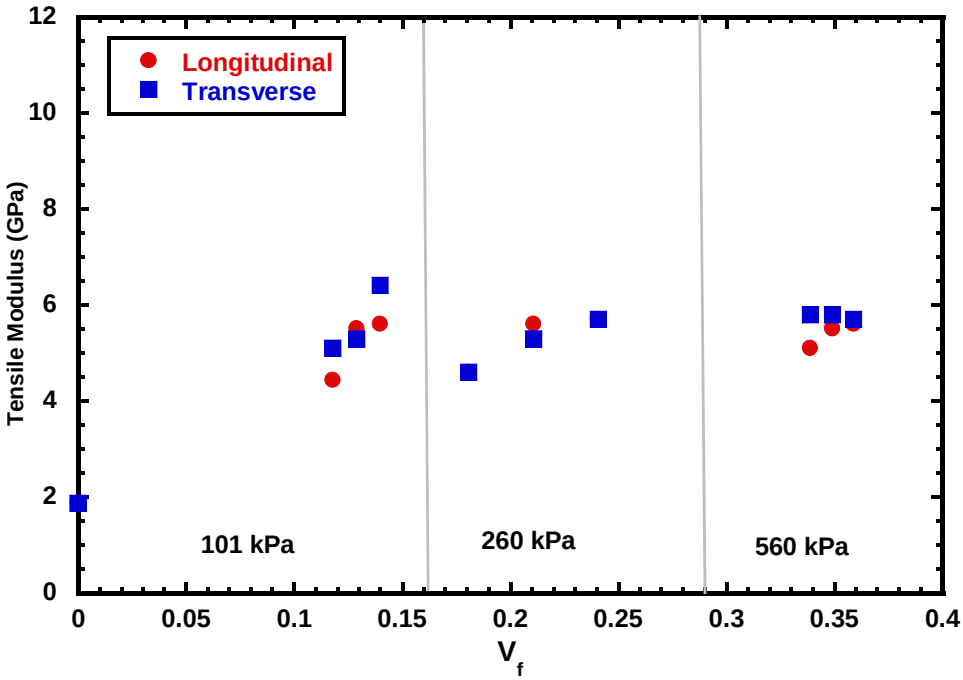

Figure 5.35. Experimental tensile modulus of 2.6-P composite in longitudinal and transverse direction

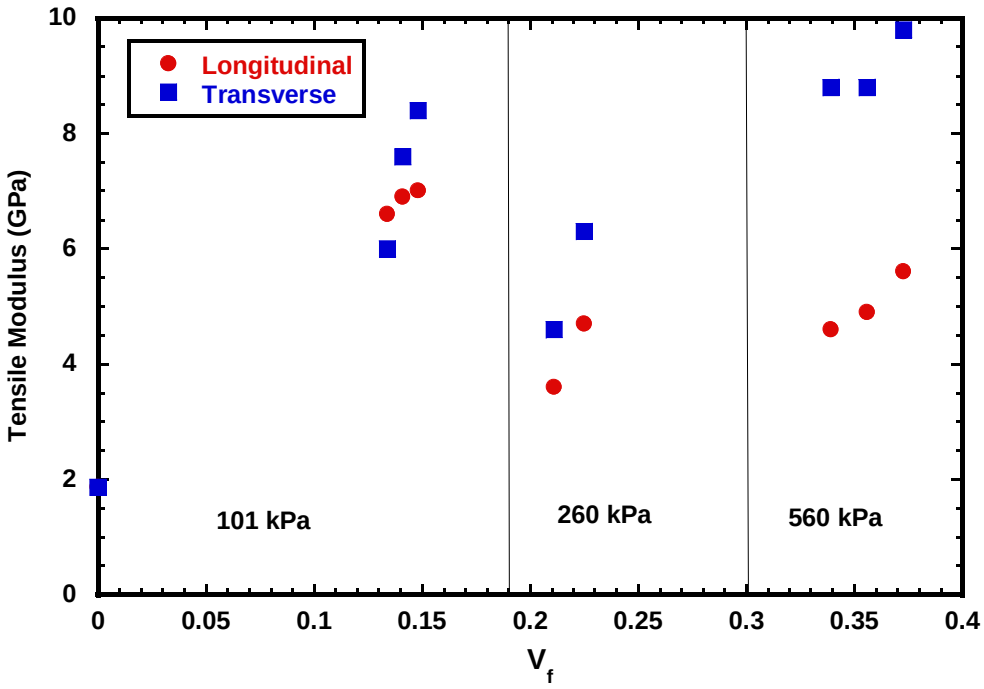

Figure 5.36. Experimental tensile modulus of 7-P composite in longitudinal and transverse direction

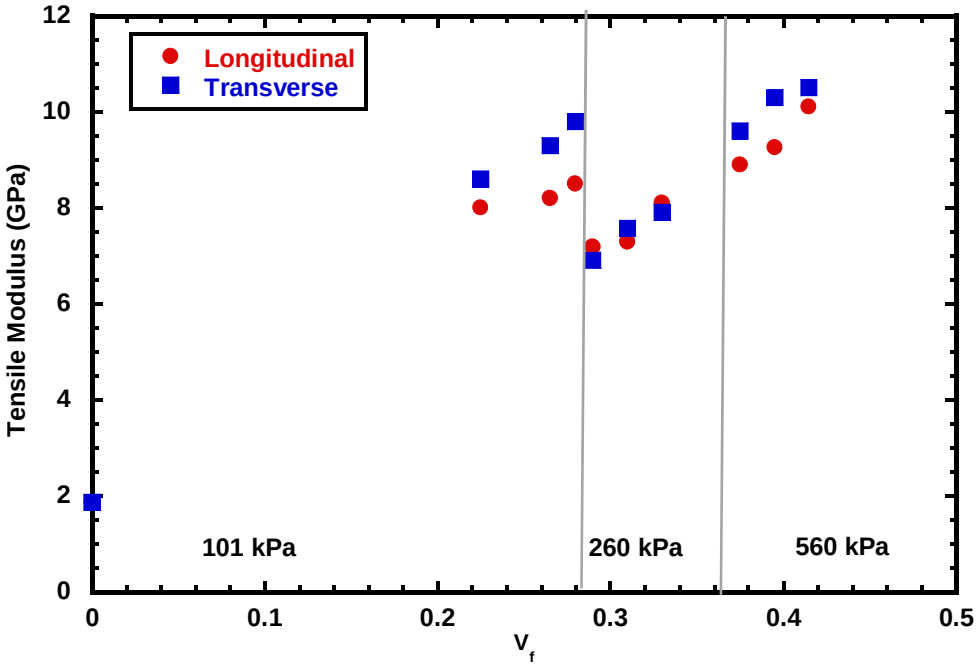

Figure 5.37. Experimental tensile modulus of 30-P composite in longitudinal and transverse direction

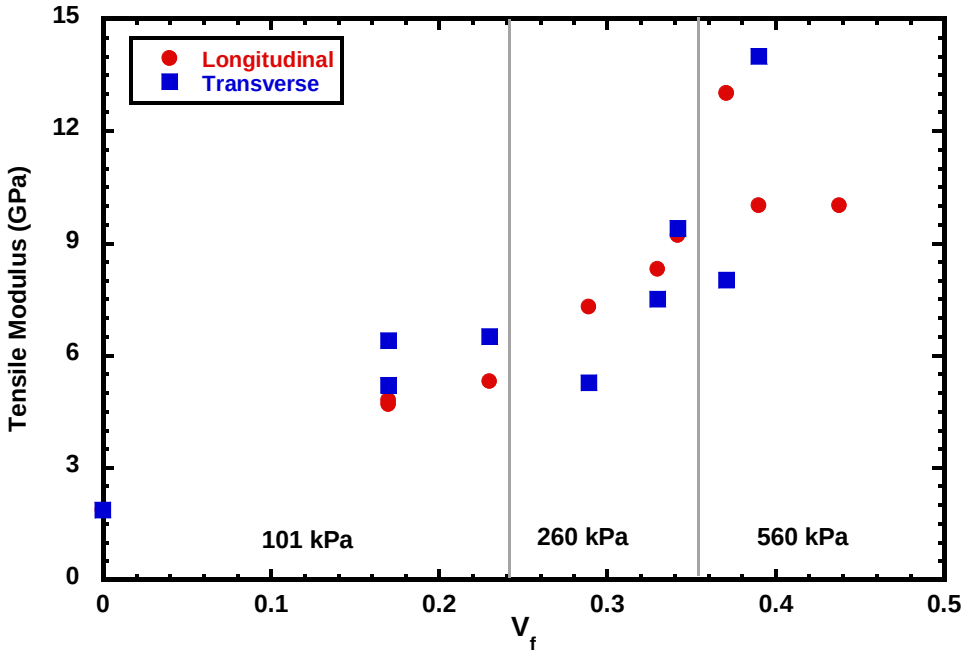

Figure 5.38. Experimental tensile modulus of 70-P composite in longitudinal and transverse direction

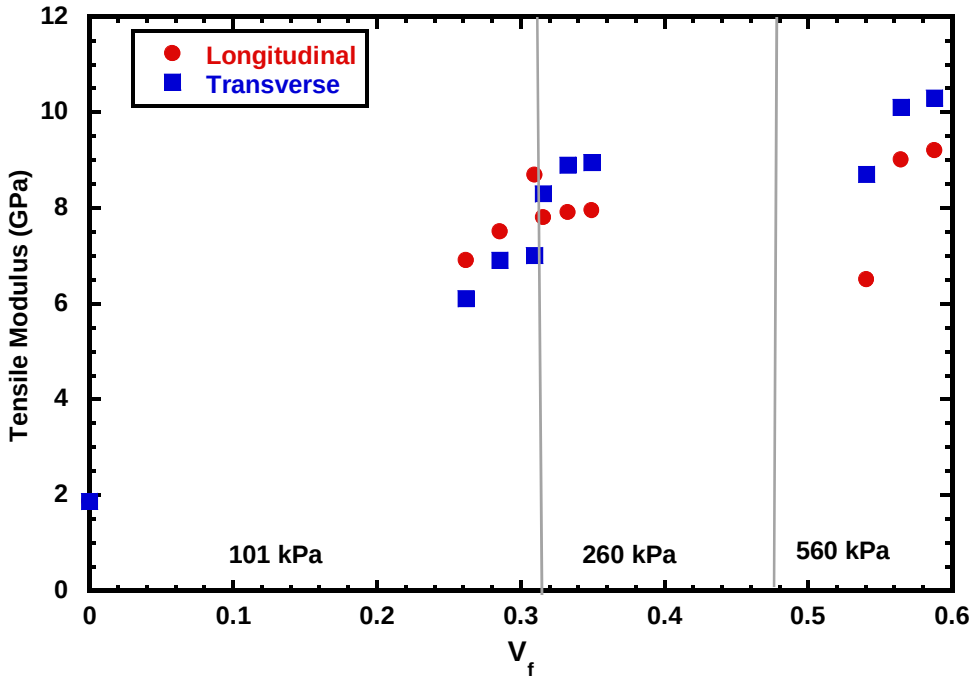

Figure 5.39. Experimental tensile modulus of 150-P composite in longitudinal and transverse direction

Despite this increase, the modulus did not follow the trend observed in V_f indicating that the FOD, which changed with pressure and punch density as observed in Figure 5.22, should have also influenced the modulus in addition to V_f. Hence, f_p plotted in Figure 5.22 is used to interpret the trend in moduli.

The values of -1 and $+1$ correspond to orientation of all fibers along the transverse direction ($\theta = 90^o$) and the longitudinal direction ($\theta = 0^o$) respectively. A value between -1 and 0 means more fibers are oriented at angles closer to 90^o than 0^o. A value between 0 and +1 means more fibers are oriented at angles closer to 0^o than 90^o. A value between -1 and +1 corresponds to a set of angles along which fibers in the composite are oriented. A value of 0 for f_p corresponds to a number of sets of orientations; for example, it can be random orientation, quasi-isotropic, bi-axial orientations with $\theta_1+\theta_2 = 90$, etc. The longitudinal modulus (E_x) is equal to the transverse modulus (E_y) only if $f_p = 0$. Hence, if $f_p < 0$, E_y will be higher than E_x and if $f_p > 0$, $E_y < E_x$. With increase in f_p from -1 to +1, E_y would decrease and E_x would increase. It should be noted that a given value of f_p can correspond to multiple sets of orientations, i.e. FODs. Hence, the magnitude of the modulus for a given f_p would depend on the FOD. The above generalizations need to be considered while interpreting the data in Figures 5.31 to 5.36.

It can be recalled from Figure 5.19 that the experimentally derived f_p is negative for all punch densities and pressures. Hence, E_y is expected to be higher than E_x. This indeed is observed in Figures 5.31 to 5.36 except when f_p is close to zero.

The difference between the moduli is small and masked by the variation in V_f. Hence, both moduli appear to be same (see 2.6-P at 260 and 560 kPa, 30-P at 260 kPa, 70-P at 260 kPa, 150-P at 101 kPa). The trend in moduli plotted in Figures 5.34 to 5.39 correlate very well with the trend in f_p as shown in Figure 5.22. When the pressure is increased from 101 to 260 kPa, the

f_p increased from negative value towards zero for 2.6-P, 7-P, 30-P, 70-P, and 150-P composites. Since fiber orientations corresponding to f_p values close to zero would be relatively more randomly oriented than those at 101 kPa, a reduction in modulus would be expected. This is observed for 2.6-P and 30-P in Figures 5.34 and 5.36, despite the increase in V_f suggesting that the decrease due to change in FOD was more than the increase due to change in V_f.

In addition to the change in the orientation angles, the frequency of fibers at each angle would also change when fibers rotate under compressive force as shown in Figure 5.21 and C.1 to C.4. These changes in frequency can increase or decrease the modulus depending on the orientation angle. This is believed to be the reason for no increase (rather than a decrease) in modulus in 70-P and 150-P composites. Despite a decrease in f_p, the modulus of the 7-P composite decreased when pressure is increased to 260 kPa, which is also believed to be due to this change in frequency of fibers for a given angle.

With a subsequent increase in pressure from 260 to 560 kPa, the modulus of 30-P, 70-P, and 150-P increased due to an increase in fiber volume fraction and a decrease in f_p. In the case of 2.6-P and 7-P, the f_p increased slightly. The reduction in modulus due to this change is believed to have offset the increase in modulus due to increase in V_f resulting in no change in modulus with increase in pressure to 560 kPa.

In order to understand the effect of punch density on the modulus, both the modulus and the fiber volume fraction values are averaged and tabulated in Table 5.8, for composites manufactured with VARTM pressure (101 kPa). The scatter in these values is also shown in this table.

For composites manufactured with VARTM pressure (101 kPa), the modulus increased with punch density until 30-P, which is believed to be due to an increase in fiber volume fraction

since the f_p values in Figure 5.19 are close to one another. With further increase in punch density, the above trend could not be clearly observed. Despite higher V_f, the modulus of 150-P composite is lower than that of 30-P and the modulus of 70-P is lower than that of 20-P composite. Since f_p values are different, the difference in FOD is believed to be the reason for this. The experimental data presented in Figures 5.34 to 5.39, are plotted together in Figure 5.40 and Figure 5.41 to highlight the trend in the effect of punch density on modulus at compaction pressures higher than 101 kPa. This plot shows no clear trend in the effect of punch density on modulus for a given fiber volume fraction, even though the fiber volume fraction increased with increase in the punch density. This behavior is due to the strong influence of FOD, which varied in a complex manner during composite manufacturing, as discussed above. This is confirmed in the next section by the good agreement between experimental modulus and the predictions based on the experimental FOD.

In contrast, the glass fiber mats, currently used in composites, are not needle punched and their composites do not show such a variation in modulus for a given fiber volume fraction. However, the modulus of 30-P hemp fiber composite is comparable to the modulus of the glass fiber composite despite slightly lower fiber volume fraction and lower fiber modulus (see Figure 5.33). Hence, increasing the needle punch density while manufacturing the natural fiber mats is definitely beneficial; however, there appears to be an optimal value, which in the case of hemp fibers used in this study is about 30-P for VARTM manufacturing.

Table 5.8. Experimental tensile modulus, strength and strain to failure of needle punched composites manufactured at 101 kPa

Compo-site	Fiber Volume Fraction (%)	Tensile Modulus (GPa)		Tensile Strength (MPa)		Strain to Failure (%)	
		Longitudinal	Transverse	Longitudinal	Transverse	Longitudinal	Transverse
Stypol 8086	0	1.869(±0.09)		34.6(±1.5)		2.54(±0.8)	
0-P	11.6 (±2.1)	4.11 (±0.48)	5.23 (±0.65)	18.36 (±3.14)	22.46 (±1.2)	0.59 (±0.2)	0.48 (±0.08)
2.6-P	12.8 (±1.1)	4.9 (±0.64)	5.59 (±0.61)	21.95 (±3.29)	25.7 (±2.3)	0.58 (±0.09)	0.48 (±0.05)
7-P	13.8 (±0.7)	6.86 (±0.18)	7.02 (±1.2)	29.50 (±2.27)	30.5 (±2.2)	0.54 (±0.03)	0.55 (±0.16)
20-P	16.4 (±1.9)	6.68 (±0.64)	6.9 (±0.6)	27.90 (±0.48)	30.0 (±1.7)	0.49 (±0.06)	0.50 (±0.07)
30-P	20.8 (±1.2)	8.29 (±0.18)	9.26 (±0.65)	36.20 (±3.02)	38.81 (±0.4)	0.62 (±0.07)	0.51 (±0.04)
70-P	18 (±3.0)	4.9 (±0.32)	6.03 (±0.32)	27.45 (±4.8)	29.7 (±3.17)	0.45 (±0.12)	0.72 (±0.08)
150-P	22.9 (±2.4)	6.66 (±0.076)	7.86 (±3.9)	25.9 (±2.82)	28.3 (±8.2)	0.49 (±0.07)	0.53 (±0.19)
Glass - Stypol	32.7 (±1.06)	8.5 (±1.4)		118.09 (±8.2)		1.8 (±0.48)	

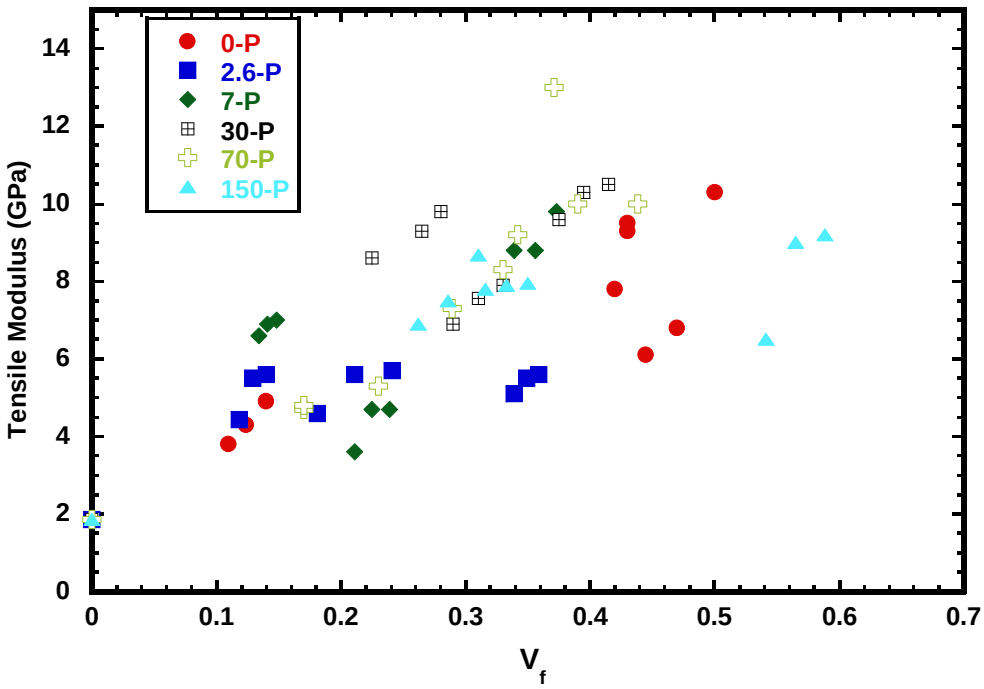

Figure 5.40. Experimental longitudinal modulus of all needle punched mat composites

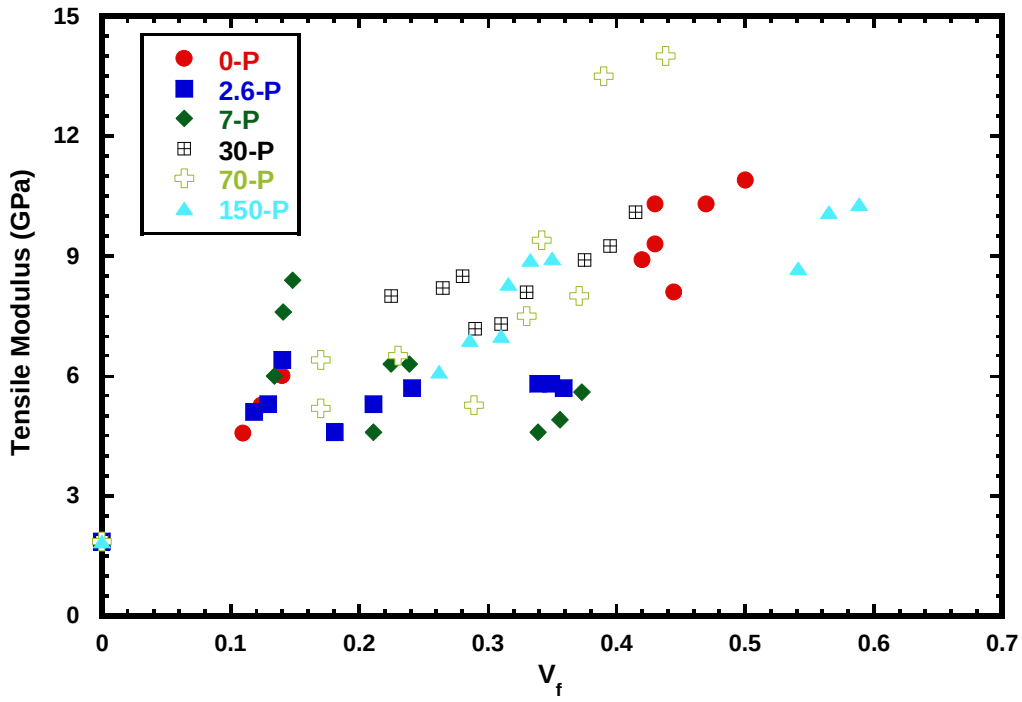

Figure 5.41. Experimental transverse modulus of all needle punched mat composite

5.5.2 Tensile Modulus – Predicted Results and Model Validation

The moduli of composites manufactured using hemp fiber mats with various punch densities were predicted using the model presented in Chapter 3, and using the procedure discussed in Chapter 4. These predictions are compared to experimental data in Figure 5.39 to Figure 5.50.

In addition, predictions using three commonly used micro-mechanical models, available in the literature, are also compared in Figure 5.42 to Figure 5.53 to evaluate the relative merits of the model developed in this study. The micro-mechanical models include the Simple Rule of Mixture given by equation 4.6 (ROM), Morais' Modified Inverse Rule of Mixture (IROM) by Equation (4.13) [117], and Halpin-Tsai model. Details of Halpin-Tsai Equation is presented in Appendix A.1.

The rule of mixture (ROM) predicts the upper boundary for the tensile modulus when all the fibers are oriented in the direction of the load. The inverse rule of mixture (IROM) predicts the lowest boundary for the tensile modulus of the composites when all the fibers are oriented perpendicular to the load direction. The experimental moduli were in between these two limits, as expected. In case of certain punch densities (0, 2.6,7, 30), the experimental moduli (either longitudinal or transverse) were found to be close to the value predicted by ROM. Since fiber orientations in these composites are not unidirectional, the predicted moduli by the rule of mixtures would be expected to be lower than what it should be. This can only be attributed to a low average fiber modulus used in the rule of mixtures. The predictions using the model developed in this thesis compare better with the experimental tensile modulus than the predictions using the rule of mixtures or Halpin-Tsai model.

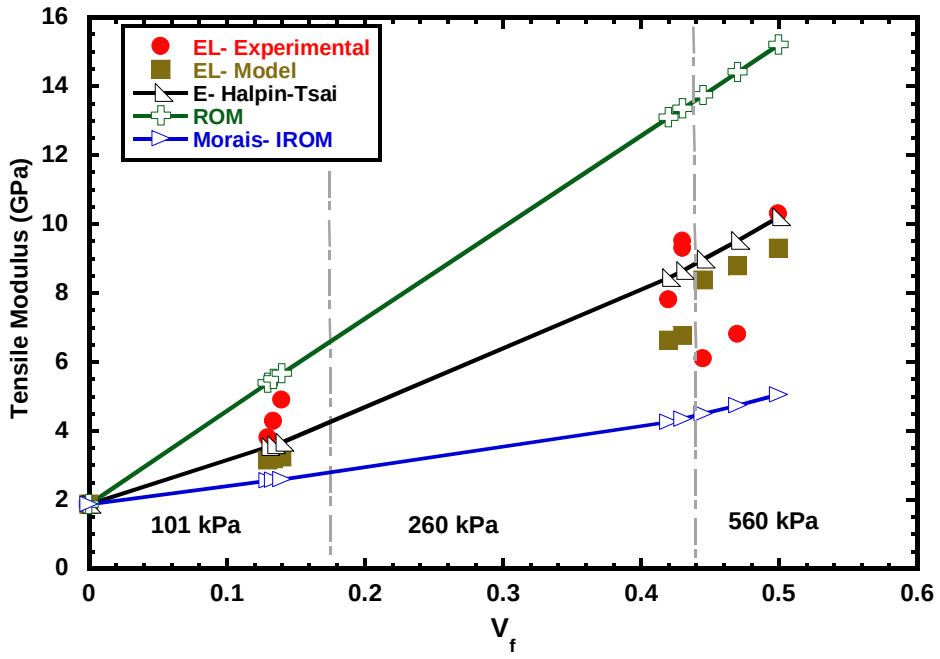

Figure 5.42. Theoretical and experimental longitudinal modulus of 0-P composite

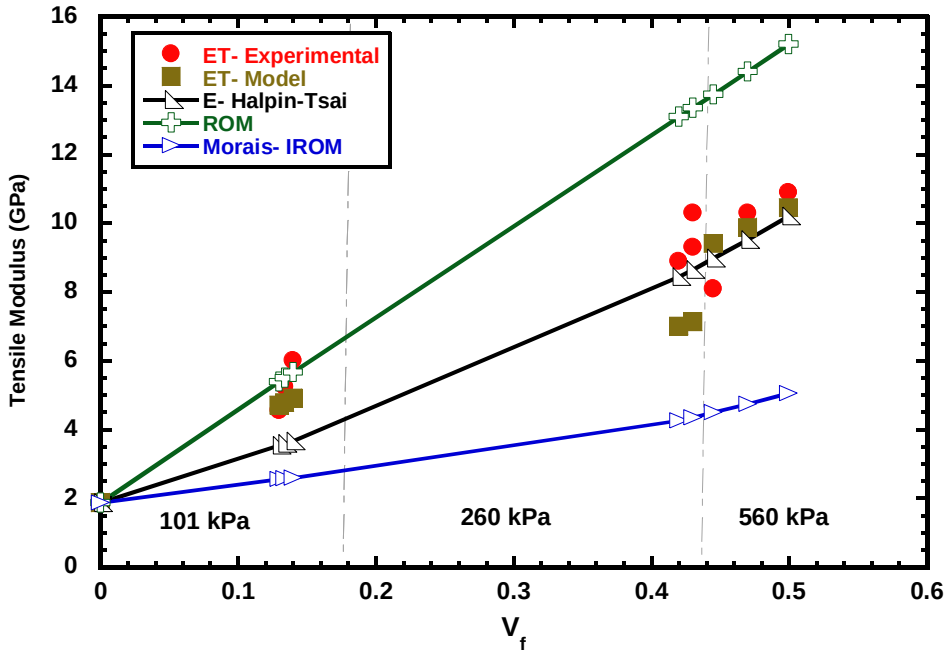

Figure 5.43. Theoretical and experimental transverse modulus of 0-P composite

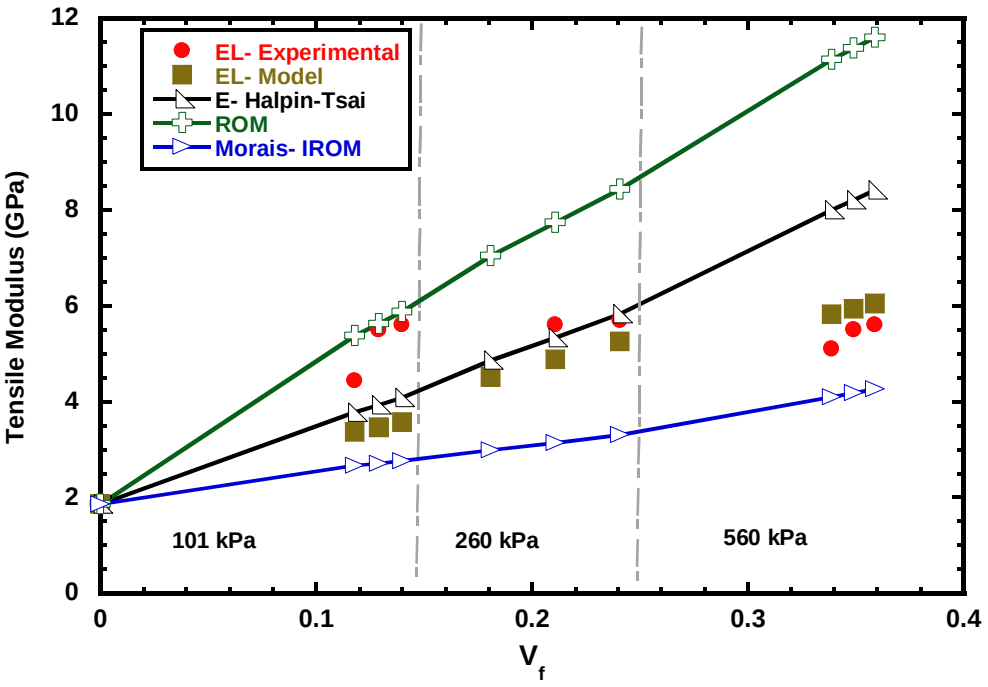

Figure 5.44. Theoretical and experimental longitudinal modulus of 2.6-P composite in longitudinal direction

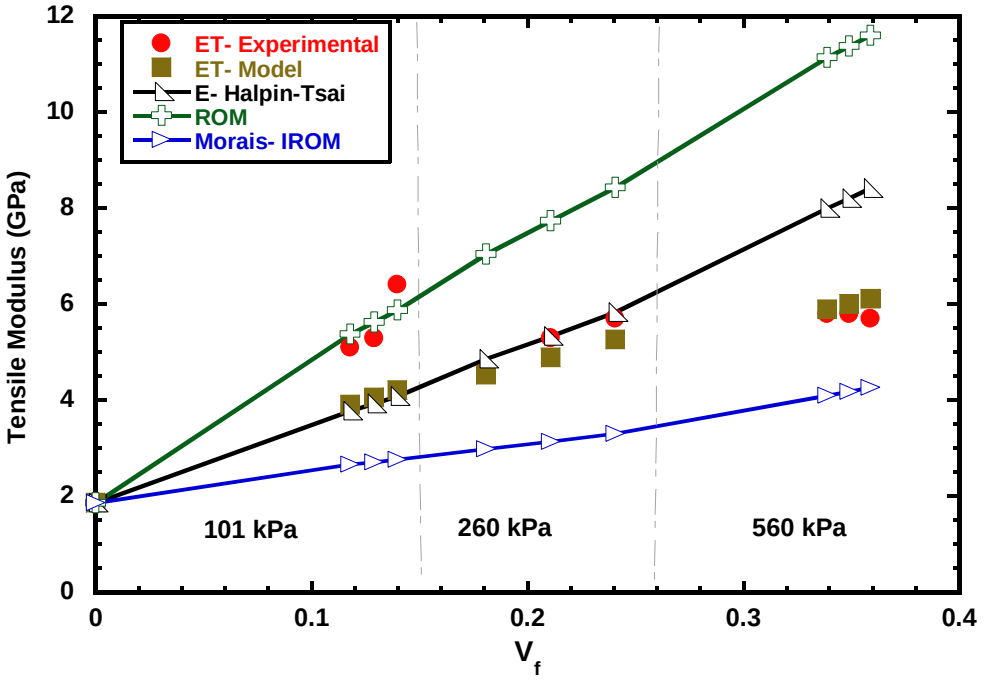

Figure 5.45. Theoretical and experimental transverse modulus of 2.6-P composite

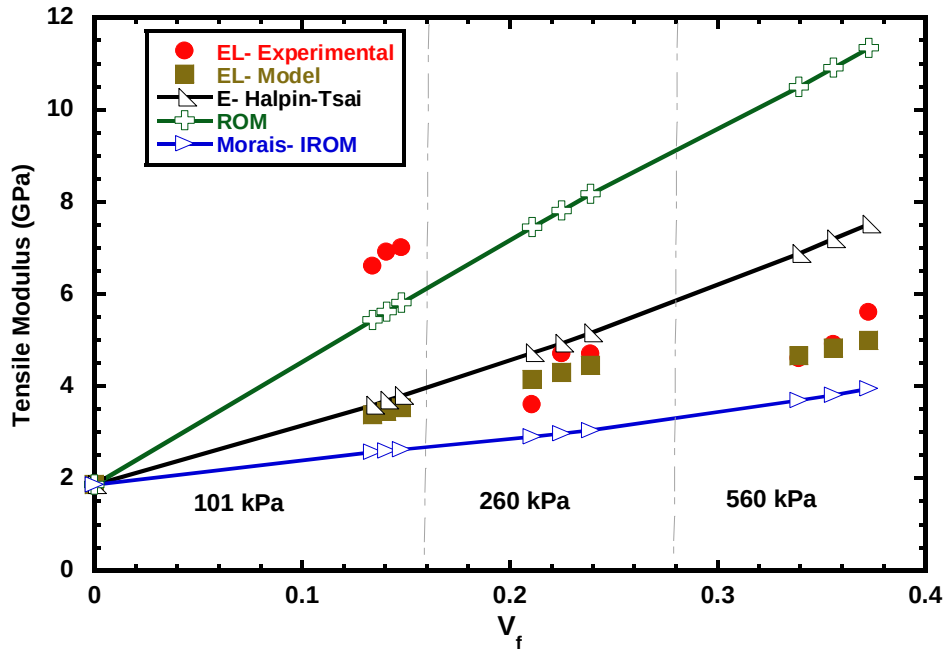

Figure 5.46. Theoretical and experimental longitudinal modulus for 7-P composite

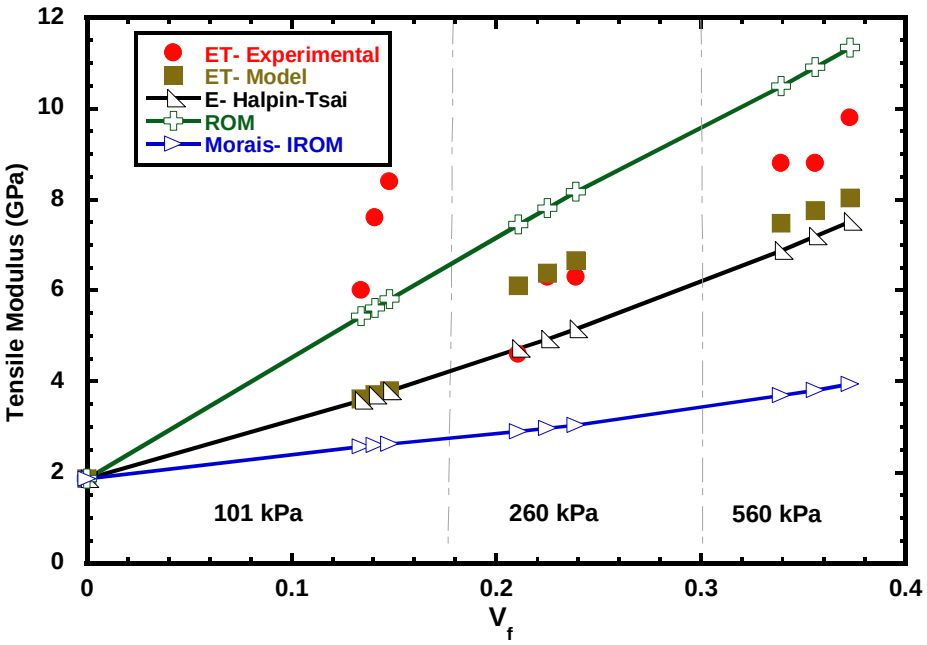

Figure 5.47. Theoretical and experimental transverse modulus for 7-P composite

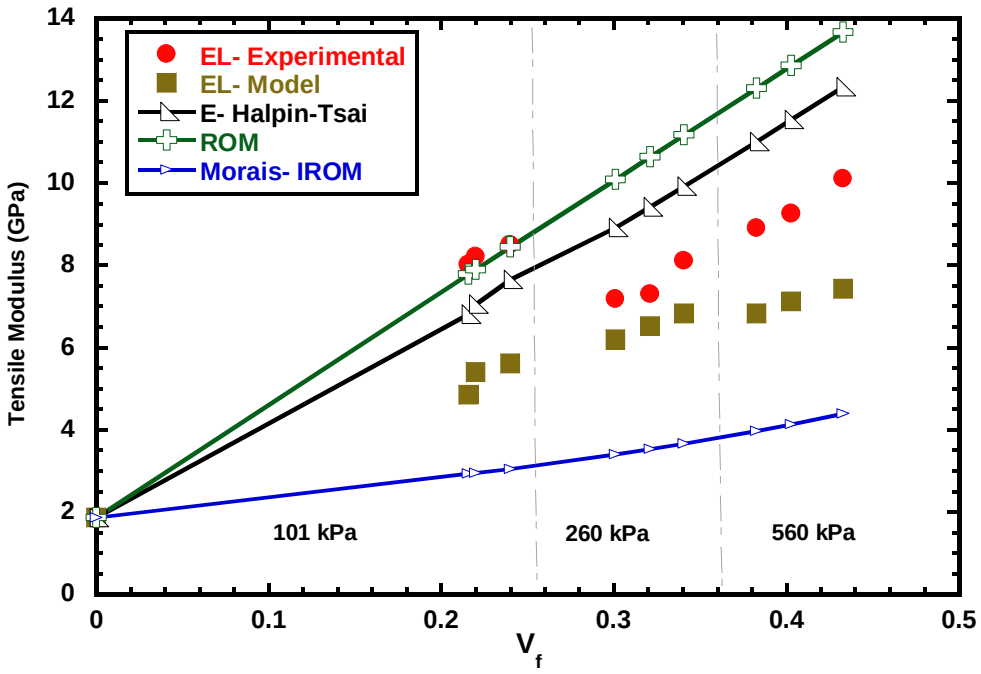

Figure 5.48. Theoretical and experimental longitudinal modulus for 30-P composite

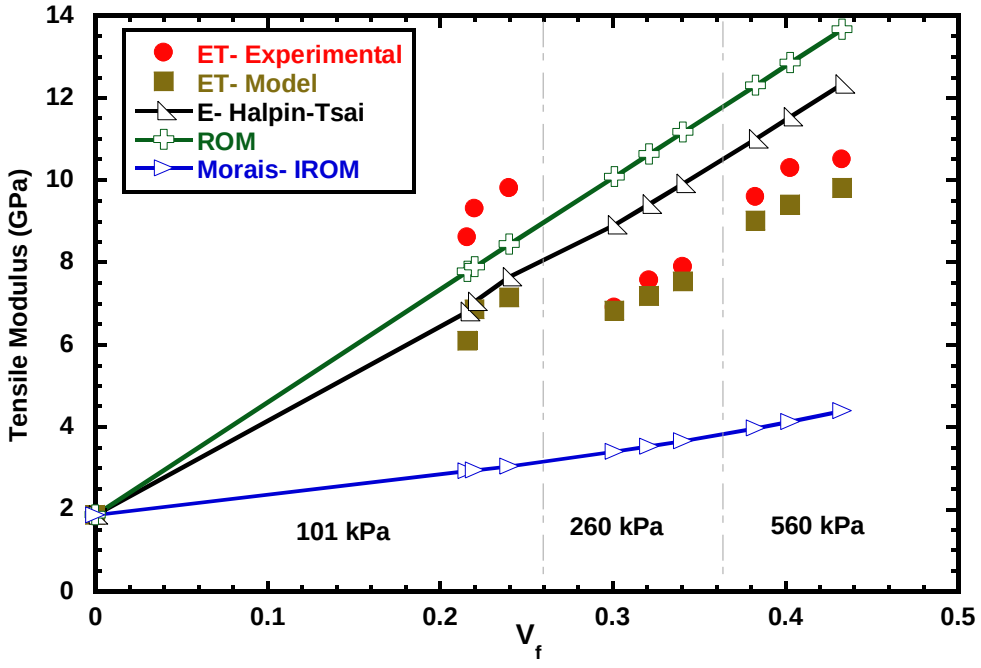

Figure 5.49. Theoretical and experimental transverse modulus for 30-P composite

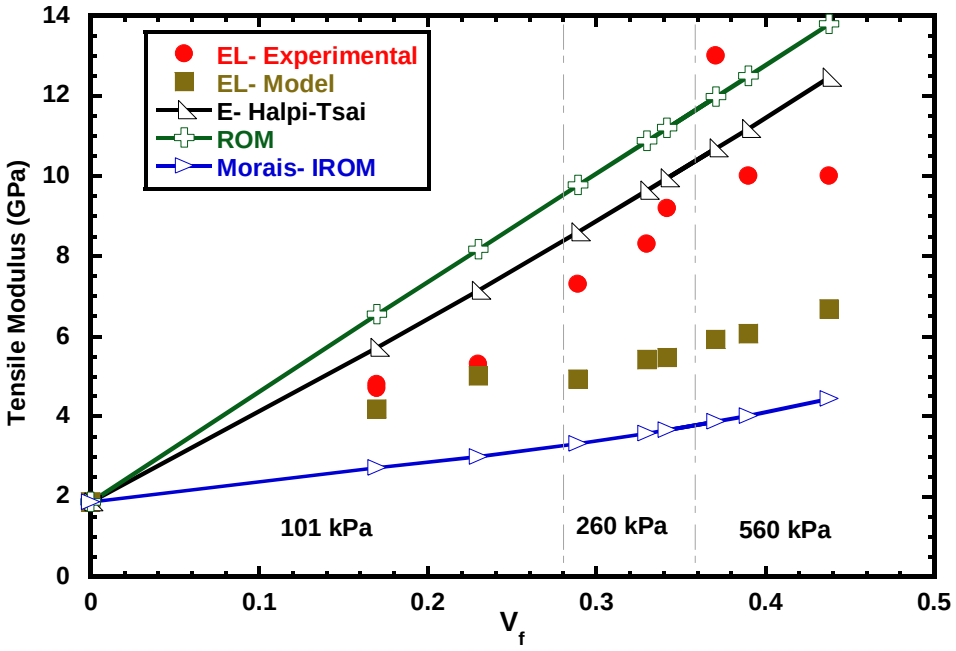

Figure 5.50. Theoretical and experimental longitudinal modulus for 70-P composite

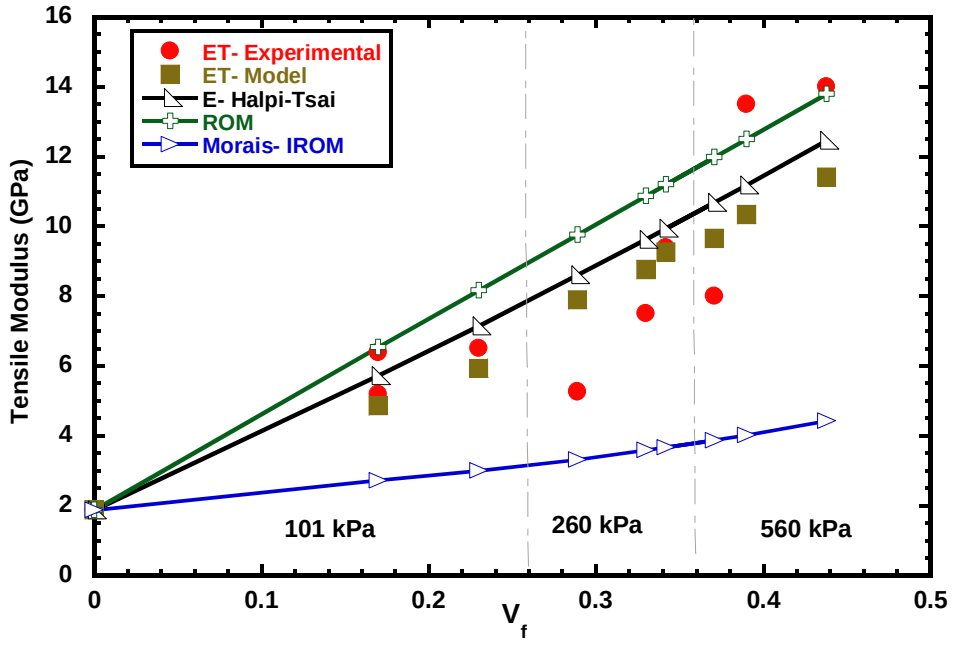

Figure 5.51. Theoretical and experimental transverse modulus for 70-P composite

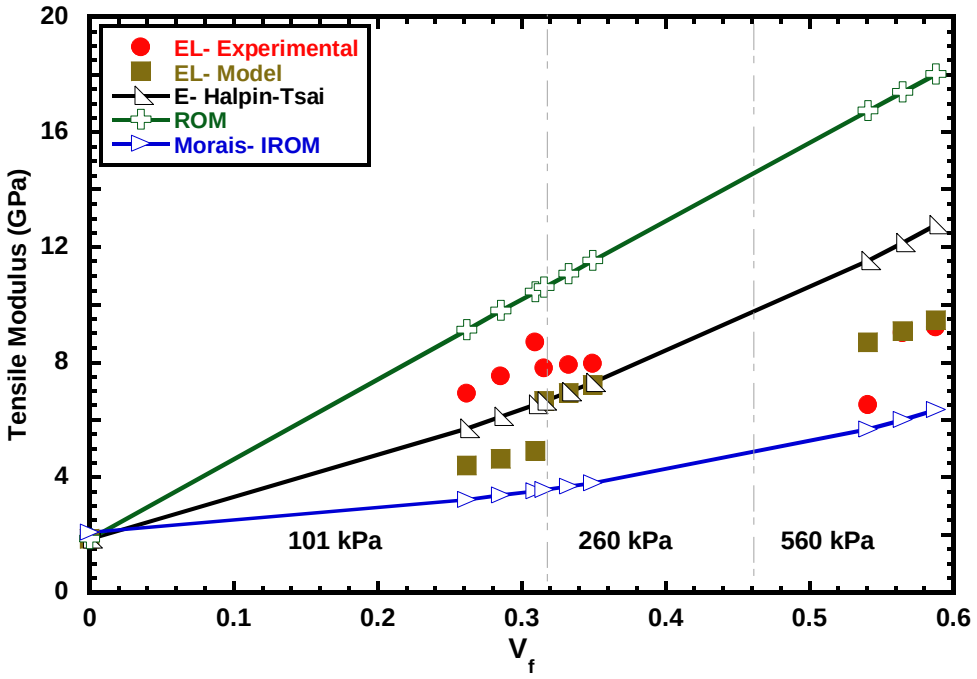

Figure 5.52. Theoretical and experimental longitudinal modulus for 150-P composite

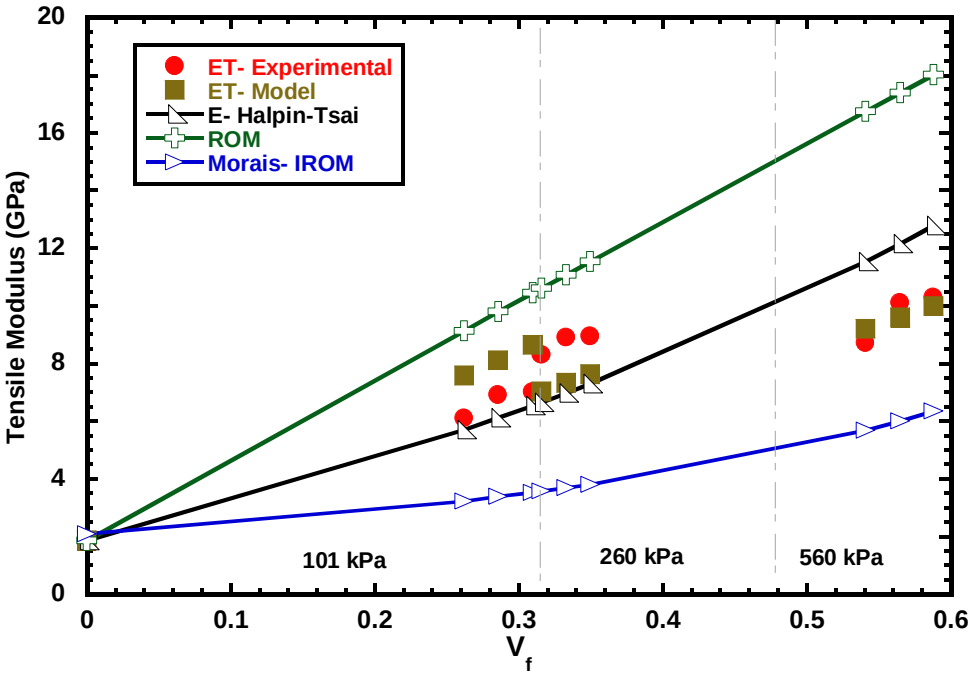

Figure 5.53. Theoretical and experimental transverse modulus for 150-P composite

The error in prediction (determined using Equation (5.5)) is tabulated in Table 5.9 and Table 5.10 for the longitudinal and the transverse tensile modulus, respectively. The values calculated for the Halpin-Tsai model are also included in these tables.

$$Error\ (\%) = \frac{E_{experimental} - E_{Theory}}{E_{experimental}} \times 100 \tag{5.5}$$

The % error in the predictions from the current model is lower than that in the predictions from Halpin-Tsai model. Moreover, the current model was able to predict the trend in the change in moduli with fiber volume fraction, for various punch densities and compaction pressure correctly, while other micro-mechanical models could not. This validates the modeling approach used in this thesis. Finally, the observed good correlation between the experimental and the predicted moduli would not be possible without the use of experimental FOD, which varied from sample to sample due to variation in punch density, or compaction pressure, or both. This supports the arguments presented in the previous section correlating f_p and moduli.

It should be noted that the predictions from the Halpin-Tsai model were based on parameter, η, which was obtained by fitting the experimental data. Hence, the moduli obtained using the Halpin-Tsai model were simulations rather than predictions.

The minimum percentage error in the moduli predicted by the current model was noticed for 30-P composite (-1% to 29% in transverse modulus) and the maximum error in predictions was noticed for 7-P composites (-32% to 55% in transverse modulus). Possible reasons for the observed error are discussed below.

One possible reason for the observed is the error in the experimental FOD used in the prediction. Because of small difference between the densities of the hemp fiber and the resin, the FOD in the manufactured composite could not be obtained using X-ray tomography. Instead, the FOD in the dry mat subjected to the same compaction pressure was characterized and used. The

compaction behavior of a dry mat is expected to be different from that of the composite due to resistance offered by the fluid pressure and lubrication in the latter. This difference is reflected in the final thicknesses of the dry mat and composite compared in Figure 5.16 and Table 5.1 for various punch densities. It can be inferred that the level of compaction was lower in the composites than in the dry mat.

Another possible reason for the error is because of variation of FOD in the mat. For 30-P mat, it is shown that the FOD changes by 10% (see Figure 5.5) in different locations of the mat. Therefore, an error of 5 to 6 % in tensile modulus predictions can be expected due to this estimation.

A third possible reason for the error is the assumption that the 3D composite can be modeled as 2D composite using the 2D lamination theory and the in-plane fiber orientation angles obtained by projecting the fibers on to the plane of loading.

A fourth possible reason is the assumption that the distribution in fiber diameter is the same in all orientations. This assumption allowed for the use of an average fiber modulus. Future work may consider variation in the distribution in the fiber diameter (and hence distribution in the fiber modulus) with orientation.

Nevertheless, it can be concluded that the model developed in this thesis is very capable of predicting the modulus of needle punched hemp fiber mat composites, manufactured using a wide range of compaction pressures. It has also helped to understand the observed trend in the experimental moduli.

Table 5.9. % Error in predictions for longitudinal modulus

Composite	Current Model (%)	Halpin-Tsai (%)
0-P	-33 +37	-24 +47
2.6-P	-37 +14	-36 +15
7-P	-50 +15	-46 +49
30-P	-39 -11	-15 +30
70-P	-54 -5	-17 +35
150-P	-43 +33	-24 +77

Table 5.10. % Error in predictions for transverse modulus

Composite	Current Model (%)	Halpin-Tsai (%)
0-P	-30 +16	-30 +11
2.6-P	-34 +7	-36 +47
7-P	-54 +32	-59 +3
30-P	-29 -1	-29 +24
70-P	-23 +49	-17 +63
150-P	+24 -17	-21 +32

5.5.3 Tensile Strength - Experimental Results

The tensile strength results for composites manufactured under VARTM pressure (101 kPa) are tabulated in Table 5.8. Similar to the modulus, the transverse strength was higher than the longitudinal strength for all punch densities. The trend in the effect of punch density on strength was similar to that observed for the modulus; the strength increased with the punch density until 30-P, beyond which the trend was not clear. The discussion in the previous section on the trend in modulus is applicable for tensile strength too.

For composites manufactured with VARTM pressure, the tensile strengths were lower than that of the matrix resin for all punch densities except 30-P, suggesting there was no reinforcement of the matrix by the fiber at the fiber volume fractions achievable using VARTM pressure. Despite having a fiber volume fraction slightly higher than 30-P, the strength of 150-P composite is lower than the strength of 30-P composite.

The longitudinal and transverse tensile strengths for all punch densities are plotted as a function of fiber volume fraction in Figure 5.54 and Figure 5.55 respectively.

The fiber volume fraction was varied by varying the compaction pressure. Both strengths increased with pressure (i.e. fiber volume fraction). Beyond a VARTM pressure of 101 kPa, the strengths of 0-P, 30-P, 70-P, and 150-P composites were higher than the resin strength indicating fiber reinforcement. In the case of 2.6-P and 7-P composites, despite the weak increase in strength, the values were still lower than the strength of the resin.

The maximum value for the strengths was recorded for composites cured at 560 kPa, in the range of 30–60 MPa. While a weak proportional relationship between the strength and the punch density could be observed at this pressure, no such trend could be observed at 260 kPa.

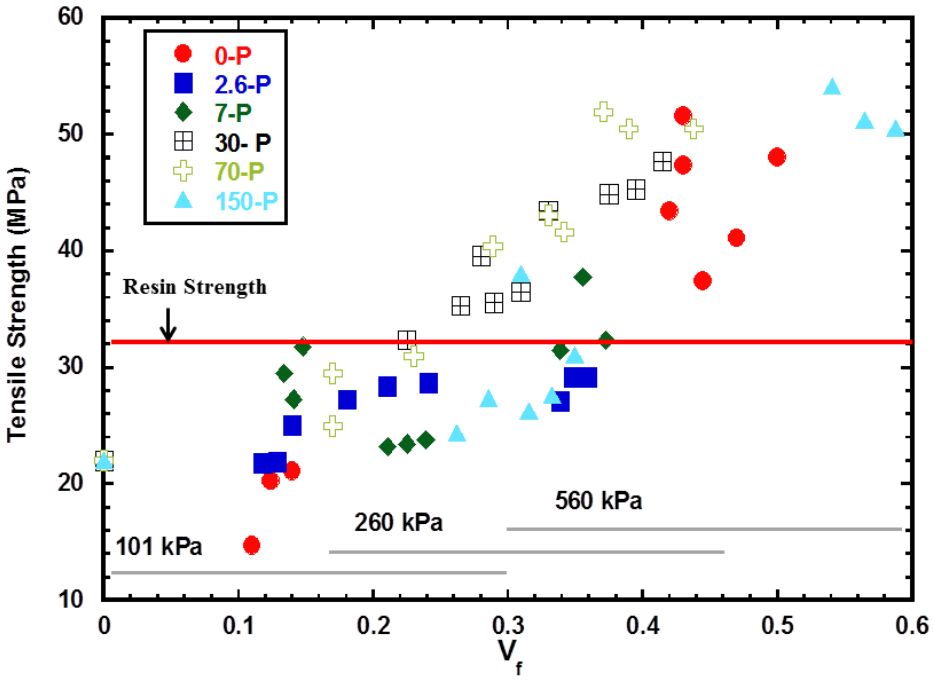

Figure 5.54. Experimental longitudinal tensile strength of needle punched composites manufactured with various manufacturing pressures

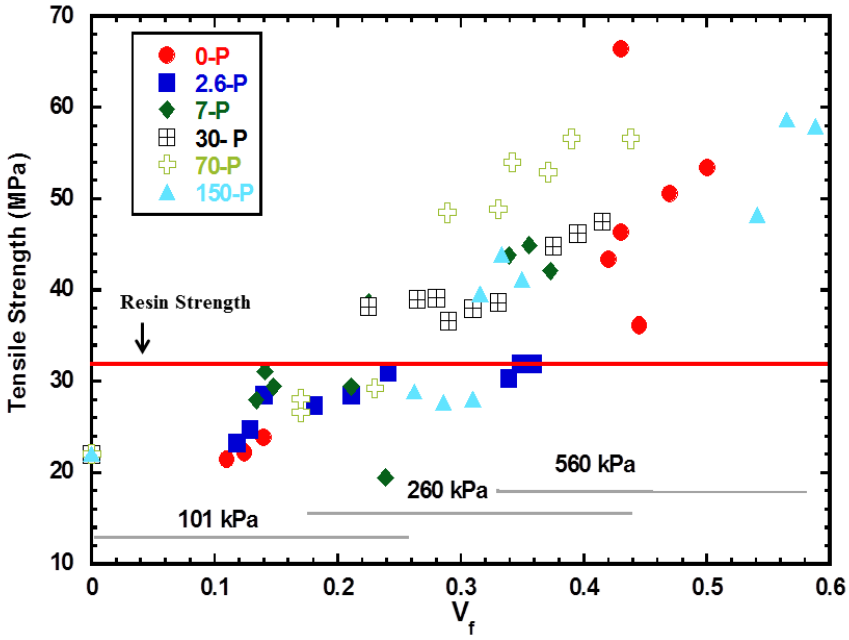

Figure 5.55. Experimental transverse tensile strength of needle punched composites manufactured using various manufacturing pressures

For all punch densities, the strength at 260 kPa was equal to, or lower than, the strength at VARTM pressure.

It can be inferred from these results that changes in fiber volume fraction, with compaction pressure, cannot explain the observed trend. Similar to its influence on modulus, a variation in FOD with punch density and compaction pressure is also believed to have influenced the tensile strength. This inference is supported by the simulation results presented below. It can be inferred from Table 5.8 that although the modulus of glass fiber composites can be matched by appropriately choosing the needle punch density, the tensile strength of hemp fiber mat composites are lower than the strength of glass fiber mat composites. This study did not treat the fibers to increase the matrix–fiber bond strength. Optimization of this bonding has been done by other students of Dr. Jayaraman's research group. While treatments increased the strength of the composite, the strength of glass fiber composites could not be reached. This is due to the higher strength of glass fibers (2 GPa for E-glass) when compared to the strength of hemp fibers (maximum of 500 MPa for fibers with less than 100 μm).

5.5.4 Tensile Strength-Predicted Results and Model Validation

The tensile strengths of needle punched hemp fiber composites were predicted using the model presented in Chapter 3 (which is referred as Ply Discounting Model (PDM) in this section) and the procedure discussed in Chapter 4. These predictions are also compared to the predictions from the Modified Micromechanical Model (MMM) presented in Appendix A.2 to evaluate the merits of the model developed in Chapter 3.

A representative tensile stress-strain curve, predicted using PDM, is compared with experimental results in Figure 5.56. Despite the assumptions in the model, the predicted curve compares very well with experimental curve. Referring to Figures 5.57 to 5.68 it is apparent the

PDM is able to predict better than other models compared in this thesis. While Lee's model predicts non-linear increase in strength with increase in fiber volume fraction, McNally et al.'s model predicts a linear increase. Besides, the tensile strength values predicted by them were much higher than the experimental values. The predictions of the MMM (which was modified in this thesis) were better than the predictions of models by McNally et al. and Lee. MMM predictions were comparable to or better than those of PDM in certain cases and inferior in other cases.

The error in the predictions was determined using Equation (5.6) and tabulated in Table 5.11 and Table 5.12 for longitudinal and transverse strengths respectively.

$$(\%\ error) = \frac{\sigma_{experimental} - \sigma_{theory}}{\sigma_{experimental}} \times 100 \tag{5.16}$$

It can be inferred from Table 5.15 and Table 5.16 that the tensile strength predicted by the PDM developed model in this thesis has the least deviation from experimental results.

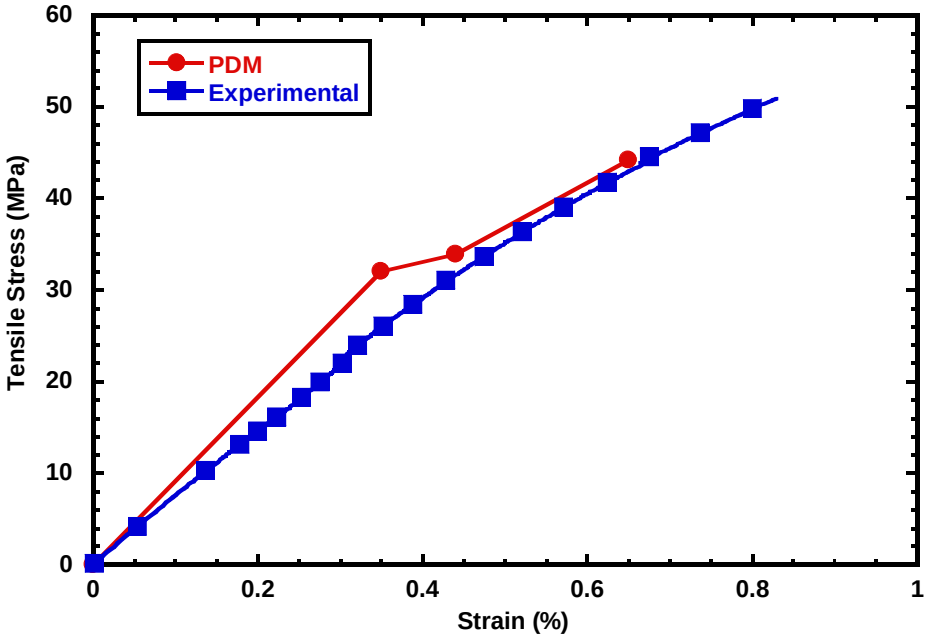

Figure 5.56. Comparison of experimental tensile stress-strain curve with the curve predicted by PDM for 70-P composite manufactured at 560 kPa

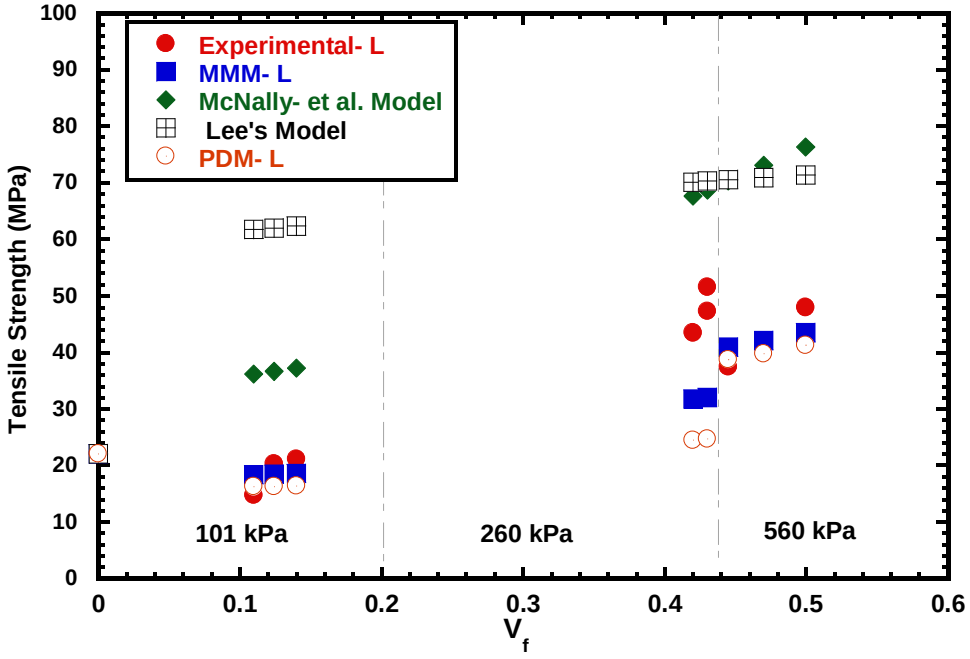

Figure 5.57. Theoretical and experimental longitudinal tensile strength for 0-P composite

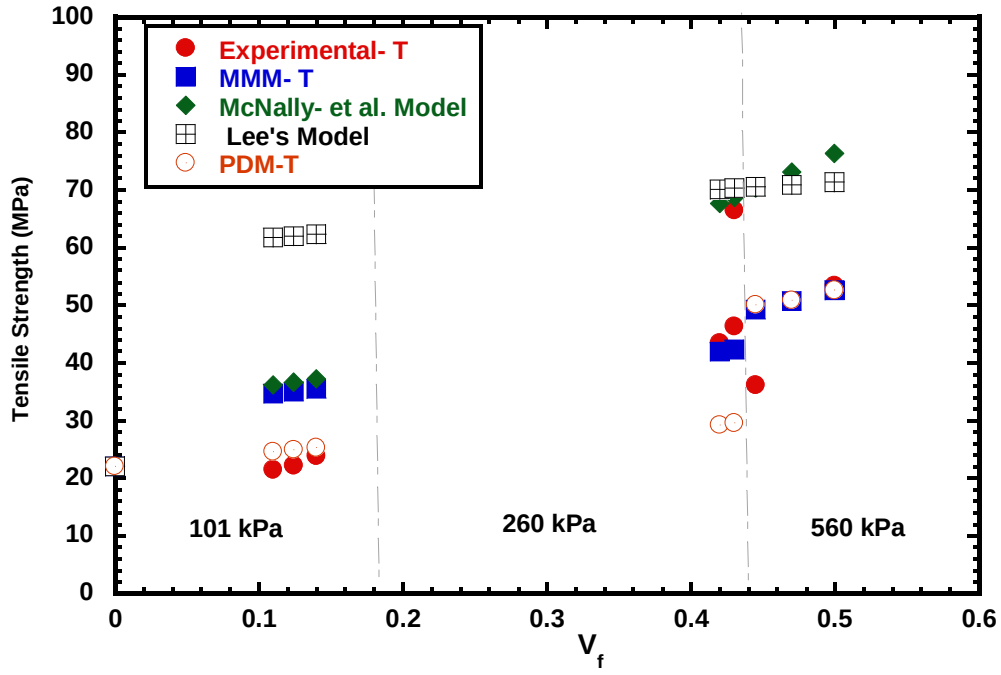

Figure 5.58. Theoretical and experimental transverse tensile strength for 0- P composite

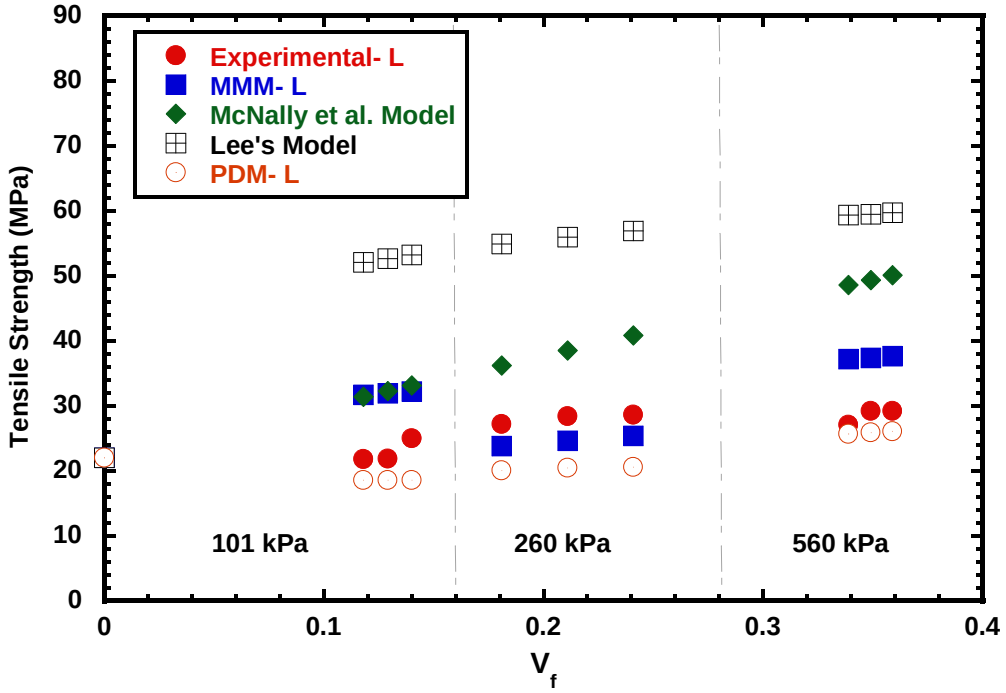

Figure 5.59. Theoretical and experimental longitudinal tensile strength for 2.6- P composite

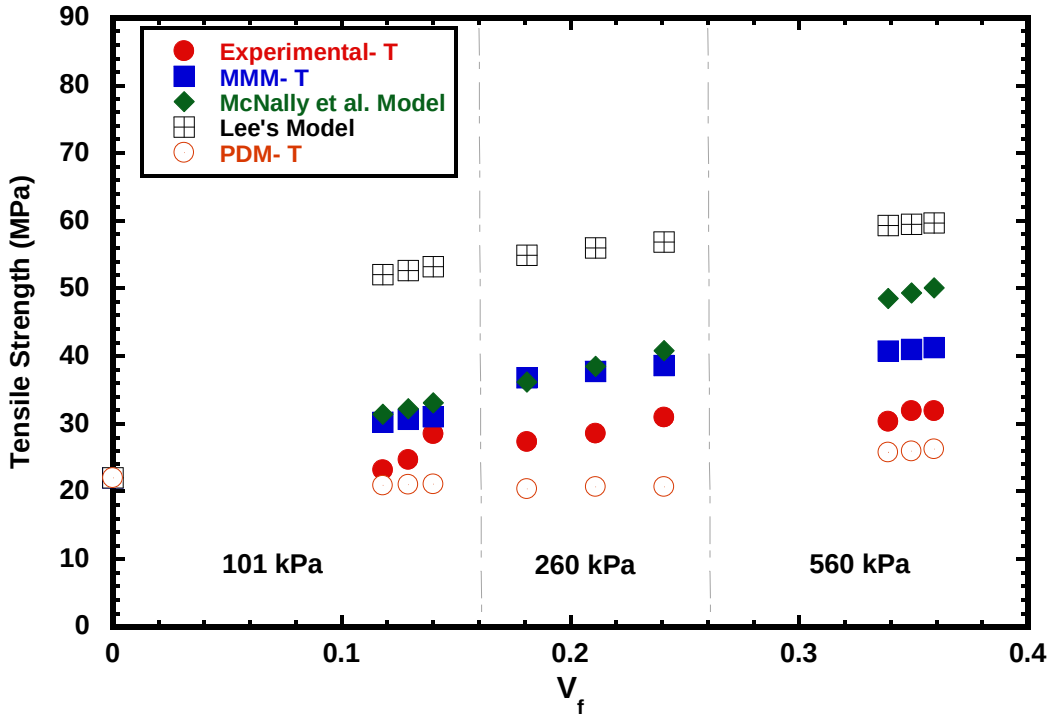

Figure 5.60. Theoretical and experimental transverse tensile strength for 2.6- P composite

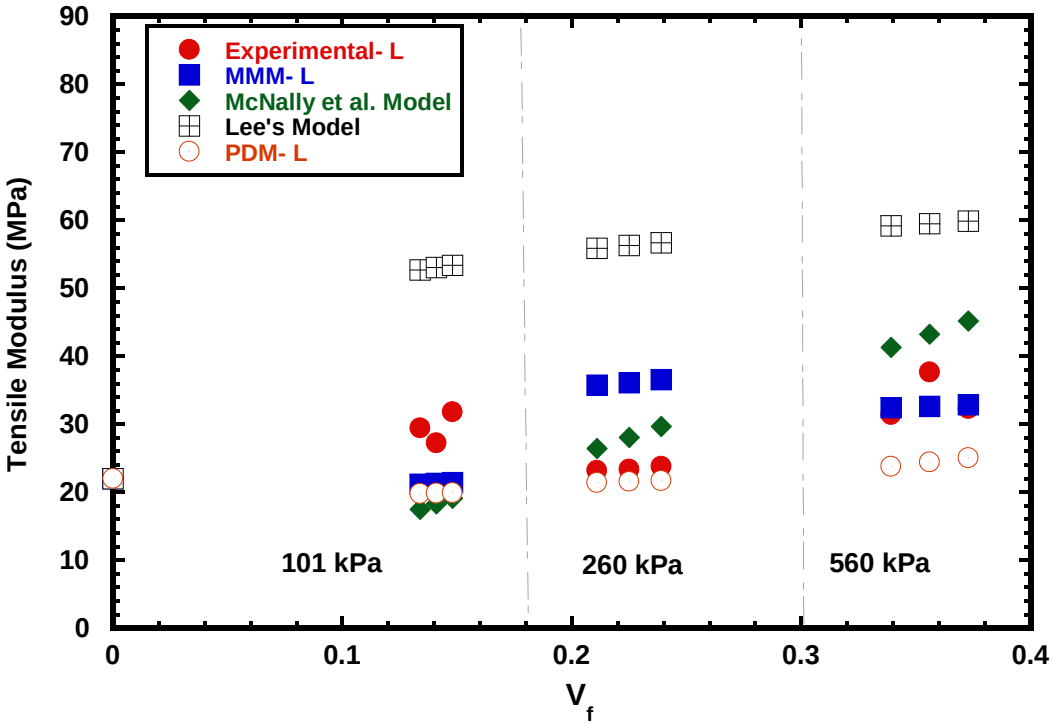

Figure 5.61. Theoretical and experimental longitudinal tensile strength for 7- P composite

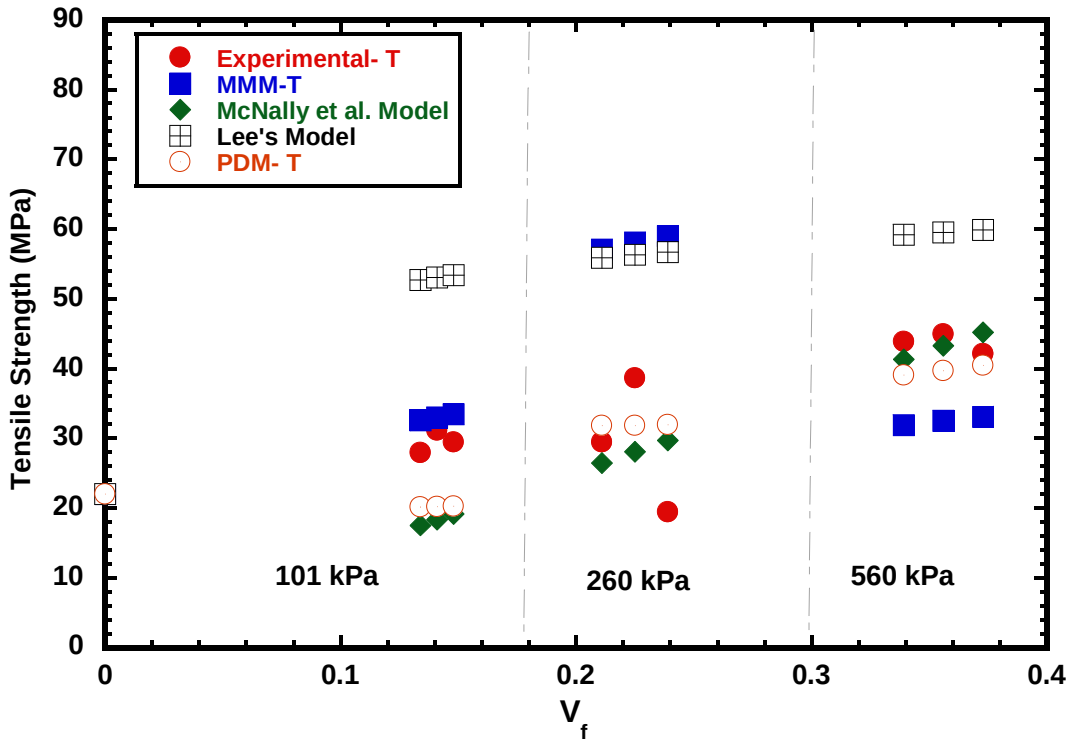

Figure 5.62. Theoretical and experimental transverse tensile strength for 7-P composite

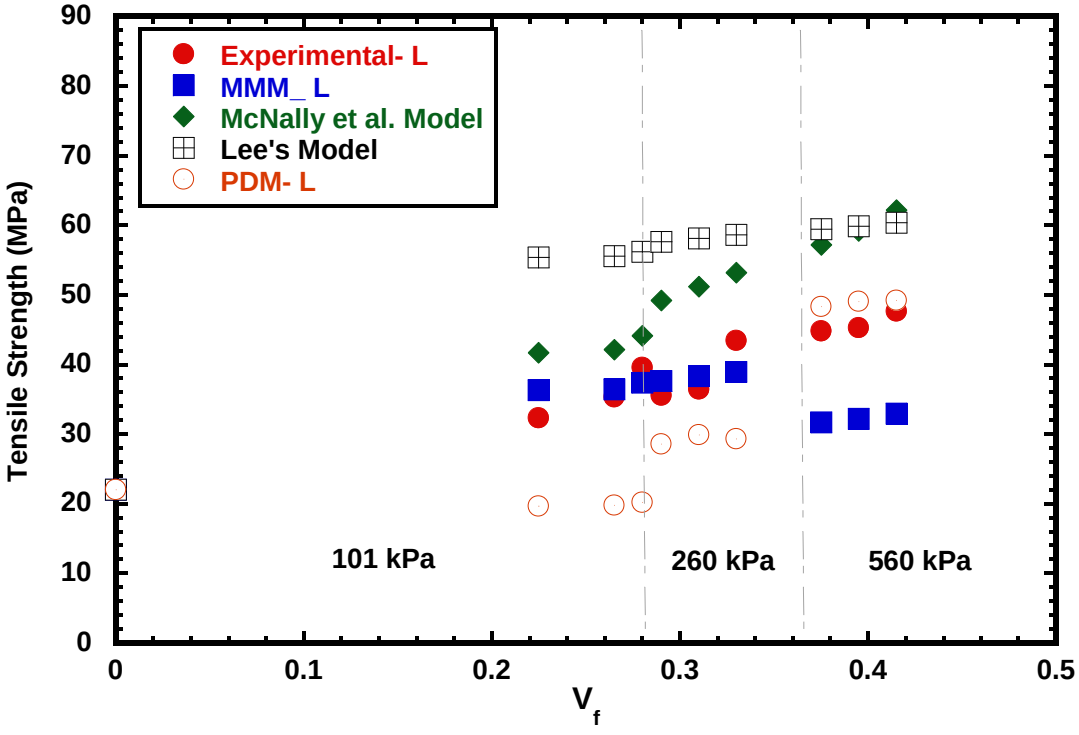

Figure 5.63. Theoretical and experimental longitudinal tensile strength for 30-P composite

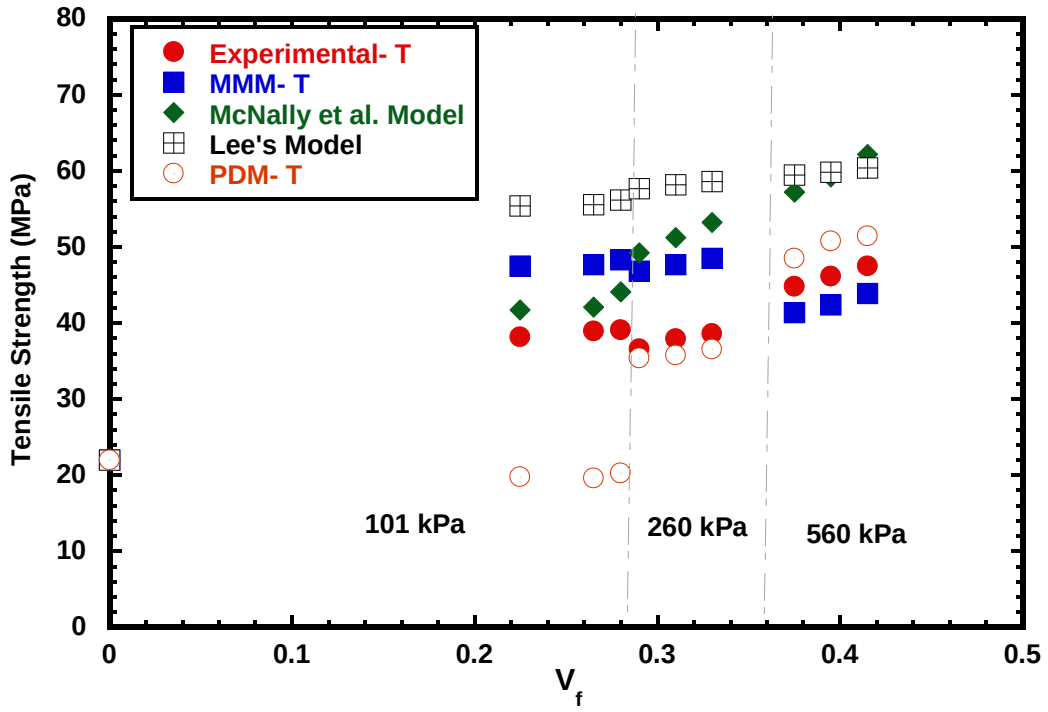

Figure 5.64. Theoretical and experimental transverse tensile strength for 30- P composite

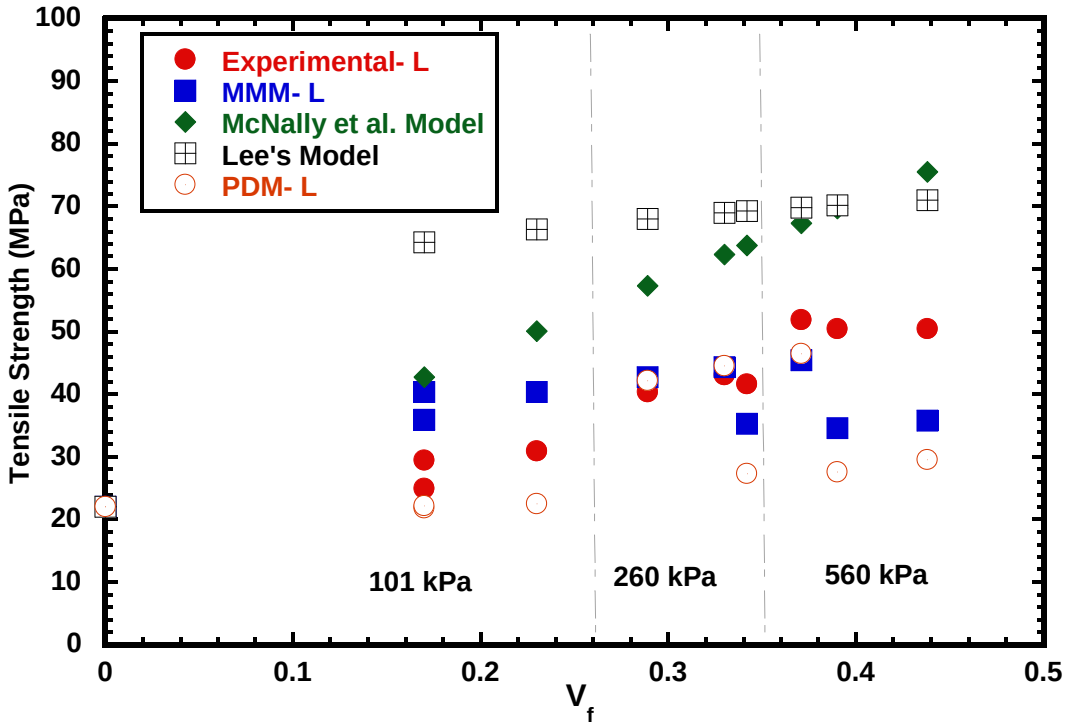

Figure 5.65. Theoretical and experimental longitudinal tensile strength for 70- P composite

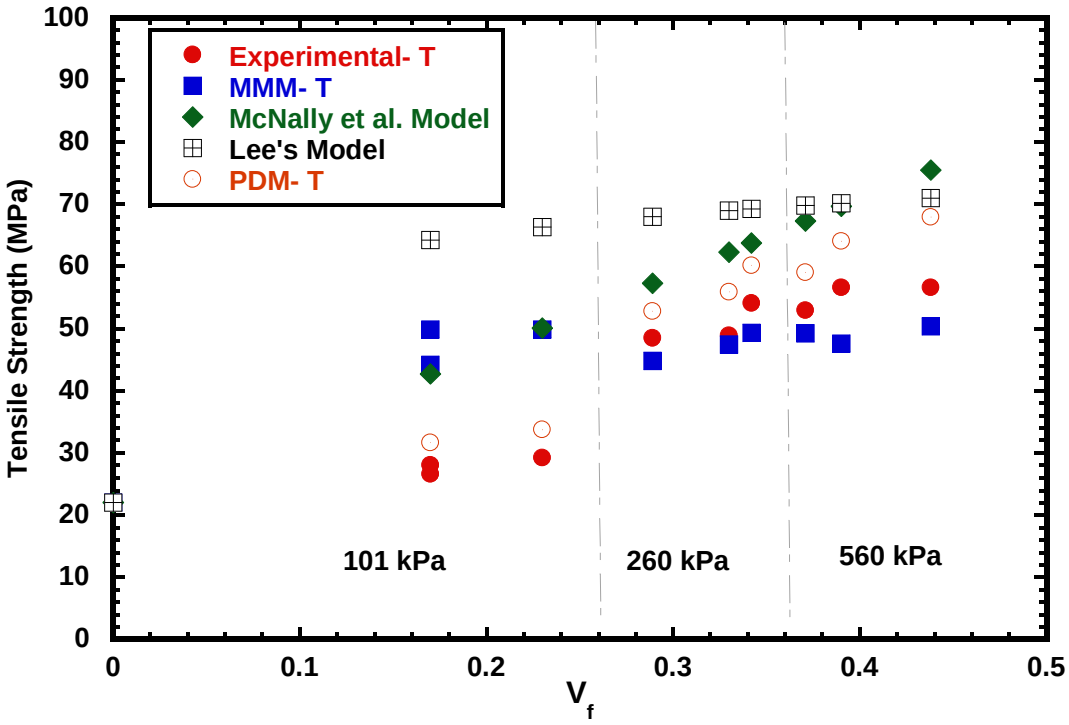

Figure 5.66. Theoretical and experimental transverse tensile strength for 70- P composite

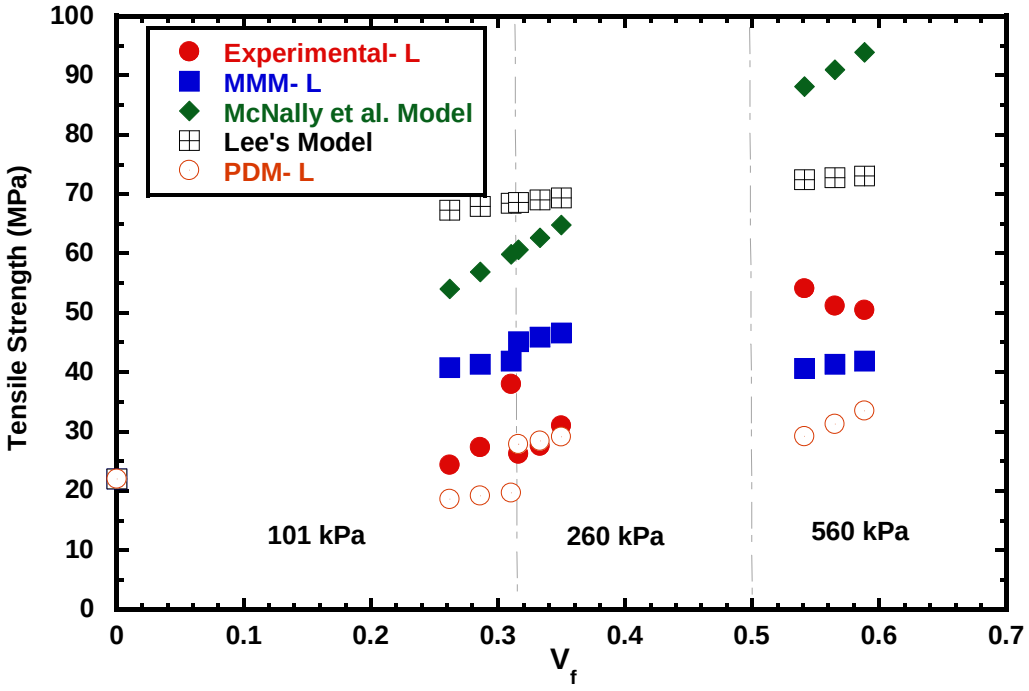

Figure 5.67. Theoretical and experimental longitudinal tensile strength for 150- P

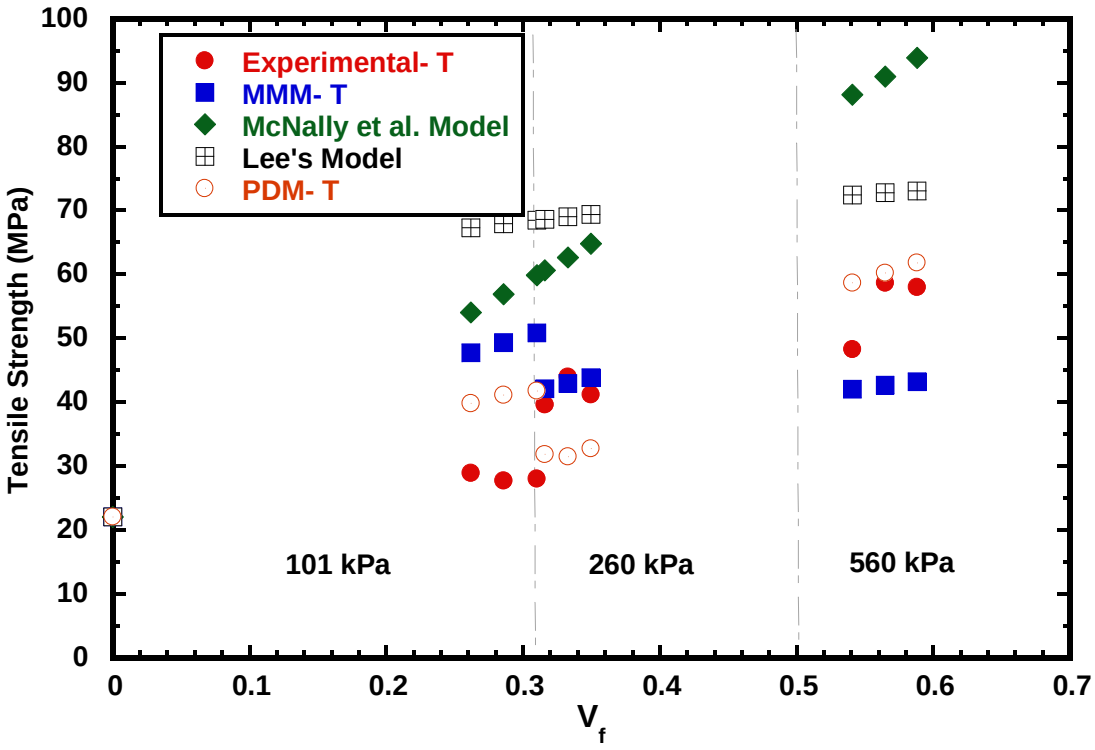

Figure 5.68. Theoretical and experimental transverse tensile strength for 150-P composite

Table 5.11. Error in prediction of longitudinal tensile strength for PDM developed in this thesis and models from literature

Composite	Developed Models		Models from Literature	
	PDM (%)	Micromechanical Model (%)	Lee's Model (%)	McNally et al.'s Model (%)
0-P	-52 +10	-37 +24	+36 +318	+33 +144
2.6-P	-26 +5	-11 +46	+97 +140	+32 +79
7-P	-37 +7	-28 +54	+57 +140	-40 +39
30-P	-48 +8	-30 +12	+26 +76	+11 +40
70-P	-45 +4	-31 +44	-34 +157	+29 +71
150-P	+6 +67	-24 +72	+33 +175	+57 +130

Table 5.12. Error in prediction of transverse tensile strength for models developed in this thesis and models from literature

Composite	Developed Models		Models from Literature	
	PDM (%)	Micromechanical Model (%)	Lee's Model (%)	McNally et al.'s Model (%)
0-P	-32 +38	-26 +13	+5 +188	+3 +68
2.6-P	-33 -10	+8 +34	+86 +124	+166 +69
7-P	-35 +64	-27 +93	+32 +191	-37 +52
30-P	-49 +9	+8 +27	+27 +57	-8 +37
70-P	+8 +19	-15 +77	+21 +143	+17 +71
150-P	-38 +49	-27 +81	+23 +144	+42 +113

PDM showed a better agreement with experimental tensile strength in most cases; a maximum deviation of −35% to 64% from experimental transverse tensile strength was recorded for 7-P composite. For the same composite, the predictions of the micromechanical model yielded a maximum deviation of −27% to 93%. The transverse strength of 70-P composite, predicted by PDM exhibited a minimum deviation of 8% to 19% from experimental results. The transverse tensile strength predicted for the same composite by the MMM was −15% to +77%.

Prediction of tensile strength is more complicated than prediction of modulus even for unidirectional continuous fiber composites, with fibers oriented in a single direction, due to difficulty in predicting the fracture initiation, propagation, and ultimate fracture.

This difficulty is increased many fold in discontinuous fiber mat composites due to a distribution in fiber length and orientation. Hemp fiber mat composites add additional complexity due to the effect of punch density on fiber orientation distribution and variation in properties of hemp fibers with diameter.

In view of this complexity, the observed difference between the predictions and experimental results is to be expected since many of the factors that influence tensile strength were either not considered or simplified. These are detailed below.

a) Error in model`s ability to account for damage progression:

Referring to Figure 5.30, it is clear that needle punched composites exhibit a ductile non-linear behavior under tensile loading. This non-linearity is due to progressive damage that occurs in the composite before final failure of the test specimen. In contrast, a brittle behavior would result in a linear stress-strain curve until final failure of the test specimen. Therefore, accurate prediction of the type of fracture is essential to accurate prediction of the tensile strength of the composite.

The MMM predicts a brittle behavior since it assumes that the composite would fracture when the damage initiation occurs; the damage initiation can be failure of the fiber or the matrix or the interface (depending on the orientation of the fiber). The MMM determines the stresses to initiate the various damage modes and adds them, in proportion to the volume fractions of fiber orientation with each type of damage, to determine the tensile strength of the composite. In reality, damage progression would follow damage initiation leading to final fracture of the composite, which has not been accounted for in the MMM developed in this thesis. The capability to simulate progressive damage (and thus differentiate between ductile and brittle laminate fracture) is the advantage of the PDM over the MMM.

For example, the PDM predicted stress-strain curve presented in Figure 5.56 corresponds to progressive failure of three ply groups before final failure of the composite. This results in a nonlinear stress-strain curve, which compares well with the experimental stress-strain curve. The predicted strength deviated minimally from the experimental value (Table 5.11 and 5.12). However, the MMM could not predict the stress-strain curve.

Despite this, the predicted failure mode was different from the experimental failure mode for some composites. For these composites, while the experimental stress-strain curve was non-linear with a ductile failure, the model predicted simultaneous fracture of all the plies, and vice versa. One possible reason is the non-consideration of a stress concentration, which is inherent in any damage initiation and progression. Another possible reason is the error in the FOD used in the simulation, as discussed in Section 5.4.2.

b) Error in predicted laminate modulus:

The error in the predicted modulus of the laminate is another source of error since this modulus is used by the PDM to predict the tensile strength. While comparing the error in the

predicted tensile moduli in Tables 5.9 and 5.10 with the errors in the predicted tensile strengths in Table 5.11 and 5.12, it is apparent that the error in the predicted tensile moduli is carried over as an error in the predicted tensile strength. For instance, an underestimation of the longitudinal and transverse tensile moduli of 2.6-P, 7-P, 30-P composite, and of the transverse moduli of 70-P and 150-P composites at 101 kPa correlate well with an underestimation of the longitudinal and transverse tensile strengths for those composites.

Hence, the possible sources of error, discussed in the previous section on modulus, such as the error in experimental FOD due to use of dry mat and small scan volume, approximation of the 3D FOD as 2D FOD, and the assumption of same fiber length and diameter distribution in all orientations, are also applicable to tensile strength too.

c) Error in hemp fiber strength:

Hemp fibers are essentially a bunch of smaller fibrils (both in diameter and length). Their mode of failure may be tensile failure of all fibrils or debonding of fibrils or a mixture of both. This structure affects the measured tensile strength of the fibers. The number of fibrils and their distribution within a hemp fiber depends on the diameter and length of the fibers. While the effect of the former on tensile strength has been accounted for, the effect of the latter has not been accounted for, which is believed to be another reason for the observed error in predicted strength. Additionally, the mat/composite manufacturing process may introduce additional fiber defects such as fiber kinking and debonding of the fibrils. The effect of these defects on fiber strength was not characterized and included in the model.

Nevertheless, it can be concluded that the models developed in this thesis are very capable of predicting the tensile strength of needle punched hemp fiber mat composites, manufactured using a wide range of compaction pressures. The developed model also helped to understand the

observed trend in the experimental moduli data in terms of the effect of fiber volume fraction and FOD.

CHAPTER 6

CONCLUSIONS

Needle punched hemp fiber mats have been manufactured and used to elucidate the effect of needle punch density on mat structure. Effect of consolidation pressure applied during composite manufacturing on composite structure has been studied; while its effect on fiber volume fraction has been studied directly, its effect on FOD has been investigated indirectly by studying the effect of consolidation pressure on mat structure.

Composites have been manufactured using mats with various punch densities and consolidation pressures, and tested for their strength and modulus. These results have been analyzed to investigate the relationship among mat manufacturing, mat structure, composite manufacturing, composite structure, and composite properties.

A modeling approach to predict the evolution of FOD and V_f during needle punching and composite manufacturing has been presented and its underlying assumption has been empirically tested. Finally, a model for predicting the modulus and the strength of needle punched mat composites has been presented and validated. Therefore, it is concluded that the overall goal and the five objectives of this thesis, stated in Section 2.7, have been successfully achieved.

6.1 Summary

A summary of accomplished tasks are presented below.

(a) Effect of needle punch density on the structure of the hemp fiber mat has been experimentally studied.

- Needle-punched hemp fiber mats have been manufactured by varying the needle punch density in the range of 0 – 150 Punches/cm^2 and used to delineate the relationship between the punch density and the mat structure, characterized by its thickness, areal density, V_f, FOD, and permeability.
- For a given areal density, with increasing the punch density the mat thickness decreases and the V_f in the mat increases. To achieve a certain mat thickness, the required punch density would increase with the areal density.
- The fiber orientation in the mat formed by air-laying was in 3D with a bias towards the width (transverse) of the mat. With increase in the needle punch density, the fibers increasingly reoriented from 3D to 2D due to compaction and stretching of the mat.
- Changes to areal density of the mat formed by air-laying, due to the lack of fine control over the process, has a significant effect on the changes in V_f and FOD due to needle punching.
- The in-plane permeability along the longitudinal direction (K_x) decreases with increase in punch density due to reduction in the porosity (i.e. increase in V_f) and does not depend on FOD.

- The through-the-thickness permeability (K_z) is dependent on both V_f and FOD; it decreases with increase in punch density due to increase in V_f as well as change in fiber orientation from 3D to 2D.

(b) Effect of consolidation pressure, applied during composite manufacturing, on composite structure and properties has been experimentally studied; while its effect on V_f has been studied directly using composites, its effect on FOD has been studied indirectly by studying the compaction of dry mats.

- V_f in needle-punched hemp composites increases with applied pressure for a given punch density and increases with punch density at an applied pressure; however, the rate of increase differs with punch density due to the effect of the latter on the compaction behavior of the composite during manufacturing
- The rate of increase in applied pressure for a unit increase in thickness (i.e. fiber volume fraction), which is a measure of rate of stiffening of the mat, varied widely with punch density highlighting the impact of mat structure on the compaction behavior. A clear trend in the effect of punch density on the rate of stiffening could not be discerned due to variation in the areal density of the mat, which altered the mat structure and hence, the compaction behavior.
- The FOD changes in a complex manner with increase in compaction pressure. Similar trend is observed for all punch densities with few exceptions. Apparent softening (instead of stiffening) at pressures above 101 kPa appears to contribute to this complex trend.
- The transverse modulus is higher than the longitudinal modulus confirming the bias observed in the FOD; The modulus of the composite is a function of both the V_f and the FOD; The modulus increases with punch density at VARTM pressure (101 kPa) due to

increase in V_f, provided the areal density is same. When the pressure increases to 260 kPa, the modulus decreases due to change in FOD, provided the increase in modulus due to increase in volume fraction is not significant. With further increase in pressure to 560 kPa, the modulus increases or does not change depending on the magnitude of contributions from change in the V_f and the FOD

- The transverse strength is more than longitudinal strength confirming the bias in FOD. The strength is a function of both the V_f and the FOD. The effect of punch density on strength is similar to that on modulus. The strength of the composite exceeds the strength of the resin only at punch densities ≥ 30.

(c) A modeling approach has been developed to predict the change in FOD during needle punching and composite manufacturing

- A model based on roll forming has been developed to predict the change in mat dimensions due to needle punching.
- Assuming a pseudo-affine deformation, the changes in mat dimensions are used with FOD in the web of fibers to predict the change in FOD due to needle punching.
- The above model could not be put to use due to lack of information on inputs required by the model. Instead, the validity of the pseudo-affine deformation has been tested by predicting the FOD using initial FOD and assumed values for changes in mat dimensions. Good correlation with experimental FOD supports this assumption.

(d) A model has been developed to predict the modulus and the strength of the needle-punched mat composites and validated using experimental results

- The mat composite has been modeled as laminate with a lay-up defined by the FOD. The lamination theory has been used to predict the modulus. Very good correlation

between the model predictions and experimental values at all consolidation pressures and punch densities confirms the effect of V_f and FOD discussed above

- Ply discounting method and maximum stress criterion have been used along with the lamination theory to predict the strength of mat composites. Good correlation between the model predictions and experimental values at all consolidation pressures and punch densities confirms the effect of V_f and FOD discussed above
- Distribution in the modulus and the strength of hemp fibers in the mat has been characterized and used in the prediction. This accounts for the distribution in the diameter and length of the fibers as well as any defects in the fiber, due to the processes of fiber extraction and needle punching.

e) The above results point to a complex relationship among mat manufacturing, mat structure, composite manufacturing, composite structure, and composite properties. The following can be concluded based on these results:

- It is advisable to use needle punching to achieve the desired V_f and properties than to achieve the same through compaction pressure. In other words higher needle punch density is preferred over higher compaction pressure to achieve the desired V_f for a given areal density, provided this does not affect permeability and degrade the properties of the fibers.

6.2 Original Contributions

To the best knowledge of the author, the following contributions are first in this area

- Comprehensive study delineating the complex relationship among mat manufacturing, mat structure, composite manufacturing, composite structure, and composite properties.
- A model to predict the modulus and the strength of needle-punched mat composites.
- A model to predict the evolution of V_f and FOD during needle punching process.

6.3. Recommendations for Future Work

- Fibers used in this thesis exhibited a large distribution in the tensile modulus and strength of the fibers. Since these, result in the distribution in the properties of composites, a fiber extraction process that minimizes the distribution in fiber properties is needed.
- In addition, the variations in the areal density of the needle punched mats have to be minimized with a better control over the processes of mat formation and needle punching in order to minimize the variation in composite properties.
- Controlled experimentation to validate the model developed for needle punching and development of a model to predict V_f and FOD during composite manufacturing. The model for modulus and strength developed in this thesis requires V_f and FOD as input. In this thesis, experimental values have been used. If a mat has to be designed to yield desired composite properties without much experimentation, then these values have to be predicted as an input to the model. The model for needle punching has not been validated in this thesis due to lack of information for many variables of this model. Further, the V_f and the FOD in the mat change during composite manufacturing and no model is currently available for this.

- Extension to 3D lamination theory

  The model for modulus and strength is based on 2D lamination theory, which uses the FOD in θ. The results of this study clearly show that fibers in needle punched mats and composites are oriented in 3D. Hence, extension of this approach using 3D lamination theory is recommended to improve the accuracy of prediction.

REFERENCES

1. AG, Q.P.C−Advanced Glass Mat Thermoplastic Composite Applications for the Automotive Industry", *Technical Information Hardstrasse*, Lenzburg, Switzerland, 2006.
2. Foulk, J.A., Chao W.Y., Akin D.E., Dodd R.B., Layton P.A., "Analysis of Flax and Cotton Fiber Fabric Blends and Recycled Polyethylene Composites", *Journal of Polymers and the Environment* 14 (2006): 15-25.
3. Mrstina, V., Fejgl F., "Needle Punching Textile Technology", Elsevier Publishing Company, 1990.
4. http://www.precisioneering.com Accessed on17/6/2013.
5. Bledzaki A., Frauk O., Sperber V.E., "Cars from Bio-fibers," *Macromolecular Materials and Engineering* 291(2006): 449-457
6. Nabi Saheb, D., Jog J.P., "Natural Fiber Polymer Composites: A Review", *Advances in Polymer Technology* 18 (1999):351-363.
7. Kandachar , P., "Opportunities for Product Developemnet for Industrial Applications in Polymer Reinforced with Natural Fibers", *Proceeding of Riso International Symposium on Materials Sciennce*, Roskilde, Denmark, 2002, 15-33.
8. Zimmermann T., "Cellulose Fibrils for Polymer Reinforcements", *Advanced Engineering Material* 6 (2004): 754- 760.
9. Anselme, P., "Main Composition of Plants and Woody tissues*", Comptes rendus hebdomadaired des séance de l'Academie des science* 3(1838):1052-1056.

10. Young, R.A., Rowell R.M., "Cellulose: Structure, Modification and Hydrolysis", Wiley-Interscience, 1986.
11. Chinga-Carrasco, G., "Cellulose Fibres, Nanofibrils and Microfibrils: the Morphological Sequence of MFC Components from a Plant Physiology and Fibre Technology Point of View", *Nanoscale Research Letters* 6(2011):1-7.
12. Garcia-Jaldon C., Vignon M. R., "Fibers from Semi-retted Hemp Bundles by Steam Explosion Treatment", *Bio-mass and Bio-energy* 14 (1998):251-260.
13. H.S, S., Industry Crops Production, 11 (2000): 73-84.
14. Hearle, J., Sparrow J.,"Mechanics of the Extension of Cotton fibers. II. Theoretical Modeling", *Journal of Applied Polymer Science* 24 (2003):1857-1874.
15. Bledzki, A., Gassan J, "Composites Reinforced with Cellulose Based Fibres," *Progress in Polymer Science* 24 (1999):221-274.
16. http://www.ccrc.uga.edu/~mao/intro/ouline.htm Accessed on: 6/17/2013.
17. Gillies, M., "Nonwoven Materials: Recent Developments",Noyes Data Corporation Park Ridge, NJ, USA, 1979.
18. Mueller, D.H., Krobjilowski, A, Schachtschneider H, "Acoustically Optimized Structural Parts Basing on Hybrid Fleeces", Procedings of the Belt-wide Cotton Conferences,:Atlanta, GA, 2002
19. Marienfeld, M.L.,"Geotextile Trends and Developments", Tappi Journal 78 (1995):143-146.
20. English, B., "Biobased, Biodegradable Geotextiles: USDA Forest Service Research Update", Proceedings of the 2nd Pacific Rim Bio-based Composites Symposium, Vancouver, Canada, 1994.

21. Woodings, C., "Regenerated Cellulose Fibres", Woodhead Publishing, 2001.
22. Hearle, J., " A Theory of The Mechanics of Needled Fabrics", Needle-felted Fabrics, Textile Trade Press, Manchester, 1972, p. 51.
23. Herman, B., "Resonance Energy Transfer Microscopy", *Methods Cell Biology* 30 (1989):219-243.
24. Byron Pipes R., McCullough R.L., Taggart D.G., "Behavior of Discontinuous Fiber Composites: Fiber Orientation", *Polymer Composites* 3 (1982):34-39.
25. Mwaikambo, L.Y., Ansell M.P., "Chemical Modification of Hemp, Sisal, Jute, and Kapok Fibers by Alkalization", *Journal of Applied Polymer Science* 84 (2002): 2222-2234.
26. Mwaikambo L., Ansell M., "Mechanical Properties of Alkali Treated Plant Fibres and Their potential as Reinforcement Materials II. Sisal fibre", *Journal of Materials Science* 41(2006):2497-2508.
27. Placet V., Trivaudey F., Cisse O., Gucheret R.V., Boubakar M.L., "Diameter Dependence of the Apparent Tensile Modulus of Hemp Fibres: A morphological, Structural or Ultrastructural Effect? ", *Composites Part A: Applied Science and Manufacturing* 43(2012):275-287.
28. Khan, R., Majibur Md., Chen Y., Belsham T., Laugue C., Landry H., Peng Q., Zhong W., "Fineness and Tensile Properties of Hemp Fibres", *Biosystems Engineering* 108 (2011):9-17.
29. Rebenfeld, L., Miller B., "Using Liquid Flow to Quantify the Pore Structure of Fibrous Materials", *Journal of the Textile Institute* 86 (1995):241-251.

30. Rouison, D., Sain M., Couturier M., "Resin Transfer Molding of Natural Fiber Reinforced Composites: Cure Simulation", *Composites Science and Technology* 64 (2004):629-644.
31. Liu X., Dai G., " Impregnation of Thermoplastic Resin in Jute Fiber Mat", *Journal of Chemical Engineering of Chinese Universities* 21 (2007):586.
32. Li, Y., "Processing of Sisal Fiber Reinforced Composites by Resin Transfer Molding", *Materials and Manufacturing Processes* 21 (2006):181-190.
33. Van Wyk C.M., "A Study of the Compressibility of Wool, with Special Reference to South African Merino Wool", Stellenbosch,Stellenbosch University, 1944.
34. Gutowski, T., Dillon G., "The Elastic Deformation of Lubricated Carbon Fiber Bundles: Comparison of Theory and Experiments," *Journal of Composite Materials* 26 (1992): 2330-2347.
35. Toll, S., Manson J.A., "Elastic Compression of a Fiber Network", *Journal of Applied Mechanics, Transactions ASME* 62 (1995): 223-226.
36. Servais, C., Michaud V., Månson J.A.E., "The Packing Stress of Impregnated Fiber Mats", *Polymer Composites* 22 (2001):298-311.
37. Kim, Y.R., McCarthy S.P., Fanucci J.P., "Compressibility and Relaxation of Fiber Reinforcements During Composite Processing," *Polymer Composites* 12 (1991): 13-19.
38. Lee, B.H., Kim H.J., Yu W.R., "Fabrication of Long and Discontinuous Natural Fiber Reinforced Polypropylene Biocomposites and Their Mechanical Properties", *Fibers and Polymers* 10 (2009): 83-90.

39. Francucci, G., Vázquez A., Rodríguez E.S., "Key Differences on the Compaction Response of Natural and Glass Fiber Preforms in Liquid Composite Molding", *Textile Research Journal* 82(2012): 1774-1785.
40. Bay, R.S., "Fiber Orientation in Injection Molded Composites: A Comparison of Theory and Experiment*", Dissertation Abstracts International* 52(1992): 233.
41. Folgar, F., C.L. Tucker, "Orientation Behavior of Fibers in Concentrated Suspensions,*" Journal of Reinforced Plastics and Composites* 3(1984):98-119.
42. Gupta, M., Wang K., "Fiber Orientation and Mechanical Properties of Short-Fiber-Reinforced Injection-Molded Composites: Simulated and Experimental results," *Polymer Composites* 14(1993):367-382.
43. Matsuoka, T.,Takabatake J.I., Inoue Y., Takahashi H., "Prediction of Fiber Orientation in Injection Molded Parts of Short-Fiber-Reinforced Thermoplastics", *Polymer Engineering and Science* 30 (1990):957-966.
44. Darlington, M., McGinley P., "Fibre Orientation Distribution in Short Fibre Reinforced Plastics", *Journal of Materials Science* 10 (1975):906-910.
45. Vaxman, A., Narkis M., Seigmann A., Kenig S., "Short-Fiber-Reinforced Thermoplastics. Part III: Effect of Fiber Length on Rheological Properties and Fiber Orientation", *Polymer Composites* 10 (1989): 454-462.
46. Johnson, R., " Examining Fiber Behavior in a Nonwoven Web Through Image Analysis of Tracer Fibers", *Tappi Journal* 71(1988):77-80.
47. Enomae, T., Han Y., Isogai A., "Nondestructive Determination of Fiber Orientation Distribution of Paper Surface by Image Analysis", *Nordic Pulp and Paper Research Journal* 21(2006):253.

48. Vahlund, C.F., Gebart B.R., “Analysis of An Image Processing Method for Fiber Orientation in Polymer Composites”, *Polymer Composites* 22 (2001):327-336.
49. Zhao, R., X. Zhou, and G. Dai, “Effect of the Microstructure of GMT on its Mechanical Properties”, *Polymer Composites* 33 (2002):1026-1035.
50. Lee S.H., Kang T.J., “Mechanical and Impact Properties of Needle Punched Nonwoven Composites”, *Journal of Composite Materials* 34(2000): 816-840.
51. Kang, T.J., Lee S.H., “Characterization of Reinforcing Web Structures in Needle Punched Nonwoven Composites”, *Journal of Composite Materials* 33(1999): 2116-2132.
52. Kang, T.J., Lee S.H., “Effect of Punching Density on the Mechanical and Thermal Properties of Needle-Punched Nonwoven Carbon/Phenolic Composites”, *Polymers & Polymer Composites* 10 (2002):521-530.
53. Miao, M., Glassey H.E., Rastogi M., “An Experimental Study of the Needled Nonwoven Process Part III: Fiber Damage Due to Needling,” *Textile Research Journal* 74 (2004): p. 485-490.
54. Wang, Y., “Effect of Consolidation Method on the Mechanical Properties of Nonwoven Fabric Reinforced Composites”, *Applied Composite Materials* 6 (1999):19-34.
55. Wuzella G., “A New Composite Material Based on Natural Fibers and a Thermoset Resin: Technology, Applications and Properties,” *WIT transactions on the Built Environment* 85 (2006): 53-62.
56. Chen, Y., Sun L., Negulescu I., Wu Q., “Comparative Study of Hemp Fiber for Nonwoven Composites”, *Journal of Industrial Hemp* 12 (2007): 27-45.

57. Van den Oever, M., Bos H., Molenveld K., “Flax Fibre Physical Structure and its Effect on Composite Properties: Impact Strength and Thermo-Mechanical Properties”, *Die Angewandte Makromolekulare Chemie* 272 (1999):71-76.
58. Van den Oever M., Bos H., Van Kemenade M., “ Influence of the Physical Structure of Flax Fibres on the Mechanical Properties of Flax Fibre Reinforced Polypropylene Composites”, *Applied Composite Materials* 7 (2000):387-402.
59. Van De Velde K., Kiekens P., “Effect of Flax/PP Panel Process Parameters on Resulting Composite Properties”, *Journal of Thermoplastic Composite Materials* 16 (2003):413-431.
60. Rodríguez E., Petrucci R., Puglia D., Kenny J., Vázquez A. “Characterization of Composites Based on Natural and Glass fibers Obtained by Vacuum Infusion”, *Journal of Composite Materials* 39 (2005):265-282.
61. Gillah, P., Irle M., Amartey S., “Development and Production of Laboratory Scale Novel MDF Panels from Composite and Nonwoven Mattresses of Sisal and Wood Fibre Mixtures”, *Holz als Roh-und Werkstoff* 58 (2000): 324-330.
62. Mwaikambo L., Ansell M., ”Hemp Fibre Reinforced Cashew Nut Shell Liquid Composites”, *Composites Science and Technology* 63 (2003):1297-1305.
63. Williams G.I., Wool R.P., ”Composites from Natural Fibers and Soy Oil Resins”, *Applied Composite Materials* 7 (2000): 421-432.
64. O’Donnell A., Wool R.P., “Natural Fiber Composites with Plant Oil-based Resin” *Composites Science and Technology* 64 (2004):1135–1145.

65. Mieck K.P., Lützkendorf R., Reussmann T., "Needle-Punched Hybrid Nonwovens of Flax and PP Fibers—Textile Semiproducts for Manufacturing of Fiber Composites", *Polymer Composites* 17 (1996):873-878.
66. Mutjé, P. Gironès J., Lopez A., Llop MF, Vilaseca F., "Hemp Strands: PP Composites by Injection Molding: Effect of Low Cost Physico-Chemical Treatments," *Journal of Reinforced Plastics and Composites* 25 (2006):313-327.
67. Hargitai, H., Racz I., Anandjiwala R., "Development of Hemp Fibre–PP Nonwoven Composites", *Macromolecular Symposia* 239 (2006): Wiley Online Library, 201-208.
68. Hargitai, H., Rácz I., Anandjiwala R.D., "Development of Hemp fiber Reinforced Polypropylene Composites", *Journal of Thermoplastic Composite Materials* 21(2008):165-174.
69. Khoathane, M., Vorster O., Sadiku E., "Hemp Fiber-reinforced 1-Pentene/Polypropylene Copolymer: The Effect of Fiber Loading on the Mechanical and Thermal Characteristics of the Composites*", Journal of Reinforced Plastics and Composites* 27 (2008):1533-1544.
70. Rouison, D., Sain M., Couturier M., "Resin Transfer Molding of Hemp Fiber Composites: Optimization of the Process and Mechanical Properties of the Materials", *Composites Science and Technology* 66 (2006):895-906.
71. Shahzad A., "Hemp Fibre and its Composites–a Review*", Journal of Composite Materials* 46 (2012):973-986.

72. Hautala M., Pasila A., Pirilä J., "Use of Hemp and Flax in Composite Manufacturing: a Search for New Production Methods", *Composites Part A: Applied Science and Manufacturing* 35 (2004):11-16.
73. Bhatnagar A., Sain M., "Processing of Cellulose Nanofiber-Reinforced Composites", *Journal of Reinforced Plastics and Composites* 24 (2005):1259-1268.
74. Epaarachi, J., Ku H., Gohel K., "A Simplified Empirical Model for Prediction of Mechanical Properties of Random Short Fiber/Vinylester composites", *Journal of Composite Materials* 44 (2010):779-788.
75. Hine, P.J., Rudolf L. H., Gusev A.A., "Numerical Simulation of the Effects of Volume Fraction, Aspect Ratio and Fibre Length Distribution on the Elastic and Thermoelastic Properties of Short Fibre Composites*", Composites Science and Technology* 62 (2002):1445-1453.
76. Kardos, J., "Critical Issues in Achieving Desirable Mechanical Properties for Short Fiber Composites", *Pure and Applied Chemistry* 57 (1985):1651-1657.
77. Liang, J.Z., "Predictions of Tensile Strength of Short Inorganic Fibre Reinforced Polymer Composites", *Polymer Testing* 30 (2011):749-752.
78. Chen, C.H., "Effective Elastic Moduli of Misoriented Short-fiber Composites", *International Journal of Solids and Structures* 33 (1996):2519-2539.
79. Fu, S.Y., Lauke B., "Effects of Fiber Length and Fiber Orientation Distributions on the Tensile Strength of Short-Fiber-Reinforced Polymers", *Composites Science and Technology* 56 (1996):1179-1190.
80. Fu, S.Y, Lauke B., "The Elastic Modulus of Misaligned Short-Fiber-Reinforced Polymers", *Composites Science and Technology* 58 (1998):389-400.

81. McGee, S.H. and R. McCullough, "Characterization of fiber orientation in short-fiber composites*", Journal of Applied Physics* 55 (1984):1394-1403.
82. Kim, J. and D. Lee, "Measurement of Fiber Orientation Angle in FRP by Intensity Method*", Journal of Materials Processing Technology* 201 (2008):755-760.
83. Esmaeili M., Zadhoush A., Javid K.M., "A New Practical Method for Theoretical Consideration of Orientation and Length Distribution in Short Fiber Composites", *Recent Advances in Textile Composites, Proceeding of 10th International Conference on Textile Composites* October, 2010, pp.157-164,
84. Facca A.G., Kortschot M.T., Yan N., "Predicting the Elastic Modulus of Natural Fibre Reinforced Thermoplastics", *Composites Part A: Applied Science and Manufacturing* 37 (2006):1660-1671.
85. Baillie C., "Green Composites: Polymer Composites and the Environment," CRC Press, 2004.
86. Ku H., Wang H., Pattarachaiya N., Trada M., "A Review on the Tensile Properties of Natural Fiber Reinforced Polymer Composites", *Composites Part B: Engineering* 42 (2011):856-873
87. Peponi L., Biagiotti J., Torre L., Kenny J.M., Mondragon, I., "Statistical Analysis of the Mechanical Properties of Natural Fibers and Their Composite Materials, I. Natural Fibers", *Polymer Composites* 29 (2008):313-320.
88. Staln, C., "Modeling of Stiffness of Wood Composite Materials" Ph.D Thesis, Lund University, 2001.

89. Mwaikambo L., Ansell M., "Mechanical Properties of Alkali Treated Plant Fibres and Their Potential as Reinforcement Materials. I. Hemp Fibres", *Journal of Materials Science* 41 (2006):2483-2496.

90. Patel, H., Reng G., Hogg P.J, Peijs T., "Hemp Fibre as Alternative to Glass Fibre in Sheet Moulding Compound Part 1; Influence of Fibre Content and Surface Treatment on Mechanical Properties", *Plastics, Rubber and Composites* 39 (2010):268-276.

91. Bledzki, A., Reihmane S., Gassan J., "Properties and Modification Methods for Vegetable Fibers for Natural Fiber Composites*", Journal of Applied Polymer Science* 59(1996):1329-1336.

92. Valadez-Gonzalez, A., Cevanets J.M., Olayo R., Herrera P.J., "Effect of Fiber Surface Treatment on the Fiber–Matrix Bond Strength of Natural Fiber Reinforced Composites", *Composites Part B: Engineering* 30 (1999):309-320.

93. Jayamol G., Sreekala M.S., Sabu T., "A Review on Interface Modification and Characterization of Natural Fiber Reinforced Plastic Composites", *Polymer Engineering & Science* 41 (2001): 1471-1485.

94. Hepworth D.G. , Steven-fountan A. , Brucea D.M. , Vincent J.F.V, "Affine versus non-affine deformation in soft biological tissues, measured by the reorientation and stretching of collagen fibers through the thickness of compressed porcine skin", *Journal of Biomechanics*,34(2001), 341-346.

95. Basu A., Wen Q., Mao X., Lubensky T. C., Janmey P. A.,Yodh A G., "Non -affine Displacements in Flexible Polymer Networks", *Macromolecules* 44 (2011), 1671-1679.

96. Wen Q., Basu A., Mao X., Lubensky T. C., Janmey P. A.,Yodh A G., " Non-affine déformations in polymer hydrogels", *Soft Matter* 8(2012), 8039.

97. Penninga J.P. , Ruiten J. V., Brouwer R. , Gabrielse W., "Orientation and structure development in melt-spun Nylon-6 fibers", *Polymer* 44 (2003), 5869- 5876.

98. Hine, P., Davidson N., Duckett R.A., Clarke A.R., Ward I.M, "Hydrostatically Extruded Glass-Fiber-Reinforced Polyoxymethylene. I: The Development of Fiber and Matrix Orientation", *Polymer Composites* 17 (1996):720-729.

99. Hoa, S.V., "Principles of the Manufacturing of Composite Materials," DEStech Publications, Inc., 2009.

100. Halpin, J. Pagano N., "The Laminate Approximation for Randomly Oriented Fibrous Composites", *Journal of Composite Materials* 3 (1969):720.

101. Kaw, A.K., "Mechanics of Composite Materials," *CRC Press, Taylor and Francis Group*,2006.

102. Shojaei A., Trochus F., Ghaffarian R., Karimian L., "An Experimental Study of Saturatedand Unsaturated Permeabilities in Resin Transfer Molding Based on UnidirectionalFlow Measurements", *Journal of Reinforced Plastics and Composites* 23 (2004):1515-1537.

103. Feih, S., Wonsyld K., Minzari D., Westermann P., Lilhott H., "Testing Procedure for the Single Fiber Fragmentation Test", 2004. Riso National Laboratory, Roskilde, Denmark.

104. *http://www.ccponline.com/* Accessed on 6/17/2013.

105. Cichocki Jr F., Thomason J., " Thermoelastic Anisotropy of a Natural Fibers", *Composites Science and Technology* 62 (2002):669-678.

106. Whitney, J.M., Riley M.B., “Elastic Stress-Strain Properties of Fiber Reinforced Composite Materials”, *Ft. Belvoir Defense Technical Information Center* 1965.

107. Whitney, J.M., “ Elastic Moduli of Unidirectional Composites with Anisotropic Filaments”, *Journal of Composite Materials* 1 (1967):188-193.

108. Harris, B., “Engineering Composite Materials,” Institute of Metals UK,1986.

109. Kelly, A., Tyson W., “Tensile Properties of Fibre-Reinforced Metals: Copper/ Tungsten and Copper/ Molybdenum”, *Journal of the Mechanics and Physics of Solids* 13 (1965):329-338.

110. Cox, H., “The Elasticity and Strength of Paper and Other Fibrous Materials”, *British Journal of Applied Physics* 3 (1952):72.

111. Stoven T, W.F., Mitschang P, Neitzel M, “Continuous Monitoring of Three Dimensional Resin Flow Through a Fiber Preform”, *Composites Part A: Applied Science and Manufacturing* 34 (2003):475–80.

112. Bickerton S, S.E.M., Graham P.J, Advani S.G, “Fabric Structure and Mold Curvature Effects on Preform Permeability and Mold Filling in the RTM Process, Part I: Experiments”, *Composites Part A: Applied Science and Manufacturing* 31 (2000):423–38.

113. Luo Y, Hoes K., Vanheule M., Sol H., Cardon A, “Permeability measurement of textile reinforcements with several test fluids, *Composites Part A: Applied Science and Manufacturing* 32 (2001):1497–504.

114. Umer R., Fernyhough A., “Characterising wood fibre mats as reinforcements for liquidcomposite moulding processes”, *Composites Part A: Applied Science and Manufacturing* 38 (2007):434-448.

115. Rodriguez E., F.G.A.A.V.Z., "Permeability–Porosity Relationshipin RTM for Different Fiberglassand Natural Reinforcements", *Journal of Composite Materials* 38 (2004):259-269.

116. Morais, A.B., "Transverse Moduli of Continuous-Fibre-Reinforced Polymers", *Composites Science and Technology* 60 (2000):997-1002.

117. Mazumdar, S., "Composites Manufacturing: Materials, Product, and Process Engineering, CRC Press, 2001.

118. Wei H.,Ton-That H., Perrin-Sarazin F., Denault J., "An improved method for single fiber tensile test of natural fibers", *Polymer Engineering Science* 50(2010), 815-826.

APPENDIX A

Introduction

In this appendix formulations and input values for different micromechanical models that are compared with the developed models, in this thesis, for tensile modulus and tensile strength are presented respectively.

A.1 Tensile Modulus

Halpin-Tsai equation [100] as shown in A.1 is used to predict the tensile modulus of needle punched composites.

$$E_{c-Halpin} = E_m \left(\frac{1+\xi\eta V_f}{1-\eta V_f} \right) \tag{A.1}$$

parameter η is given by equation (A.2)

$$\eta = \frac{\left(\frac{E_f}{E_m}\right)-1}{\left(\frac{E_f}{E_m}\right)+\xi} \tag{A.2}$$

where ξ is the shape parameter. The significance of the parameter ξ is that it takes in to account the packing arrangement and the geometry of the reinforcing the fibers. A variety of empirical equations for ξ are available in the literature and they depend on the shape of the reinforcing fibers [106]. In this thesis, parameter η is estimated by fitting average experimental tensile modulus, in transverse and longitudinal direction for each needle punch density, with Equation (A.1). The empirically fitted η is tabulated in Table A.1.

Table A.1. Empirically fitted η for different needle punch density composites

Composite	$\boldsymbol{\eta}$
0-P	10
2.6 -P	8
7-P	10
30-P	30
70 -P	8
150-P	9

A.2. Tensile Strength Predictions Using Modified Micromechanical Model (MMM)

In this section The MMM model that is used to predict the tensile strength of needle punched hemp mat composites are explained. Two other models available in literature that are compared with PDM model in Section 5.5.4 are also presented.

In MMM approach, the mat composite is modeled as a single layer with a distribution in fiber orientation. A modified rule of mixture [108] is used to estimate the tensile strength of needle punched composite. The effect of orientation is accounted for in Equation (4.15) which is developed for tensile strength of unidirectional fiber composites.

It is well known that a continuous fiber unidirectional lamina would fail by one of the three failure modes depending on the orientation of the fiber axis with respect to loading axis. This is illustrated in A.1, where in strength of unidirectional lamina is plotted as a function of orientation angle. For small values ($\theta < \theta_0$), the composite fail by fiber fracture and strength of the composite (σ_θ) is calculated given by

$$\sigma_\theta = \sigma_{LC} sec^2\theta \qquad (0 \leq \theta \leq \theta_0) \qquad \text{(A.3)}$$

where σ_{Lc} is the strength of the composite when all the fibers are aligned in the direction of the applied load and

$$\theta_0 = tan^{-1}(\frac{\tau_6}{\sigma_{LC}}) \qquad \text{(A.4)}$$

where $\tau_6$is the shear strength of the composites.

At intermediate angles, the composite fails by shear and the strength of the composite is given by

$$\sigma_\theta = \frac{\tau_6}{sin\theta cos\theta} \qquad (\theta_0 \leq \theta \leq \theta_1) \tag{A.5}$$

where $\tau_{6,u}$ is the shear strength of the composite and

$$\theta_1 = tan^{-1}\left(\frac{\sigma_{2,u}}{\tau_{6,u}}\right) \tag{A.6}$$

Beyond θ_1, the composite would fail by normal failure

$$\sigma_\theta sin^2\theta = \sigma_{2,u} \qquad \left(\theta_1 \leq \theta \leq \frac{\pi}{2}\right) \tag{A.7}$$

Needle punched hemp mat composites, have fibers with orientation distributed from ^{0}0 to ^{0}90. Therefore, the average strength of the composite can be calculated by summing the contribution from fibers at ach orientation as

$$\sigma_c = \sum_0^{N_f} f(\theta)\sigma_\theta \tag{A.8}$$

where N_f is the number of fibers, $f(\theta)$ is the normalized frequency of fibers oriented in θ such that $\int_0^{\frac{\pi}{2}} f(\theta)d\theta = 1$.

Substituting Equations (A.3), (A.5), and (A.7) into Equation (A.8) yields:

$$\sigma_c = \sum_0^{\theta_0} f(\theta)\sigma_{LC}sec^2\theta + \sum_{\theta_0}^{\theta_1} f(\theta)\frac{\tau_c}{sin\theta cos\theta} + \sum_{\theta_1}^{\frac{\pi}{2}} f(\theta)\frac{\sigma_m}{\sin(\theta)^2} \tag{A.9}$$

σ_{LC} , calculated based on the Equation (4.15), is substituted in Equation (A.9) to determine the tensile strength of the needle punched composite

The input data required for the MMM are the distribution in the length of the hemp fibers in the mats and θ_1 and θ_0. The former was determined experimentally and modeled using a Weibull distribution. The model-fit parameters (*a* and *b*) along with minimum and maximum length are tabulated in Table 4.4. The latters are tabulated in Table A.2 and A.3.

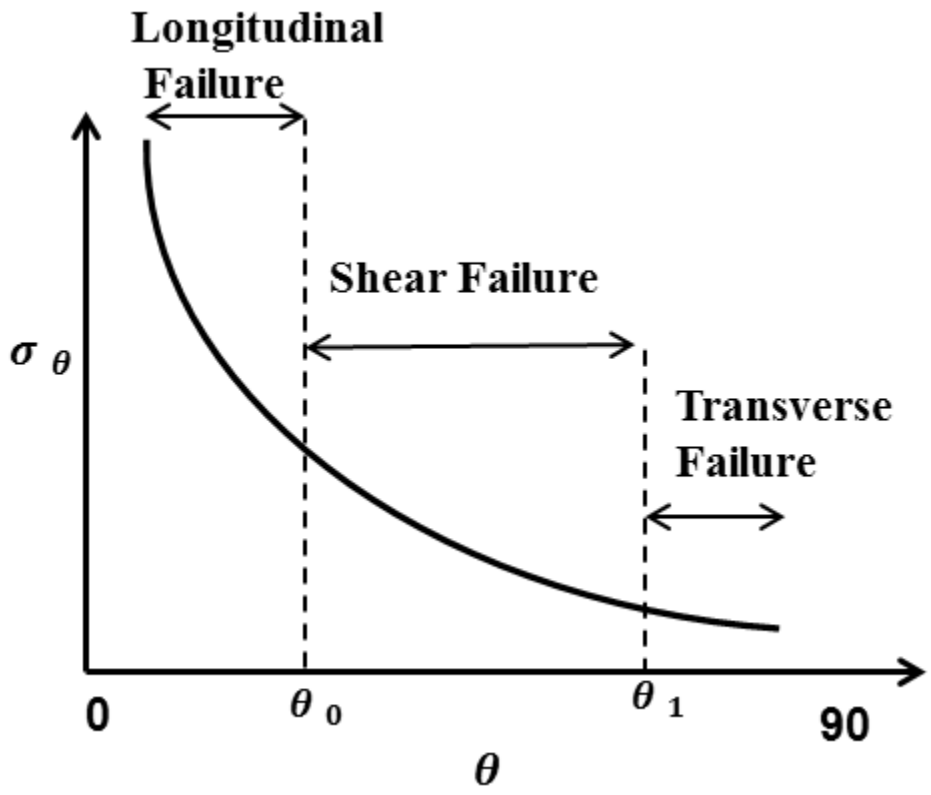

Figure A.1. Strength of a unidirectional lamina as a function of orientation of the fibers

Table A.2. Experimental input values for MMM

$\sigma_m^{'}$ (MPa)	$\theta_1 = tan^{-1}\left(\frac{\tau_m}{\sigma_m^{'}}\right)$
20	63.019^0

Table A.3. Fiber orientation angle for transition from longitudinal composite failure (i.e. fiber fracture) to shear failure (θ_0)

Composite ID	$\boldsymbol{\theta_0}$
No P	3^0
No P-260	5^0
No P-560	6^0
2.6 P	3.1^0
2.6 P-260	4.2^0
2.6 P-560	5.2^0
7 P	3.2^0
7 P-260	4.1^0
7 P-560	5.3^0
30 P	3.7^0
30 P-260	4.6^0
30 P-560	5.4^0
70 P	3.1^0
70P-260	4.2^0
70P-560	5.1^0
150P	4.1^0
150P-260	5.2^0
150P-560	7.3^0

Predictions using two other micromechanical models available in the literature are also compared with the predictions using the PDM model that is developed in this thesis to evaluate the relative merits of these models with respect to those available in the literature Both of these

models took in to account the effect of length and orientation of fibers on tensile strength of the composite. For the effect of length, both used simple and widely accepted shear lag theory, introduced by Cox [110] and developed by Kelly and Tyson[109]. The first model is the one developed by McNally et al. [108] represented by Equation (A.10).

$$\sigma_c = D\left[\sum_{l_i=l_{min}}^{l_i=l_c} \frac{V_{fi}\tau l_i}{d} + \sum_{l_j=l_c}^{l_j=l_{max}} \sigma_f V_{fj}\left(1-\frac{l_c}{2l_j}\right)\right] + V_m\sigma'_m \qquad \text{(A.10)}$$

In this model, to the effect of fiber orientation is taken into account using an empirically fitted factor (*D*) [106].

The second model is that developed by Lee [38] and have been applied successfully to predict the tensile strength of discontinuous fiber glass composite . In this model, represented by Equations (A.11) and (A.12), the in-plane orientation of fibers is assumed to be random.

$$\sigma_{CL} = \frac{2\tau}{\pi}\left\{2 + ln\left[\frac{\left(1-\frac{l_C}{2L}\right)\sigma_f\sigma_m V_f + \sigma_m\sigma'_m V_m}{\tau^2}\right]\right\} \quad for \quad L \geq l_c \qquad \text{(A.11)}$$

$$\sigma_{CL} = \frac{2\tau}{\pi}\left\{2 + ln\left[\frac{\tau(l_f/d_f)\sigma_m V_f + \sigma_m^2 V_m}{\tau^2}\right]\right\} \quad for \quad L < l_c \qquad \text{(A.12)}$$

Various parameters in this equation have been defined above. Lee's model is one of the few simple micromechanical models that have used a constant value $\left(\frac{1}{\pi}\right)$ for orientation of fibers. The constant value used for orientation factor in these models differentiates it from the PDM and MMM models that is introduced in this thesis that use FOD instead of constant values.

APPENDIX B

Distribution of tensile strength and tensile modulus of hemp mats with different needle punch density is presented in this Appendix.

B.1. Tensile Modulus of Hemp Fibers

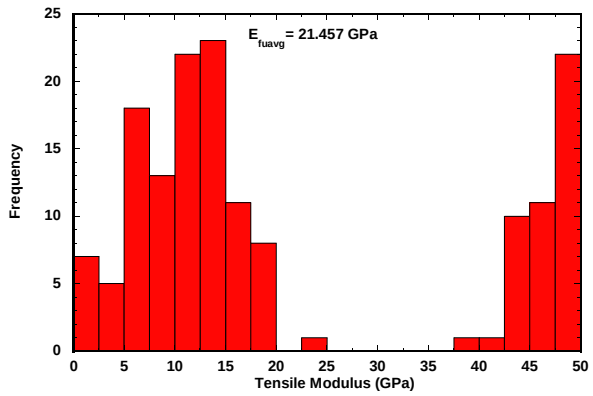

Figure B.1. Distribution of tensile modulus in 2.6-P hemp mat

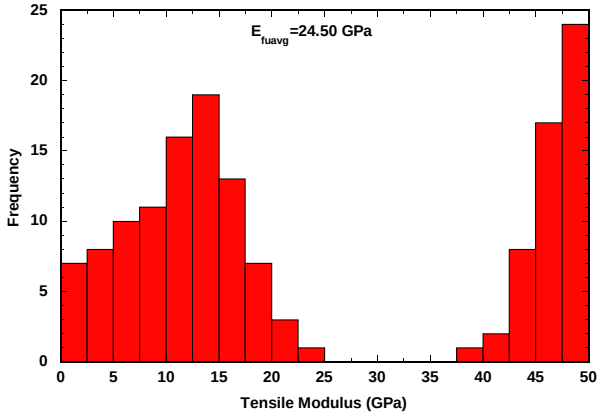

Figure B.2. Distribution of tensile modulus in 7-P hemp mat

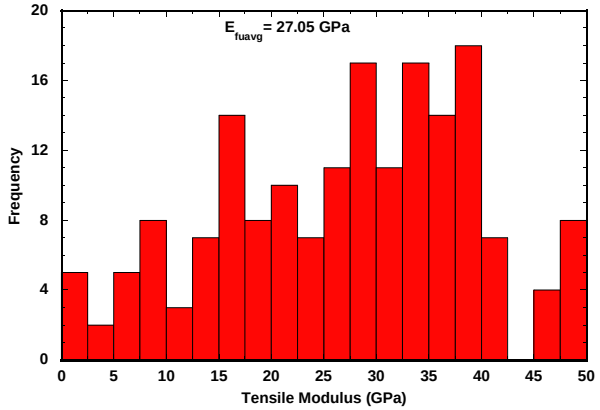

Figure B.3. Distribution of tensile modulus in 30-P hemp mat

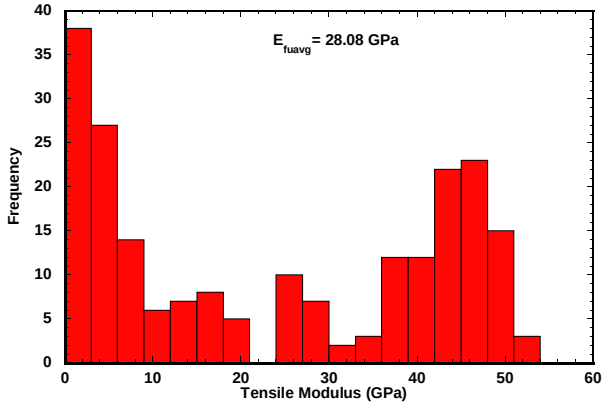

Figure B.4. Distribution of tensile modulus in 70-P hemp mat

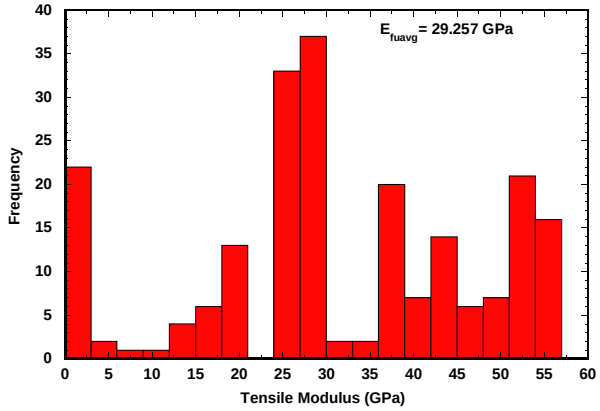

Figure B.5. Distribution of tensile modulus in 150-P hemp mat

B.2 Tensile Strength of Hemp Fibers

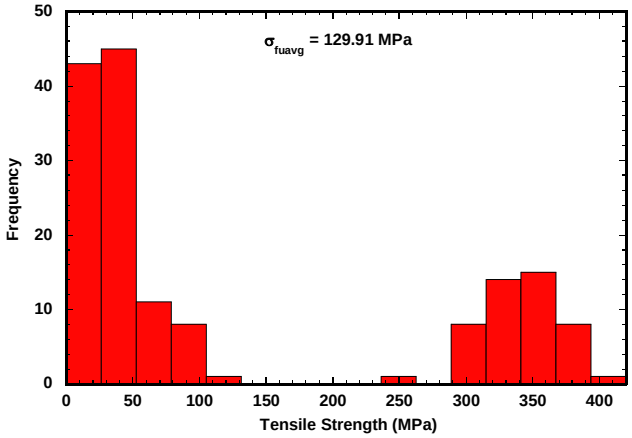

Figure B.6. Distribution of tensile strength in 2.6-P hemp mat

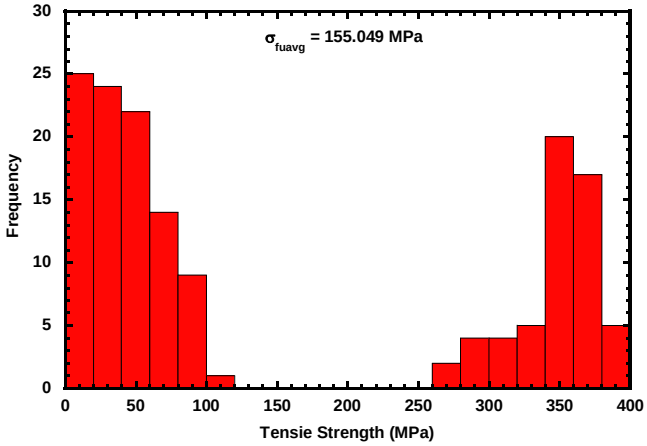

Figure B.7. Distribution of tensile strength in 7- P hemp mat

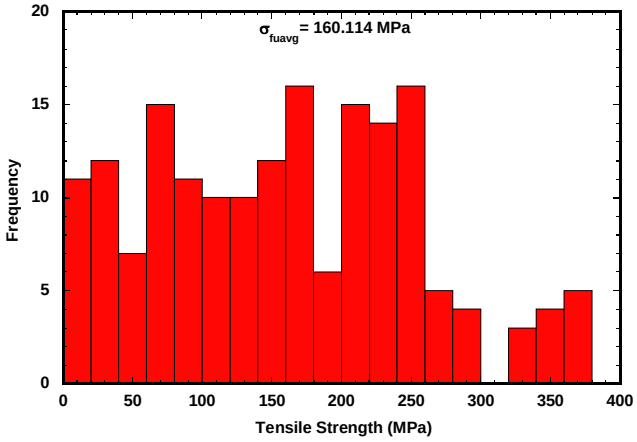

Figure B.8. Distribution of tensile strength in 30–P hemp mat

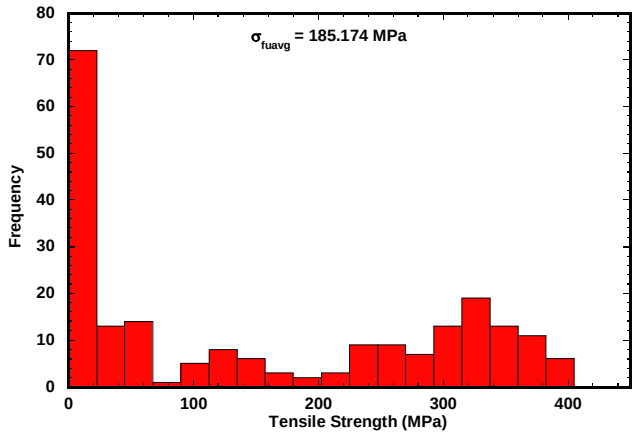

Figure B.9. Distribution of tensile strength in 70–P hemp mat

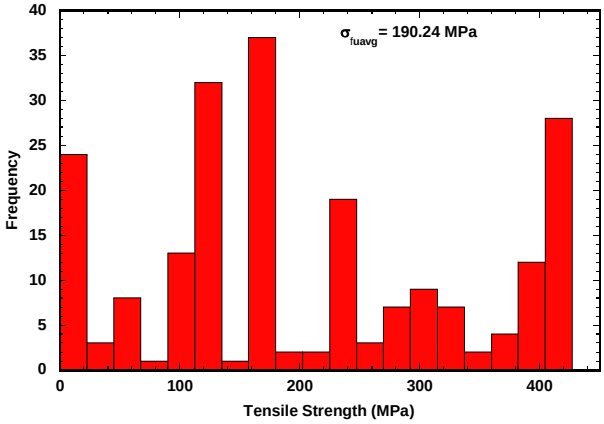

Figure B.10. Distribution of tensile strength in 150–P hemp mat

APPENDIX C

In this appendix the experimental FOD for θ and φ of hemp mats at different compaction pressures are presented.

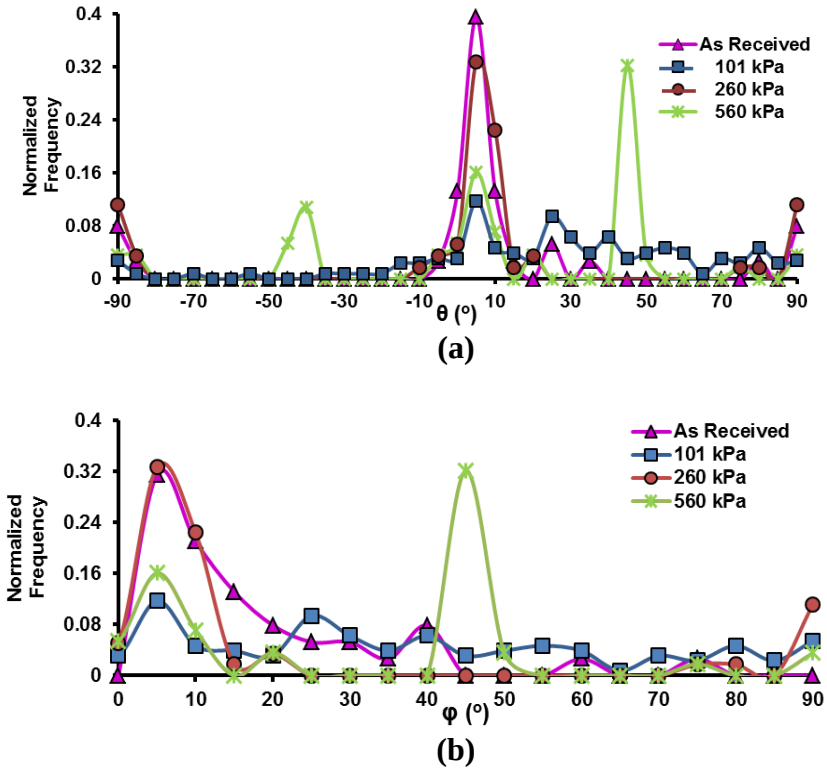

Figure C.1. Effect of compaction pressure on FOD for 7-P (a) in- plane orientation θ, (b) out of plane orientation φ

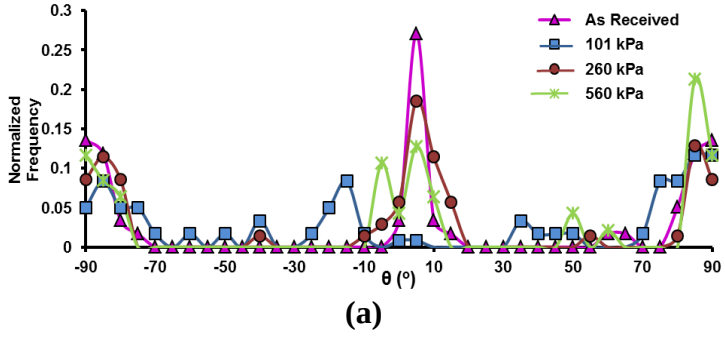

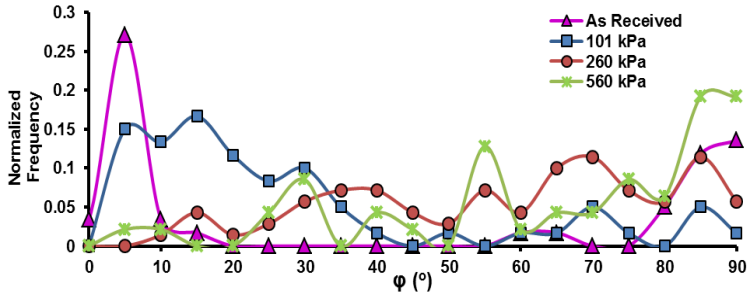

(b)

Figure C.2. Effect of compaction pressure on FOD for 30-P (a) in- plane orientation θ, (b) out of plane orientation φ

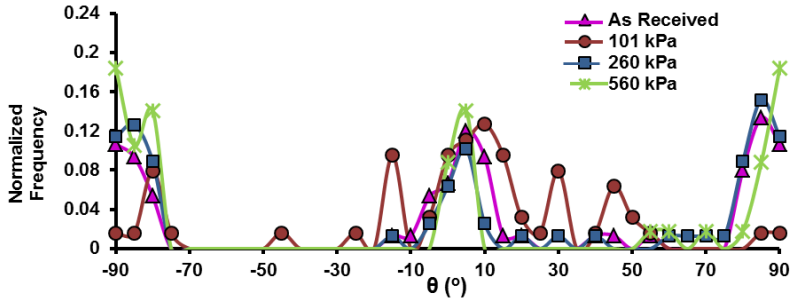

(a)

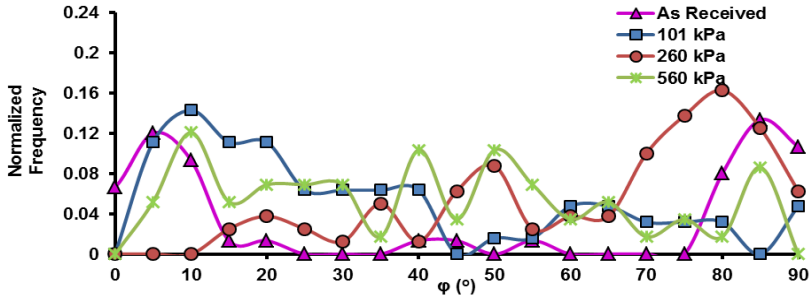

(b)

Figure C.3. Effect of compaction pressure on FOD for 70-P (a) in- plane orientation θ, (b) out of plane orientation φ

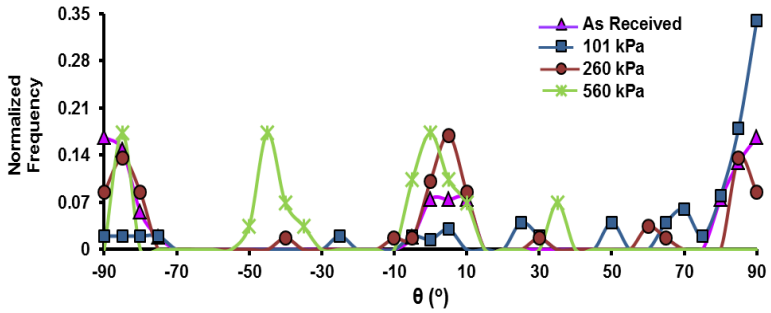

(a)

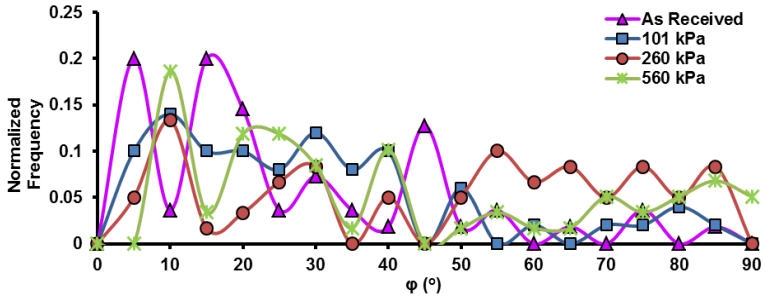

(b)

Figure C.4. Effect of compaction pressure on FOD for 150-P (a) in- plane orientation θ, (b) out of plane orientation φ

C.2. Effect of Needle Punching on FOD of Hemp Mats

In this section the predicted FOD of hemp mats after needle punching is compared with experimental FODs.

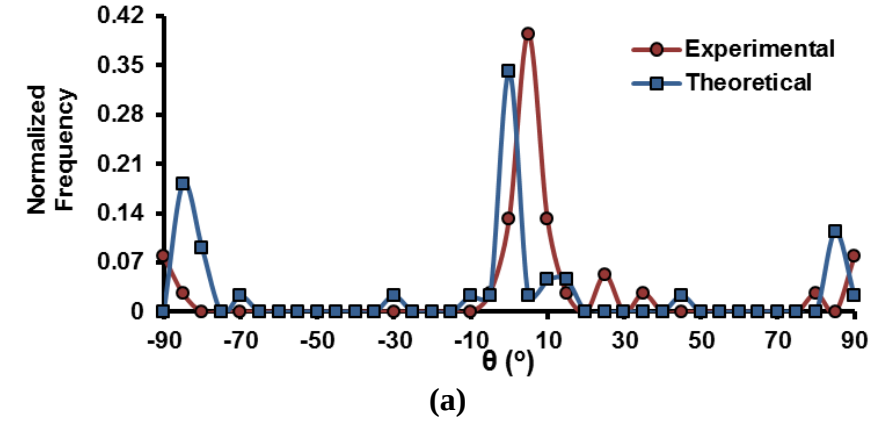

(a)

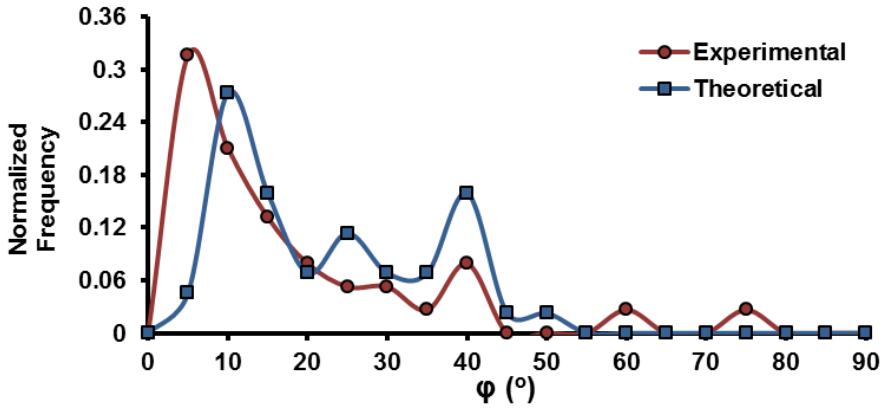

(b)

Figure C.5. Predicted and experimental FOD of 7-P mat (a) in- plane orientation θ, (b) out of plane orientation φ

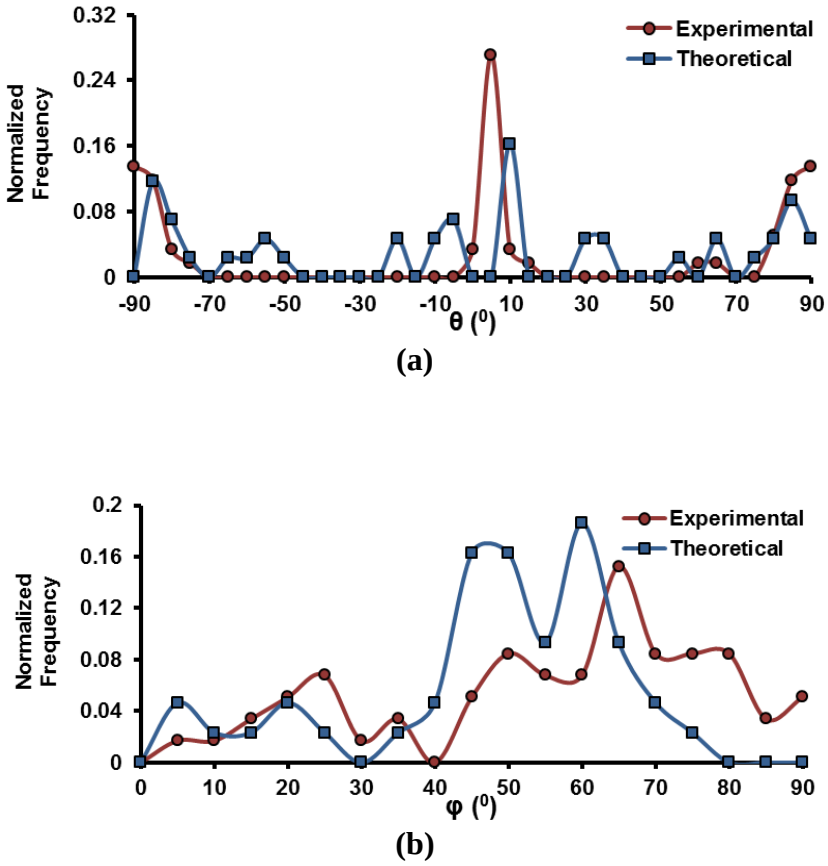

Figure C.6. Predicted and experimental FOD of 30-P mat (a) in- plane orientation θ, (b) out of plane orientation φ

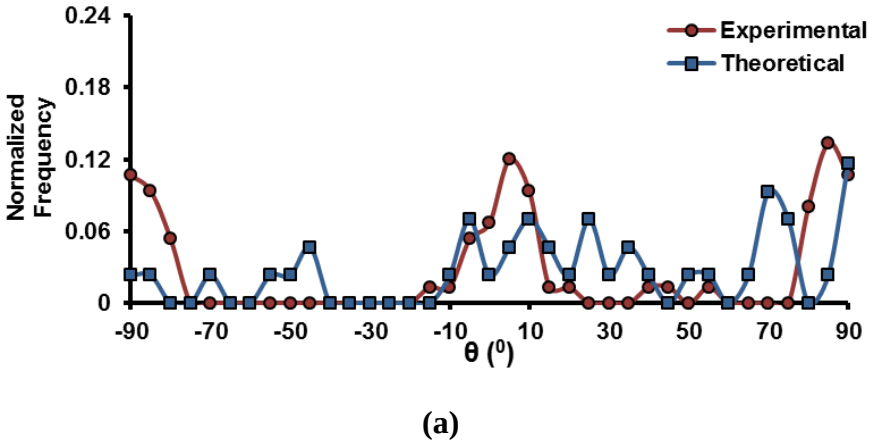

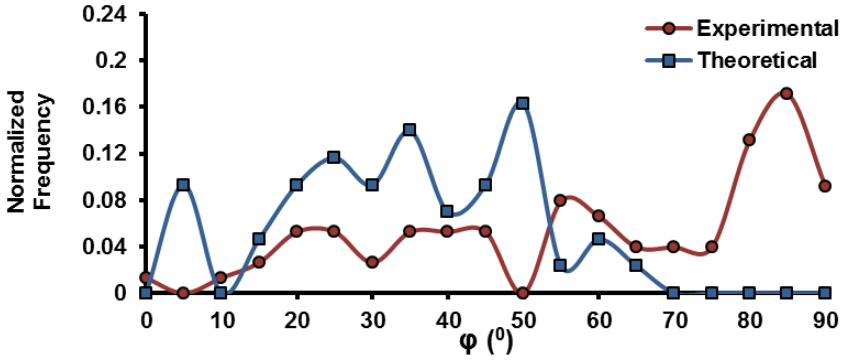

(b)

Figure C.7. Predicted and experimental FOD of 70-P mat (a) in- plane orientation θ, (c) out of plane orientation φ

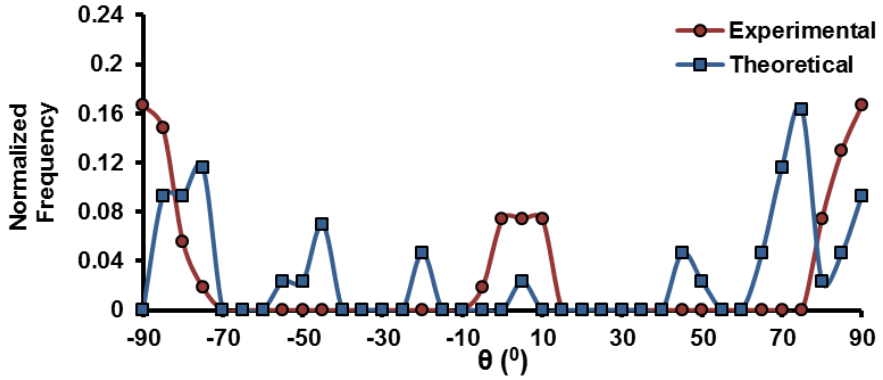

(a)

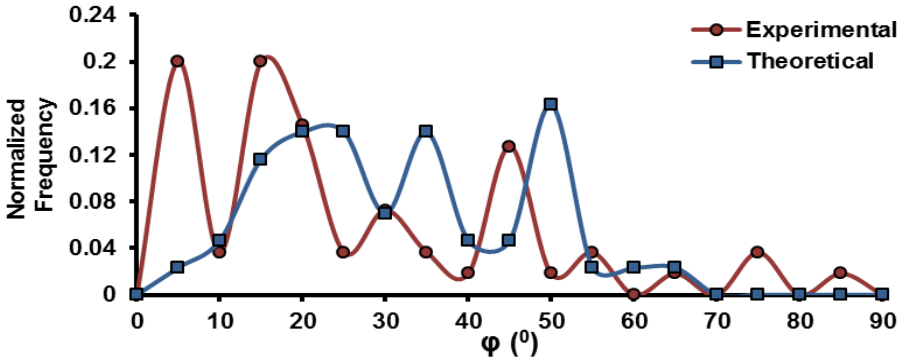

(b)

Figure C.8. Predicted and experimental FOD of 150-P mat (a) in- plane orientation θ, (b) out of plane orientation φ

C.3. Effect of Compaction Pressure on FOD of Hemp Mats

In this section the predicted FOD of hemp mats after compacting at pressures of 101, 260 and 560 kPa are compared with experimental FODs.

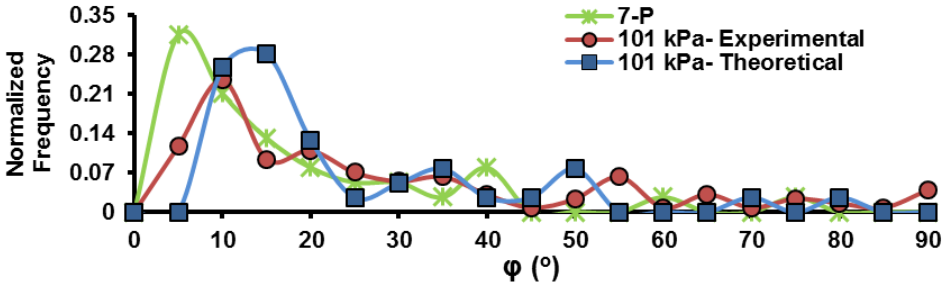

(a)

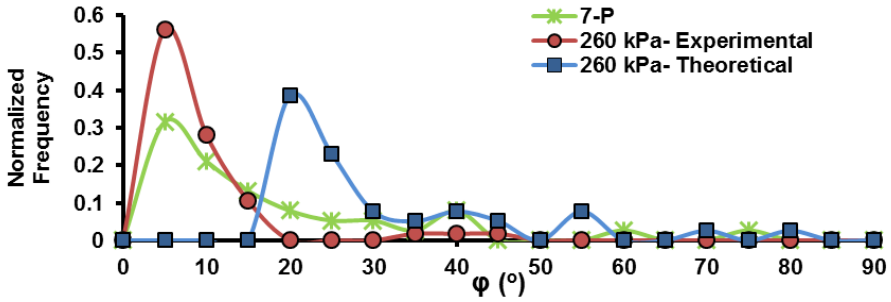

(b)

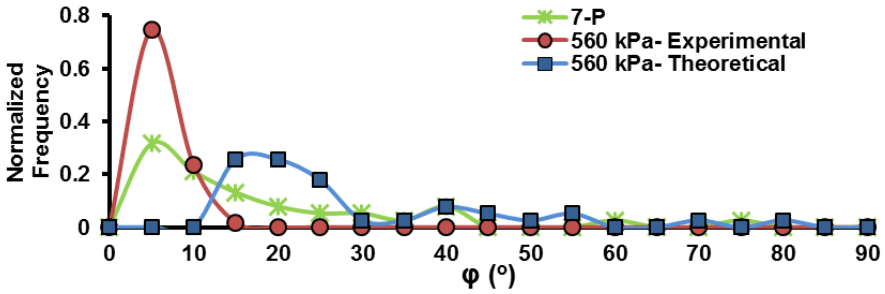

(c)

Figure C.9. The predicted and experimental FOD of φ for 7-P mat in (a) 101 kPa and (b) 260 kPa (c) 560 kPa compaction pressure

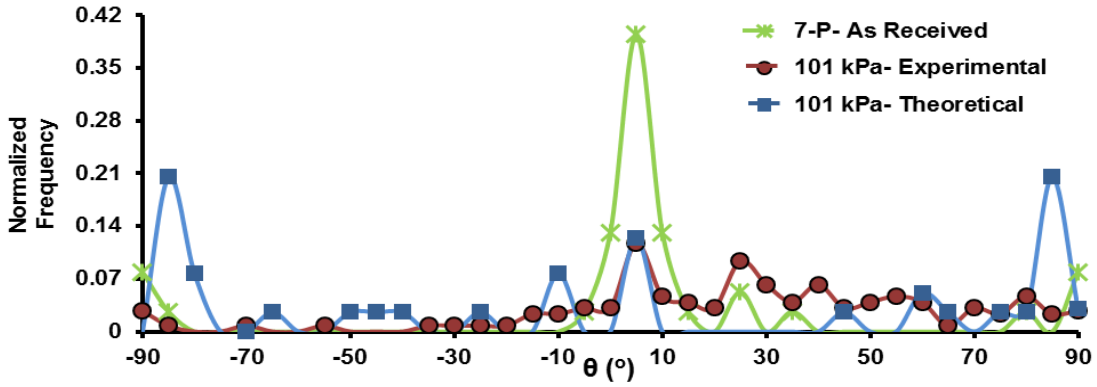

(a)

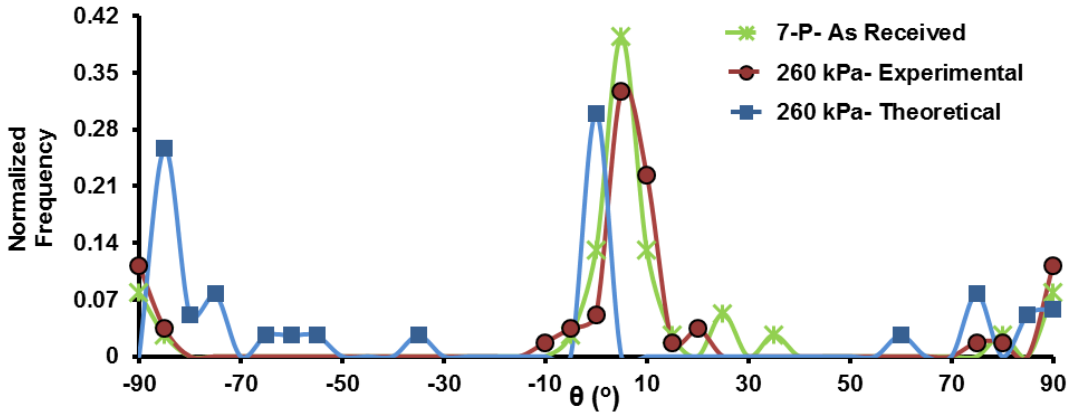

(b)

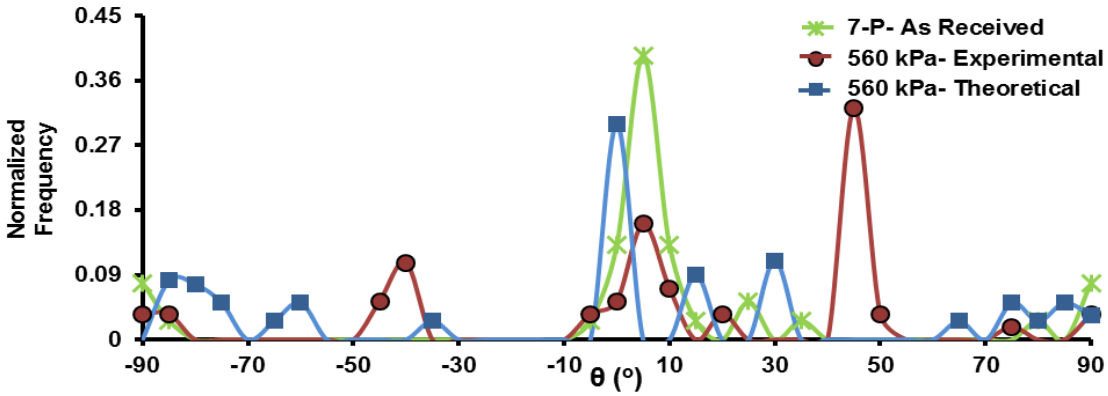

(c)

Figure C.10. The predicted and experimental FOD of θ for 7-P mat in (a) 101 kPa and (b) 260 kPa (c) 560 kPa compaction pressure

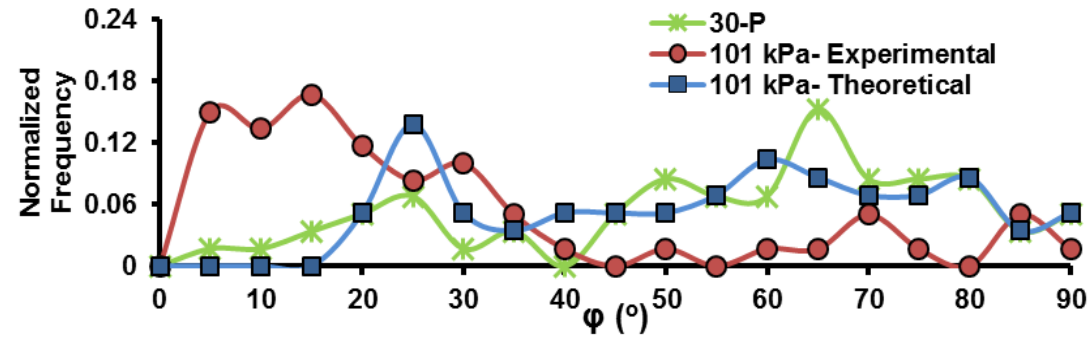

(a)

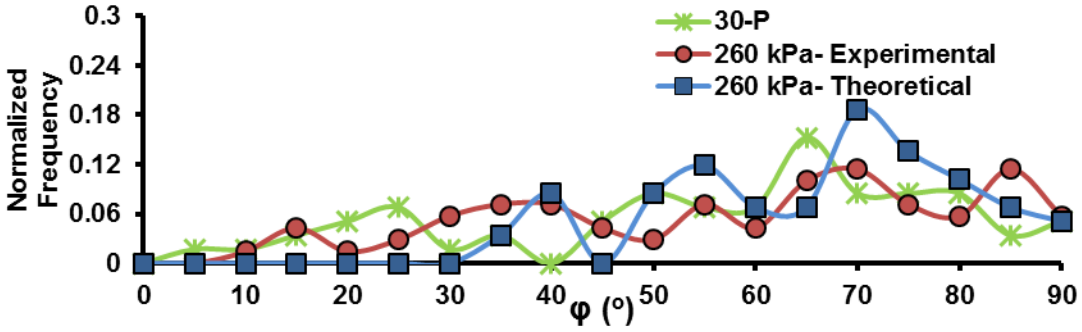

(b)

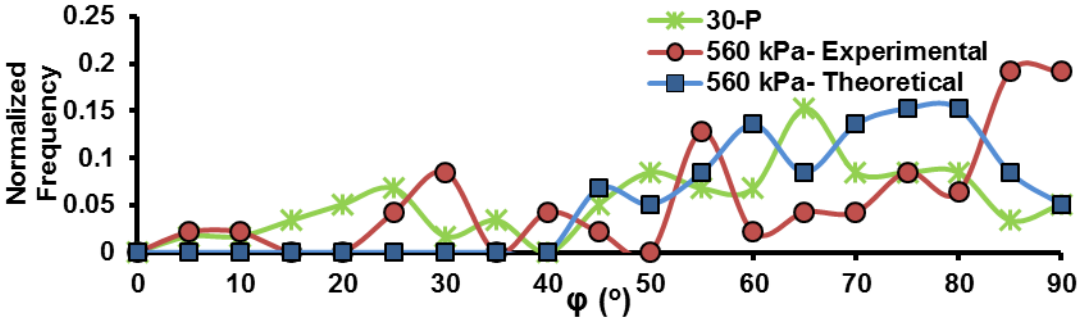

(c)

Figure C.11. The predicted and experimental FOD of φ for 30-P mat in (a) 101 kPa and (b) 260 kPa (c) 560 kPa compaction pressure

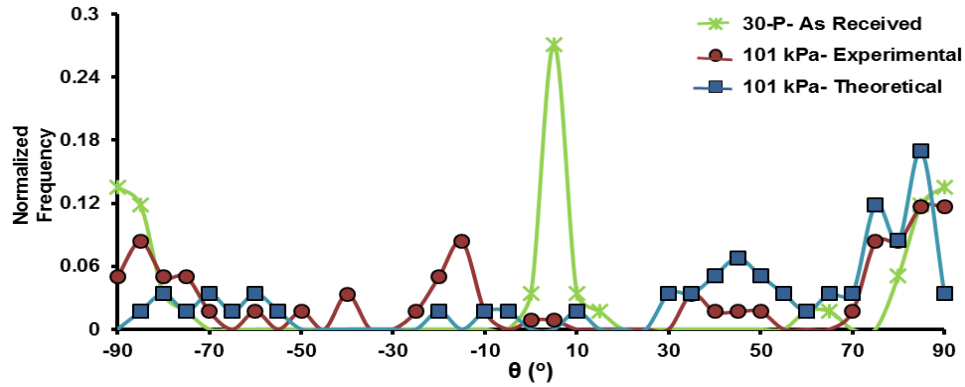

(a)

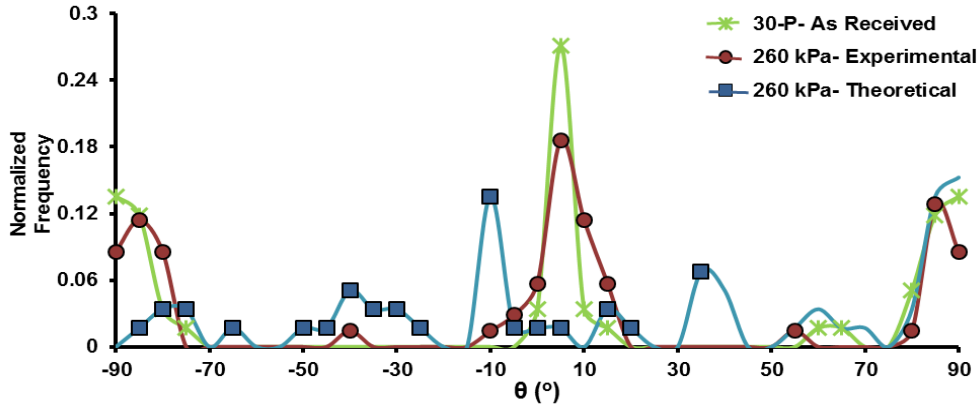

(b)

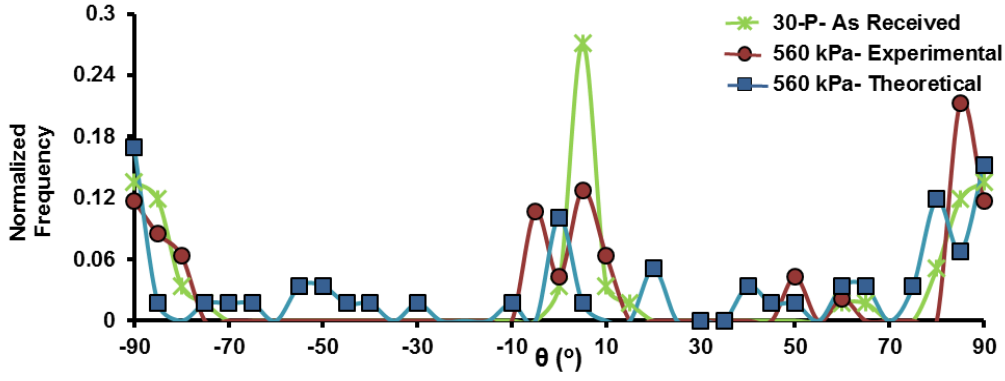

(c)

Figure C.12. The predicted and experimental FOD of θ for 30-P mat in (a) 101 kPa and (b) 260 kPa (c) 560 kPa compaction pressure

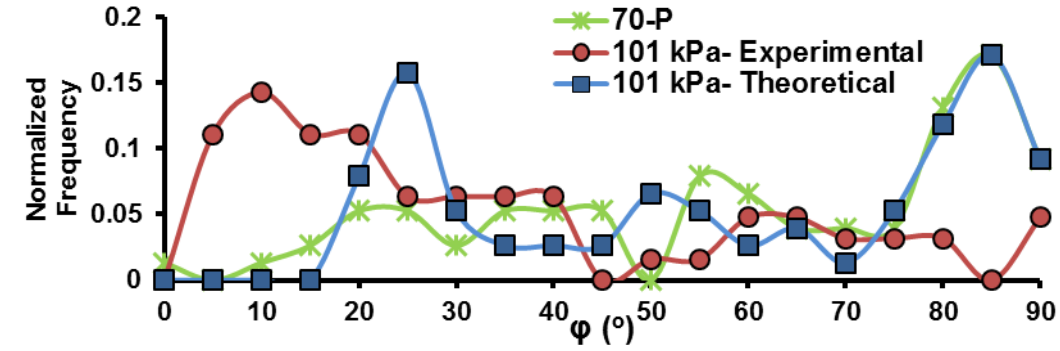

(a)

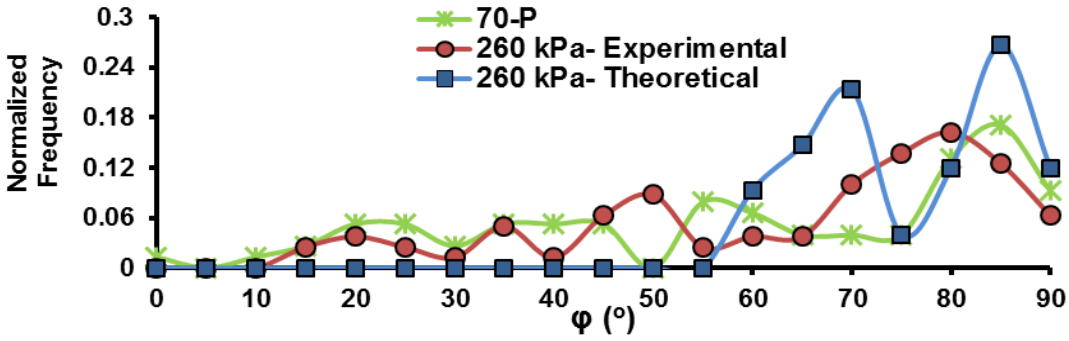

(b)

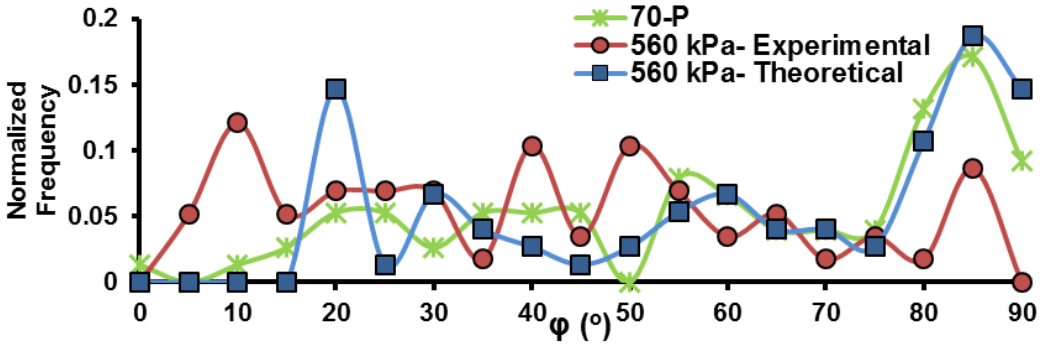

(c)

Figure C.13. The predicted and experimental FOD of φ for 70-P mat in (a) 101 kPa and (b) 260 kPa (c) 560 kPa compaction pressure

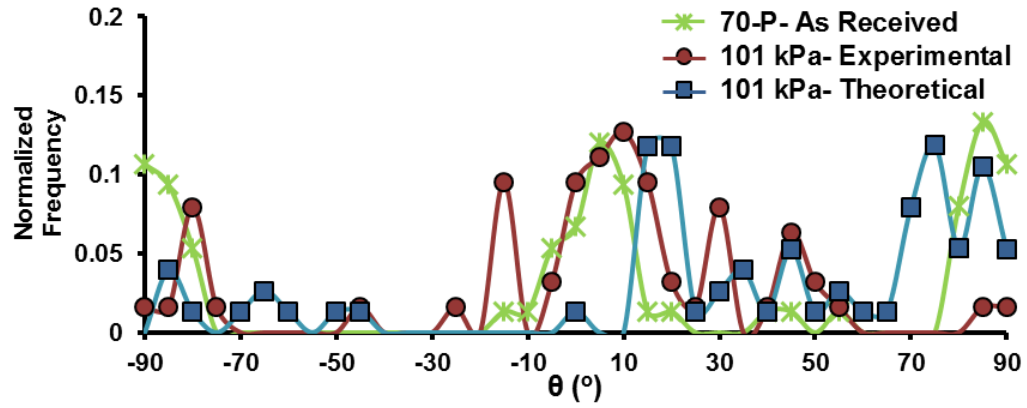

(a)

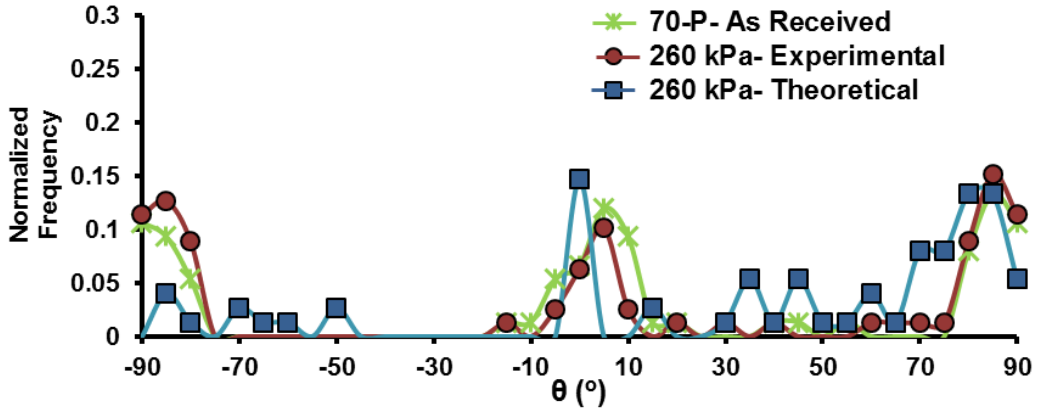

(b)

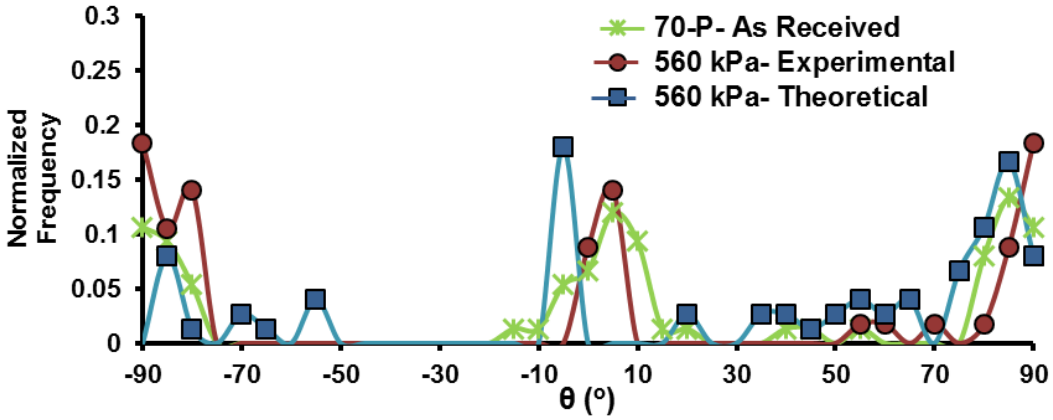

(c)

Figure C.14. The predicted and experimental FOD of θ for 70-P mat in (a) 101 kPa and (b) 260 kPa (c) 560 kPa compaction pressure

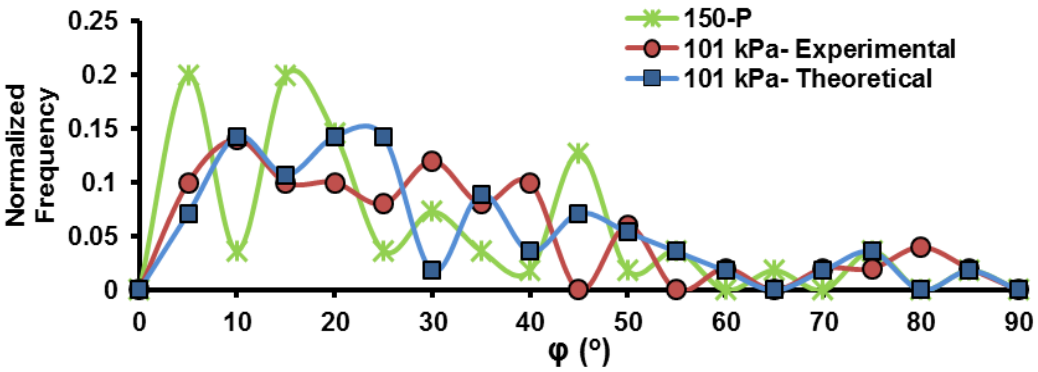

(a)

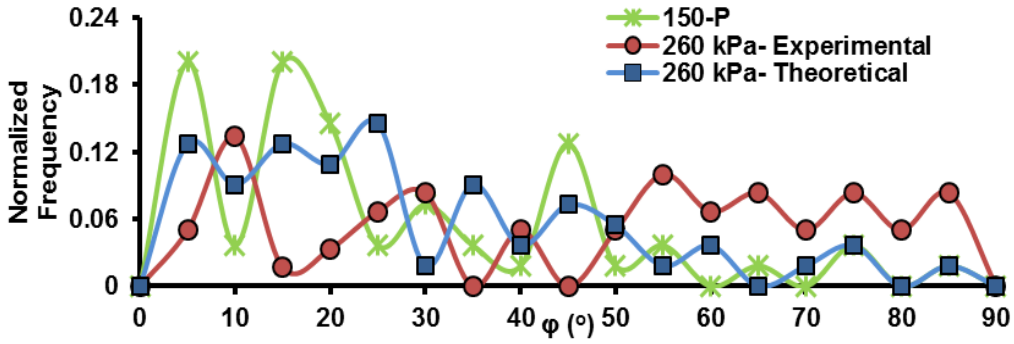

(b)

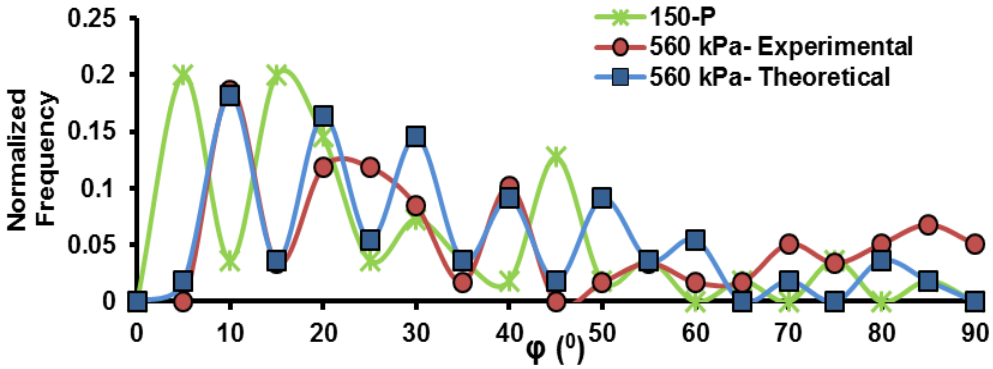

(c)

Figure C.15. The predicted and experimental FOD of φ for 150-P mat in (a) 101 kPa and (b) 260 kPa (c) 560 kPa compaction pressure

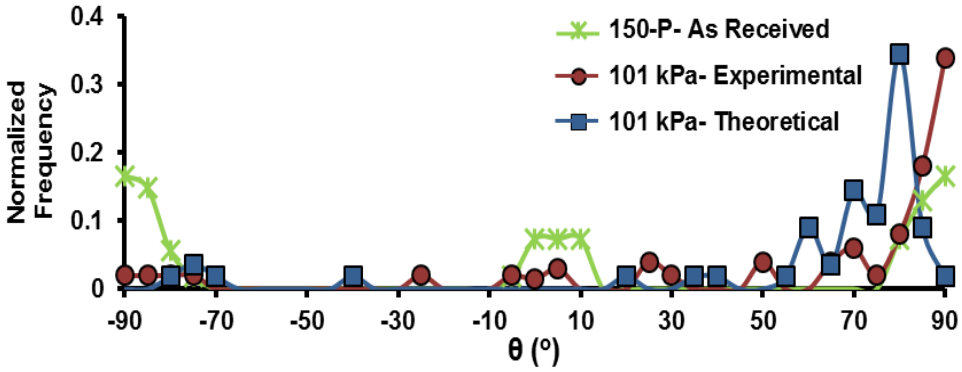

(a)

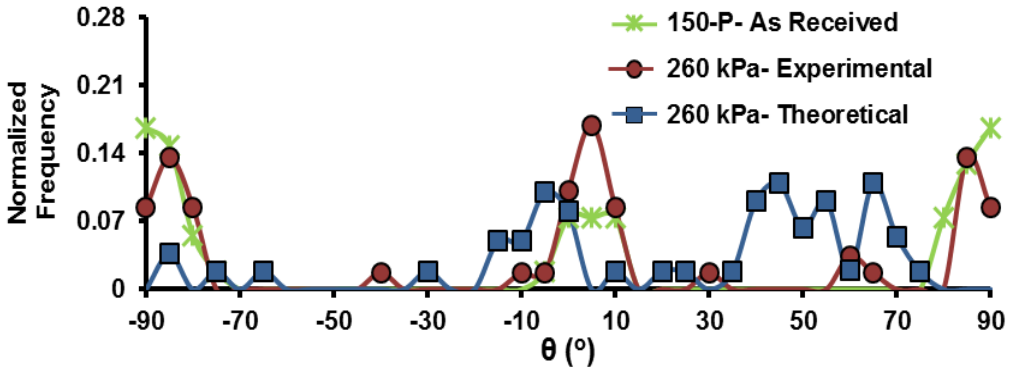

(b)

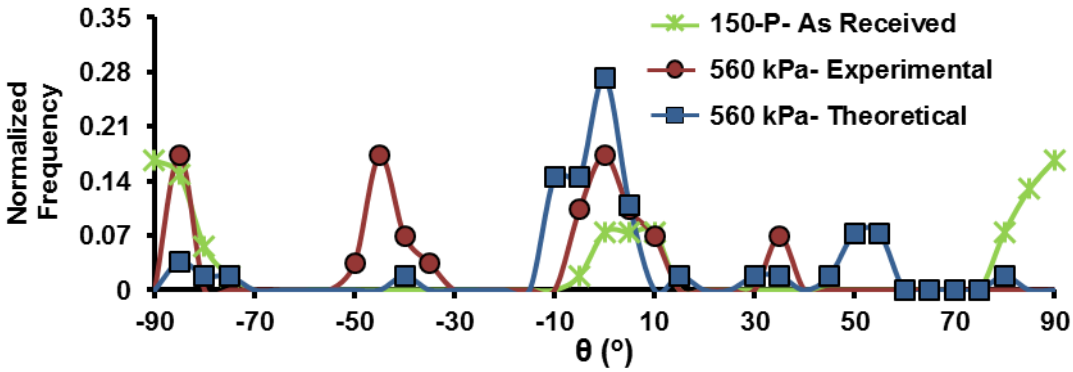

(c)

Figure C.16. The predicted and experimental FOD of θ for 150-P mat in (a) 101 kPa and (b) 260 kPa (c) 560 kPa compaction pressure